UNIVERSIDAD DE CANTABRIA

Escuela Técnica Superior de
Ingenieros de Caminos Canales y Puertos

# A STATISTICAL FATIGUE MODEL COVERING THE TENSION AND COMPRESSION WÖHLER FIELDS AND ALLOWING DAMAGE ACCUMULATION

**Author**
**María Luisa Ruiz Ripoll**

**Directors**
Prof. Dr. Enrique Castillo Ron (Universidad de Cantabria)
Prof. Dr. Alfonso Fernández Canteli (Universidad de Oviedo)

**Santander, 2008**

***A mis padres,***
***a mi hermana,***
***a Álvaro...***

*"No hay enigmas, si un problema puede plantearse, es que puede resolverse"*
Ludwig Wittgenstein, filósofo (1889–1951)

*"En el fondo, los científicos somos gente con suerte: podemos jugar a lo que queramos durante toda la vida"*
Lee Smolin, físico (1955–today)

*"A theory can be proved by experiment; but no path leads from experiment to the birth of a theory"*
Albert Einstein, científico (1879-1955)

# Acknowledgements

It is well known that these pages of a PhD thesis are the most widely read pages of the entire publication. I will try to write these lines as emotional as possible, because the conclusion of all this work, all this time has to be sincere.

Thanks to my supervisors Enrique and Alfonso. They have given me the opportunity of be the scientist that I am today, and have the pleasure of knowing many new.

Thanks to Hernán and Paola, good mates during this long travel.

Thanks for the financial, academic and technical support of Empa (Swiss Federal Laboratories for Testing and Research at Dübendorf (Switzerland)). Thanks to Roland for his daily supervision of my work and all the help that he gave me during this year. Thanks to Evelyne, for the good moments expended in our office. Thanks to the durability group, because they were with me always. Thanks to G. Terrasi for his supervision. Thanks to Sandro and Walti, my best German professors, my Empa uncles, for the personal support. Thanks to Christian, Alex, Berni, Ali, Peter, each one has a important contribution during the time I have been in Swizterland.

Thanks to my friends, Luba, Vanessa, Claire and Martin, for the personal support. During my time in Zürich I have shared my best time with all of you giving me advices, surprises and making me smile when I needed it, always perfect!.

Thanks to the existence of the cities Santander and Zürich. In them I discovered myself as the happiest person in the world. They are the most beautiful cities that I know, and I wish to come back to each one during all my life to experience between their fantastic beaches, forests, mountains and lakes fantastic moments.

Thanks to my family. To my parents, Javier and Luisa, because they have been always there, even thousand of kilometers apart. I am the person that I am because of them. Thanks to my sister Lidia, during all my life she has been the perfect sister and friend. Thanks “peque”.

Thanks to Álvaro, my motivation. He has suffered with me all the good and bad moments during this stage, and always he has given me the best. Today I am here because of you. You are my energy.

And I would like to thank to the rest of the people that should be here, but I have forgotten and they supported me in one or another way.

M. Luisa Ruiz Ripoll
October 30, 2008
Ciudad Real, Spain

# Contents

# List of Figures

# List of Tables

# Part I

# Sinopsis de la Tesis Doctoral en Castellano

# Chapter 1

# Sinopsis de la Tesis Doctoral en Castellano

## 1.1 Objeto y objetivos de la investigación

El presente trabajo pretende aportar un avance en el conocimiento del comportamiento de materiales metálicos sometidos a cargas cíclicas mediante el desarrollo de un nuevo modelo probabilístico de fatiga de materiales.

De acuerdo al Capítulo 8 de la Normativa de los Estudios de Doctorado de la Universidad de Cantabria, al Real Decreto 778/1998 y a la normativa de la Universidad de Cantabria, los principales requisitos para la obtención del títutlo de Doctor son:

- Estar en posesión de título de Licenciado, Arquitecto, Ingeniero o equivalente u homologado a ellos.
- Realizar y aprobar los cursos, seminarios y trabajos de investigación tutelados del programa de doctorado correspondiente.
- Presentar y aprobar una tesis doctoral consistente en un trabajo original de investigación.

En el presente documento la doctoranda María Luisa Ruiz Ripoll presenta las contribuciones necesarias que avalan el cumplimiento de estos requisitos optando al título de Doctor por la Universidad de Cantabria.

Esta tesis doctoral ha sido realizada dentro del *Departamento de Matemática Aplicada y Ciencias de la Computación* de la Universidad de Cantabria, dentro del *Programa Interdepartamental I04: Desarrollo y Aplicación de Modelos en Ingeniería Civil*.

Esta tesis doctoral a su vez opta al título de doctorado europeo, habiéndose realizado las estancias mínimas fuera de España en un centro de investigación de otro Estado europeo cursando estudios o realizando trabajos de investigación que le hayan sido reconocidos por el Departamento responsable del programa, de acuerdo con el Capítulo 15 de la Normativa de los Estudios de Doctorado de la Universidad de Cantabria, al Real Decreto 778/1998 y a la normativa de la Universidad de Cantabria.

Debido a que la tesis doctoral está escrita en una lengua distinta a la castellana, debe contener un apartado suficientemente amplio, escrito en castellano en el que se incluyan las contribuciones, resultados y conclusiones obtenidas durante la elaboración de la misma, siendo este el objetivo del capítulo en el que nos encontramos.

La presente tesis doctoral, titulada: *"A Statistical Fatigue Model Covering the Tension and Compression Wöhler Fields and Allowing Damage Accumulation"* (*Modelo Estadístico de Fatiga para el Análisis del Campo de Wöhler Bajo Tensión y Compresión, Incluyendo el Cálculo de Acumulacin de Daño*) está redactado en lengua inglesa, por ello es necesario que contenga un apartado en castellano que se compone de las siguientes secciones:

1. Objeto y objetivos de la investigación.
2. Planteamiento y metodología utilizada.
3. Aportaciones originales.
4. Conclusiones y futuras líneas de investigación.

### 1.1.1 Introducción, hipótesis y objetivos de la investigación

Los trabajos existentes en la literatura de fatiga no han resuelto todavía el problema de la acumulación de daño debida a una historia de cargas arbitraria, ni desde el punto de vista teórico ni desde el punto de vista práctico y de laboratorio. Este problema es sin embargo crucial en la ingeniería práctica para diseño de estructuras. Se plantea el desarrollo de un modelo probabilístico que sirva como base para el análisis a fatiga de materiales metálicos sometidos a cualquier espectro de carga en cualquier rango de la misma (tensión, compresión o mixto).

Se pretende por tanto, dar una respuesta teórica y práctica a un campo de investigación ampliamente explorado antes, pero que no ha llegado a obtener una expresión matemática que involucre conceptos estadísticos, físicos y del comportamiento del material para el tipo de carga descrito anteriormente, de manera que sirva como base para el comienzo de una nueva forma de abordar la fatiga de los materiales basada en un nuevo modelo.

La principales motivaciones de esta tesis doctoral son dos. La primera de ellas es el ahorro económico que supone un buen conocimiento del comportamiento de los materiales frente al fenómeno de la fatiga. Los daños por fatiga siguen siendo de los más elevados en el diseño ingenieril al igual que las inversiones realizadas para su prevención. El coste anual debido a la fatiga de los materiales en Estados Unidos es de alrededor de un 3% del producto interior bruto (GON) [59], [94]. El otro motivo es el aumento de la fiabilidad en el cálculo de la vida última (comportamiento a fatiga) de un material sometido a cargas cíclicas.

Esta tesis doctoral es la continuación del trabajo realizado por los directores de tesis de la autora del trabajo, quienes desde los años ochenta del pasado siglo desarrollan, implementan y mejoran modelos para la fatiga de los materiales. Son destacables algunos de los últimos trabajos de estos autores, en los que mediante un modelo tipo Weibull se predice la vida última a fatiga y su daño acumulado, de un material sometido a cualquier historia de carga.

Las **hipótesis** utilizadas para el desarrollo de esta investigación son las siguientes:

1. Los modelos existentes para el análisis a fatiga hoy en día no satisfacen todos las condiciones físicas, experimentales y estadísticas para un buen modelo.
2. Un modelo útil para definir el comportamiento de materiales debe satisfacer estas condiciones.
3. Los materiales utilizados en esta investigación son normalmente metálicos y longitudinales.
4. Se supone el *principio del eslabón más débil*: *"Si un elemento longitudinal es dividido en n subelementos, la vida última del material vendrá dada por la vida última del elemento más débil"*.

5. Se supone que la acumulación del daño en un material comienza cuando la probabilidad de fallo es nula, y el fallo total se produce cuando dicha probabilidad es igual a uno.

Tras haber realizado una pequeña introducción al problema y haber dispuesto las hipótesis de trabajo, los **objetivos** que se plantean en esta tesis doctoral son los siguientes:

1. Desarrollar un estado del arte de la fatiga de los materiales donde se muestren los principales modelos usados hasta la fecha para la estimación y el análisis del comportamiento del material sujeto a cargas cíclicas. Realizar una discusión de las ventajas y desventajas de cada uno de ellos.

2. Detectar los principales problemas existentes en estos modelos y en las estrategia de ensayos utilizados en el análisis a fatiga de los materiales.

3. Desarrollar un nuevo modelo para la fatiga de los materiales que cubra todo el rango de cargas (tensión y compresión) para el campo de Wöhler para cualquier historia de carga. La derivación del modelo estará basada en la teoría de ecuaciones funcionales.

4. Realizar una discusión de las medidas de daño actuales y proponer nuevas, seleccionando las más adecuadas para el análisis a fatiga.

5. Analizar el daño acumulado con el modelo probabilístico propuesto.

6. Proponer una buena estrategia de ensayos para la obtención de los mejores resultados de laboratorio posibles y por lo tanto, las mejores estimaciones para los parámetros del modelo.

7. Diseñar una serie de ensayos experimentales para la evaluación y validación del modelo teórico.

8. Analizar los resultados obtenidos para validar el modelo.

9. Basándose en los resultados obtenidos y su analisis, presentar las principales conclusiones del trabajo realizado.

## 1.2 Planteamiento y metodología utilizada

La definición de una buena metodología trae consigo la obtención de buenos resultados y una buena organización en tiempo y trabajo. En esta tesis doctoral se han seguido los siguientes pasos (ver figura 1.1):

1. Análisis del problema: cuáles han sido los hechos a lo largo de la historia que han propiciado que el hombre se interese por ese problema y quiera solucionarlo?. Corresponde al capítulo 3 de la tesis doctoral.

2. Comprensión del problema: En el que se realiza un análisis de las causas que provocan esas situaciones y entendiendo qué factores entran a tomar parte de su evolución y desarrollo. Definición del término *fatiga de materiales*. Todos estos conceptos se analizan en los capítulos 3 y 4 de esta tesis doctoral.

3. Desarrollo: donde se establecen las bases y se desarrollan las aportaciones científicas necesarias para la mejora y el análisis de materiales sujetos a este tipo de solicitaciones. Los capítulos 5 y 6 sientan las bases necesarias para la derivación y aplicación del modelo de fatiga propuesto.

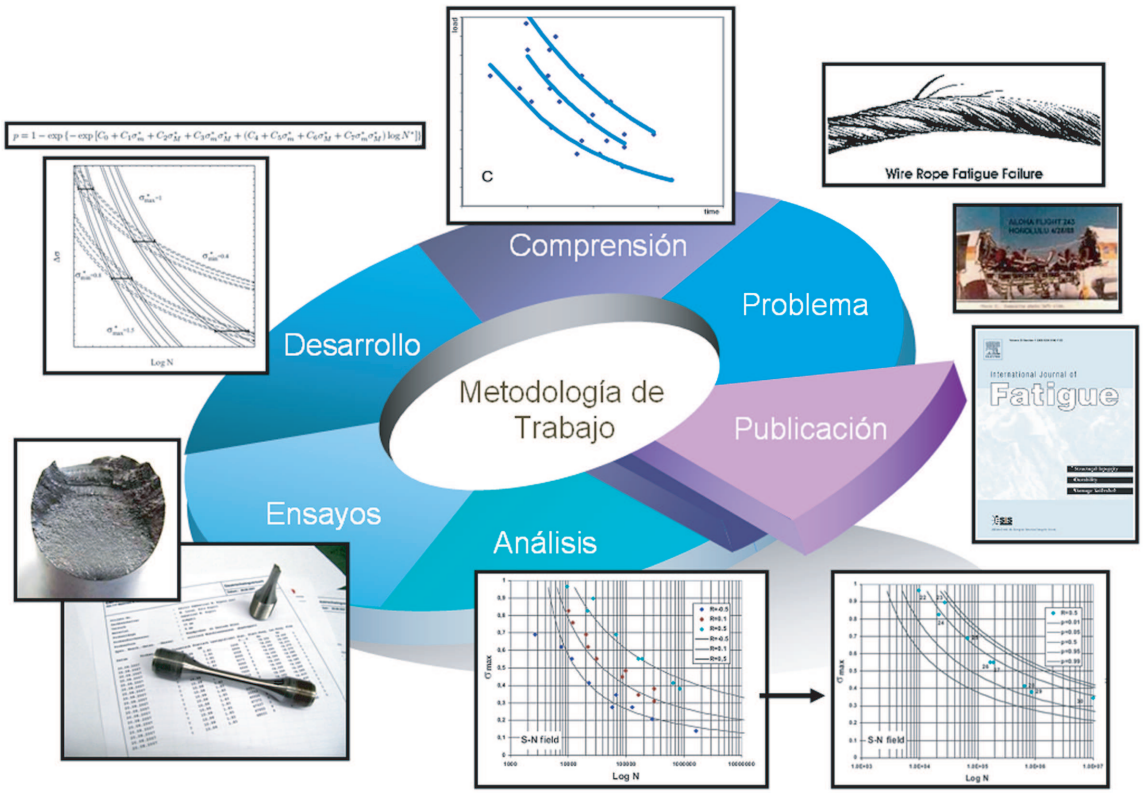


Figura 1.1: Metodología de trabajo seguida en la elaboración de la tesis doctoral.

4. Ensayos experimentales: cuyo objetivo es la obtención de datos que posteriormente se analizarán para validar el modelo teórico propuesto en el punto anterior. Capítulos 7 y 8 de la tesis doctoral.

5. Análisis de los resultados obtenidos: cuyo objetivo es la validación del modelo teórico. Capítulos 7 y 8 de la tesis doctoral.

6. Publicación: de las principales contribuciones al campo científico internacional. Este último paso de la investigación se ha ido realizando a lo largo de la elaboración de la tesis doctoral y queda plasmado en artículos enviados a revistas internacionales con índice de impacto.

## 1.3 Aportaciones originales

### 1.3.1 Los modelos Weibull y Gumbel basados en el campo S–N

**(chapter 6: The Weibull and Gumbel S–N field stress based fatigue models)**

A continuación se presenta, desarrolla y analiza de manera teórica el modelo propuesto por los autores. Algunos de los aspectos que se estudiarán son las condiciones tanto físicas, como estadísticas y de compatibilidad que definen el problema, las restricciones del modelo, las

propiedades del mismo, los submodelos resultantes y los métodos de estimación propuestos para el conocimiento de los parámetros del modelo.

Se propone en primer lugar un modelo general de fatiga que incluye la consideración de la tensión media, con un modelo probabilístico tipo Weibull de 9 parámetros. Posteriormente, tras el análisis del mismo se llega a la expresión final de un modelo probabilístico tipo Gumbel basado en 8 parámetros característicos del material.

Las **principales aportaciones** de este modelo son:

- De acuerdo con el Teorema de Buckingham [31], solo deben utilizarse variables adimensionales en modelos de regresión. Esto implica que el modelo sea sencillo y que los parámetros obtenidos a su vez sean variables adimensionales.
- El modelo no se basa en hipótesis arbitrarias, sino en propiedades físicas y estadísticas que son necesarias en cualquier modelo de fatiga.
- El modelo revela información estadística que no sólo incluye valores medios, sino que analiza la variabilidad del modelo y con ello, el conocimiento de la probabilidad en cada momento.
- El modelo puede usarse para todo el rango de cargas: tensión, compresión y/o mixto.
- El modelo puede extrapolarse a cualquier otra condición de cargas tras la estimación de los parámetros característicos del material.

Considérese un material sujeto a unas cargas constantes mínimas y máximas que denominaremos $\sigma_m$ y $\sigma_M$ por simplicidad (sección 6.2). Sabiendo que $N$ es el número de ciclos al que este material rompe, el objetivo es conocer la probabilidad de rotura $p$ del material sujeto a dichas cargas. Para la derivación del modelo se tiene en cuenta que $p$ está relacionada con los términos $N, \sigma_m$ y $\sigma_M$. Con estos conceptos en mente, el procedimiento es el siguiente: Primero, se parte del modelo presentado por Castillo et al. [39]:

$$p = 1 - \exp\left\{ - \left[ \frac{(\log N^* - B)\,(\sigma_M^* - \sigma_m^* - C) - E}{D} \right]^A \right\}, \tag{1.1}$$

donde $A$ representa el parámetro de forma de la función de distribucion tipo Weibull; $B$, representa el valor límite en la vida última del material, asíntota vertical de la curva S–N; $C$, el límite de endurancia; $E$, define la posición en la que se encuentra el percentil cero de la hipérbola y $D$, representa de escala de la función de distribución de Weibull (figura 1.2).

A continuación se aplica la condición de compatibilidad en el sentido de que: *Si se ejecuta un ensayo de fatiga a carga constante oscilante entre $\sigma_m$ y $\sigma_M$, podemos derivar el modelo correspondiente a dos casos particulares, (a) con $\sigma_m$ constante o (b) con $\sigma_M$ constante, pero en ambos casos el modelo es el mismo* [42]. Esta condición de compatibilidad se representa en la figura 1.3, donde las intersecciones entre curvas con $\sigma_m$ y $\sigma_M$ constantes se definen como líneas horizontales.

Sabiendo que si se toma $A \to \infty$ (see [37] and [40]), el modelo pasa a ser tipo Gumbel, la expresión final del modelo propuesto es:

$$p = 1 - \exp\left\{ - \exp\left[ C_0 + C_1\sigma_m^* + C_2\sigma_M^* + C_3\sigma_m^*\sigma_M^* + (C_4 + C_5\sigma_m^* + C_6\sigma_M^* + C_7\sigma_m^*\sigma_M^*) \log N^* \right] \right\}, \tag{1.2}$$

donde $C_0, C_1, C_2, C_3, C_4, C_5, C_6$ y $C_7$ son los parámetros que definen el modelo y las variables $\sigma_m^*, \sigma_M^*$ y $N^*$ se definen como $\sigma_m^* = \sigma_m/\sigma_0; \sigma_M^* = \sigma_M/\sigma_0$ y $N^* = N/N_0$, donde $\sigma_0$ y $N_0$ son variables utilizadas para adimensionalizar el problema.

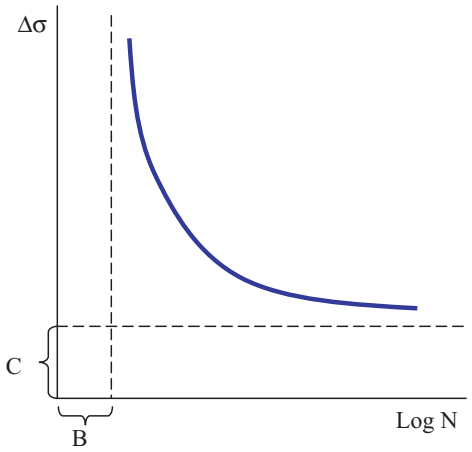


Figura 1.2: Representación esquemática del significado físico de las variables $B$ y $C$ del modelo de Castillo et al. [39].

Para hacer el modelo estadística y físicamente compatible, deben tenerse en cuenta algunas **restricciones** (sección 6.4):

- Restricciones físicas: Las asíntotas en ambos ejes deben ser positivas y decrecientes con respecto a las variables del modelo ($\sigma_m$, $\sigma_M$ y $\log N$).
- Restricciones estadísticas: la función de distribución debe ser creciente con respecto a las variables del modelo y la curvatura del modelo debe ser siempre positiva.

La estimación de los parámetros del modelo se lleva a cabo mediante dos métodos diferentes: máxima verosimilitud y regresión por mínimos cuadrados (sección 6.6.1 y 6.6.2). Para el caso de máxima verosimilitud, el problema se reduce a maximizar la función objetivo (1.3) con respecto a los parámetros del modelo $C_i$, sujeta a las restricciones descritas enteriormente, desarrolladas en la sección 6.4

$$L = \sum_{i \in I_1} \left[ H(N_i^*) + \log\left(C_4 + C_5\sigma_{m_i}^* + C_6\sigma_{M_i}^* + C_7\sigma_{m_i}^*\sigma_{M_i}^*\right) - \log(N_i^*) \right] - \sum_{i \in I_1 \cup I_0} \exp(H(N_i^*)), \quad (1.3)$$

donde $H(N_i) = C_0 + C_1\sigma_{m_i}^* + C_2\sigma_{M_i}^* + C_3\sigma_{m_i}^*\sigma_{M_i}^* + \left(C_4 + C_5\sigma_{m_i}^* + C_6\sigma_{M_i}^* + C_7\sigma_{m_i}^*\sigma_{M_i}^*\right)\log N_i^*$.

En el caso de la regresión, la función objetivo es ahora

$$Q = \sum_{i=1}^{n} \left( \log N + \frac{C_0 + C_2\sigma_{max}^* + C_1 R\sigma_{max}^* + C_3 R{\sigma_{max}^*}^2 + \gamma}{C_4 + C_6\sigma_{max}^* + C_5 R\sigma_{max}^* + C_7 R{\sigma_{max}^*}^2} \right)^2, \quad (1.4)$$

sujeta también a las restricciones descritas en la sección 6.4, definiéndose $R$ como $R = \sigma_m/\sigma_M$.

Con el fin de usar el modelo en la práctica, se definen ahora una estrategia basada en los siguientes pasos:

**Paso 1:** *Diseño de la estrategia de ensayos.* Se definen el número de series así como la distribución tensional de los distintos puntos a ensayar, intentando cubrir el mayor rango tensional posible.

**Paso 2:** *Elección de las variables normalizadas $N_0$ y $\sigma_0$.* Con ellas se realiza la adimensionalización de las variables.

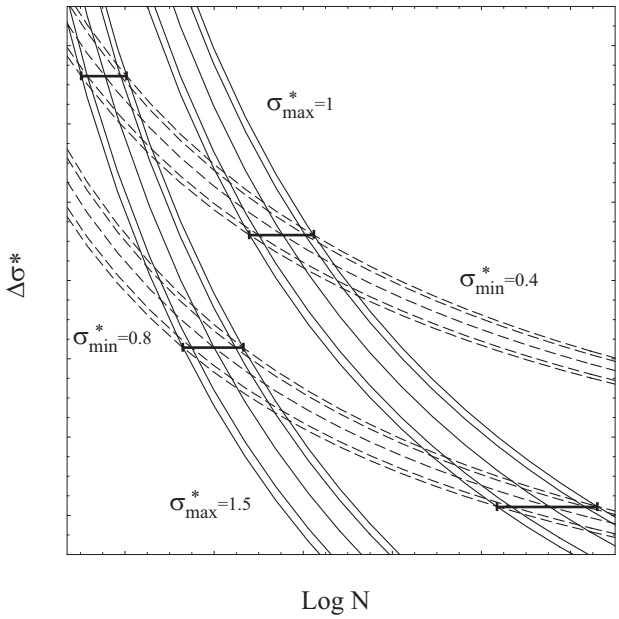


Figura 1.3: Esquema de las curvas de Wöhler para los percentiles $\{0.01, 0.05, 0.5, 0.95, 0.99\}$ con un $\sigma^*_{max} = 1$ y $\sigma^*_{max} = 1.5$, y $\sigma^*_{min} = 0.4$ y $\sigma^*_{min} = 0.8$ [42].

**Paso 3:** *Estimación de los parámetros del modelo.* Utilizando para ello cualquiera de los dos métodos definidos anteriormente (Ecuaciones (1.3) y (1.4)).

**Paso 4:** *Extrapolación del problema a otras condiciones tensionales cualesquiera.* Empleando el modelo (1.2) y los parámetros $C_1, C_2, C_3, C_4, C_5, C_6, C_7$, $\log N_0$ y $\sigma_0$ para cualquier otra condición de ensayos.

### 1.3.2 Validación experimental del modelo

**(chapter 7: Experimental validation of the model)**

La validación experimental del modelo se ha llevado a cabo a partir de los resultados obtenidos tras varias series de ensayos realizados en el departamento de *Materials Science and Technology* del laboratorio federal suizo de ensayos e investigación Empa-Dübendorf.

Se estudia el comportamiento de dos aceros de características estáticas y mecánicas diferentes (tabla 7.1):

- Acero con baja aleación de cromo, 42CrMo4, (DIN-1.7225) con $R_m = 1067MPa$ y $R_y = 975.3MPa$.
- Aleación de aluminio, AlMgSi1 (DIN-3.2315) con $R_m = 391.7MPa$ y $R_{p_{0.2}} = 364.3MPa$.

Las muestras son descritas en la sección 7.3. Los ensayos se enmarcan dentro de la normativa ASTM E606 [5], manteniéndose constante $\sigma_M$. Para cada material se eligieron cuatro series con diferentes $\sigma_M = cte$ y variables $\sigma_m$ teniendo en cuenta la posición del límite de endurancia (figura 1.4, (a)) y el límite de plasticidad de cada material (figura 1.4, (b)). Para la realización de los ensayos se utilizó una máquina vibrophore de alta frecuencia, con capacidad de 150 Hz de frecuencia.

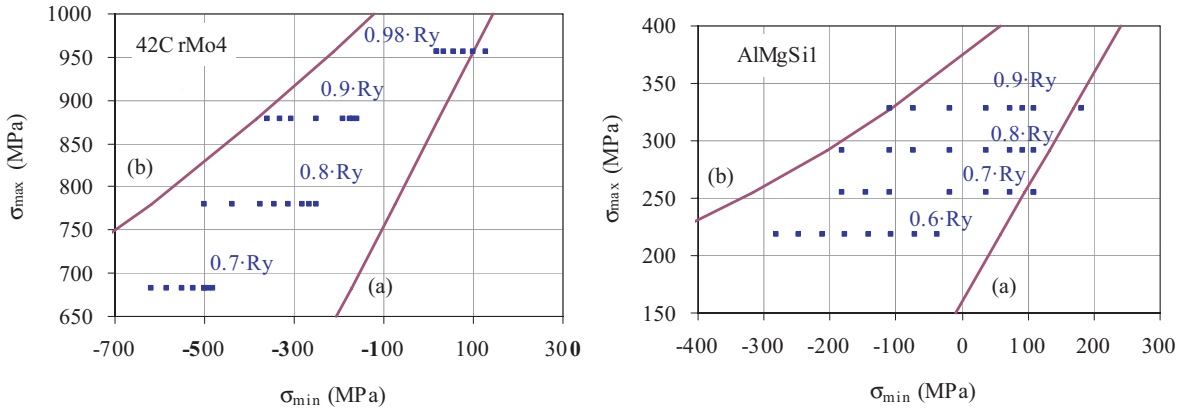


Figura 1.4: Representación esquemática de la distribución tensional de los ensayos. A la izquierda el acero 42CrMo4, a la derecha la aleación AlMgSi1. (a) límite de plasticidad, (b) límite de endurancia del material.

La adimensionalización se lleva cabo definiendo $\sigma_0 = \max(\sigma_{M_i})$, que corresponde con los valores $\sigma_0 = 0.98R_y$ MPa para el 42CrMo4 y $\sigma_0 = 0.9R_{p_{0.2}}$ MPa para el AlMgSi1. En el caso de $N_0 = \max(N_i)$ los valores elegidos corresponden con $N_0 = 532000$ ciclos para el 42CrMo4 and $N_0 = 526500$ ciclos para el AlMgSi1.

Los resultados obtenidos se presentan en las tablas 1.1, 1.2 y las figuras 1.5 y 1.6 (secciones 7.6.2 y 7.6.3):

**Acero 42CrMo4** La tendencia resultante en las curvas S–N es lineal ya que $C_4 = C_5 = C_7 = 0$. Los datos tienen una gran dispersión y ello dificulta la estimación de los parámetros del modelo, aunque los resultados son aceptables (figura 1.5, tabla 1.1).

**Aleación AlMgSi1** En este caso, la tendencia de las curvas que definen el campo de Wöhler no es lineal. Sólo los parámetros $C_4$ y $C_5$ son nulos. La dispersión es menor que en el primer material y la estimación parece haber tenido mejor resultado (figura 1.6, tabla 1.2).

Table 1.1: Parámetros obtenidos para el acero 42CrMo4.

| Case | $C_0$ | $C_1$ | $C_2$ | $C_3$ | $C_4$ | $C_5$ | $C_6$ | $C_7$ |
|---|---|---|---|---|---|---|---|---|
| Max. Ver. | -79.066 | -63.141 | 85.309 | 38.297 | 0.000 | 0.000 | 2.394 | 0.000 |
| Min. Cuad. | -77.338 | -53.530 | 83.913 | 26.824 | 0.000 | 0.000 | 2.570 | 0.000 |

Table 1.2: Parámetros obtenidos para la aleación AlMgSi1.

| Case | $C_0$ | $C_1$ | $C_2$ | $C_3$ | $C_4$ | $C_5$ | $C_6$ | $C_7$ |
|---|---|---|---|---|---|---|---|---|
| Max. Ver. | -78.507 | -31.357 | 101.460 | -34.960 | 0.000 | 0.000 | 13.302 | -8.642 |
| Min. Cuad, | -24.737 | -16.091 | 31.803 | -4.569 | 1.619 | -1.619 | 2.837 | -0.377 |

Para validar el modelo se utilizan los métodos de Kolmogoronov-Smirnov, el Test de uniformidad $\chi^2$ y el análisis de los gráficos PP y QQ. La conclusión final a la que se llega tras

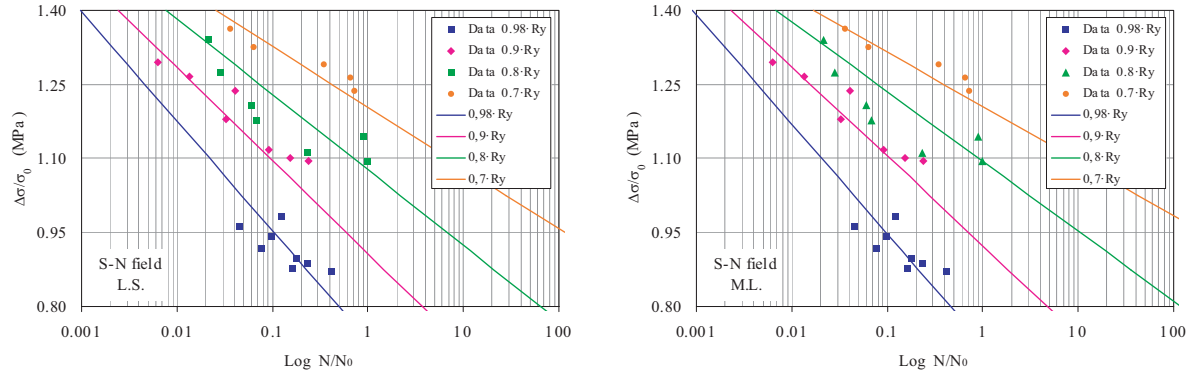


Figura 1.5: Campo de Wöhler resultante para el acero 42CrMo4 con los parámetros obtenidos por el método de máxima verosimilitud (figura de la derecha) y regresión por mínimos cuadrados (figura de la izquierda).

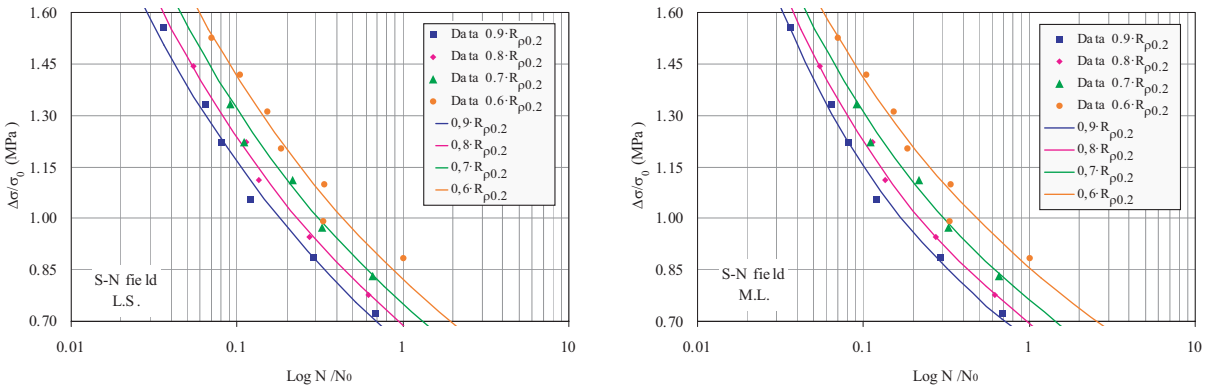


Figura 1.6: Campo de Wöhler resultante para la aleación AlMgSi1 con los parámetros obtenidos por el método de máxima verosimilitud (figura de la derecha) y regresión por mínimos cuadrados (figura de la izquierda).

la validación experimental del modelo es que para ambos materiales los resultados obtenidos muestran una buena estimación de los parámetros, aunque en el caso de la aleación AlMgSi1 los resultados son mejores, debido quizás a la dispersión de los datos.

Por último, conociendo los parámetros del modelo para cualquiera de los materiales, se puede extrapolar el problema a otras condiciones tensionales. Como ejemplo se puede predecir la vida última asociada a las cargas conocidas representando el campo de isoprobabilidad P–S–N (ver figura 1.7).

### 1.3.3 Análisis del daño acumulado

**(chapter 8: Damage measures and damage accumulation)**

Existen diversas formulaciones para el análisis del daño acumulado, pero como vemos en la tabla 8.1 la mayoría de ellas no son una buena herramienta para medir el daño en un cierto

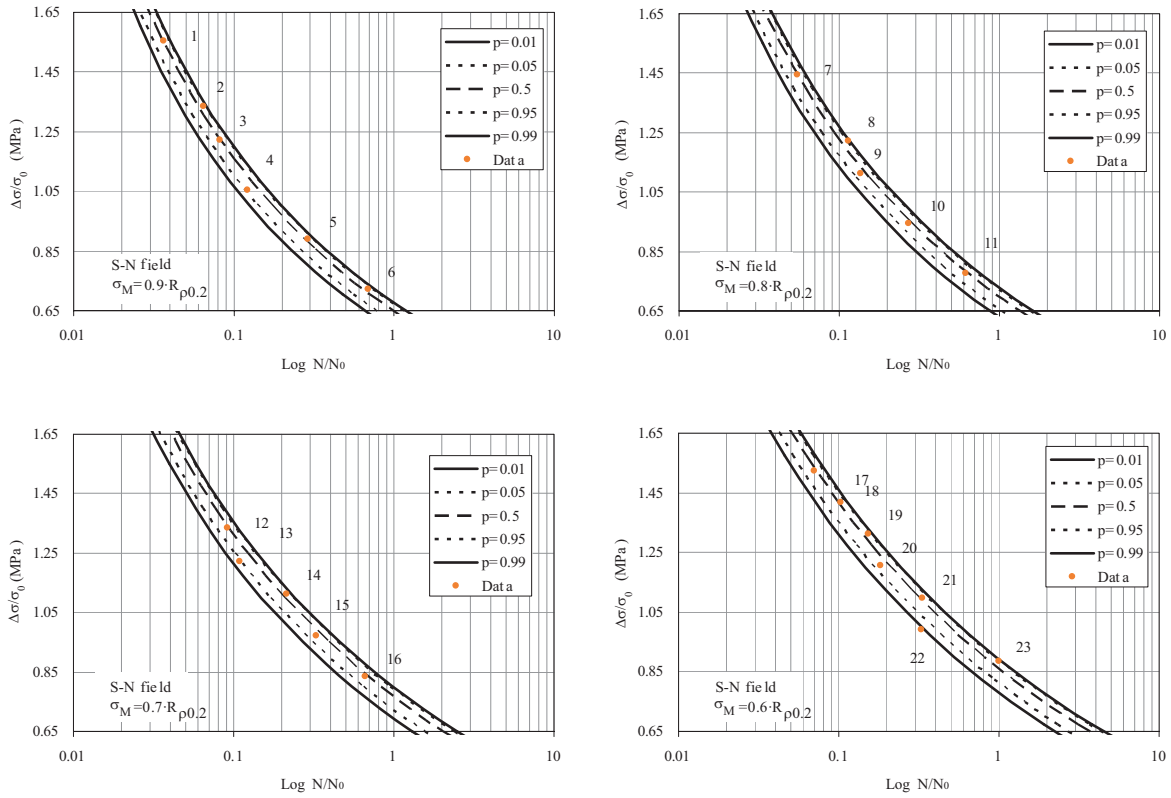


Figura 1.7: Represesntación del campo de isoprobabilidad P–S–N para la aleación AlMgSi1. Los percentiles representados corresponden con los valores 0.01,0.05, 0.50, 0.95 y 0.99.

momento. Algunas de las consideraciones/propiedades que una medida de daño debe cumplir son:

**Propiedad 1.- Incrementar con el daño:** El daño incrementa cuando incrementa la medida del daño analizada.

**Propiedad 2.- Interpretabilidad:** La medida de daño debe ser clara y comprensible.

**Propiedad 3.- Medida adimensional:** Para evitar problemas de unidades en la estimacion de la vida última a fatiga de un material es mejor trabajar con variables adimensionales.

**Propiedad 4.- Conocimiento del rango:** El rango de variación de la medida de daño debe ser fijo, conocido, independiente de la carga y si puede ser, también del material.

**Propiedad 5.- Función de distribución conocida:** Para conocer la probabilidad de fallo de una pieza, es necesario conocer la función de distribución de la probabilidad de esa medida de daño.

Por lo tanto, después de analizar la tabla 8.1 en función de las propiedades descritas anteriormente, queda claro que la probabilidad de daño, derivada de la expresión del modelo Gumbel (6.13) derivado en el capítulo 6 es la mejor medida que podemos utilizar para analizar el daño acumulado de un material sujeto a cargas cíclicas.

La figura 1.3 es un ejemplo de curva de isoprobabilidad del campo de Wöhler, donde se representa el daño (probabilidad de fallo) para un material sometido a distintos rangos de carga. Existen dos reglas que son útiles a la hora de evaluar el daño en cualquier espectro de carga:

1. ***Regla de la iso-probabilidad:*** *Dos historias de carga producen el mismo daño si la probabilidad de fallo es la misma para ambos casos.*

2. ***Regla de la proporcionalidad:*** *El daño producido por debajo del cero por ciento es proporcional al número de ciclos, con un máximo valor de uno.*

Para evaluar la acumulación del daño, el procedimiento es el siguiente (ver figura 8.2):

1. El daño inicial es nulo ($p = 0$).

2. El daño $p$ tras el primer ciclo es calculado con el nivel de cargas considerado para ese ciclo.

3. El número equivalente de ciclos asociados a un daño $p$ para un nivel de cargas ($\sigma_m^* = \sigma_m^*(N)$ y $\sigma_M^* = \sigma_M^*(N)$), para $N^* = 2$, utilizando la función inversa de (6.13) es:

$$\log N_{eq}^* = \frac{\log(-\log(1-p)) - (C_0 + C_1\sigma_m^* + C_2\sigma_M^* + C_3\sigma_m^*\sigma_M^*)}{C_4 + C_5\sigma_m^* + C_6\sigma_M^* + C_7\sigma_m^*\sigma_M^*} \tag{1.5}$$

4. El daño acumulado, representado mediante la probabilidad de fallo, es calculado mediante la fórmula recursiva:

$$P_{N+\Delta N} = F(N_{eq}^* + \Delta N, \sigma_m^*(N), \sigma_M^*(N)), \tag{1.6}$$

   que obtiene el daño acumulado tras $N + \Delta N$ ciclos cuando la unidad esta sujeta a un nivel de cargas dado por $\sigma_m^*(N)$ y $\sigma_M^*(N)$.

5. Tras este punto, el daño puede ser calculado en base a los percentiles, solo repitiendo los pasos 3 y 4 sucesivamente, hasta que se alcance el nivel de daño requerido.

A continuación, diferentes tipos de cargas son analizados para validar la capacidad del modelo descrito en el capítulo 6. Se han estudiado dos casos:

- Daño acumulado frente a carga constante.
- Daño acumulado frente a carga variable, de variación lineal.

**Daño acumulado ante cargas constantes**

Se analizan a continuación tres historias de cargas diferentes. Todos los casos tienen un valor constante $\Delta\sigma(N) = 1130MPa$, que corresponde con un $\Delta\sigma^* = 1.099$ ($\sigma_0 = 955.5$ MPa), pero cada uno de ellos tiene diferente valores de $\sigma_M$, $\sigma_m$ y $\sigma_{mean}$. Las características de cada una de las historias de carga se muestran en la tabla 8.2. La figura 1.8 muestra las distintas cargas aplicadas.

Los resultados se muestran en la tabla 8.3 y figura 1.9. En la tabla 8.3 se muestran los diferentes valores de número de ciclos para diversas probabilidades ($p = 0.01, 0.1, 0.5, 0.9$ y $p = 0.99$). Se puede apreciar el efecto de $\sigma_{mean}$ en el daño acumulado, mayores valores de $\sigma_{mean}$ corresponden con mayores valores de probabilidad de fallo.

$$\sigma_{mean_{(a)}^*} < \sigma_{mean_{(c)}^*} < \sigma_{mean_{(b)}^*} \rightarrow N_{(a)}^* > N_{(c)}^* > N_{(b)}^*$$

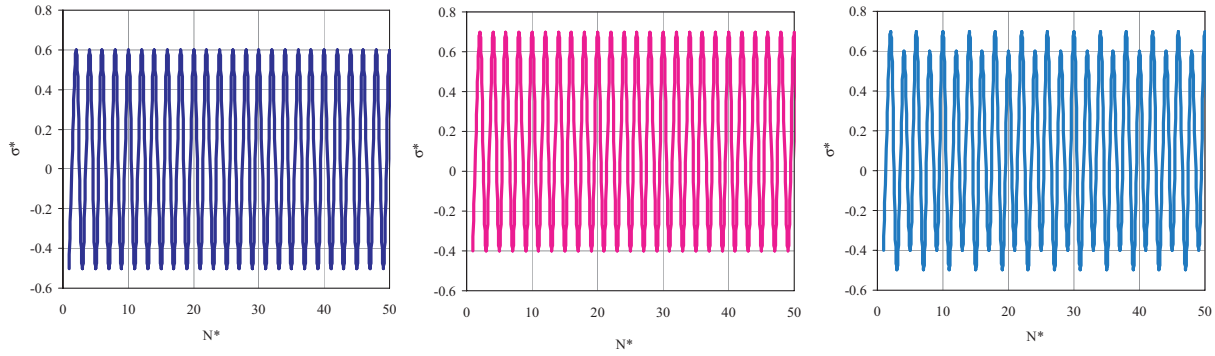


Figura 1.8: Diferentes historias de carga utilizadas para el análisis del daño acumulado, cuando $\Delta\sigma = 1050$ MPa $\rightarrow \Delta\sigma^* = 1.099$ ($\sigma_0 = 955.5$ MPa). (a) $\sigma_m^* = -0.500$, $\sigma_M^* = 0.599$; (b) $\sigma_m^* = -0.399$, $\sigma_M^* = 0.700$; (c) $\sigma_m^* = -0.500$, $\sigma_M^* = 0.599$ para los ciclos impares y, $\sigma_m^* = -0.399$, $\sigma_M^* = 0.700$ en los ciclos pares.

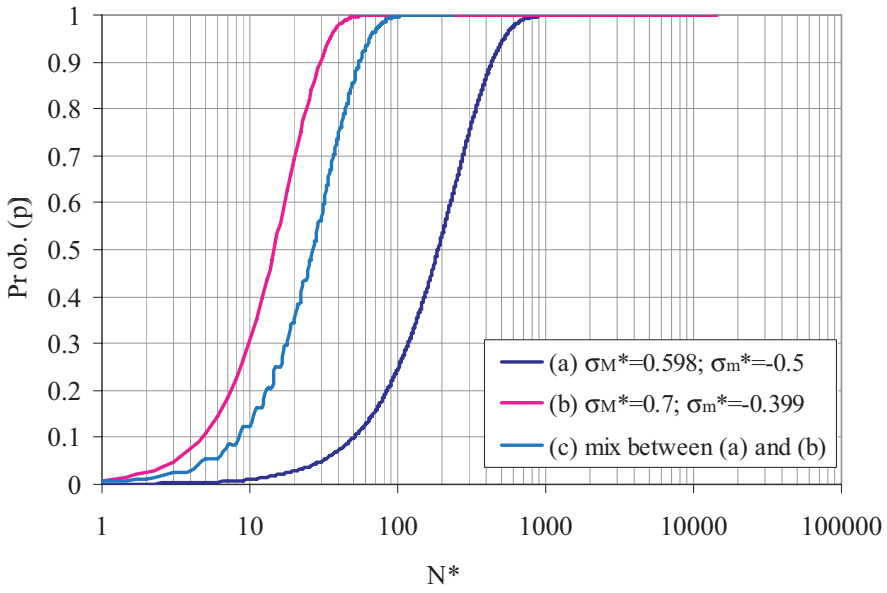


Figura 1.9: Funciones de distribución obtenidas para las distintas historias de cargas utilizadas en el daño acumulado cuando $\Delta\sigma = 1050$ MPa $\rightarrow \Delta\sigma^* = 1.099$ ($\sigma_0 = 955.5$ MPa). (a) $\sigma_m^* = -0.500$, $\sigma_M^* = 0.599$; (b) $\sigma_m^* = -0.399$, $\sigma_M^* = 0.700$; (c) $\sigma_m^* = -0.500$, $\sigma_M^* = 0.599$ para los ciclos impares y, $\sigma_m^* = -0.399$, $\sigma_M^* = 0.700$ en los ciclos pares.

Se ha realizado también un estudio de la influencia de la existencia de discontinuidades con mayor amplitud dentro de un espectro de carga constante. El estudio se ha llevado a cabo mediante el análisis de tres casos diferentes (ver figura 1.10):

- **Caso a:** La discontinuidad se sitúa al comienzo de la secuencia de carga ($N^* = 10$).
- **Caso b:** La discontinuidad se sitúa en la mitad de la secuencia de carga ($N^* = 100$).
- **Caso c:** Cuando exsiten dos discontinuidades, situadas en $N^* = 10$ y $N^* = 30$.

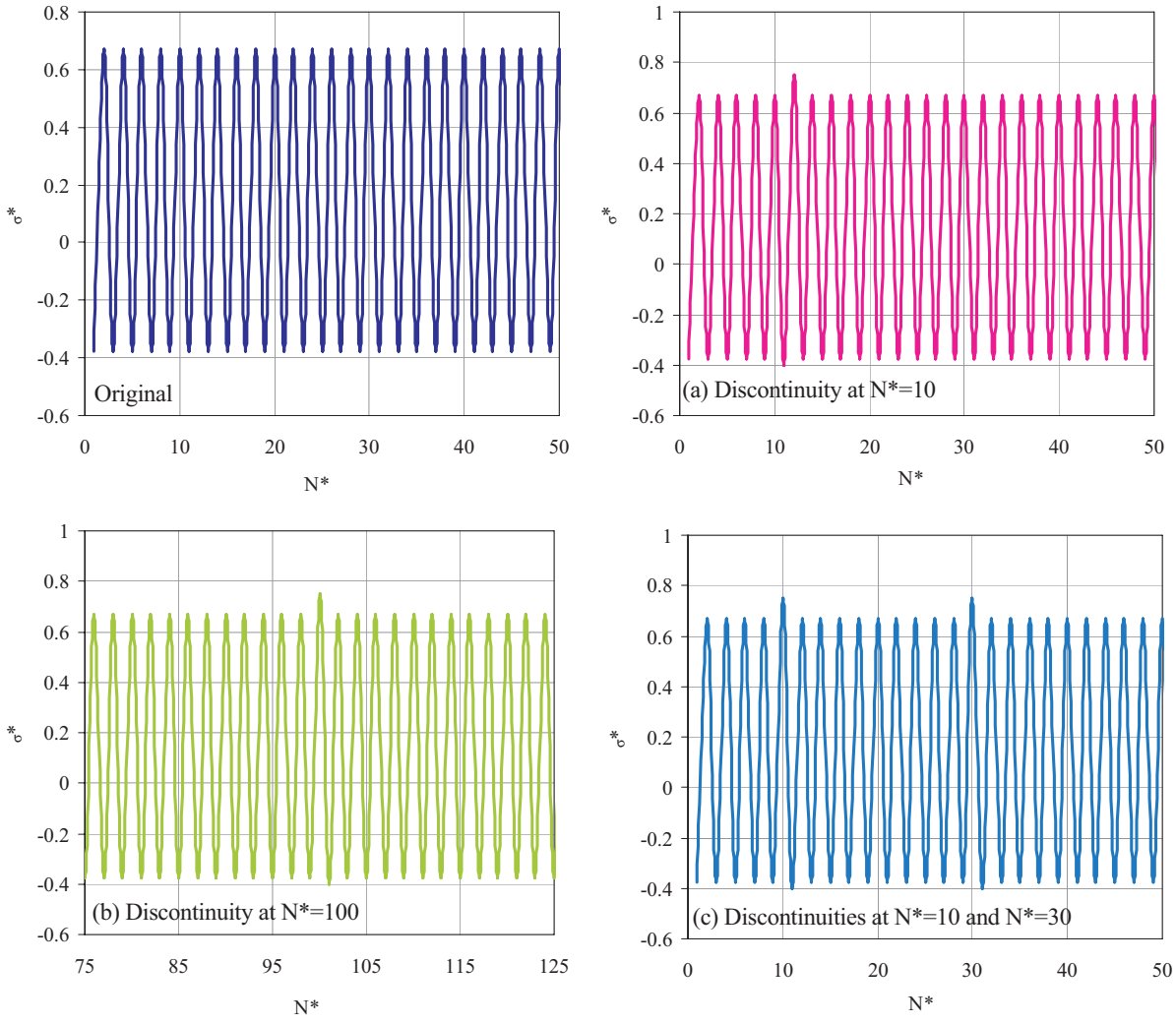


Figura 1.10: Historias de cargas utilizadas para el análisis de la influencia de existencia de discontinuidades dentro de un espectro de carga constante. De arriba hacia abajo y de izquierda a derecha: secuencia origial (sin discontinuidades), secuencia con discontinuidad situada en $N^* = 10$, secuencia con discontinuidad situada en $N^* = 100$ y secuencia en la que las discontinuidades se sitúan en $N^* = 10$ y $N^* = 30$ (para un valor de $N_0 = 532000$ ciclos).

Se observa que la existencia de discontinuidades con mayor amplitud de carga (un aumento de un 10% sobre el resto de los ciclos) influye en la probabilidad de fallo. Esta probabilidad se ve modificada en función de donde se encuentre el ciclo en cuestión. En todos los casos en los que existe una discontinuidad de este tipo el especimen rompe antes que en el caso original sin discontinuidades (ver tabla 8.4 y figura 1.11). Por otro lado, el peor caso es en el que existen

más de una discontinuidad durante la secuencia de carga. El incremento de la probabilidad es función del número equivalente de ciclos ($N^*_{eq}$) que depende a su vez de la probabilidad de rotura en el ciclo anterior (Equaciones (1.5) y (1.6)), por ello, la evolución de las probabilidades es diferente aunque el incremento en todos los casos sea el mismo.

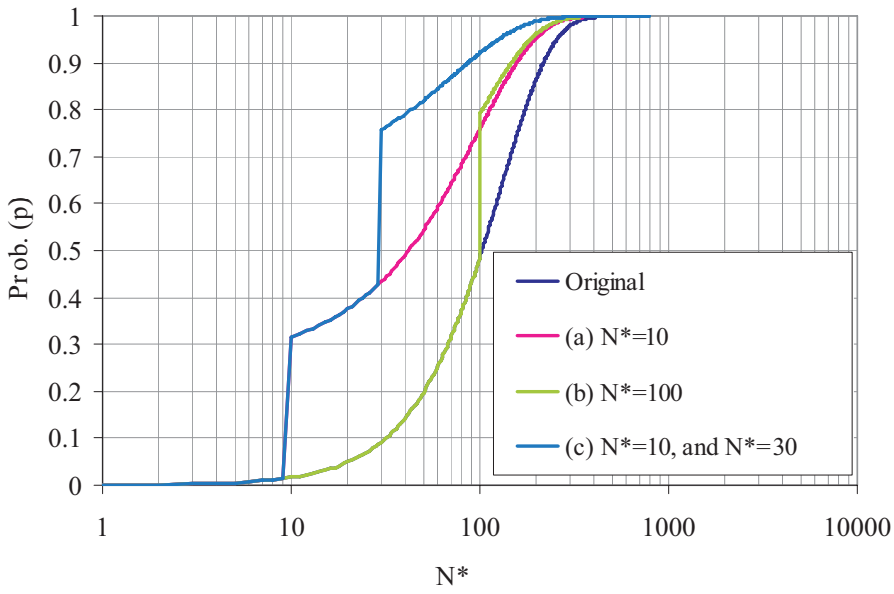


Figura 1.11: Funciones de probabilidad obtenidas del análisis de la influencia de existencia de discontinuidades dentro de un espectro de carga constante. De arriba hacia abajo y de izquierda a derecha: secuencia original (sin discontinuidades), secuencia con discontinuidad situada en $N^* = 10$, secuencia con discontinuidad situada en $N^* = 100$ y secuencia en la que las discontinuidades se sitúan en $N^* = 10$ y $N^* = 30$ (para un valor de $N_0 = 532000$ ciclos).

### Daño acumulado ante cargas variables

Se ha realizado el estudio de tres grupos diferentes de historias de carga variable (ver figura 1.12). A saber:

1. Historia de carga con $\sigma^*_m$ constante y variable $\sigma^*_M$.
2. Historia de carga con $\sigma^*_M$ constante y variable $\sigma^*_m$.
3. Historia de carga con $\sigma^*_M$ y $\sigma^*_m$ variables.

La forma general de estas expresiones es $\Delta\sigma^* = m \cdot N^* + n = \sigma^*_M - \sigma^*_m$, donde $\sigma^*_M = m_1 \cdot N^* + n_1$ y $\sigma^*_m = m_2 \cdot N^* + n_2$. Los valores de los parámetros $m_1, m_2, m, n_1, n_2$ y $n$ se definen en la tabla 8.5.

Como se puede observar en la figura 1.12 hay dos espectros diferentes en cada grupo de carga. El objetivo es conocer la variación del daño cuando se tienen espectros con la misma forma pero simétricos, tal y como se muestra en la figura 1.13, donde la duda es si $p_A$ y $p_B$ serán iguales.

Los resultados se muestran en la figura 1.14. Se puede apreciar como en el segundo espectro de cada grupo (designado con las letras $a_2, b_2$ y $c_2$) el daño acumulado crece más rápidamente.

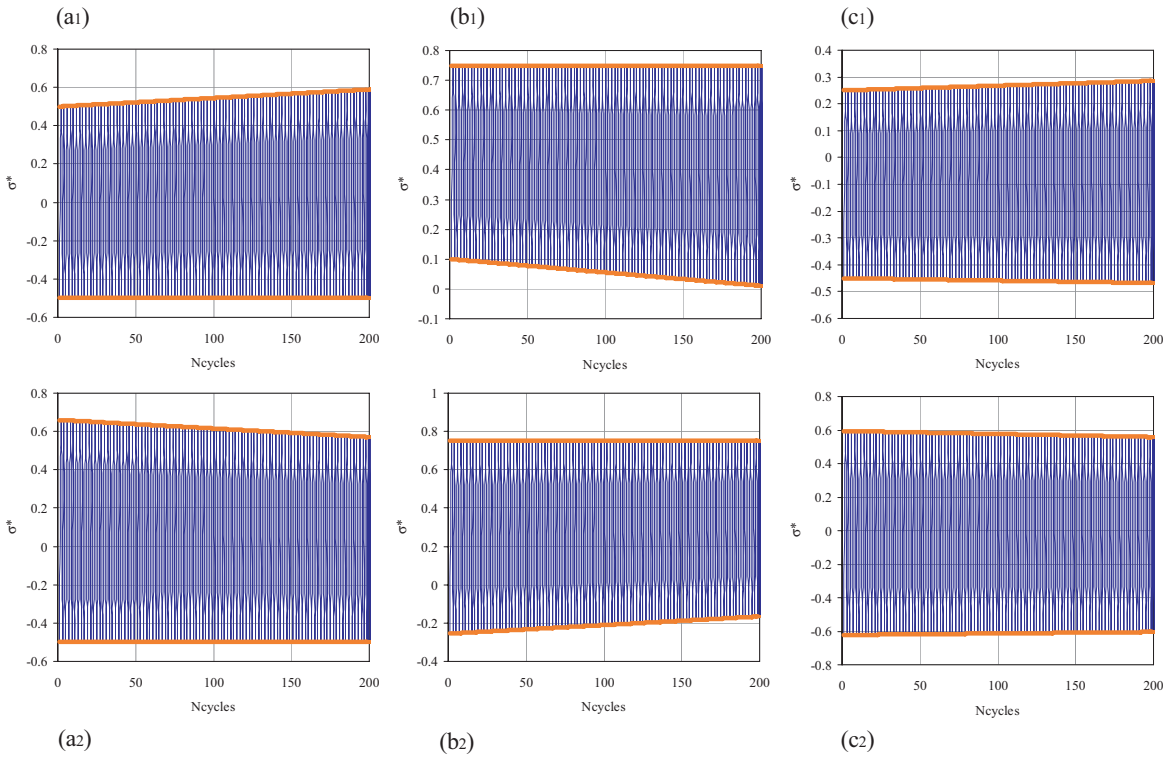


Figura 1.12: Historias de carga variable analizadas en el estudio del daño acumulado: $(a_1), (a_2)$ constante $\sigma_m^*$ y variable $\sigma_M^*$, $(b_1, b_2)$ constante $\sigma_M^*$ y variable $\sigma_m^*$, $(c_1, c_2)$ variable $\sigma_M^*$ y $\sigma_m^*$.

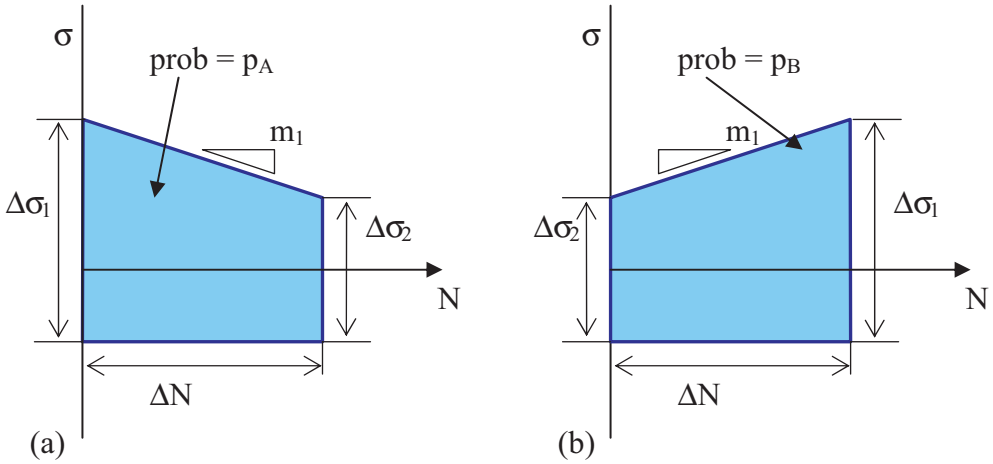


Figura 1.13: Esquema representativo del problema simétrico.

Esto es debido a que el daño en estos espectros comienza por un valor no nulo como en el caso primero (denominados por $a_1, b_1$ y $c_1$).

La comparación de los resultados entre todas las funciones de distribución obtenidas muestra que el daño acumulado incrementa con el valor de $\sigma_{mean}$ (ver figura 1.15): Por lo tanto, si la

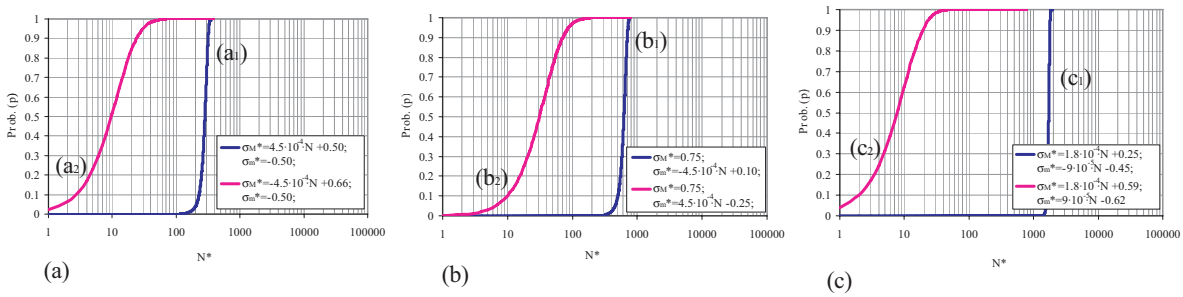


Figura 1.14: Funciones de distribución obtenidas tras el análisis de diversas historias de carga variable: $(a_1), (a_2)$ constante $\sigma_m^*$ y variable $\sigma_M^*$, $(b_1, b_2)$ constante $\sigma_M^*$ y variable $\sigma_m^*$, $(c_1, c_2)$ variable $\sigma_M^*$ y $\sigma_m^*$.

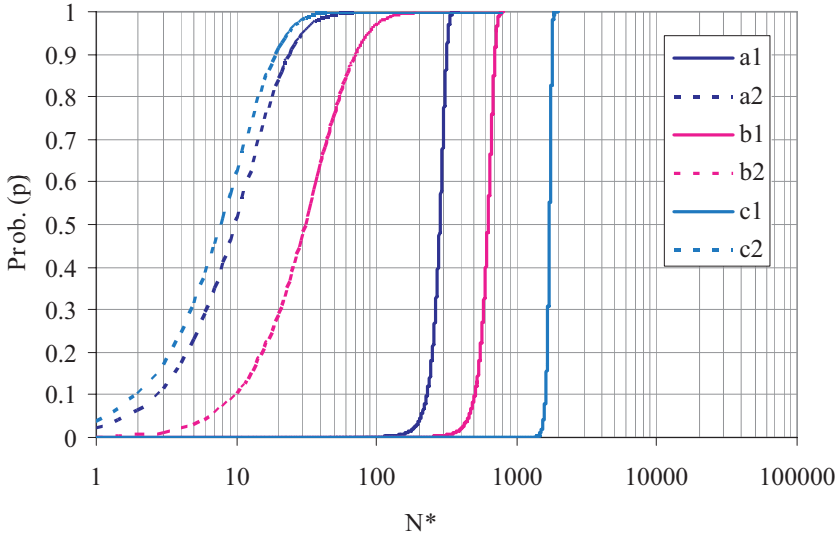


Figura 1.15: Funciones de distribución obtenidas tras el análisis del daño acumulado en diferentes historias de carga: $(a_1), (a_2)$ constante $\sigma_m^*$ y variable $\sigma_M^*$, $(b_1, b_2)$ constante $\sigma_M^*$ y variable $\sigma_m^*$, $(c_1, c_2)$ $\sigma_M^*$ y $\sigma_m^*$ variables.

relación entre las tensiones medias es

$$\sigma_{mean_{c_2}} > \sigma_{mean_{a_2}} > \sigma_{mean_{a_1}} > \sigma_{mean_{b_2}} > \sigma_{mean_{b_1}} > \sigma_{mean_{c_1}}$$

la probabilidad de fallo se relaciona del siguiente modo

$$p_{failure_{c_2}} > p_{failure_{a_2}} > p_{failure_{a_1}} > p_{failure_{b_2}} > p_{failure_{b_1}} > p_{failure_{c_1}}$$

y por conclusión

$$N^*_{failure_{c_2}} < N^*_{failure_{a_2}} < N^*_{failure_{a_1}} < N^*_{failure_{b_2}} < N^*_{failure_{b_1}} > N^*_{failure_{c_1}}$$

En la tabla 8.6 se representan los valores de número de ciclos $N^*$ para las distintas probabilidades de fallo ($p = 0.01, 0.1, 0.5, 0.9$ y $0.99$).

## 1.4 Conclusiones y futuras líneas de investigación

### 1.4.1 Conclusiones

**(chapter 9: Conclusions)**

Las principales conclusiones obtenidas tras la realización de este trabajo de investigación son:

**Modelo de fatiga propuesto**

- Se ha desarrollado un nuevo modelo que analiza la vida a fatiga para cualquier tipo de carga y para cualquier rango de la misma (tensión, compresión y/o mixto). Además la derivación del modelo se lleva a cabo teniendo en cuenta condiciones físicas, estadísticas y de compatibilidad, resultanto por tanto un modelo potente y con gran capacidad de adaptación ante todo tipo de datos y materiales metálicos.
- El modelo depende de 8 parámetros $C_i$ que pueden ser estimados mediante diferentes métodos. Por otro lado, el modelo incluye una gran información estadística, entre la que podemos destacar la capacidad para conocer la probabilidad de fallo para cualquier estado de carga y número de ciclos.

**Validación experimental del modelo**

- Se ha validado el modelo mediante la realización y análisis de resultados con dos materiales metálicos de diferentes comportamientos a fatiga.
- Los resultados obtenidos muestran la capacidad de adaptación del modelo a diferentes materiales en diferentes estados de carga, mostrándose diferentes tendencias en las curvas S–N (tensión–número de ciclos).
- La distribución de los puntos no afecta a la estimación de los parámetros, pero es necesario tener un conjunto de datos que se distribuyan al máximo posible en todo el rango de cargas.
- Diferentes casos (submodelos) han sido obtenidos gracias a la libertad del modelo para la elección de los mejores parámetros para cada material analizado.
- Se ha realizado también la validación del modelo gracias a datos obtenidos de otras referencias bibliográficas ajustadas anteriormente a otros modelos de fatiga. Estas validaciones tenían en cuenta diferentes condiciones de carga, por ejemplo con niveles constantes de diferentes ratios de tensiones $R$.
- Se ha validado la capacidad de extrapolación del modelo mediante la elaboración de los campos P–S–N o mediante la reestimación de los parámetros tras la eliminación de algunas de las series originales.

**Análisis del daño acumulado**

- La probabilidad de fallo es un buena medida del daño acumulado ya que permite la evaluación de la probabilidad de fallo directamente. De hecho, las curvas P–S–N de Wöhler interpretan de una manera sencilla el daño del material en cada momento.

- El modelo propuesto es útil para el análisis del daño en cualquier tipo de historia de carga: constante o linealmente variable, para todo el rango de tensiones.
- El factor que tiene más influencia en la evolución del daño es la tensión media. Conociendo su distribución a lo largo del tiempo y conociendo los parámetros del modelo resulta sencillo conocer el daño acumulado para un momento preciso.

### 1.4.2 Futuras líneas de investigación

**(chapter 9: Conclusions)**

Tras la elaboración de la tesis doctoral nuevos temas de investigación surgen derivados de los analizados en el presente proyecto de investigación. Por ello, las futuras líneas de investigación que se plantean son:

- Realizar la validación del modelo teórico para otros materiales metálicos, ampliando el rango de materiales que cuentan con el conocimiento de los parámetros característicos del modelo propuesto.
- Comprobar la validez del nuevo modelo para las zonas de bajo y alto número de ciclos, en las cuales el comportamiento del material puede diferente. Con ello se conocería con mayor grado de seguridad el grado de utilidad del modelo en dichos rangos, básicos para distintas aplicaciones ingenieriles como el sector aeroespacial o automovilístico.
- Investigar en la estrategia de ensayos para desarrollar una metodología de ensayos óptima.
- Estudiar el efecto de otros factores en el proceso del daño acumulado. A lo largo de la historia la influencia de la frecuencia se supone nula en la vida última de material [102], pero esto no es completamente cierto cuando se analizan otros factores como corrosión, altas temperaturas o cargas aleatorias. Esta influencia depende del material analizado y ensayo realizado (ver [14], [16], [102] o [119]). El efecto de las altas temperaturas es también un factor del cual se debe conocer su influencia. Es conocido en el diseño de materiales metálicos utilizados en la industria aeroespacial que los materiales están sujetos a cargas variables en combinación con altas temperaturas.
- Comprobar el modelo para otro tipo de materiales (no metálicos), materiales heterogéneos (hormigón), o nuevos materiales en los que algunas propiedades se han modificado para obtener mejores respuestas a este tipo de solicitaciones.

# Part II

# Presentation and State of the Art

# Chapter 2

# Presentation

The present doctoral thesis aims at contributing to the advance in the state of knowledge of the fatigue behavior of materials. New models are proposed for analyzing fatigue failure and predicting fatigue damage as a function of lifetime, stress level and stress range.
The document is addressed to engineers and researches who want to improve their knowledge with a new model that covers the tension and compression Wöhler fields, so as to scientists who want to explore a new research field.

## 2.1 Justification

In material science, *fatigue* is the progressive and localized structural damage that occurs when a material is subjected to cyclic loading. The first researches in this field (19th. century) discovered, that if they represented load versus time to failure (lifetime), a relation between these two variables would exist. This relation can be represented by different mathematical expressions such as those in the right part of figure 2.1 where it is possible to observe some of these different representations. Find the best expression to define the lifetime of a piece subject to fatigue is one of the most important aims of these researches.

The fatigue mechanism is present practically in all structures, machine components and vehicles, which are subjected to repeated loads and can lead to damage of the material involved, until it develops into the component failure.

Fatigue failures continue to be a major concern in engineering design. The economic costs of fracture and its prevention are quite large, and they involve situations in which cyclic loads are at least a contributing factor. But these costs arise from the occurrence or prevention of fatigue failure. So one of the first motivations for this doctoral thesis is to find a new model which saves cost to engineers working with this problem.

Taking into account all the previous researches in this field, the author of this doctoral thesis tries to find, with a new statistical model, the best expression to fit the fatigue life data, subject to physical, statistical and other type of conditions.

This doctoral thesis must be considered as one step further in the line developed by the thesis directors. In particular, we refer to previous works such as those dealing with Weibull

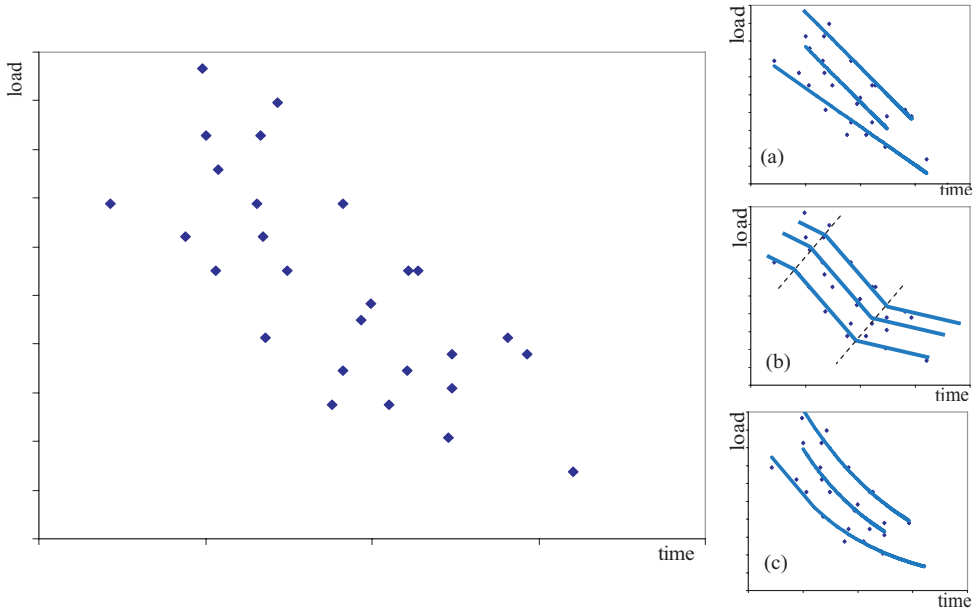


Figure 2.1: Schematic representation of a typical fatigue plot of the fatigue life data, and some different fits: (a) linear fit, (b) piece wise linear fit, (c) nonlinear fit.

models used to predict fatigue lifetime and damage accumulation in a material subject to any stress history.

## 2.2 Hypotheses

The hypotheses utilized for the development of this research were the followings:

1. The models used for fatigue analysis at present time do not satisfy all required physical, experimental and statistical conditions for a satisfactory model from a physical and engineering points of view.
2. A model able to define the fatigue behavior of the material and satisfying these conditions can be obtained.
3. The materials used in this research field of fatigue are typically metallic and some important structural elements are longitudinal.
4. It is assumed that the *weakest link principle* is satisfied: If a longitudinal element is divided into $n$ sub-elements, its fatigue life must be the fatigue life of its weakest component.

## 2.3 Objectives

In the following lines, the objectives of this research are described. These objectives define the characteristics, methods and developments of this doctoral thesis, and are as follows:

1. Perform a state of the art on fatigue of materials, showing the main models used to estimate and analyze the fatigue behavior of materials and discuss the advantages and shortcomings of each one.

2. Detect the main problems of existing models and testing strategies used in fatigue analysis.

3. Develop a new fatigue model covering the tension and compression Wöhler field for any stress history, based on the application of functional equation theory for its definition.

4. Discuss existing damage measures and propose new ones, selecting the most adequate to be used in fatigue.

5. Study and analyze damage accumulation with the proposed statistical models and damage measures.

6. Propose a good testing strategy to obtain the best laboratory results, that is, those leadings to the best possible estimates of the model parameters.

7. Design and perform a series of experimental tests to evaluate and validate and the theoretical model.

8. Run the test and analyze the test results to validate the model.

9. Based on the results and their analysis, present the main conclusions with respect to the model and testing strategies.

## 2.4 Introduction

This doctoral thesis has been done at the Department of Applied Mathematics and Computational Sciences of the University of Cantabria, inside the program: *Development and Applications of Models in Civil Engineering*.

The directors are Professors Enrique Castillo Ron and Alfonso Fernández Canteli.

The experimental tests have been done inside an experimental fatigue program launched at Empa (Swiss Federal Laboratories for Testing and Research at Dübendorf (Switzerland)).

The doctoral thesis is organized in four parts as follows:

1. **Presentation and state of the art:** In this part, an introduction and the state of the art about fatigue is discussed.

2. **Theoretical contributions:** The proposed fatigue models are presented, and some aspects about them are analyzed, including their derivations model, restrictions and properties, resulting sub-models and parameter estimation methods.

3. **Experimental validation of the models:** Here the model is validated based on laboratory tests at constant stress range and variable load histories. Furthermore, damage accumulation theories are analyzed and a comparison among these theories using the new models is made.

4. **Conclusions:** Finally, the conclusions of the doctoral thesis are given, together with, some proposals for the future lines of research in this field.

# Chapter 3

# State of the Art

The aim of this Chapter is to introduce the readers in the fatigue world and understand its different approaches. In this Chapter, an introduction to the fatigue problem is presented. In the first section, some history issues are analyzed and some basic concepts of fatigue are introduced. In sections 3.2, 3.3 and 3.4 the basic approaches to fatigue, the fracture based, stress based and strain based approaches are presented.

## 3.1 Introduction to the fatigue problem

### 3.1.1 The fatigue problem in engineering

The history of the mechanical failures due to fatigue has been studied or analyzed for more than 150 years. August Wöhler was one of the first who tested mine hoist chains under cyclic loading in Germany around 1828, but started fatigue work in Germany in the 1850s and, motivated by railway axle failures, he began to test irons, steels and other materials to design strategies for avoiding fatigue failure. He demonstrated that fatigue was affected not only by cyclic stresses, but also by the accompanying steady (mean) stresses. More detailed studies by the Wöhler followers, like Gerber and Goodman, together with the early work on fatigue and subsequent efforts up to the 1950s are reviewed in a paper by Mann [91].

Actually, fatigue failures continue to be a major concern in engineering design. The economic costs of fracture and its prevention are quite large, and 80% of these costs involve situations in which cyclic loads are at least a contributing factor to failure. For example, the anual cost of fatigue materials in the United States is about 3% of the gross national product (GPN) (see [94] and [59]). But these costs arise from the occurrence or prevention of fatigue failure for ground and rail vehicles, aircrafts, bridges, cranes, equipment, offshore oil well structures and everyday household items like toys and sport equipments.

At present, there are three different approaches to fatigue mechanisms and failures. The *stress-based approach* was developed in 1955, and the corresponding analysis is based on the nominal stresses in the affected region of the engineering component. The second approach is the *strain-based approach*, which involves a more detailed analysis of the localized yielding that may occur at stress raises during cyclic loading. The last one is the *fracture mechanics approach*, which specifically treats growing cracks by the methods of fracture mechanics.

### 3.1.2 Fatigue concepts

#### Description of cyclic loading

The *constant stress amplitude test* involves cycling between minimum and maximum stress constant levels [59] (see figure 3.1).

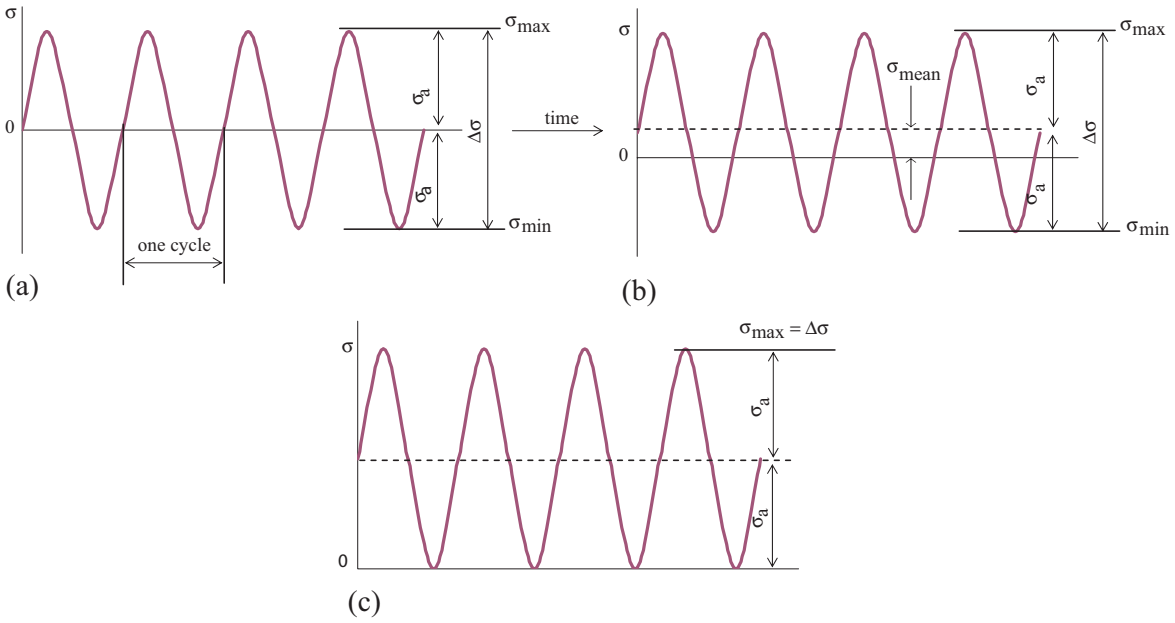


Figure 3.1: Illustration of the constant stress amplitude test and three different cases: (a) $\sigma_{mean} = 0$, (b) $\sigma_{mean} \neq 0$ and (c) $\sigma_{min} = 0$ [59].

The stress range $\Delta\sigma = \sigma_{max} - \sigma_{min}$ is the difference between the maximum and the minimum stress values. Averaging the maximum and the minimum values we obtain the *mean stress*, $\sigma_{mean}$:

$$\sigma_{mean} = \frac{\sigma_{max} + \sigma_{min}}{2}. \tag{3.1}$$

Another important parameter is the *stress amplitude*, $\sigma_a$, that is, the half range of stress range:

$$\sigma_a = \frac{\Delta\sigma}{2} = \frac{\sigma_{max} - \sigma_{min}}{2}. \tag{3.2}$$

Another two parameters useful in the fatigue problems, are the *stress ratio, R,* and the *amplitude ratio, A* [59]:

$$R = \frac{\sigma_{min}}{\sigma_{max}}; \quad A = \frac{\sigma_a}{\sigma_{mean}}. \tag{3.3}$$

Some interesting relationships derived from all the above equations are:

$$\sigma_a = \frac{\Delta\sigma}{2} = \frac{\sigma_{max}}{2}(1 - R); \quad \sigma_{mean} = \frac{\sigma_{max}}{2}(1 + R)$$
$$R = \frac{1 - A}{1 + A}; \qquad A = \frac{1 - R}{1 + R} \tag{3.4}$$

### Stress versus lifetime (S–N) curves

A *stress-life curve*, also called *S–N curve* is the representation of fatigue tests from a number of different stress levels [59]. If a test specimen of a material or an engineering component is subjected to a sufficiently severe cyclic stress, a fatigue crack (or other damage) will develop, leading to complete failure of the member. If the test is repeated at a higher stress level, the number of cycles to failure will be smaller. Since the number of cycles to failure reaches very high values data are usually plotted on a logarithmic scale (see figure 3.2).

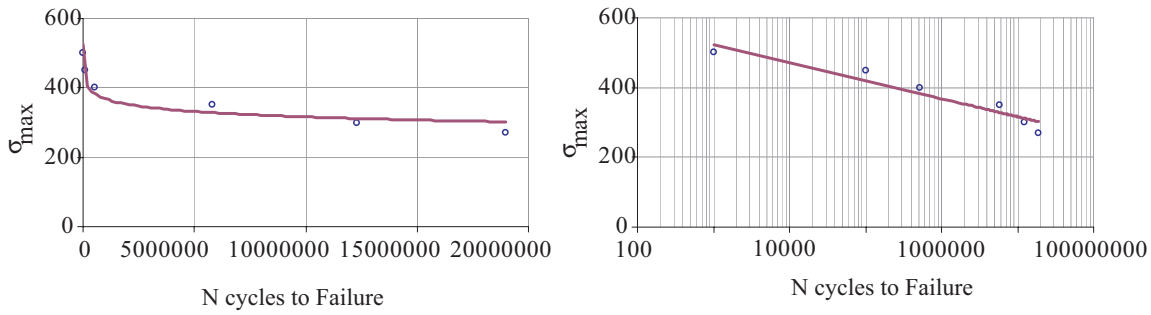


Figure 3.2: Example of a S–N curve [59]. The left side corresponds to a representation on an arithmetic scale of $N$. The right side shows a representation on a logarithmic scale of $N$.

The *endurance limit* or *fatigue limit* [59] is the lower stress amplitude below which fatigue failure does not occur under ordinary conditions. This occurs with materials like plain carbon and low alloy steels.

The term *fatigue strength* [59] is used to specify a stress amplitude value from an S–N curve at a particular life of interest. Hence, the fatigue strength at $10^5$ cycles is simply the stress amplitude corresponding to $N = 10^5$.

## 3.2 Fatigue under the fracture mechanics point of view

Engineering analysis of crack growth is often required, and can be done using the stress intensity factor, $K$, of fracture mechanics [59]:

$$K = F\sigma\sqrt{\pi a}, \tag{3.5}$$

where $a$ is crack length, $\sigma$ is stress, usually defined based on the gross area of the un-cracked member, and $F$ is a dimensionless function depending on the geometry. The value of $F$ is affected by the relative crack length, $\alpha = a/b$, where $b$ is a width dimension of the member such that $\alpha = 1$ for complete cracking. The rate of fatigue crack growth is controlled by $K$. Hence, under constant amplitude cycling loading, the dependence of $K$ on $a$ and $F$ causes cracks to accelerate as they grow.

### 3.2.1 Definitions for fatigue crack growth

Consider a growing crack that increases its length by an amount $\Delta a$ due to the application of a number of cycles $\Delta N$. The rate of crack growth with cycles can be characterized by the ratio $\Delta a/\Delta N$, for small intervals, i.e. by the derivative $da/dN$ [59].

Assume that the applied loading is cyclic with constant values of the loads $\sigma_{min}$ and $\sigma_{max}$. For fatigue crack growth, it is conventional to use the stress range $\Delta\sigma$ and the standard stress

ratio $R$. The primary variable affecting the growth rate of a crack is the range of the stress intensity factor. This can be calculated from the stress range as:

$$\Delta K = F\Delta\sigma\sqrt{\pi a}. \tag{3.6}$$

The value of $F$ depends only on the geometry and the relative crack length just as if the loading were not cyclic. Since $K$ and $\sigma$ are proportional for a given crack length, according to Equation (3.5), the maximum, minimum, range and ratio $R$ for $K$ during a loading cycle [59], are given by:

$$\begin{aligned} K_{max} &= F\sigma_{max}\sqrt{\pi a}; \qquad & K_{min} &= F\sigma_{min}\sqrt{\pi a} \\ \Delta K &= K_{max} - K_{min}; \qquad & R &= \frac{K_{max}}{K_{min}}. \end{aligned} \tag{3.7}$$

### 3.2.2 Describing material fatigue crack growth behavior

For a given material and set conditions, the crack growth behavior can be described by the relationship between cyclic crack growth rate $da/dN$ and stress intensity range $\Delta K$ [59]. Some test data and the corresponding fitted curve for a material are shown on a log-log plot in figure 3.3. There are three different states in a material during crack growth, in which geometry, environment conditions, stresses and material have a big influence on the material behavior:

1. Initialization,

2. Propagation,

3. Unstable rapid growth and fail of structure.

At low growth rates, the curve generally becomes step and appears to approach a vertical asymptote denoted $\Delta K_{th}$, which is called the *fatigue crack growth threshold* [59]. This quantity is interpreted as a lower limiting value of $\Delta K$ below which crack growth does not ordinarily occur.

At intermediate values of $\Delta K$, there is often a straight line type of behavior on the log-log plot as in this case. A relationship representing this line is:

$$\frac{da}{dN} = C(\Delta K)^m, \tag{3.8}$$

where $C$ is a constant and $m$ is the slope on the log-log plot. This equation is attributed to P.C. Paris, who first used it and who was influential in the first application of fracture mechanics to fatigue in the early 1960s.

At high growth rates, the curve may again become steep. This is due to rapid unstable crack growth just prior to final failure of the test specimen. Such behavior can occur where the plastic zone is small, in which case the curve approaches an asymptote corresponding to $K_{max} = K_c$, the fracture toughness of the material and thickness of interest. Rapid inestable growth at high $\Delta K$ sometimes involves fully plastic yielding. In such cases, the use of $\Delta_K$ for this portion of the curve is improper because the theoretical limitations of the $K$ concept are exceeded. Figure 3.3 is a typical representation of this kind of curves.

Constant $C$ and $m$ for the intermediate region, where Equation (3.8) applies, have been suggested by Barson for various classes of steel [19]. The value of $m$ is important as it indicates the degree of sensitivity of the growth rate to stress.

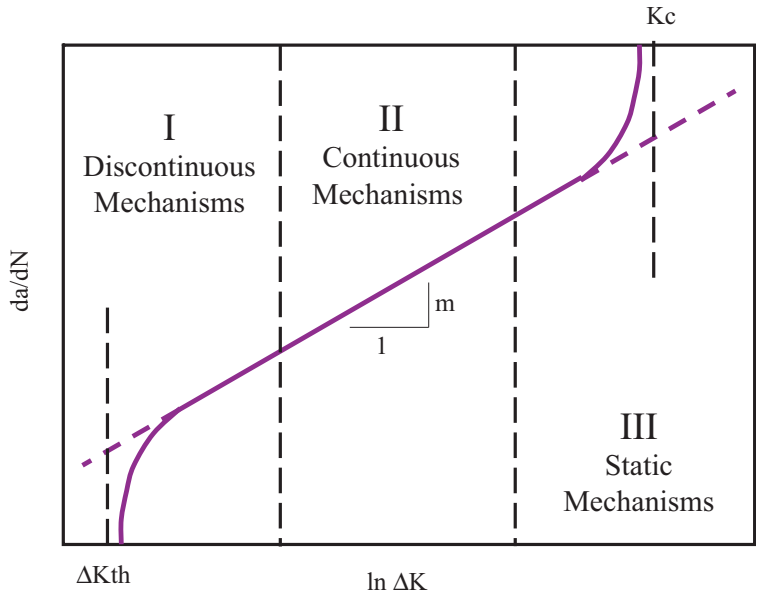


Figure 3.3: Schematic representation of crack propagation. Typical Paris curve [106].

### 3.2.3 Influence of different parameters on fatigue crack growth

**Effects of $R = \frac{S_{min}}{S_{max}}$ on fatigue crack growth:** An increase in the $R$ ratio of the cyclic loading causes growth rates for a given $\Delta K$ to become larger [59]. The effect is generally more pronounced for more brittle materials.

Various empirical relationships are employed for characterizing the effect of $R$ on $da/dN$ vs. $\Delta K$ curves. One is the Walker Equation:

$$\overline{\Delta K} = K_{max}(1-R)^{\gamma}; \quad \frac{da}{dN} = C\left(\frac{\Delta K}{(1-R)^{1-\gamma}}\right)^{m}, \tag{3.9}$$

where $\gamma$ is a constant for the material and $\overline{\Delta K}$ is an equivalent zero-to-tension ($R = 0$) stress intensity that causes the same growth rate as the actual $K_{max}$, $R$ combination.

**Effect on $\Delta K_{th}$:** The $R$ ratio generally has a strong effect on the material behavior at low growth rates, hence also on the threshold value $\Delta K_{th}$ [59]. This occurs even for low strength metals where there is little effect at intermediate growth rates. The lower limit of the scatter shown corresponds to $\Delta K_{th}$ as follows:

$$\Delta K_{th} = 7.0(1-0.85R)MPa\sqrt{m}, \quad R \geq 0.1. \tag{3.10}$$

Based on Barson [19], these equations appear to represent a reasonable worst-case estimate for a wide range of steels. However, lower values of $\Delta K_{th}$ may apply for highly strengthened steels (similar trends occur for other classes of metals).

**Environmental effects:** Similar considerations of inspection for cracks, and a similar need for life estimates, exist where crack growth is caused by a hostile chemical environment, a situation

termed *environmentally assisted cracking* ($EAC$) [59]. There are several physical mechanisms that occur.

In situations of environmental crack growth during an unchanging static load, the crack growth life can be estimated based on fracture mechanics, is a manner analogous to the procedures described above for fatigue crack growth under constant amplitude loading. The parameter controlling crack growth is simply the static value $K$ of the stress intensity factor, as determined from the applied static stress and the current crack length. Growth rates for the material are characterized by the use of $da/dt$ versus $K$ curve, where $da/dt$ is the time-based growth rate, or *crack velocity*, also denoted $\dot{a}$.

$$\dot{a} = \frac{da}{dt} = AK^n, \tag{3.11}$$

where $A$ and $n$ are material constants that depend on the particular environment and are affected by temperature.

### 3.2.4 Fatigue laws

There are two different types of parameters that can affect fatigue crack growth [23]:

- Intrinsic parameters of material: Young's modulus, yield stress, cyclic and metallurgic properties of material, etc.
- Extrinsic parameters: Test conditions, temperature, geometry, $R$ ratio, etc.

**Models based on crack propagation:** In 1963 Paris and Erdogan [106] proposed the most commonly used law for crack propagations (Equation (3.8) and figure 3.3). In this figure three different parts can be analyzed:

- Part I: In which a big influence of microstructure, mean stresses and environment conditions takes place (discontinuos mechanisms).
- Part II: Paris's Law is described here. There is an influence of microstructure, stresses, environment conditions and geometry of specimen (continuos mechanisms).
- Part III: Finally, in this part, previous parameters have a big influence.

Broek and Schijve [117] proposed an empirical equation to describe the crack growth:

$$\frac{da}{dN} = C_1 \left( \frac{\Delta K}{1-R} \right)^3 \exp(-C_2 R), \tag{3.12}$$

where $C_1$ and $C_2$ are characteristic parameter of the material, and $R$ is the stress ratio.

Forman et al. [67] assuming that crack failure occurs when $K = K_c$, derivated from Equation (3.12), the following expression:

$$\frac{da}{dN} = \frac{C\Delta K^m}{(1-R)K_c - \Delta K}. \tag{3.13}$$

Frost and Dugdale [69] analyzed diverse material taking into account dimension considerations and experimental results:

$$\frac{da}{dN} = (P + Q\overline{\sigma})\Delta\sigma^3 a, \tag{3.14}$$

where $P$ and $Q$ are material parameters.

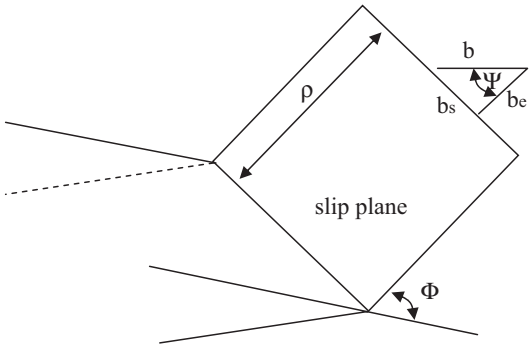


Figure 3.4: Schematic representation of the Yokobori problem, [134].

**Models based on theory of dislocation:** This model is based on the crack growth when a movement on dislocation at the head of the crack is produced.

The most used model was defined by Bilby et al. [25], which supposed a plain strain. The stress concentration derivates in the growth of a plastic region. Furthermore, there is a friction strength opposite to this movement. This situation leads to equilibrium when there is a movement at the head of the crack.

Yokobori [134] defines a cinetic theory to describe the strain between dislocations.

$$f_\tau = \tau_{p,\Phi} b_e = \frac{K_I b}{\sqrt{8\pi p}} \sin\Phi \cos\frac{\Phi}{2} \cos\psi, \tag{3.15}$$

$$f_i = -\frac{\mu b^2}{4\pi\rho}\left(\frac{1}{1-\upsilon}\right), \tag{3.16}$$

where $\rho$ is the distance from the head of crack to the dislocation, $\Phi$ is the angle formed with the propagation direction, $f_\tau$ is the strength applied and $f_i$ is the image strength (see figure 3.4).

**Models based on the material behavior:** This is the third mode of studying crack growth. The models here are more complex than others based on the theories exposed above.

Pook and Frost [109] define the stress distribution at the crack head, when there is a crack of a length $2a$ and subject to a cyclic load (from 0 to $\sigma$):

$$\frac{da}{dN} = \frac{9}{\pi}\frac{K_I^2}{E}, \tag{3.17}$$

$$\frac{da}{dN} = \frac{9}{\pi}\frac{K_I(1-\upsilon^2)^2}{E}, \tag{3.18}$$

where Equation (3.17) corresponds to plain stress and Equation (3.18) corresponds to plain strain.

## 3.3 Stress based approach to fatigue

### 3.3.1 Estimated S–N curve of a component based on ultimate tensile strength

In the event that experimental S–N data are not available, methods for estimating the S–N behavior of a component becomes useful and crucial for the design process. Large amounts of

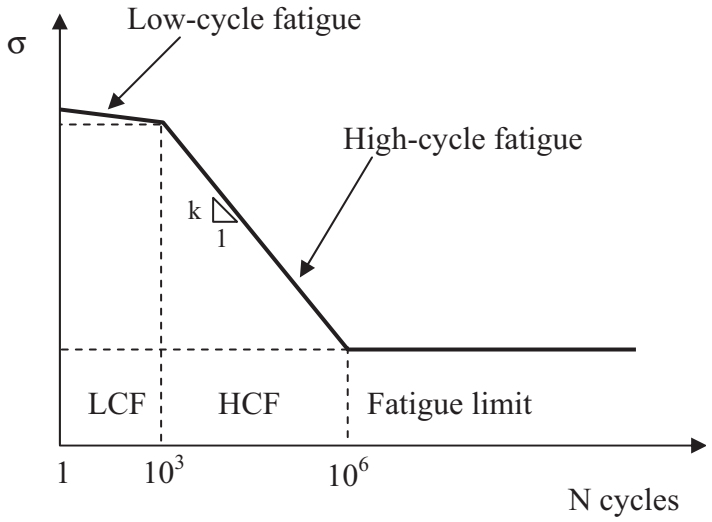


Figure 3.5: Schematic of a S–N curve for steels [59].

S–N data have been historically generated based on fully reversed rotating bending testing on standard specimens. The standard test specimen is described in [135].

The S–N curve derived from the standard specimens under loads can be constructed as a piecewise-continuous curve. As shown schematically in figure 3.5, there are two inclined linear segments and one horizontal segment in a typical $\log S$-$\log N$ curve. The two inclined linear segments represent the low-cycle fatigue ($LCF$) and high-cycle fatigue ($HCF$) regions, and the horizontal asymptote represents the fatigue limit.

For specimens made of steels, the fatigue strength values at 1, $10^3$, $10^6$ cycles define an S–N curve.

### 3.3.2 Fatigue strength testing

The objective of the fatigue strength test (also called the *fatigue limit test*, *the strength test*, or *the response test* [59]) is to estimate a statistical distribution of the fatigue strength at a specific fatigue life. The mean fatigue limit has to be first estimated, and a fatigue life test is then conducted at a stress level a little higher than the estimated mean.

Two typical data reduction techniques, the Dixon-Mood [57] and the Zhang-Kececioglu [136] methods, are used to determine the statistical parameters of the test results.

### 3.3.3 Mean stress effect

Fatigue damage of a component correlates strongly with the applied stress amplitude or applied stress range and is also influenced by the mean stress (see [59] and [135]). If mean stress is higher, the possibilities of stay near to tensile stress are bigger, and in this moment, the failure can be produced by the static parameter of the material. There is very little or no effect of mean stress on fatigue strength in the low-cycle fatigue region in which the large amounts of plastic deformation hide any beneficial or detrimental effect of a mean stress.

Early empirical models by Gerber [73], Goodman [74], Haigh [79], and Soderberg [124] were proposed to compensate for the tensile normal mean stress effects on high–cycle fatigue strength.

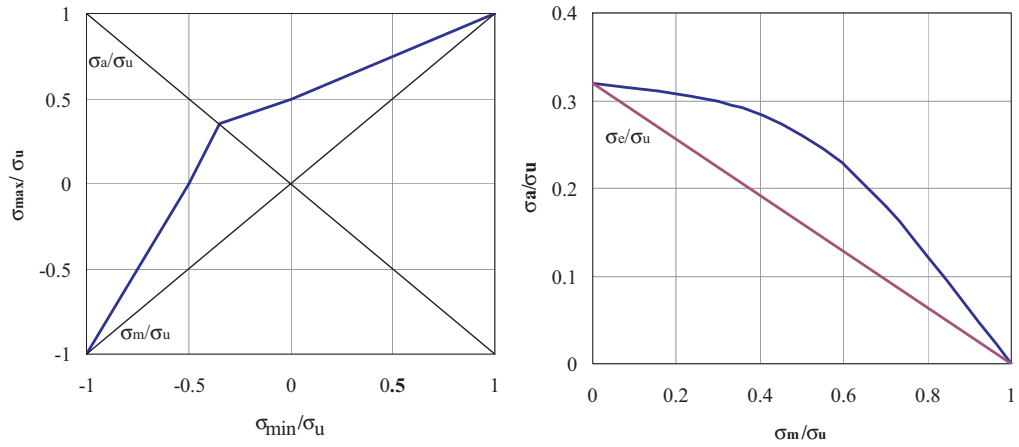


Figure 3.6: Different diagrams of mean stress corrections. Gerber's and Goodman's diagrams (left) and Haigh's plot for Gerber's and Goodman's diagrams (right) [135].

In 1874, Gerber proposed a parabolic representation of the Wöhler fatigue limit data on a plot of $\sigma_{max}/\sigma_u$ versus $\sigma_{min}/\sigma_u$ as shown in figure 3.6, where $\sigma_u$ is the stress failure. In 1899, Goodman introduced a theoretical line representing the available fatigue data and justified the use of the impact criterion on the basis that it was easy, simple to use, and provided a good fit to the data. In 1917, Haigh first plotted fatigue data for brasses on a $\sigma_a$ versus $\sigma_m$ plot. figure 3.6 illustrates the Haigh plot of the Gerber and the Goodman mean stress corrections. The ordinate of the Haigh plot is the normalized fatigue limit, and the maximum mean stress is limited to the ultimate strength $S_u$. The curve connecting these two points on the two axes represents combinations of stress amplitudes and means stresses given at the fatigue limit life.

Mathematically, the Gerber parabola and the Goodman line in Haighs coordinates can be expressed as the following expressions:

- Gerber's mean stress correction:
$$\sigma_e = \frac{\sigma_a}{1 - \frac{\sigma_m{}^2}{\sigma_u}}. \tag{3.19}$$

- Goodman's mean stress correction:
$$\sigma_e = \frac{\sigma_a}{1 - \frac{\sigma_m}{\sigma_u}}. \tag{3.20}$$

- Soderberg's mean stress correction: In this case, the maximum normal stress should be limited to the yield strength $\sigma_y$:
$$\sigma_e = \frac{\sigma_a}{1 - \frac{\sigma_m}{\sigma_y}}. \tag{3.21}$$

It is conservative to assume that for most ductile materials, the compressive normal mean stress does not benefit fatigue strength. This means that the fully reversed stress amplitude is the same as the stress amplitude if the normal mean stress is negative. A modified Goodman diagram for both tensile and compressive normal mean stresses is schematically illustrated in

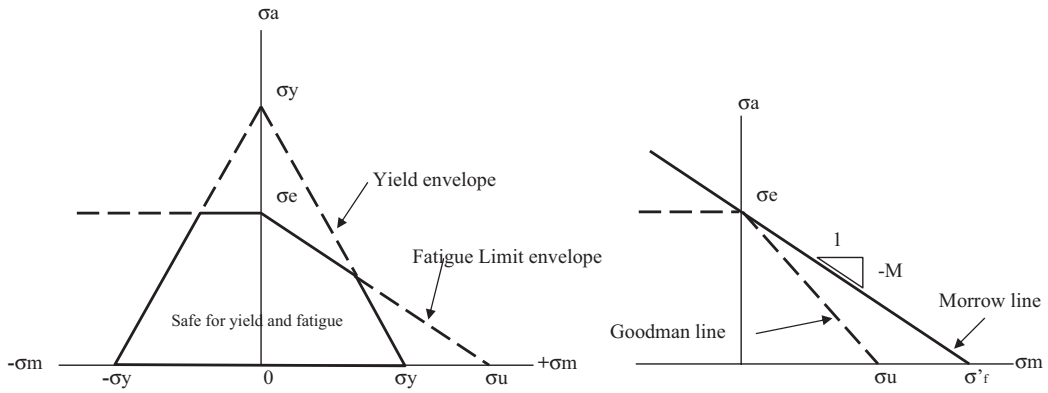


Figure 3.7: Different diagrams of mean stress corrections. Comparison between Goodman's and Morrow's mean stress models (left side). Models for combined fatigue limit and yield in ductile materials (right side)[135].

the Haigh plot at the fatigue limit as shown in figure 3.7. Wilson and Haigh [131] introduced the line of constant yield strength as an additional constraint for ductile materials on the safe design stress region, named the safe design region for fatigue limit and yield strength, shown in figure 3.7.

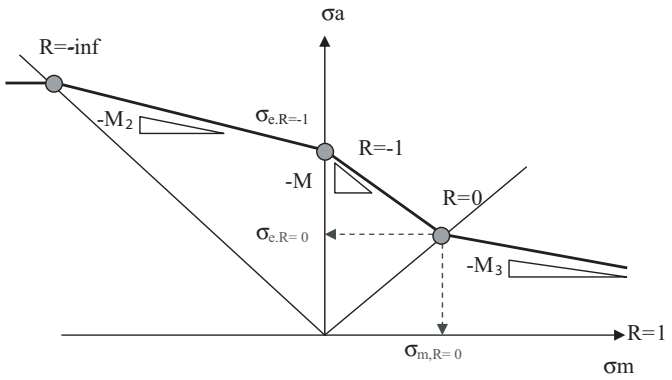


Figure 3.8: Mean stress sensitivity factors [135].

Morrow [97] suggested that the stress amplitude plus the mean stress could never exceed the fatigue strength coefficient, the fatigue strength at one reversal:

$$\sigma_{ar} = \frac{\sigma_a}{1 - \frac{\sigma_m}{\sigma'_f}}. \tag{3.22}$$

For relatively small mean stress loading, the Morrow approach is considered better than the Goodman method. The Goodman mean stress correction formula should only be used if none of the fatigue properties are available [135]. For relatively large mean stress conditions, an empirical model based on the concept of the mean stress sensitivity factor was introduced. As illustrated in figure 3.8, $M$ factors were found to vary in different mean stress levels (Radaj and Sonsino, [111]). For example, the mean stress sensitivity factor for low mean stress loading

$(-1 \leq R < 0)$ denoted by $M$, is defined as follows:

$$M = \frac{\sigma_{e,R=-1} - \sigma_{e,R=0}}{\sigma_{e,R=0}}. \tag{3.23}$$

The mean stress sensitivity factor for loading with low, compressive mean stress levels $(-\infty \leq R < 1)$ denotes $M_2$ and varies from 0 to $M$. The mean stress sensitivity factor for higher mean stress levels $(0 \leq R \leq 1$ or $S_m > S_a)$ denoting $M_3$ is usually lower than M by a factor of 3 $(M_3 \approx M/3)$. This is based on the empirical observation that loading with high mean and small amplitude shows higher damaging effects than that predicted by M. It is also found by Schütz [118] that the M factor for a material increases with a higher ultimate strength, as illustrated in figure 3.9.

If the baseline S–N curve was generated by specimens under $R = 0$ loading, it is required to convert any positive mean offset loading to an equivalent $R = 0$ loading. For a given mean stress sensitivity factor, the following conversion formula is used:

$$S_{ar,R=0} = \frac{\sigma_a + M \times S_m}{M + 1}. \tag{3.24}$$

This equation is popular in spot welded fatigue life prediction because single spot weld laboratory specimens cannot resist any compression that leads to local buckling of the metal sheet. Thus, these specimens are often subjected to $R = 0$ loading for the generation of a baseline S–N curve. Any shear mean stress can be considered positive because signs of shear are arbitrarily chosen.

Experimental fatigue data indicate that shear mean stress has little effect on fatigue strength of un-notched members under torsion [135]. Where significant stress raises are present in a component subjected to torsional loading, the state of stress at high-stress-concentration areas deviates from pure shear. Thus, experimental results under these conditions show a shear mean stress detrimental to the fatigue strength approximately as significant as that observed for bending stresses in other load cases. It is recommended to use the Goodman equation in $\tau_a - \tau_m$ for notched torsion members for which the ultimate shear strength $S_{us}$ is given.

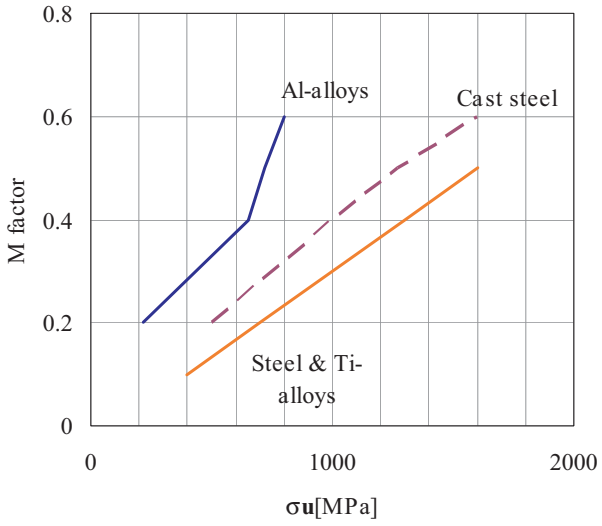


Figure 3.9: Mean stress sensitivity factors [135].

### 3.3.4 Trends in S–N curves

S–N curves are characteristic for each material, and they are affected by a variety of factors. In this subsection environment, frequency of cycling, microstructure, residual stresses and surface effects will be studied [59].

Now, some of these aspects are analyzed to know the influence in the trends of S–N curves, when one or more of these aspects are presented in material tests.

**Effects of environment and frequency of cycling:** Hostile chemical environments can accelerate the initiation and growth of fatigue cracks. One mechanism is the development of corrosion pits by chemical reactions and dissolution of material at the crack tip. Gasses in air can act as a hostile environment, especially at high temperature.

Fatigue life varying with frequency of cycling in such situations, the life in cycles being shorter for slower frequencies (see figure 3.10).

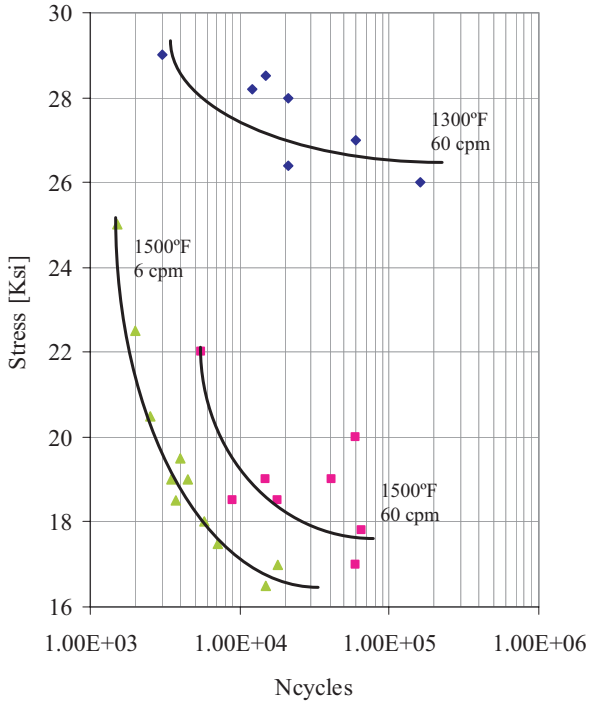


Figure 3.10: Temperature and frequency effects on the S–N curve for a nickel-base alloy Inconel [32].

**Effects of microstructure:** A change in the microstructure or surface condition has the potencial of altering the S–N curve, especially at long fatigue lives. In metals resistance to fatigue is generally enhanced by reducing the size of inclusions and voids.

Microstructure of materials often vary with direction, such as the elongation of grains and inclusions in the rolling direction of metal plates. Fatigue resistance may be lower in directions where the stress is normal to the long direction of such and elongated or layered grain structure.

**Effects of residual stresses and surface effects:** The internal stresses in the material are called *residual stresses*. This can be beneficial or not depending on the type of stresses. In the case of compressive residual stresses they are beneficial because the material attempts to recover its original size by elastic deformation.

Smoother surfaces that result from more careful machining in general improve resistance to fatigue, although some machining procedures are harmful, as they introduce tensile residual stresses.

### 3.3.5 Variable amplitude loading

Practical applications usually involve stress amplitudes that change in an irregular manner. This doctoral thesis has the objective (see Section 2.3) to validate the proposed model (see Chapter 6) for all kinds of spectra (see Chapter 8).

Cycles can be counted using time histories of the loading parameter of interest, such as force, torque, stress, strain, acceleration, or deflection. In the next lines several cycle counting techniques will be analyzed to reduce a complicated variable amplitude loading history into a number of discrete simple constant amplitude loading events, which are associated with fatigue damage.

There are different methods for obtaining life estimates for such loadings. One of them is the Palmgren-Miner Rule (see Section 4.2.2), developed in the 1920s for predicting the life of ball bearings and then, until 1945 with the appearance of Miner's paper. For cases that exhibit constant amplitude loading with or without mean offset loading, the determination of the amplitude of a cycle and the number of cycles experienced by a component is a straightforward exercise.

There are two different groups of cycle counting [135]: *One-parameter cycle counting methods* and *two parameter cycle counting methods*. The first one, called *peak-valley*, have been commonly used for extracting the number of cycles in a complex loading history. These methods are unsatisfactory for the purpose of describing a loading cycle and fail to link the loading cycles to the local stress - strain hysteresis behavior that is known to have a strong influence on fatigue failure. Thus, these methods are considered inadequate for fatigue damage analysis and we only study a method of the second group.

Two–parameter cycle counting methods, such as the *rain–flow* cycle counting method, can faithfully represent variable-amplitude cyclic loading. Dowling [58] states that the rain-flow counting method is generally regarded as the method leading to better predictions of fatigue life. It can identify events in a complex loading sequence that are compatible with constant-amplitude fatigue data. Matsuishi and Endo [93] were the first in developing the rain–flow cycle counting method based on the analogy of raindrops falling on a pagoda roof and running down the edges of the roof. A number of variations of this original scheme have been published in various applications.

**Three–point cycle counting method** SAE [114] and the ASTM [1] standards, use this kind of counting method. The three–point cycle counting rule uses three consecutive points in a load–time history to determine whether a cycle is formed (see figure 3.11):

$$\Delta\sigma_1 = |\sigma_1 - \sigma_2| \quad ; \qquad \Delta\sigma_2 = |\sigma_2 - \sigma_3| \tag{3.25}$$

$$\begin{aligned} \Delta\sigma_1 \leq \Delta\sigma_2 \quad &\rightarrow \quad \text{One cycle is counted} \\ \Delta\sigma_1 > \Delta\sigma_2 \quad &\rightarrow \quad \text{No cycle is counted} \end{aligned}$$

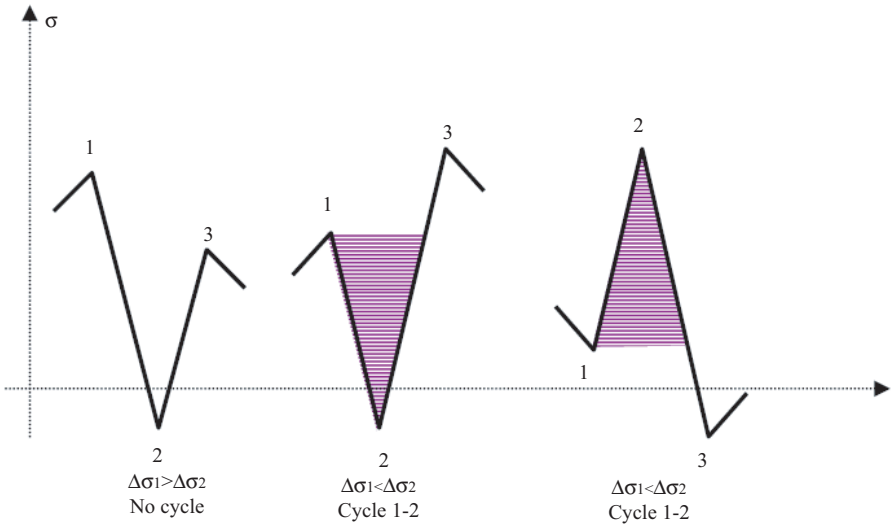


Figure 3.11: Rules of the three–point rain–flow cycle counting [135].

So the cycle identification rule is applied to check every three consecutive points from the beginning until a closed loop is defined.

**Four–point cycle counting method** Similar to the three–point cycle counting method, the four–point cycle counting rule uses four consecutive points to extract a cycle. figure 3.12 illustrates the principles for two possible cycles counted in a nominal stress–time history and the corresponding local $stress - strain$ response.

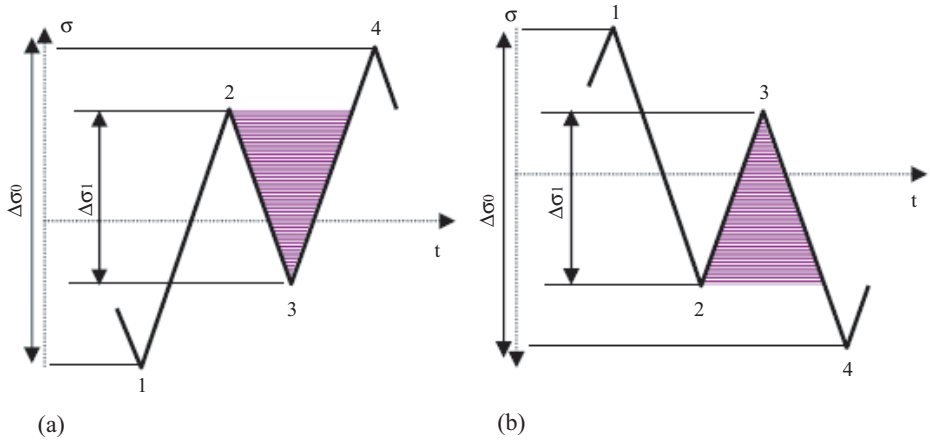


Figure 3.12: Rules of the four–point rain–flow cycle counting [135].

Two possible cycles are defined: one with a hanging cycle in (a) and another with a standing cycle in (b) in figure 3.12. The four consecutive stress points $(\sigma_1, \sigma_2, \sigma_3, \sigma_4)$ define the inner $(\Delta\sigma_1 = |\sigma_2 - \sigma_3|)$ and the outer stress range $(\Delta\sigma_0 = |\sigma_1 - \sigma_4|)$. If the inner stress range is less than or equal to the outer stress range $(\Delta\sigma_1 \leq \Delta\sigma_0)$ and the points comprising the inner stress range are bounded by (between) the points of the outer stress range, the inner cycle from

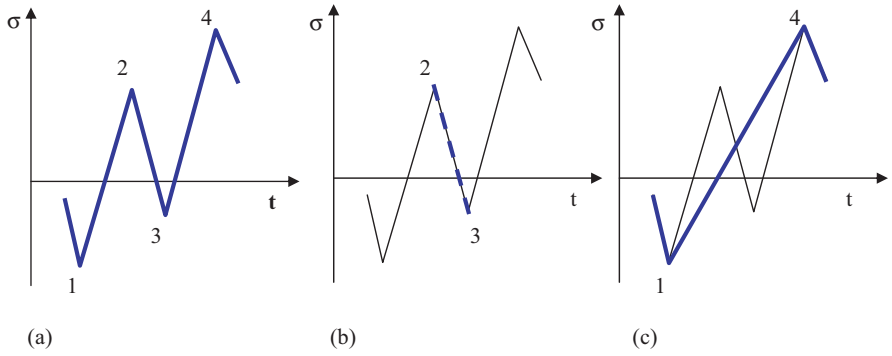


Figure 3.13: Example of four–point rain flow cycle counting [135]. (a) original loading, (b) extraction of cycle,(c) reconstruction of the load.

$\sigma_2$ to $\sigma_3$ is extracted, the two inner points discarded, and the two outer points ($\sigma_1$ and $\sigma_4$) connected to each other. In figure 3.13 an example of this technic is shown, where (a) is the original loading, (b) defines which cycle will be extracted and (c) represents the final loading. Otherwise, no cycle is counted, and the same check is done for the next four consecutive stress points ($\sigma_2$, $\sigma_3$, $\sigma_4$, $\sigma_5$) until no data remain.

Unlike the three point rainflow cycle counting method, this technique does not guarantee that all the data points will form closed cycles. The remaining data points that cannot constitute a cycle are called the *residue*.

Often, it is necessary to consider the results from cycle counting and reconstruct a load-time history as an input to fatigue testing or simulation. A method to reconstruct a new load-time history is based on the four-point counting matrix, the procedure for reconstruction is the reverse process of the four-point cycle extraction (for more information see [135]).

## 3.4 Strain based approach to fatigue

In the previous section, the analysis and design of components using stress–based fatigue life prediction techniques were presented. This approach to the fatigue analysis of components works well for situations in which only elastic stresses and strains are present. These components may appear to have nominally cyclic elastic stresses, but notches, welds, or other stress concentrations present in the component may result in local cyclic plastic deformation. Under these conditions, another approach that uses the local strains as the governing fatigue parameter (the local strain-life method) was developed in the late 1950s and has been shown to be more effective in predicting the fatigue life of a component [135].

The local strain–life method is based on the assumption that the life spent on crack nucleation and small crack growth of a notched component can be approximated by a smooth laboratory specimen under the same cyclic deformation at the crack initiation site (see figure 3.14).

The local strain-life method can be used proactively for a component during early design stages. The local strain-life method is preferred if the load history is irregular or random and where the mean stress and the load sequence effects are thought to be of importance. This method also provides a rational approach to differentiate the high–cycle fatigue and the low–cycle fatigue regimes and to include the local notch plasticity and mean stress effect on fatigue life.

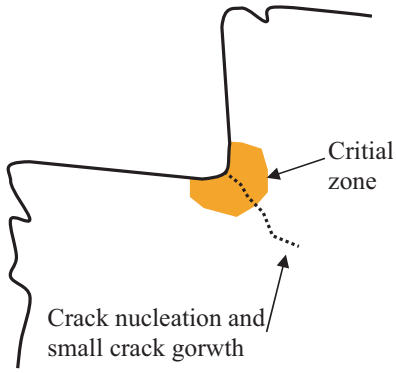


Figure 3.14: Concept of the local strain-life approach.

### 3.4.1 Analysis of monotonic and cyclic stress-strain behavior of materials

**Monotonic mechanical properties:** The following parameters are determined, from monotonic tensile tests, in table 3.1. It is not possible to explain these properties without explaining first the meaning of the $\sigma - \epsilon$ curve (see figure 3.15, right side).

Instead of the original dimensions of the specimen, the true stress ($\sigma$) and the true strain ($\epsilon$) are defined by using the instantaneous cross–sectional area ($A$) and length ($l$). They are expressed as follows:

$$\sigma = \frac{P}{A} \rightarrow \sigma = S(1+e)$$
$$\epsilon = \int_{l_0}^{l} \frac{dl}{l} = \ln \frac{l}{l_0} \rightarrow \ln(1+e). \tag{3.26}$$

These relationships are only valid up to the onset of necking in the specimen.

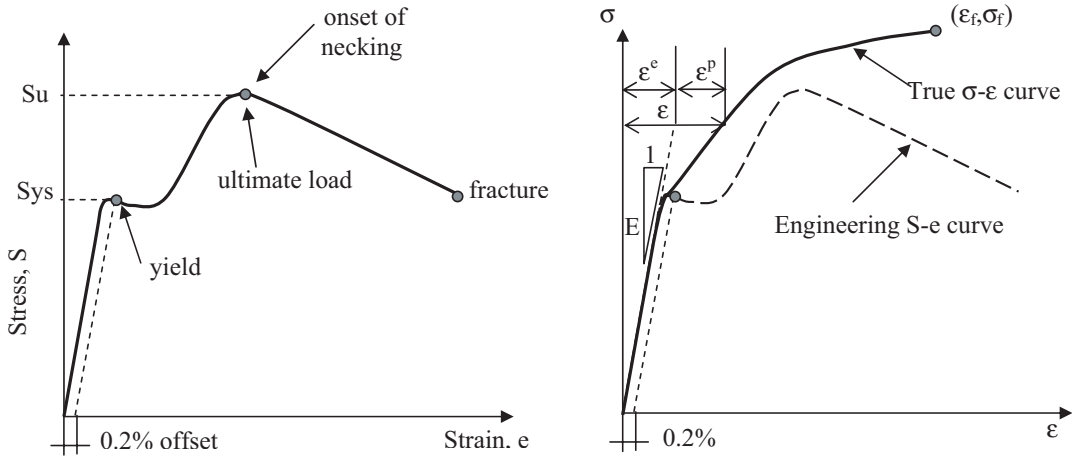


Figure 3.15: Engineering stress–strain curve (left) and true stress-strain curve (right) [135].

The engineering stress (S) and engineering strain (e) relationship is determined by monotonic tensile tests performed on smooth, cylindrical specimens. Engineering stresses and strains are defined by using the original cross-sectional area ($A_0$) and original length ($l_0$) of the test

Table 3.1: Monotonic mechanical properties

| Parameter | Definition |
|---|---|
| $\sigma_{ys}$ | 0.2% Offset yield strength |
| $\sigma_u$ | Ultimate tensile strength |
| $\%RA$ | Percent reduction area |
| $\%EI$ | Percent elongation |
| E | Modulus of elasticity |
| K | Monotonic strength coefficient |
| n | Monotonic strain hardening exponent |
| $\sigma_f$ | True fracture strength |
| $\epsilon_f$ | True fracture ductility |

specimen:

$$S = \frac{P}{A_0} \quad ; \quad e = \frac{\Delta l}{l_0}. \tag{3.27}$$

Four parameters can be measured directly from the engineering stress-strain relationship: yield strength ($\sigma_y$), ultimate tensile strength ($\sigma_u$), percentage elongation ($\%EI$), and reduction in area ($\%RA$). A typical engineering stress–strain curve is plotted in figure 3.15 (left). The yield strength represents the limit of elastic behavior and is commonly defined as the stress associated with 0.2% plastic strain. The ultimate tensile strength is the maximum load carrying capability of a specimen.

Both percent elongation and reduction in area are measured by assembling a fractured tensile specimen together and measuring the final length ($l_f$) and final cross–sectional area ($A_f$). These two parameters are the measure of metal ductility prior to fracture and are defined as follows:

$$\%EI = 100 \times \frac{l_f - l_0}{l_0} \quad ; \quad \%RA = 100 \times \frac{A_f - A_0}{A_0}. \tag{3.28}$$

If the strain abroach of an element, subject to a load, we can assume that the total strain can be decomposed into elastic ($\epsilon^e$) and plastic strain ($\epsilon^p$) components, the true stress versus true strain plot shown in figure 3.15 (right) is often described by the following equation (Ramberg and Osgood [112]):

$$\epsilon = \epsilon^e + \epsilon^p = \frac{\sigma}{E} + \left(\frac{\sigma}{K}\right)^{1/n}, \tag{3.29}$$

where $E$ is the Young modulus. The material constants $K$ and $n$ describe the monotonic stress-plastic strain relationship and can be evaluated by the least–squares fit to the data plotted on a log-log graph ($\sigma = K(\epsilon^p)^n$). In accordance with the ASTM Standard E739 [3], when performing the least–squares fit, the logarithms of the stresses are assumed to be statistically dependent and the logarithms of the plastic strain statistically independent.

Finally, the true fracture ductility $\epsilon_f$ is the true strain at final fracture and is calculated as follows (applying the Bridgman correction factor [29]):

$$\epsilon_f = \ln\left(\frac{100}{100 - \%RA}\right). \tag{3.30}$$

Table 3.2: Cyclic material properties: steady–state cyclic behavior

| Parameter | Definition |
|---|---|
| $\sigma'_y$ | 0.2% Offset yield strength |
| $K'$ | Monotonic strength coefficient |
| $n'$ | Monotonic strain hardening exponent |

**Cyclic material properties:** The cyclic stable stress-strain response is the hysteresis loop and is identified in figure 3.16. The hysteresis loop defined by the total strain range ($\Delta\epsilon$) and the total stress range ($\Delta\sigma$) represents the elastic plus plastic work on a material undergoing loading and unloading. Usually, the stabilized hysteresis loop is taken at half of the fatigue life.

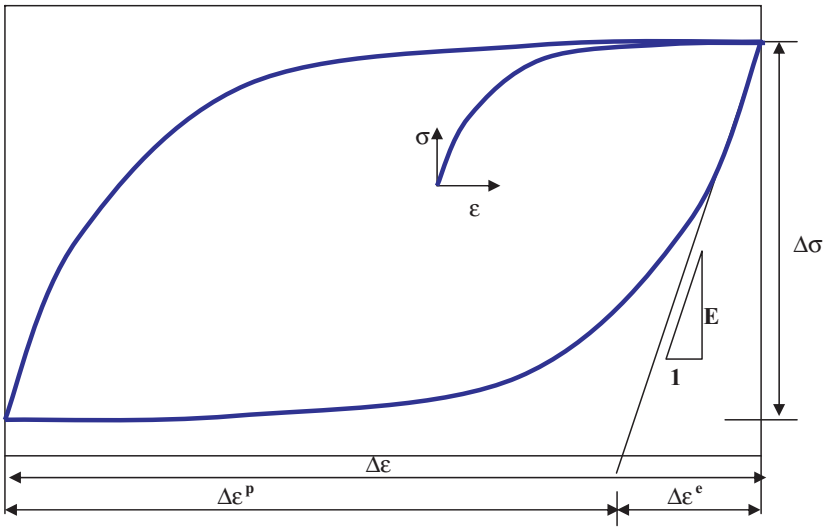


Figure 3.16: Hysteresis loop.

The properties determined from the steady–state cyclic stress  strain response are defined in table 3.2.

It also states that the material should have symmetric behavior in tension and compression. The hysteresis loop equation is defined by:

$$\Delta\epsilon = \frac{\Delta\sigma}{E} + 2\left(\frac{\Delta\sigma}{2K'}\right)^{1/n'} . \tag{3.31}$$

Equation (3.31) has been widely used for describing and tracking the stress-strain behavior under variable amplitude loading conditions.

The cyclic stress-strain curve reflects the resistance of a material to cyclic deformation and can be different from the monotonic stress-strain curve. Typically, metals with a high monotonic strain-hardening exponent ($n > 0.2$) will harden whereas those with a low monotonic strain hardening exponent ($n < 0.1$) will cyclically soften. A rule of thumb (Bannantine [18]) is that the material will harden if $\sigma_u/\sigma_y > 1.4$ and the material will soften if $\sigma_u/\sigma_y < 1.2$.

The properties that are determined from stabilized hysteresis loops and strain-life data are defined in table 3.3: Based on the proposal by Morrow [98], the relation of the total strain

Table 3.3: Cyclic material properties: constant-amplitude fatigue behavior

| Parameter | Definition |
|---|---|
| $\sigma'_f$ | Fatigue strength coefficient |
| $b$ | Fatigue strength exponent, usually varying between -0.04 and -0.05 for metals |
| $\epsilon'_f$ | Fatigue ductility coefficient |
| $c$ | Fatigue ductility exponent, usually varying between -0.3 and -1.0 for metals |
| $2N_T$ | Transition fatigue life in reversals |

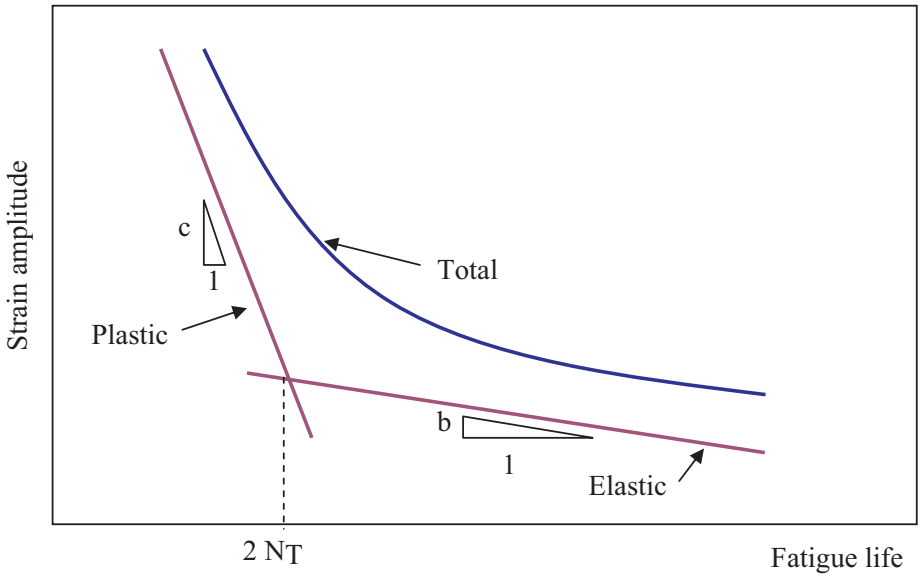


Figure 3.17: Schematic total strain-life curve [135].

amplitude ($\epsilon_a$) and the fatigue life in reversals to failure ($2N_f$ ) can be expressed in the following form:

$$\epsilon_a = \frac{\sigma'_f}{E}(2N_f)^b + \epsilon'_f(2N_f)^c. \tag{3.32}$$

Equation (3.32), called the *strain-life equation*, is the foundation for the strain - based approach for fatigue. This equation is the summation of two separate curves for elastic strain amplitude life ($\epsilon_a^e - 2N_f$) and for plastic strain amplitude - life ($\epsilon_a^p - 2N_f$). Dividing the Basquin [20] equation by the modulus of elasticity gives the equation for the elastic strain amplitude–life curve (first part in Equation (3.32)). Both Manson [92] and Coffin [50] simultaneously proposed the equation for the plastic strain amplitude–life curve (second part of Equation (3.32)). When plotted on log-log scales, both curves become straight lines as shown in figure 3.17.

### 3.4.2 Mean stress correction methods

Here mean stress correction methods are studied, as in Section 3.3.3. In designing for durability, the presence of a nonzero mean normal stress can influence fatigue behavior of materials because a tensile or a compressive normal mean stress has been shown to be responsible for accelerating or decelerating crack initiation and growth (like in stress approach to fatigue (Section 3.3.3).

Many models have been proposed to quantify the effect of mean stresses on fatigue behavior.

The commonly used models in the ground vehicle industry are those by Morrow [97] and by Smith, Watson, and Topper [123].

**Morrow's mean stress correction method:** Morrow has proposed the following relationship when a mean stress is present:

$$\epsilon_a = \frac{\sigma'_f - \sigma_m}{E}(2N_f)^b + \epsilon'_f(2N_f)^c. \tag{3.33}$$

This equation implies that the mean normal stress can be taken into account by modifying the elastic part of the strain-life curve by the mean stress ($\sigma_m$).

This correction is used for steels and used with considerable success in the long-life regime when plastic strain amplitude is of little significance.

**Smith–Watson–Topper (SWT) model:** Smith, Watson, and Topper [123] proposed a method that assumes that the amount of fatigue damage in a cycle is determined by $\sigma_{max}\epsilon_a$, where $\sigma_{max}$ is the maximum tensile stress and $\epsilon_a$ the strain amplitude. Also, the SWT parameter is simply a statement that $\sigma_{max}\epsilon_a$ *for a fully reversed test is equal to* $\sigma_{max}\epsilon_a$ *for a mean stress test.* Thus, this concept can be generalized and expressed in the following mathematical form (Langlais and Vogel, [88]):

$$\sigma_{max}\epsilon_a = \sigma_{a,rev}\epsilon_{a,rev} \rightarrow \sigma_{max} > 0, \tag{3.34}$$

where $\sigma_{a,rev}$ and $\epsilon_{a,rev}$ are the fully reversed stress and strain amplitudes, respectively, that produce an equivalent fatigue damage due to the SWT parameter.

The SWT parameter predicts no fatigue damage if the maximum tensile stress becomes zero and negative. The SWT formula has been successfully applied to grey cast iron, hardened carbon steels and micro-alloyed steels.

# Chapter 4

# Models Used in Fatigue

The aim of this Chapter is to explain the different models used in fatigue from the stress approach point of view. The advantages and disadvantages of each model are analyzed, discovering which of them predict better fatigue lifetime. The Chapter is organized as follow: first, a short overview is given in section 4.1. In sections 4.2 and 4.3 different models are analyzed. In section 4.4 an analysis and discussion about the models presented above is made.

## 4.1 Overview

From the physical point of view, fatigue failure (fracture) is the result of plastic strain accumulation [86]. However, fatigue processes preceding fracture are too complicated and it is therefore not possible to describe fatigue curves using only simple physical conceptions. On the other hand, all fatigue properties associated with fatigue curves (fatigue limit, the slope of the fatigue curve in the range of finite life, etc.) are not strictly defined physical quantities but only engineering properties of materials. The result of these two facts is only a phenomenological description of fatigue curves and it seems that a purely physical approach will not be successful for the next few years.

All the important functions for the description of fatigue curves can be divided into several groups according to the geometrical shapes of their graphs. No special attention will be paid to the classical trivial models of the fatigue curves covering the regions of finite life and permanent fatigue limit. To this purpose a broken straight line with two arms (oblique and horizontal) is used.

The fatigue model historical evolution is shown in table 4.1. The very first ideas were arisen from August Wöhler, who started work in Germany in the 1850s. Then others, like Basquin, Palmgrem, Miner, Dixon and Mood, Castillo et al. developed new models to describe this material behavior ([20], [22], [37]–[49], [57], [107] and [126]).

In the following sections, the most important models are studied and analyzed to show the evolution of the state of knowledge in this field.

Table 4.1: Historical evolution of principal fatigue models.

| Year | Author | Main contribution |
|---|---|---|
| 1850s | August Wöhler | First approximation to fatigue of materials |
| 1910 | Basquin | Fatigue strain approach model |
| 1924 | Palmgren | Creation of one of the most used rule in fatigue |
| 1945 | Miner | Development of Palmgren ideas → Palmgren–Miner rule |
| 1948 | Dixon & Mood | Use of Up & Down method in fatigue |
| 1972 | Basteraine | Statistical evaluation of fatigue models |
| 1981 | Spindel & Haibach | Statistics applied to shape of S–N curves |
| 1985 | Castillo et al. | Hyperbolic approximation to the lifetime stress level curves |
| 1999 | Pascual & Meeker | Use of the random fatigue–limit method |
| 2001 | Kohout & Vechet | Create a model covering low, medium and high cycles region |
| 2001 | Castillo & Fernández-Canteli | A Weibull model for lifetime evaluation and prediction |
| 2006 | Castillo & Fernández-Canteli | A Weibull model for fatigue damage due to any stress history |

## 4.2 Models used in fatigue

In this section the most important models used in fatigue are described.

### 4.2.1 The Basquin model

Since A. Wöhler begun to study what happened with the material subject to cyclic loads, many functions have been suggested to present the material behavior. The Basquin function [130] represents a hyperbola with an exponent parameter ($b$ is a negative number). Other models, such as the Stromeyer, Palmgren or Weibull [130] are modifications or generalizations of the Basquin model

$$\sigma(N) = aN^b. \tag{4.1}$$

The simple Basquin function [20] describes the dependence of fatigue limit of finite life $N$ on the number of cycles $N$. This, can be extended also to the *low–cycle region*

$$\sigma(N) = a(N + B)^b, \tag{4.2}$$

as well as to the *high–cycle region*

$$\sigma(N) = aN^b + \sigma_\infty, \tag{4.3}$$

a function which is called the *Stromeyer function* [128], where $\sigma_\infty$, is the permanent fatigue limit. A model valid in both the low- and the high–cycle regions:

$$\sigma(N) = a(N + B)^b + \sigma_\infty, \tag{4.4}$$

which is called the *Palmgren function.*

### 4.2.2 The Palmgren–Miner rule

This model is one of the most used in fatigue of materials. The model was created by Palmgren in 1924, but it begun to be popularized by Miner in 1945.

To understand the problem, consider a situation of variable amplitude loading, as illustrated in figure 8.6. A certain stress amplitude $\sigma_{a1}$ is applied for a number of cycles $N_1$, where the number of cycles to failure from the S–N curve for $\sigma_{a1}$ is $N_{f1}$. The fraction of life used is then

$N_1/N_{f_1}$. Now let another stress amplitude $\sigma_{a2}$, corresponding to $N_{f2}$ on the S–N curve, be applied for $N_2$ cycles. An additional fraction of the life $N_2/N_{f_2}$ is then used. The *Palmgren-Miner rule* [59], simply states that fatigue failure is expected when such life fractions sum to unity, when 100% of the life is exhausted:

$$\frac{N_1}{N_{f1}} + \frac{N_2}{N_{f2}} + \frac{N_3}{N_{f3}} + ... = \sum \frac{N_i}{N_{fi}} = 1. \tag{4.5}$$

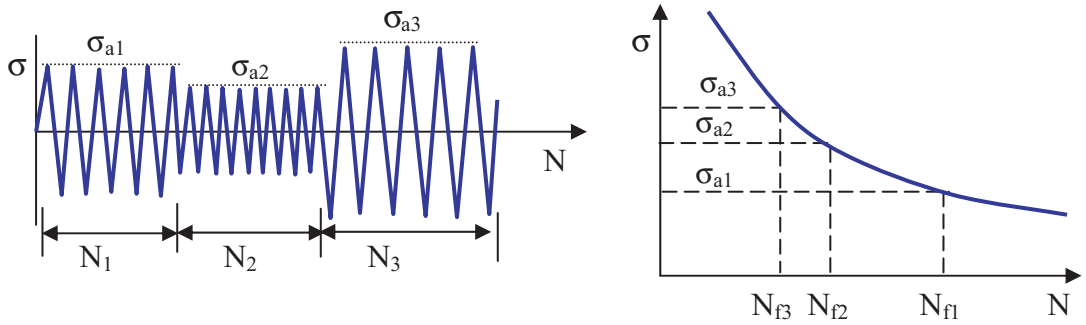


Figure 4.1: Use of the Palmgren–Miner rule for life prediction for variable amplitude loading which is completely reversed [59].

Some cycles of the variable amplitude loading may involve mean stresses. Equivalent completely reversed stresses then need to be calculated before applying a completely reversed S–N curve, or else a life equation applied that already incorporates mean stress effects, studied in section 3.4.2. In addition, the stress range caused by changing the mean level also needs to be considered in summing cycle ratios.

### 4.2.3 The up–and–down method

In daily practice some continuous variables appear such that they cannot be measured directly. This is for example the case of the fatigue endurance limit, i.e., the stress level below which the fatigue failure does not occur. Unfortunately, once an specimen subject to a fatigue experiment at the stress level $\Delta\sigma$ has failed it cannot be tested again at a lower stress level to see if failure occurs at that level. Thus, the population variable is characterized by a continuous variable (the endurance limit) which cannot be measured in practice. All we can do is to select some stress level and determine whether the endurance limit is below or above such a level.

This type of situation arises in many fields of actual research. There are several common procedures to deal with the problem of estimation, as for example the up-and-down method.

Originally, this method was used for obtaining sensitivity data and developed and used in explosives research. But the method may be employed in any sensitivity experiment. The technique consists of choosing several stress levels:

$$\ldots, \Delta\sigma_2, \Delta\sigma_1, \Delta\sigma_0, \Delta\sigma_{-1}, \Delta\sigma_{-2}, \ldots$$

and start the test at level $\Delta\sigma_0$. If the specimen fails, we move downward to $\Delta\sigma_{-1}$, and upwards to $\Delta\sigma_1$, otherwise. Then, the process is repeated a number of times $t$. The results of the experiment consists of the stress levels $\Delta\sigma_i$ and the binary values $\gamma_i$ where 1 means survival and 0, failure.

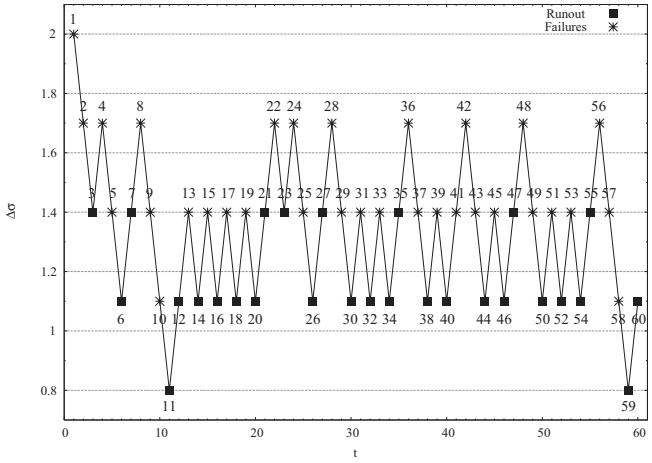


Figure 4.2: Illustration of the up-and-down method using the Dixon and Mood data and showing the five stress levels [48].

The result of such a experiment can be represented as in figure 4.2, where we have used data reported by Dixon and Mood [57] and the failures (asterisks) are the data points followed by data points in an upper level, and the survivals (squares) are the data points followed by another data points in a lower level.

The principal advantages proposed by the authors were two: the primary advantage of this method was that it automatically concentrates testing near the mean so, that this increases the accuracy with which the mean can be estimated. A second advantage is that the statistical analysis was quite simple in certain circumstances whereas the analysis for the ordinary method is rather tedious. But, the method had one obvious disadvantage in certain kind of experiments because it requires that each specimen be tested separately.

**Some conditions on the experiments** These conditions are:

1. The analysis requires that the variate under analysis be normally distributed. It is therefore necessary that the natural variate be transformed to one which does have the normal distribution.

2. The sample size must be large if the analysis to be described is to be applicable. As it turns out, the effective sample size is only about half the actual sample size. The statistical analysis is based on large sample theory so that if one uses the analysis on a sample of size forty, he will in effect be using large sample theory on a sample of size twenty. Measures of reliability may well be very misleading if the sample size is less than forty or fifty.

3. The interval between testing levels should be approximately equal to the standard deviation. This condition will be well enough satisfied if the interval actually used is less than twice the standard deviation.

**Statistical analysis** The simple method of analysis given in this section is applicable only when all the conditions described in the preceding lines are fulfilled.

To describe the statistical analysis the authors again revert to the explosives experiment in describing the method. Suppose it is known for the given type of explosive that the logarithms

of the critical heights are normally distributed. Letting $h$ represent the height, $y = \log h$ will then be the normally distributed variate. We shall call $y$ the normalized height, and represent the mean and variance of its distribution by $\mu$ and $\sigma^2$. The experiment is performed by choosing an initial height for the first test, say $h_0$. This should be chosen near the anticipated mean. The other testing levels are determined so that the values of the normalized height $y$ are equally spaced. If $d$ is the preliminary estimate of $a$, and if $y_0 = \log h_0$, then the actual testing heights are obtained by putting $\log h = y_0 \pm d$, $y_0 \pm 2d$,..., and solving for $h$. The heights will then be so spaced that the transformed variate is equally spaced with spacing equal to its anticipated standard deviation. All computations are done in terms of $y$.

The estimates of $\mu$ and $\sigma$ are based on the first two moments of the $y$ values using the frequencies $n_i$. But since the y values are equally spaced, the moments are more easily computed in terms of the two sums:

$$\begin{aligned} A &= \sum i n_i, \\ B &= \sum i^2 n_i. \end{aligned} \tag{4.6}$$

That is,

$$\mu = y' + d\left(\frac{A}{N} \pm \frac{1}{2}\right), \tag{4.7}$$

where $y'$ is the normalized height corresponding to the lowest level. The standard deviation is:

$$\sigma = 1.62d\left(\frac{NB - A^2}{N^2} + 0.29\right). \tag{4.8}$$

### 4.2.4 The Bastenaire model

The author [22], presents a probabilistic description of constant stress amplitude fatigue-test results, using the experimental and theoretical results of previous research work. This description includes the S–N curves (or equiprobability of fracture curves), P–S curves (or stress–response curves), P–N curves (cumulative distribution functions of fatigue endurance), and accounts for the occurrence of run-outs. The application of this method is demonstrated through five examples for each of which several hundred test results are available.

The purpose of this model [22], is to demonstrate the application of a new statistical method of evaluation based on the same underlying mathematical model to the experimental data collected. Furthermore, this model is one of the first models in which the P–S–N fields are presented, being useful in the definition of the model proposed in this doctoral thesis and described totally in Chapters 5, 6 and 7.

**General expression for the probability of fatigue failure:** It has long been known that the scatter of fatigue lives in constant stress amplitude tests could be represented using a set of equiprobability curves in a P–S–N diagram [68]. The P–S–N diagram is a simple method of representing the following relationship between the probability of fracture $p$, the stress amplitude $S$, and the number of load cycles $N$

$$p = F(S, N). \tag{4.9}$$

The two quantities $S$ and $N$ are assumed to be independent variables to which the experimenter can assign any values since he is at liberty to carry out a test that may last up to $N$ cycles under stress S and examine whether or not the specimen sustains this number of cycles without

fracturing, $p$ is the probability of fracture regarded as one of two alternatives. However, $F(S, N)$ is also the cumulative distribution function ($CDF$) of the number of cycles to fracture ($NCF$) regarded as a random variate.

If a group of specimens is allocated to each stress level, it is possible to estimate the probability of fracture $F(S_i, N)$ from the proportion of specimens broken in the $i_{th}$ group before N cycles are completed.

For any given value of $S$, the value of $N$ which is such that $F(S, N_p) = p$ is the $p_{th}$ quantile of the distribution of the $NCF$ which can be denoted by $N_p$

$$F(S_p, N) = p. \tag{4.10}$$

If it is assumed that $p$ increases when either $S$ or $N$ increases then

$$\frac{\partial F}{\partial S} > 0; \quad \frac{\partial F}{\partial N} > 0 \tag{4.11}$$

Differentiating Equation (4.11), we obtain:

$$p = \frac{\partial F}{\partial S} dS + \frac{\partial F}{\partial N} dN. \tag{4.12}$$

In the case of $dp = 0$,

$$\frac{dS_p}{dN} = -\frac{\partial F}{\partial N} / \frac{\partial F}{\partial S}. \tag{4.13}$$

Using the above equations, we find that $dS_p/dN < 0$. For constant $p$, $S_p$ is, therefore, a decreasing function of $N$, as shown by the schematic equiprobability curves of figure 4.3.

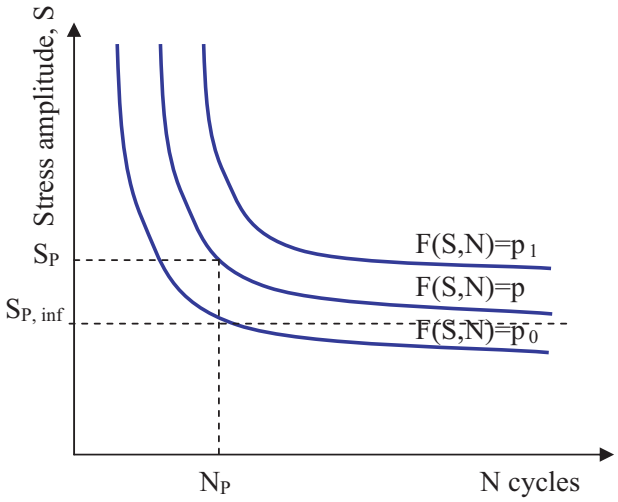


Figure 4.3: Schematic diagram of equiprobability of fracture curves [22].

The following remarks are useful for the determination of the limit to the stress–response curves when $N$ tends to infinity:

1. $S$ is a stress amplitude and, therefore, cannot be negative.
2. A zero stress amplitude can be assumed to produce no fatigue effects in a material. $S_p$ being a bounded decreasing function of $N$, a limit $Ep \geq 0$ to $S_p$ always exists (except, perhaps for $p = 1$, for which $S_p$ may not be defined).

3. That a limiting stress–response curve certainly exists, though it may possess two different shapes.

Bastenaire shows that it is advantageous to plot the proportions of specimens failing before $N$ load cycles have been completed on a normal or logistic probability scale. If a straight line is obtained on probability paper, it can be conc1uded that the threshold stresses are normally distributed with a standard deviation shown by the slope of the straight line.

However, the stress-response curves do not have to be normal. This concept will be analyzed in Section 4.3 and Chapter 6. The failure of a material is an extremal process and there are other distributions (like Gumbel or Weibull distributions) that can represent better this behavior of the material.

Making the hypotheses that the stress–response curves are normal, one only needs to assume that two parameters, a location parameter $\mu$ and a scatter parameter $\sigma$, are sufficient to represent these curves which may equally well derive from the normal, logistic, extreme value or some other distribution.

For any given value of N, $\mu$ and $\sigma$ depend on $N$ and should really be regarded as two functions $\mu(N)$ and $\sigma(N)$. Denoting the cumulative distribution function of the reduced variate by $F$, the probability of fracture can be expressed by the following equation

$$p = F\left(\frac{S-\mu(N)}{\sigma(N)}\right). \tag{4.14}$$

**Representation of the equiprobability curves using a transformed variate:** Now, the aim of this subsection is to obtain the general expression that can describe the problem and the better solution. For this, it is necessary to take into account the boundary conditions to transform Equation (5.36) into a general function.

Equation (5.36) shows that $P$=constant if $(S-\mu(N))/\sigma(N)$ is constant. In particular, if $S-\mu(N)=0$ then $P=F(0)$. It has been shown that $S_P$ tends to a limit $E_P \geq 0$ when $N \to \infty$ (endurance limit).

A new function

$$\varphi(N) = \mu(N) - \mu(\infty), \tag{4.15}$$

is introduced, one can express $\mu(N)$ as

$$\mu(N) = \varphi(N) + \mu(\infty), \tag{4.16}$$

where $\varphi(N)$ is a decreasing function of $N$ tending to zero as $N \to \infty$. Using Equations (5.36) and (4.16), and knowing that $\mu(\infty) = E$,

$$p = F\left(\frac{S-\varphi(N)-E}{\sigma(N)}\right). \tag{4.17}$$

This equation can be used to account for the main features of the NCF distributions.

A contribution of Bastenaire is the representation of the S–$\varphi$ field, in where is represented the variable $\varphi(NCF)$ in a diagram. Replacing the usual S–N system of coordinates by $S, \varphi$, the equiprobability curves can be represented in a new diagram. The equation of the $F(0)$ equiprobability curve is

$$S_{F0} = \varphi(N) + E. \tag{4.18}$$

This equation shows that by plotting $\varphi$ instead of $N$ as the abscissa, the $F(0)$ equiprobability curve is represented by a straight line.

More generally, assuming that $F$ is the cdf of a continuous random variate, F is monotonic, and P will be constant in Equation (4.17) if, and only if, the argument of F is constant, say

$$u = \left( \frac{S - \varphi(N) - E}{\sigma(N)} \right), \tag{4.19}$$

where $u$ is a constant.

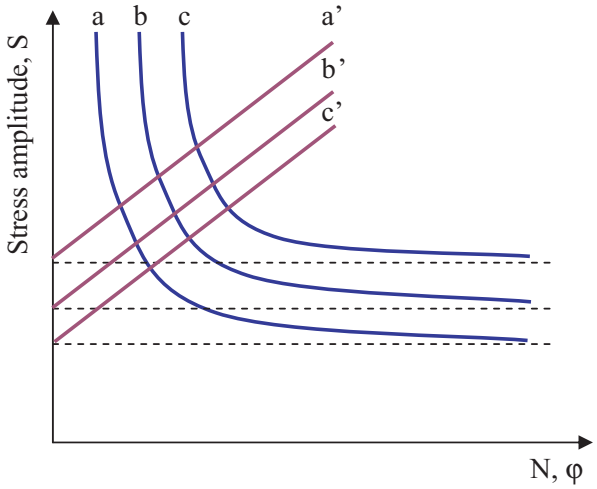


Figure 4.4: S–N and S–$\varphi$ diagrams. Letters a, b, c correspond to S–N field. Letters a', b', c' correspond to the $\varphi$–N field [22].

The general equation of the equiprobability curves can be written as

$$S_p = \varphi(N) + E + u\sigma(N). \tag{4.20}$$

The S–N and S–$\varphi$ systems of coordinates are superimposed in figure 4.4 to show how they are related. figure 4.4 also shows how the distributions of $S$ and $\varphi$ differ. For any given value of $N$, there is no practical limit to the stress amplitude which can be applied to specimens and the stress–response curve can be explored up to stresses at which the probability of fracture is nearly unity. In contrast with this, an increase in the number of cycles for a given stress value produces a decrease in $\varphi(N)$ which is bounded at zero and the proportion of failures tends to a limit.

As a final remark, Equation (4.17) shows that the value of $\varphi$ for which $p = F(0)$ is $\varphi = S - E$. When a value of $S$ less than $E$ is chosen as a test stress, this value is negative though the observed values of $\varphi$ are all positive. This is so because the central value of a distribution can be outside the range of the observed values.

The distributions of $\phi(N)$ at different stress levels differ mainly in location and in the proportion of observations cut off at $\phi = 0$ but can be expected to be very similar in shape. This is in contrast with the distributions of fatigue lives which (even though plotted on a logarithmic scale) change markedly in shape when the stress changes. Bastenaire explains [22], that the logarithm of the $NCF$ is distributed normally only at intermediate stress levels. When the stress decreases, the scatter and skewness of these distributions increase to a considerable degree, and the proportion of broken specimens tends to a limit as the number of applied load cycles increases.

**More general transformation of the number of cycles to fracture:** Bastenaire studied different real cases [21], but, unfortunately, $S_{F(0)} = (A/N) + E$ is not always a convenient equation for the median equiprobability curve. This is unfortunate, not only because $A/N$ is a simple function, but also because, if $A/N$ is distributed normally, so is $1/N$. Similarity, if a linear relationship holds between $A/N$ and $S$, it also holds between $1/N$ and $S$. No prior knowledge of coefficient $A$ is, therefore, necessary to check the validity of this relationship, and $A$ can be estimated later by means of a linear regression.

For a number of materials and testing conditions [21], the median equiprobability curve can be represented by the following equation:

$$N = \frac{A \exp[-c(S-E)]}{(S-E)}, \tag{4.21}$$

in which $A$, $c$, and $E$ are coefficients. Making $c = 0$ we obtain $S_{F(0)} = (A/N) + E$.

A more general formula is

$$N + B = \frac{A \exp[-c(S-E)]}{(S-E)}, \tag{4.22}$$

with an additional coefficient $B$ (see figure 4.5). If it is assumed that Equation (4.22) can be

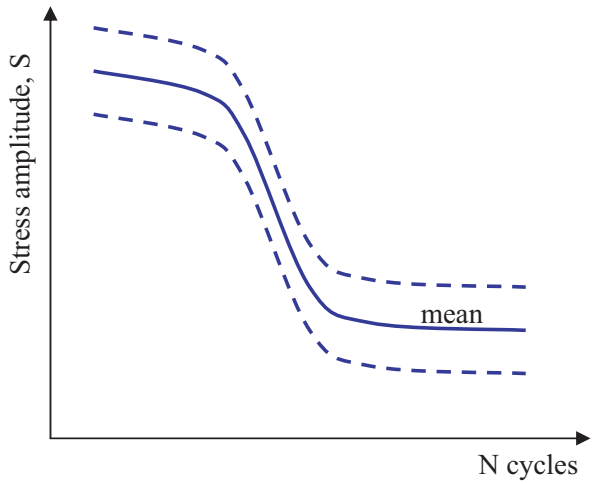


Figure 4.5: Bastenaire schematic curve [126].

used to represent the $F(0)$ equiprobability curve, and knowing that when $N \to \infty$, $S_{F(0)} \to E$, we can obtain

$$N + B = \frac{A \exp[-c\varphi]}{\varphi}. \tag{4.23}$$

Finally, sorting elements of Equation (4.23) we can obtain the general expression of the Bastenaire Model

$$N = \frac{A \exp\left[-\left(\frac{S-E}{B}\right)^{C}\right]}{S-E}. \tag{4.24}$$

**Example of application:** The schematic diagram of figure 4.4 can now be used to plot real values. This is done in figure 4.6 in which the results for five materials are plotted together. The estimated means of $\varphi(NCF)$ are plotted in the abscissas axis and the stresses in the ordinates axis.

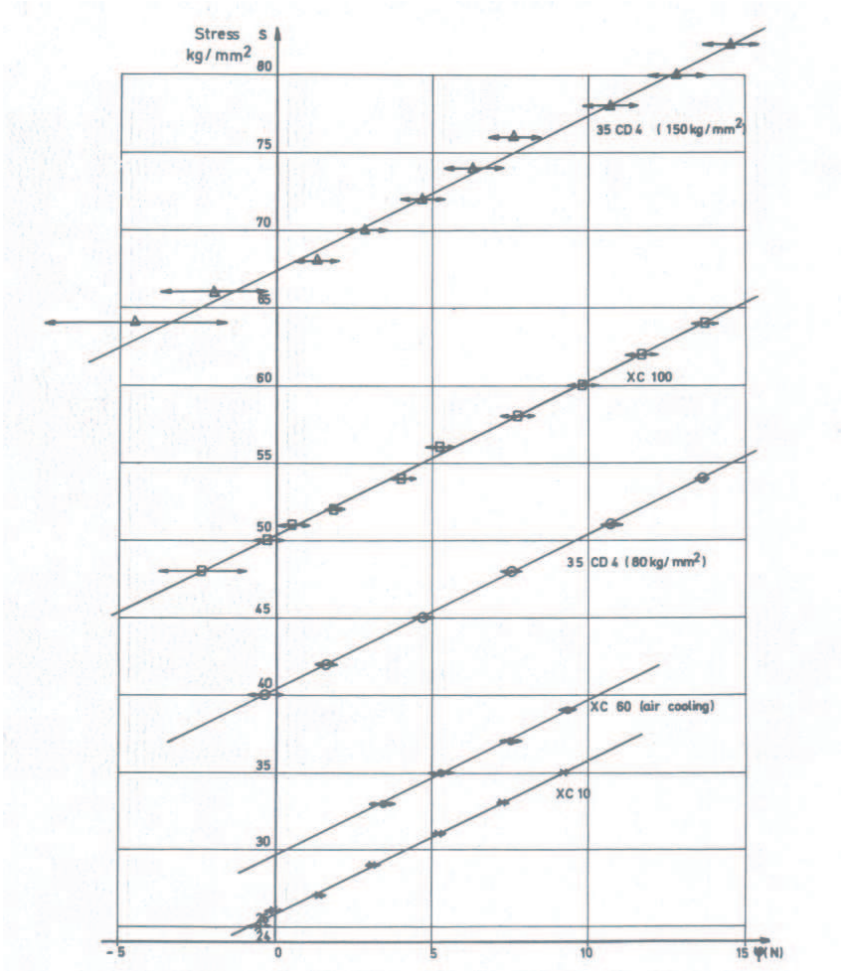


Figure 4.6: Experimental S–$\varphi$ diagram for five different steels. figure from [22].

The main purpose of this diagram is not to plot each S–N curve in the form of a straight line: indeed, nearly any relationship can be represented by a straight line using suitable coordinates.

figure 4.6 represent estimated mean values. Plotting hundreds of individual test results for each material was not feasible on the S–$\varphi$ diagram. A better image of their distributions is given by the cumulative frequency curves shown in figure 4.7.

### 4.2.5 The Spindel and Haibach model

The method proposed by the authors [126] tries to find the cutoff point, that is, the endurance at which conventionally shaped S–N curves change to the horizontal.

The determination of the shape of S–N curves is not a purely academic exercise. It is found in cumulative damage calculation that the position of the cutoff point has a considerable effect on the stress that is calculated as tolerable for a given load spectrum when such calculations are

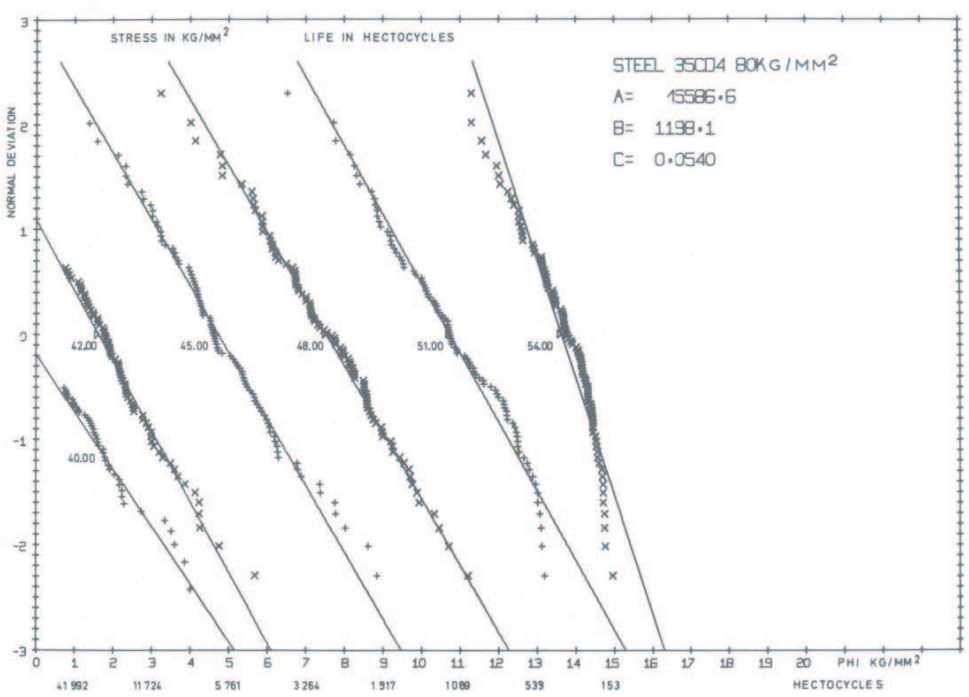


Figure 4.7: Cumulative frequency curves of $\varphi(NCF)$ for steel 33CD4 (treated to $80kg/mm^2$). This curve correspond with the third curve in figure 4.6. figure from [22].

based on Miner's rule [76]. Considerable differences are found, not only in the stress at the endurance limit, but also in the fatigue strength for loading spectra calculated for high–endurance values, that is, values above $10^7$ cycles where experimental verification is not practicable because of the testing time and cost.

The authors developed a new method that would determine the best common slope to fit a number of sets of individual test data.

**Possible definitions of the S–N curve:** Any statistical analysis must be based on some assumptions about the shape of the S–N curve, however large or small the number of parameters used to define it. The straight–line approximation may be found to give a poor fit in the case of good data. The assumption that the logarithm of the endurance are normally distributed with the same standard deviation at all stress levels is evidently untrue. The $S$ shaped types of S–N curves, like those suggested by Weibull [130] or Bastenaire [22] (Section 4.2.4), may be considered to provide a more appropriate representation.

**Possible statistical methods:** The method of analysis appropriate in any given case should be selected on the principle that the simplest statistical model that will fit the available data with acceptable precision is the right one to use. Precision refers to the inferences drawn about the parent population that might have produced the data rather that to a description of the individual set of data.

Multiple regression may be appropriate for well documented data. Otherwise the regression and the confidence limits calculated will be distorted. In any case, if the data contain run-outs, a method based on maximum likelihood is needed to take account of these.

A graphical analysis developed on the assumption of a uniform shape of the S–N curves for comparable test series but allowing for variation in the parameter $S_a$ (stress amplitude) that defines the fatigue strength at $2 \times 10^6$ cycles has been described elsewhere in detail [78].

In the next lines, two different forms for determining the parameters of the distributions are analyzed. The first is the combination of set of data, used with normal distribution data. The second one is the maximum likelihood method.

**Combining set of data:** This technique can be illustrated by applying it to samples drawn from a normally distributed population: If the population means is $\mu$ and its variance is $\sigma^2$, the probability of drawing a sample value $y_i$ is

$$\frac{1}{\sigma\sqrt{2\pi}} \exp\left[-\frac{1}{2}\left(\frac{y_i-\mu}{\sigma}\right)^2\right] dy, \tag{4.25}$$

the logarithm of which is

$$-\frac{1}{2}\left(\frac{y_i-\mu}{\sigma}\right)^2 - \ln\sigma + \ln\frac{dy}{\sqrt{2\pi}}. \tag{4.26}$$

The last term in the expression is constant for all values of $\mu$ and $\sigma$ and, therefore, of no interest in likelihood ratio

$$L = -\frac{1}{2}\left(\frac{1}{\sigma^2}\sum_1^n (y_i-\mu)^2 + n\ln\sigma^2\right) = -\frac{n}{2}\left(\frac{1}{\sigma^2}((\bar{y}-\mu)^2+s^2) + \ln\sigma^2\right). \tag{4.27}$$

For run-outs in fatigue test, the probability is given by the condition that no failure has occurred up to certain value of $y_i$, where $y_i$ is the logarithm of the endurance. The probability is

$$\frac{1}{\sqrt{2\pi}} \int_{-\infty}^{(y_i-\mu)/\sigma} \exp\left[-\frac{1}{2}\xi^2\right] d\xi \tag{4.28}$$

and the likelihood is

$$\ln\left(\frac{1}{\sqrt{2\pi}} \int_{-\infty}^{(y_i-\mu)/\sigma} \exp\left[-\frac{1}{2}\xi^2\right] d\xi\right). \tag{4.29}$$

**The Likelihood method applied to S–N curves:** The only difference between this calculation and a form of regression analysis is that both $\mu$ and $\sigma$ become functions of the independent variable $x$.

When the prevoius method is applied to the analysis to S–N data, the transformed variables $\log N$ and $\log S_a$ are most commonly used. To specify the shape of the S–N curve the following information is needed:

1. The fatigue strength $S_A$ at $2 \times 10^6$ cycles,
2. The slope, $k$,
3. The standard deviation, $s$, of $\log N$ and $\log S_a$, and
4. The position of change of slope $N_E$ at stress $S_E$ are to be considered as parameters of a simple model (see figure 4.8)

An additional parameter, $\alpha$, was introduced to specify the mode of transition and the typical values are in the interval $\alpha \in [10, 100]$. For $\alpha = \infty$, the model degenerates to the

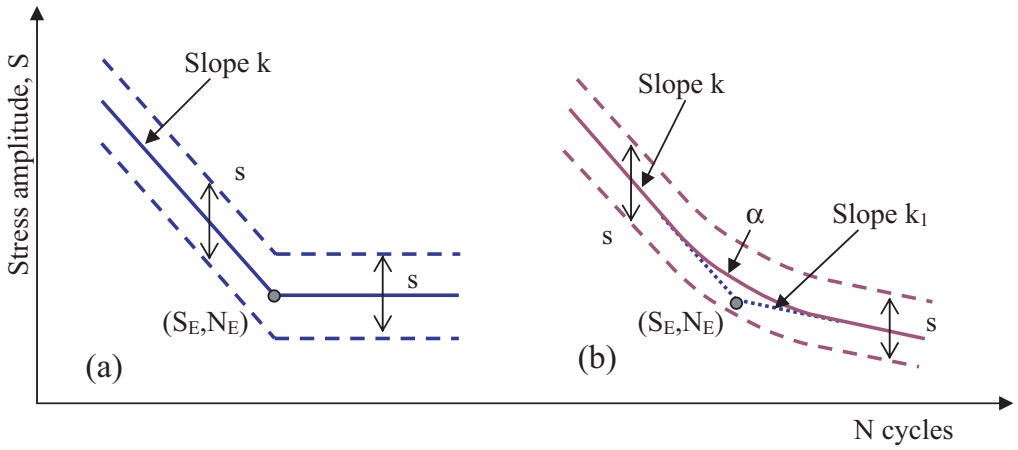


Figure 4.8: Shapes of S–N curve considered: (a) simple model, (b) extended model [126].

simple one changing slope abruptly. Analytically, the S–N curve for the extended model is given by the equation

$$Y = 0.5(k + k_1)x + 0.5(k - k_1)\left(|x| + \frac{1}{\alpha}\ln\left[1 + \exp(-2\alpha|x|)\right]\right), \tag{4.30}$$

where $Y = \log N/N_F$, and $x = \log S/S_E$.

**Example of application:** The described method of determining the shape of the S–N curves will be illustrated in the next lines. The data is presented in table 4.2 and in figure 4.9.

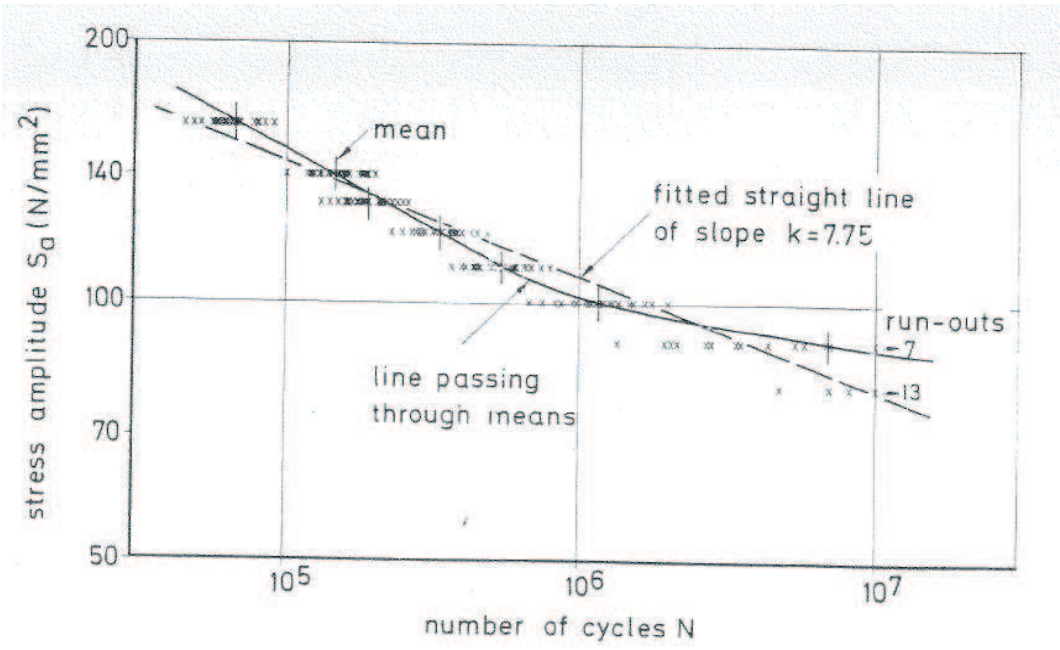


Figure 4.9: S–N curve established by 20 tests per stress level [126].

Table 4.2: Jointly best supported parameters of the S–N curve as a function of the cutoff points derived for the data from figure 4.9. figure from [126]

| Run No. | Cutoff $N_E$ | Slope $k$ | SD of logS $s$ | Endurance Limit, $S_E$ | Likelihood method | Additional criterium |
|---|---|---|---|---|---|---|
| Slope changing abruptly to the horizontal | | | | | | |
| 1 | $0.6 \cdot 10^6$ | 4.00 | 0.0326 | 98.1 | 213.0 | |
| 2 | $1.0 \cdot 10^6$ | 5.00 | 0.0228 | 94.8 | 203.9 | |
| 3 | $1.5 \cdot 10^6$ | 5.50 | 0.0176 | 91.2 | 236.5 | |
| 4 | $2.0 \cdot 10^6$ | 6.00 | 0.0162 | 89.5 | 236.5 | |
| 5 | $3.0 \cdot 10^6$ | 6.50 | 0.0175 | 86.7 | 221.6 | |
| 6 | $10.0 \cdot 10^6$ | 7.75 | 0.0246 | 79.5 | 130.7 | |
| Slope changing continuously to the horizontal ($\alpha = 20$) | | | | | | |
| 7 | $2.0 \cdot 10^6$ | 4.00 | 0.0215 | 76.8 | 249.5 | 249.0 |
| 8 | $3.0 \cdot 10^6$ | 5.00 | 0.0194 | 75.2 | 251.7 | 250.9 |
| 9 | $5.0 \cdot 10^6$ | 5.50 | 0.0176 | 72.6 | 250.8 | 248.2 |
| 10($\alpha = 25$) | $3.0 \cdot 10^6$ | 5.25 | 0.0185 | 77.8 | 251.1 | |

The determination of the cutoff point depends of the type of curve we chose. In the case of an S–N curve with the slope changing abruptly to the horizontal, the best supported cutoff point is found by interpolation between points 3 and 4 (see table 4.2). And better fit is obtained with a continuously changing slope (see figure 4.9).

The value of $N_E$ is found to be slightly lower, and the confidence limits become narrower when the additional criterion is used (see figure 4.10).

### 4.2.6 The Pascual and Meeker model

This model [107], describes the relationship between fatigue life and applied stress and provides and illustrates the corresponding data analysis methods. This work is motivated by the need to develop and present quantitative fatigue–life information used in the design of jet engines.

Fatigue data are often presented in the form of a median S–N curve, a log–log plot of cyclic stress or strain $s$ versus the median fatigue life $N$. An extension of this concept is the $p$ quantile S–N curves, also called *S–N–P curves*, a generalization that relates the $p$ quantile of fatigue life to the applied stress or strain. Thus, each curve represents a constant probability of failure $p$, as a function of $s$. We shall use the 0.05 and 0.95 quantile S–N curves to illustrate the variability of fatigue life.

Fatigue data on ferrous and titanium alloys indicate that experimental units tested below a particular stress level are unlikely to fail [107]. The S–N curve for these materials exhibits a strong curvature and an asymptotic behavior near the fatigue limit. Most nonferrous metals such as aluminum, copper, and magnesium appear not to have a fatigue limit.

For nonferrous materials, it is common practice to define the "fatigue strength" to be the stress level below which failure will not occur before an arbitrary large number of cycles. Collins [52] and Dieter [56] defined fatigue strength as such and used the term fatigue limit to imply infinite life. On the other hand, to represent fatigue strength at a prescribed long but finite life, Nelson [101], and Colangelo and Heiser [51], used the term endurance limit, whereas others use the term fatigue limit.

There are two main considerations in modeling the relationship between the applied stress

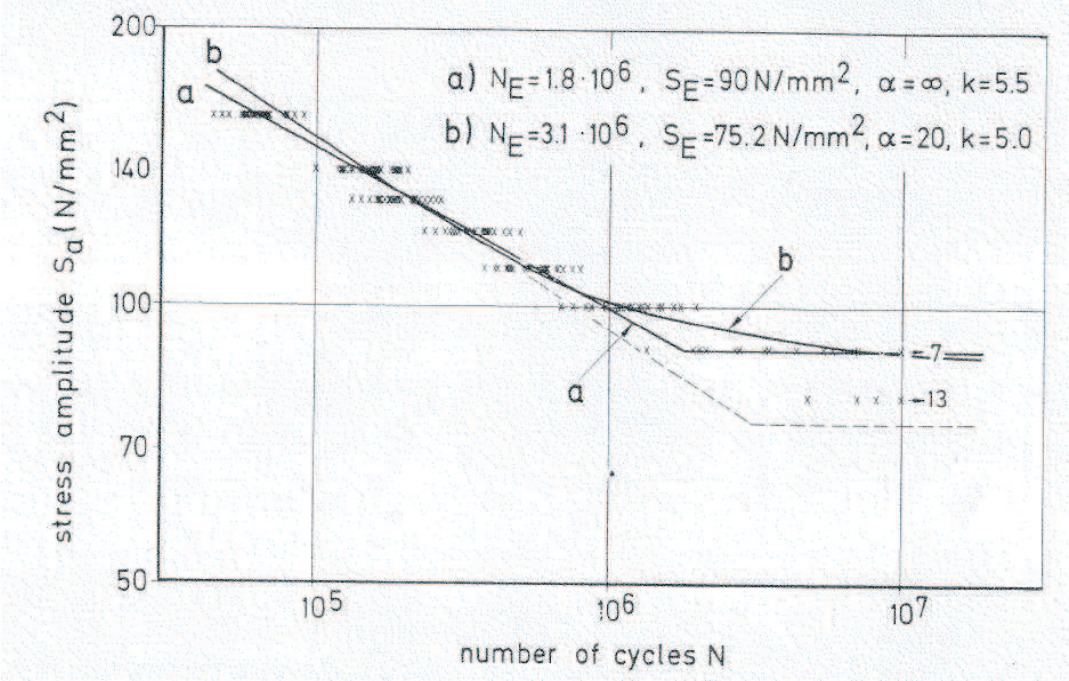


Figure 4.10: Best supported S–N curves: (a) changing slope abruptly to the horizontal; (b) changing slope continuously to the horizontal as fitted to the set of data from figure 4.9. figure from [126].

and fatigue life. First, often the standard deviation of fatigue life decreases as the applied stress increases. Second, curvature in fatigue curves suggests the inclusion of a fatigue limit in the statistical model for fatigue life. The random fatigue-limit model describes both characteristics.

Let $Y$ be the fatigue life and $s$ the stress level. We model $Y$ as

$$\log(Y) = \beta_0 + \beta_1 \log(s - \gamma) + \epsilon, \tag{4.31}$$

where $\beta_0$, and $\beta_1$ are fatigue curve coefficients, $\gamma$ is the fatigue limit of the specimen, $\epsilon$ is the error term, and log denotes natural logarithm. Let $V = \log(\gamma)$, and suppose that $V$ has probability density function (pdf)

$$f_V(v; \mu_\gamma; \sigma_\gamma) = \frac{1}{\sigma_\gamma} \phi_V \left( \frac{v - \mu_\gamma}{\sigma_\gamma} \right), \tag{4.32}$$

with location and scale parameters $\mu_\gamma$ and $\sigma_\gamma$, respectively. $\phi_V()$ is either the standardized smallest extreme value (sev) or normal pdf.

Let $x = \log(s)$ and $W = \log(Y)$. Assume that, conditioned on a fixed value of $V < x, W|V$ has pdf

$$f_{W|V}(w; \beta_0; \beta_1; \sigma; x; v) = \frac{1}{\sigma} \phi_{W|V} \left( \frac{w - (\beta_0 + \beta_1 \log(\exp x - \exp v))}{\sigma} \right) \tag{4.33}$$

with location parameter $\beta_0 + \beta_1 \log(\exp x - \exp v)$ and scale parameter $\sigma$. $\phi_{W|V}$ either the standardized *sev* or normal *pdf*. The marginal *pdf* of $W$ is given by

$$f_W(w; x\theta) = \int_{-\infty}^{\infty} \frac{1}{\sigma\sigma} \phi_{W|V} \left( \frac{w - \mu(x, v, \theta)}{\sigma} \right) \phi_V \left( \frac{v - \mu_\gamma}{\sigma_\gamma} \right) dv, \tag{4.34}$$

where $\theta = (\beta_0; \beta_1; \sigma; \mu_\gamma; \sigma_\gamma)$ and $\mu(x, \upsilon, \theta) = \beta_0 + \beta_1 \log(\exp x - \exp \upsilon)$.The marginal cumulative distribution function (*cdf*) of $W$ is given by

$$F_W(w; x\theta) = \int_{-\infty}^{\infty} \frac{1}{\sigma} \Phi_{W|V} \left( \frac{w - \mu(x, \upsilon, \theta)}{\sigma} \right) \phi_V \left( \frac{\upsilon - \mu_\gamma}{\sigma_\gamma} \right) d\upsilon, \tag{4.35}$$

where $\Phi_{W|V}$ is the cdf of $W|V$. We will refer to this statistical model as the random fatigue-limit model. There are no closed forms for the density and distribution functions of $W$.

To estimate the parameters of the random fatigue-limit model the authors use ML methods. Statistical theory suggests that ML estimators, in general, have favorable asymptotic (large-sample) properties. For "large" sample sizes and under certain conditions on the fatigue life distribution, the distribution of ML estimators is approximately multivariate normal with mean vector equal to the vector of true values being estimated and standard deviations no larger than that of any other competing estimators.

When fatigue limits exist, plots of fatigue life versus stress–strain often exhibit curvature at lower stress–strain levels. Moreover, in most fatigue experiments, the variance of fatigue life decreases as stress–strain increases and the standard deviation is often modeled as a monotonic function of stress–strain.

### 4.2.7 The Kohout and Vechet models

The authors present a complex function that can be used in all range of lifetime (from low–cycle fatigue region to high–cycle region). But this function can be reduced in other simpler expressions to make the use of the model easier in one special part.

A new function is proposed for the description of fatigue curves in both low and high–cycle fatigue regions [86], i.e. for the whole region of cycles from tensile strength to permanent fatigue limit (usually described by the Palmgren function). In each cycle region it can be simplified; in fact it changes into the Basquin function in the region of finite life and an analogy of the Stromeyer function for the high–cycle fatigue region can also be obtained (Equations (4.2) and (4.4)).

The contribution of the present authors (Kohout and Vechet [85] and [84]) consists in extending the Basquin function to the low and the high–cycle regions symmetrically, besides replacing N with $N + B$ for the extension to the low-cycle region:

$$\sigma(N) = aN^b \rightarrow \sigma(N) = a(N + B)^b, \tag{4.36}$$

where $a$ is a parameter of the Basquin and some other functions (extrapolated value of function or of the tangent in the point of inflexion for $N = l$)[MPa], $b$ a parameter of the Basquin and some other functions (in log-log fit the slope of oblique asymptote or of the tangent in the point of inflexion), and $B, C$ is a parameter of new function (see figure 4.11).

For its extension to the high–cycle region, in some cases $1/N$ has been replaced with $1/N + 1/C$, obtaining:

$$\sigma(N) = aN^b = a \left( \frac{1}{N} \right)^{-b} \rightarrow \sigma(N) = a \left( \frac{1}{N} + \frac{1}{C} \right)^{-b} = a \left( \frac{NC}{N + C} \right)^b. \tag{4.37}$$

Finally, both extensions can be made simultaneously, but because $B << C$ (their values differ by many orders of magnitude) quantity B can be neglected in the sum $B + C$ resulting the function:

$$\sigma(N) = a \left( \frac{(N + B)C}{N + C} \right)^b \tag{4.38}$$

It represents the new function for the description of fatigue curves in both the low- and the high–cycle fatigue regions, i.e. over the whole range of lifetime.

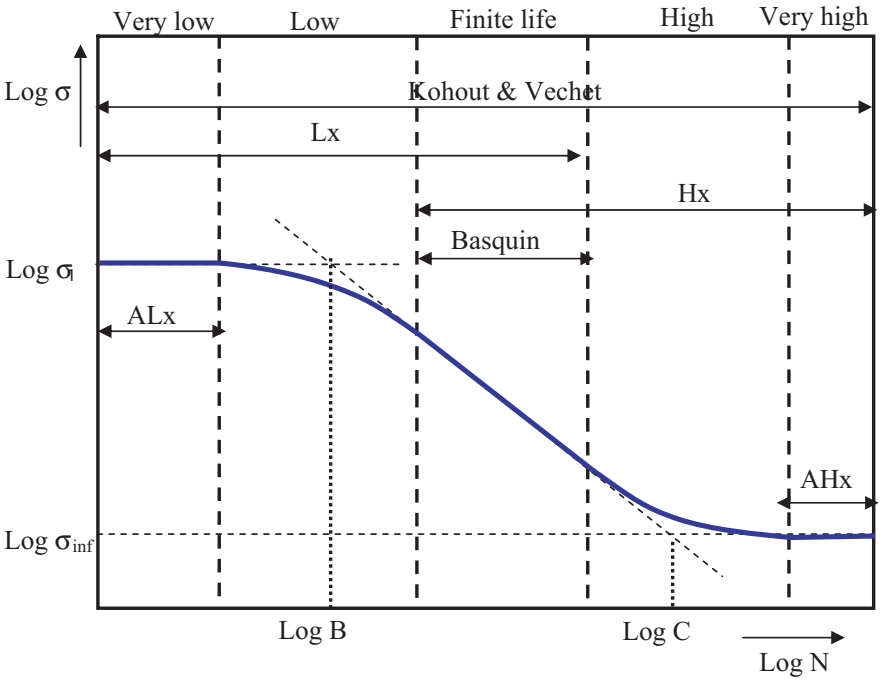


Figure 4.11: Regions of validity of its simplified forms [86].

The new function (Equation (4.38)) can be simplified for various regions of the number of cycles. The regions of the number of cycles where the above relations are valid are shown in figure 4.11. Region named $L_X$ represents the very low–cycle region, which corresponds with Equation (4.2). Similarly, region $H_X$ represents the very high–cycle region (Equation (4.37)) and regions $AL_X$ and $AH_X$, which corresponds with asymptotes of Equations (4.2) and (4.37), that is:

$$\begin{aligned} \sigma(N) = aB^b = \sigma_1 \quad &\rightarrow \quad AL_X, \\ \sigma(N) = aC^b = \sigma_\infty \quad &\rightarrow \quad AH_X. \end{aligned} \tag{4.39}$$

Comparing the curves corresponding to the new ($H_x$) and the Stromeyer functions in figure 4.12 it can be seen that in the range of experimental values the curves differ in their positions only unsubstantially and the values of fatigue limit for $10 \cdot 10^7$ cycles are practically identical. But the curves differ substantially in their directions (slopes) in the margins of measured range. For a very high number of cycles the curve corresponding to the new function is practically constant with stress values only slightly lower than the fatigue limit for $10 \times 10^7$ cycles.

For a low number of the cycles the curve of new function merges with the oblique asymptote while the slope of the Stromeyer curve substantially increases with decreasing number of cycles. In both cases the extrapolation by means of the new function is substantially closer to reality than the extrapolation by the Stromeyer curve. The asymptotes of the new function can be used for estimation as well as extrapolation of the fatigue curve and they are nearly identical to the broken straight line used earlier as the fatigue curve.

All the above means that the new function ($H_x$) is very suitable for extrapolating out of the range of measured data while the use of the Stromeyer function cannot be recommended to this purpose.

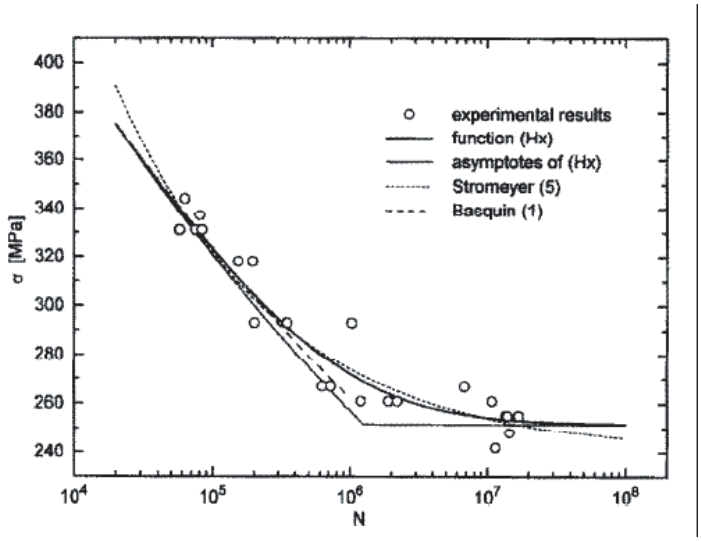


Figure 4.12: Comparison of regressions by the Basquin function (Equation (4.1)) for $N << 10^6$, the Stromeyer function (Equation (4.36)), and new function ($Hx$) with its asymptotes. figure from [86].

## 4.3 New statistical models: Castillo's models

In 1985, a hyperbolic approximation of the lifetime stress level curves was developed by Castillo et al. [37]. starting with this model, several methods have been presented by this researcher with the aim of find the best model to define the lifetime (stress approach) of a material ([35], [39], [42], [36], [37] and [44]). These models for the analysis of lifetime data are derived based on physical and statistical considerations.

When modeling fatigue and other similar lifetime data, models such as those in table 4.1 are selected mainly because of their mathematical tractability, simplicity and/or concordance with the data. But, models should be derived based on physical and statistical considerations. These considerations require that fatigue models should satisfy the following considerations (see [37] and [44]):

1. **Weakest link principle:** If a longitudinal element is divided into $n$ sub-elements, its fatigue life must be the fatigue life of the weakest element [62]. The weakness of a subpiece is determined by the size of its largest crack and the stress it is subjected to.

2. **Independence:** The fatigue strengths of two non-over lapping subelements are independent random variables.

3. **Stability:** The cumulative distribution function (cdf) model must be valid for all lengths, but with different parameters.

4. **Limit value:** The cdf should encompass extreme lengths. Thus, the cdf must belong to a family of asymptotic functions.

5. **Limited range of the random variables involved:** The variables have a finite lower end, which must coincide with the theoretical lower end of the selected cdf.

6. **Compatibility:** The distribution of lifetime given stress level should be compatible with the distribution of the stress level given lifetime; that is, if $F_X(x, y)$ is the cdf of $X$ given $y$, and $F_Y(y, x)$ is the cdf of $Y$ given $x$ then

$$F_X(x, y) = F_Y(y, x). \tag{4.40}$$

With all these model conditions (see [35], [39], [42], [36], [37] and [44]) the authors proposed a new solution to the problem. In particular they dealt and gave adequate answers to the following questions [36]:

**Question 1:** Is it possible to extrapolate S–N curves derived from laboratory results for a given stress level to another stress level conditions?

**Question 2:** We can one predict the fatigue damage associated with a given arbitrary pair $\sigma_{max}; \sigma_{min}$ from laboratory results obtained for a given stress level?

**Question 3:** If the answers to the above two questions are negative, we can ask the following question: what is the minimum information required to make the above extrapolation possible?

**Question 4:** Are the existing fatigue models able to adequately use this information to achieve the above aims? If the answer is negative, what changes are required in the models to solve the problem?

**Question 5:** What is the associated testing strategy (test design) able to produce the data required by the valid model?

**Question 6:** Once the lab tests have been conducted and the model selected, are there models and explicit formulas to perform the above extrapolation or interpolation?

### 4.3.1 The general model for lifetime evaluation: The Weibull model

In this subsection we introduce the Weibull model (see [35], [38], [36], [48]) with some of its properties, applicable to lifetime problems.

Like the Bastenaire model, studied in Section 4.2.4, this model is based on the implementation of a probability distribution to define the relation between lifetime and loads (P–S–N curves). But in this case, contrary to Bastenaire and Spindel and Haibach hypothesis (see [22], [126]), the probability function is not a normal distribution. In fatigue the probability of failure can be assumed ro be an extremal distribution, in this case a Weibull distribution.

The cumulative distribution function (cdf) of the three–parameter Weibull family is given by:

$$F(x; \lambda, \delta, \beta) = 1 - \exp\left[-\left(\frac{x-\lambda}{\delta}\right)^{\beta}\right] \quad x \geq \lambda \quad ; \quad -\infty < \lambda < \infty, \delta > 0, \beta > 0, \tag{4.41}$$

where $F(x; \lambda, \delta, \beta)$ represents the probability of the event $X \leq x$, and $\delta, \lambda$ and $\beta$ are the scale, the location (minimum possible value of the random variable $X$), and the shape parameter, respectively. When $X$ has the cumulative distribution function in 4.41 we write $X \sim W(x; \lambda, \delta, \beta)$.

Its mean and variance are:

$$\begin{aligned} \mu &= \lambda + \delta\Gamma[1 + 1/\beta] \\ \sigma^2 &= \delta^2[\Gamma[1 + 2/\beta] - \Gamma^2[1 + 1/\beta]], \end{aligned} \tag{4.42}$$

and the corresponding percentiles are:

$$x_p = \lambda + \delta[-\log(1 - p)]^{1/\beta} \quad ; \quad 0 \leq p \leq 1. \tag{4.43}$$

Before selecting a model to solve an engineering problem, the relevant variables involved must be identified. By previous experience, accumulated in the study of the fatigue phenomenon, we know that the five variables initially involved in the fatigue problem are: $p, N, N_0, \Delta\sigma$ and $\Delta\sigma_0$, where $p$ is the probability of fatigue failure of a piece when subject to $N$ cycles at a stress range $\Delta\sigma$, $N_0$ is the threshold value for $N$, the minimum lifetime for any $\Delta\sigma$, and $\Delta\sigma_0$ is the endurance limit, below which fatigue failure does not occur.

However, this initial number of variables can be reduced. The $\prod$ Theorem allows representing any existing relation among the initial variables in terms of another smaller set of non-dimensional variables. In fact, a dimensional analysis of the initial set of 5 variables leads to a set of 3 non-dimensional variables. It seems convenient to choose $N/N_0$, $\Delta\sigma/\Delta\sigma_0$ and $P$ as these variables.

Solving the problem with functional equation ([49] and [45]), the resulting model is:

$$F(N^*, \Delta\sigma^*) = 1 - \exp\left[-\left[\frac{(N^* - B)(\Delta\sigma^* - C) - \lambda}{\delta}\right]^{\beta}\right] \quad ; \quad N^* \geq B + \frac{\lambda}{\Delta\sigma^* - C}, \tag{4.44}$$

where $N^* = N/N_{ref}$ and $\Delta\sigma^* = \Delta\sigma/\Delta\sigma_{ref}$, $N_{ref}$ and $\Delta\sigma_{ref}$ are the number of cycles and the stress level of reference, respectively, $B, C, \lambda, \delta$ and $\beta$ are the non-dimensional model parameters. Their physical meanings (figure 4.13) are the following:

B: threshold value of lifetime.

C: endurance limit.

$\lambda$: position of the corresponding zero-percentile hyperbola.

$\delta$: scale factor.

$\beta$: Weibull shape parameter of the whole cdf in the S–N field.

We note that the percentile curves are hyperbolas which share the asymptotes.
The principal conclusions of this model may be summarized as follows:

1. The use of non-dimensional variables simplifies the problem under consideration and clarifies what is the minimal set of variables, or functions of them, which are relevant to the problem, and allows working with non-dimensional parameters that have many important advantages, apart from independency of the set of selected units, as a better numerical behavior.

2. Physical and engineering considerations allow rejecting many models non satisfying the associated constraints. These considerations can be written, in many cases, in terms of functional equations, that lead to explicit forms for the mathematical and statistical models.

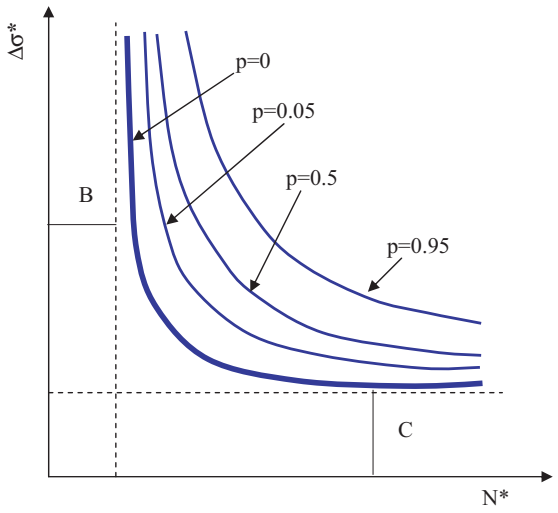


Figure 4.13: Graphical representation of the Weibull model. Percentiles curves representing the relationship between lifetime, $N^*$, and stress range, $\Delta\sigma^*$, in the S–N field [44].

3. A Weibull based model for the S–N field has been obtained by solving a functional equation. This model is useful not only to fit fatigue data, but also to explain the fatigue behavior of longitudinal elements.

4. There are two types of parameters. One is related to the non-dimensional variables, and used for normalization purposes and includes the threshold parameters $N_0$ and $\Delta\sigma_0$. Other type of parameters are statistical parameters, as the location parameter $\lambda$, the scale parameter $\delta$, and the shape parameter $\beta$.

5. The probabilities of failure associated with a given load history can be easily calculated.

The authors have been working with other aspect in the model. A comparison between the up–and–down method (Section 3.4) and the Weibull model has been made by the authors, concluding that the up-and-down method neglects important information contained in the data making it very expensive and inefficient when compared with other alternative models [48]. Furthermore, the problem of estimating the $S-N$ field based on samples with different lengths and testing the hypothesis of length independence of fatigue lifetimes has also been analyzed by the authors, concluding that the length independence assumption cannot be accepted for the prestressing wires data, while it is a reasonable assumption for the prestressing strands data [**?**].

Model (4.41) has been studied and successfully applied to different cases of lifetime problems such as plain concrete, prestressed wires and strands with different lengths, etc.

## 4.4 Discussion

The last two sections study the principal models used in fatigue to predict and estimate the lifetime of a material. In this section, the advantages and shortcomings of these models are analyzed and discussed.

This chapter has analyzed nine models used in fatigue. The main conclusions after comparing them are:

- The Basquin model [20] and the Palmgren–Miner rule [59] make an approximation to fatigue law easier.
- There are models which analyze the fatigue in all the fatigue regions (low–cycle region and high–cycle region). Kohout & Vechet model [86] are part of this group. But the parameter estimation is complex.
- Some of these models, such as the up–and–down method or the Spindel & Haibach model [126] are used to determine the endurante limit of a material.
- The Palmegren–Miner's rule allows us analyze a variable load history, but the model needs to know the behavior of the material in each stress level for a constant load.
- The relation between probability of failure, stress level and number of cycles to failure (P–S–N) is provided in Bastenaire [22], Pascual & Meeker [107] and Castillo's models ([38] and [36]).
- Only Castillo's model and Pascual and Meeker Model, define the probability of failure with an extremal distribution. In the other cases the authors choose normal distributions, but this distribution is not valid for the fatigue of material (extremal process).
- The only model that can be extrapolated to other range of loads after the model parameters have been estimated is the Castillo model. Remember that in the Bastenaire model, when the author represents points outside the estimation range, he obtains negative values of $\varphi$.

An evolution of fatigue models has been presented in these sections. All of them allow analyzing different stress histories, some constant and other variable load histories, but none of them can be used to study the behavior of material in all the load range, i.e. mixing tension and compression loads.

Actually, the most useful models are based on statistic and probabilistic concepts, like Castillo's Model. So, the principal aim of this thesis is to develop a new statistic and probabilistic model covering the tension and compression Wöhler fields.

# Chapter 5

# Use of Functional Equations

The aim of this Chapter is to introduce readers into the field of functional equations which have shown very useful in some applications, such as model design. We are aware that this is not an easy task, and that any effort to bring together mathematicians and engineers, as experience shows, has many related difficulties.
The model derived in chapter 6 has been obtained thanks to this theory.

## 5.1 Introduction

The modeling or idealization of the problem under consideration (structure, road, harbor, water supply system, etc.) should be sufficiently simple, logically irrefutable, admitting a mathematical solution, and, at the same time, represent sufficiently well the actual problem. Experienced engineers and scientists know how a successful design depends on an adequate selection of the model and method of analysis. As in any other branch of knowledge, the selection of the idealized model should be achieved by detecting and representing the essential first-order factors, and discarding or neglecting the inessential second order factors.

Functional equations are a tool that avoids arbitrariness and allows selection of models to be based on adequate constraints.

Though the theory of functional equations is very old (some examples of functional equations appear in Oresme (see [103], [104]), Napier (see [100], [101]), Kepler [82], Galileo [71], Abel (see [8],[9] and [10]), not only technicians but many mathematicians are still unaware of the power of this important field of Mathematics and in many fields of Applied Science. This chapter is based on the Castillo et al.'s book (see [46]) and others as Aczél [12], Rassias [113], Balasubrahmayan [17], Anatolij [15], Small [120], Balasubrahmayan [17] and Smital [121].

One of the most appealing characteristics of functional equations is their capacity for model design. In fact, conditions required by many models to be adequate replicas of reality can be written as functional equations. Thus, the engineer finds there an appropriate tool for his design purposes. In this manner, functions are not arbitrarily chosen; on the contrary, they appear as the only solutions to the adequate set of requirements.

We can also cite other ideas about functional equations: *"the theory of functional equations is fascinating because of its instrinsic mathematical beauty as well as its applications.[...] In this*

*field one deals with mathematical identities where the solutions strongly depend upon the domains and the regularity assumptions required for the unknows. Proofs are usually clear, clean, short: elegant arguments come up. Sometimes the equations give you just a little information, but, by using the powerful methods that the theory provides, you can say quite a lot about the general solutions."* said by Cl. Alsina [12].

There exist diverse bibliography where we can find new ideas and methods to solve new problems. We cite here some examples where an extensive study of topics related with functional equations and inequalities is made (see [12] and [113]).

### 5.1.1 One example of functional equation: area of a rectangle (Legendre [89])

Assume that the formula of the area of a rectangle is unknown but given by $f(a, b)$, where $f$ is an unknown function, $b$ is its basis and $a$ is its height. Consider figure 5.1(left) in which the rectangle of basis $b$ and height $a$ has been horizontally divided in two different sub-rectangles with the same basis $b$ and heights $a_1$ and $a_2$, respectively. According to our assumptions, the areas of the sub-rectangles and the initial rectangle cannot be calculated, but they can be expressed in terms of our unknown $f$ function as $f(a_1, b)$, $f(a_2, b)$, and $f(a_1 + a_2, b)$, respectively. Similarly, we can perform the division vertically, as shown in the right rectangle of the same figure, and write the areas of the resulting rectangles as $f(a, b_1)$, $f(a, b_2)$, and $f(a, b_1 + b_2)$, respectively.

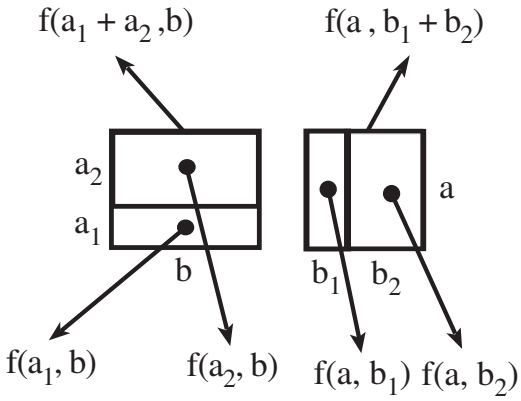


Figure 5.1: Basic rectangles. figure from [46].

Stating that the areas of the initial rectangles must be equal to the sum of the areas of the sub-rectangles, we get the functional equations

$$\begin{aligned} f(a_1 + a_2, b) &= f(a_1, b) + f(a_2, b) \\ f(a, b_1 + b_2) &= f(a, b_1) + f(a, b_2). \end{aligned} \tag{5.1}$$

Because $b$ is constant in the first equation and $a$ is constant in the second, both equations become Cauchy's Equation, we have

$$f(a, b) = c_1(b)a = c_2(a)b,$$

where $c_1(b)$ and $c_2(a)$ are initially arbitrary functions, but due to the second identity, they must satisfy the condition

$$\frac{c_1(b)}{b} = \frac{c_2(a)}{a} = c,$$

which implies

$$f(a, b) = cab, \tag{5.2}$$

where $c$ is an arbitrary positive constant.

As a consequence, the area of a rectangle is the product of its basis $a$, its height $b$ and a constant $c$.

This proves that the area of a rectangle is not the well known "basis × height", but "a constant × basis × height". The constant takes care of the units we use for the basis, the height and the area. This means that if $b$ is measured in inches, $h$ in feet, and we want $f$ in square miles, the constant must be different from the constant required for the case of $b$ measured in meters, $h$ in kilometers, and $f$ in square meters.

The interesting result is that functional equations discover the need to consider the units of measure.

## 5.2 History of functional equations

The use of the functional equations comes from much longer period that the formal mathematic discipline has existed.

One of the first mathematician who worked with functional equations was **Nicole Oresme** (1323-1382), who provided an indirect definition of linear functions by means of a functional equation. In 1352, Oresme wrote the *Tratatus de configurationibus qualitatum et motuun* in which the definition of a functional relationship between two variables is defined, and furthermore he defined the idea of that one can express this relationship geometrically by what we would now call a graph (well ahead of Réné Descartes) [120].

We have three distinct real numbers $x$, $y$ and $z$, which describe a linear functional equation. Associated with $x$, $y$ and $z$ we have a variable that can be writen as $f(x)$, $f(y)$ and $f(z)$, respectively. The function $f$ is defined to be linear (i.e. a quality which is uniform) if:

$$\frac{y - x}{z - y} = \frac{f(y) - f(x)}{f(z) - f(y)}, \tag{5.3}$$

for all distinct values of $x$, $y$ and $z$.

What makes Oresme's definition a functional equation is that $f$ is treated abstractly: one may plug any function into this equation to see whether the equation is satisfied for all possible values of $x$, $y$, and $z$. We can compare this with the standard definition to be found in most modern textbooks which say that a linear funciton is one of the form:

$$f(x) = ax + b, \tag{5.4}$$

for some $a$ and $b$.

Over the next few hundred years, functional equations were used but no general theory of such equation arose. Other important mathematician was **Gregory of Saint–Vicent** (1584–1667), whose work on the hyperbola made implicit use of the functional equation $f(xy) = f(x) + f(y)$, pioneered the theory of the logarithm.

In the year 1647 he wrote *Opus Geometricum quadraturae circuli et sectionum coni*, in which the deal is to present methods for calculating areas and the properties of conic sections. He made great progress on the problem of logarithm using purely geometric arguments: *"If a planar region is stretched horizontally by a given factor, and simultaneously shrunk vertically by*

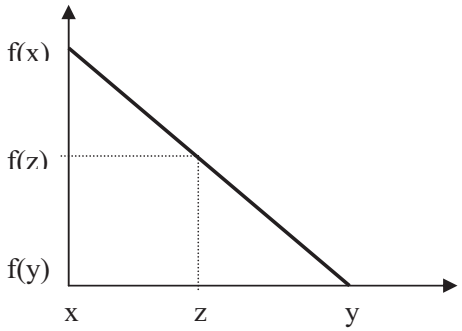


Figure 5.2: Schematic definition of linear functions [120].

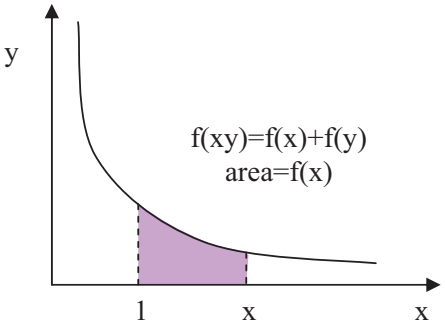


Figure 5.3: Schematic definition of logarithmic functions [120].

*the same factor, then the resulting region will have an area which is equal to that of the original region"*, both regions have the same area. Thus, using the scaling argument we have:

$$f(x) = f(xy) - f(y), \tag{5.5}$$

or equivalently,

$$f(xy) = f(x) + f(y), \tag{5.6}$$

That is a functional equation for the family of logarithms. However, the theoretical work which links this functional equation to the family of logarithms had to wait for the work of Augustin-Louis Cauchy [120].

The subject of functional equations is more properly dated from the work of **A. L. Cauchy**, born in 1789. The functional equation that is particularly associated with Cauchy is:

$$f(x + y) = f(x) + f(y), \tag{5.7}$$

for a real $x$ and $y$, and is now called *Cauchy's equation*. It is required to find all real-valued functions $f$ satisfying Equation (5.7), but any function of the form

$$f(x) = ax, \tag{5.8}$$

can satisfied the Cauchy's equation (always with $a$ a real number).

Historically, **Jean d'Alambert** precedes Cauchy. However in the context of functional equations, it seems more natural to consider his contribution after Cauchy. In his efforts to

understand the principles of combinations of forces, d'Alambert was led to the equation:

$$g(x+y)+g(x-y)=2g(x)g(y), \tag{5.9}$$

where $0 \leq y \leq x \leq \pi/2$. This equation is called d'Alambert equation. Find the solution for this equation is not easy. The Equation (5.9) is reminiscent of a trigonometric identity, thus we need to look inside trigonometric functions to look for the solution [121]. Finally, the solution to this equation has the form:

$$g(x) = b\cos ax, \tag{5.10}$$

for suitable chosen constant $a, b$. However, letting $x = y = 0$ in Equation (5.9) reduces it to the equation $g(0) = g(0)^2$, telling us that $g(0) = 0$ or $g(0) = 1$, that correspond with $b = 0$ or $b = 1$ respectively. The constant $a$ turns out to be arbitrary.

To finish with this review of the firsts mathematicians who worked with functional equations, we present next **Charles Babbage**. One property that both Cauchy's and d'Alambert's equations have in common is that, although they involve functions of a single variable, the equations are formulated using two variables, namely $x$ and $y$, but Babbage investigated other class of completely different functional equations [120].

Babbage is the founder of modern computing and with a different engine. One of his inventions is the cowcatcher, a remarkable device that was attached to the front of trains to remove obstacles (such as cows) that might cause the train to be derailed. On 1815, one paper changes the life of this mathematician. This paper defines some mathematical calculus about direct and inverse functions. Babbage defines a set of functions that satisfied this calculus, thus, a set of functional equations and their solutions increasing generality and complexity to the functional equation theory.

## 5.3 Basic concepts and definitions

It is not easy to give a precise definition of functional equation. Castillo et al. in [46] define some ***concepts*** to make the understanding of the problem easier.

**Definition 5.1** ***Functional equation:*** *In a broader sense, a functional equation can be considered as an equation which involves independent variables, known functions, unknown functions and constants; but we exclude differential equations, integral equations and other kinds of equations containing infinitesimal operations. In our equations, the main operation is the substitution of known or unknown functions into known or unknown functions.*

**Definition 5.2** ***System of functional equations:*** *A system of functional equations is a set of $n \geq 2$ functional equations.*

**Definition 5.3** ***Domain of a functional equation:*** *Given a functional equation, the set of all values of the variables, on which it is supposed to hold, is called its domain (not to be confused with the domain of definition of each known or unknown function appearing in it).*

If the functional equation comes from a physical problem we can talk about its *natural domain*, as the set of values of the variables with a physical sense.

Sometimes we find functional equations which are stated on a *restricted domain*, that is, restricted when compared with their natural or initial domain. In this case two different names have been proposed: *"functional equations on restricted domains"*, [87], and *"conditional functional equations"*, [55].

It is interesting to point out that the domain of the functional equation can be independent of the unknown functions or dependent on them.

**Definition 5.4** ***Particular solution*** *We say that a function or a set of functions is a particular solution of a functional equation or system if, and only if, it satisfies the functional equation or system in its domain of definition.*

**Definition 5.5** ***General solution*** *Given a class of functions $\mathcal{F}$, the general solution of a functional equation or system is the totality of particular solutions in that class.*

To obtain the general solution of a functional equation (or system), the following considerations must be taken into account:

1. The general solution of the functional equations can depend on one or more arbitrary constants.
2. In addition to arbitrary constants, arbitrary functions can appear in the general solution. Thus, an infinite number of point conditions could be necessary to get a unique solution.
3. Unlike any other kind of equations, a single equation can determine several unknown functions.
4. To have a well defined equation, its domain of definition (integer, real, complex, etc.) and the domains and ranges of the functions appearing in the functional equation or system should be clearly established. It is important to mention that the general solution of a given functional equation is strongly dependent on its domain of definition.
5. To have a well defined equation, the class (continuity, measurability, differentiability, integrability, etc.) of admissible functions should be given.

To solve a functional equation we have to solve three important points:

1. The equation $E[\mathbf{f}, \mathbf{x}] = 0$.
2. Its domain $D$.
3. The class $\mathcal{F}$ of admissible functions (including domains and ranges).

Thus, a functional equation can be considered as a triplet $(E, D, \mathcal{F})$. This means that we are interested in all functions $f \in \mathcal{F}$ such that

$$E[\mathbf{f}, \mathbf{x}] = 0, \ \ \forall \mathbf{x} \in D,$$

where $\mathbf{f}$ and $\mathbf{x}$ are the vectors of unknown functions and variables, respectively.

Sometimes it is interesting to compare the general solutions of the same functional equation but with different domains and/or classes of admissible functions; that is, the solution of the equation with restricted or enlarged domains or classes of admissible functions. In other words, we want to compare the general solutions of

$$E\left[\mathbf{f}, \mathbf{x}\right] = 0, \ \ \forall \mathbf{x} \in D_1, \ \ \mathbf{f} \in \mathcal{F}_1 \tag{5.11}$$

and

$$E\left[\mathbf{f}, \mathbf{x}\right] = 0, \ \ \forall \mathbf{x} \in D_2, \ \ \mathbf{f} \in \mathcal{F}_2. \tag{5.12}$$

If the sets of all solutions of (5.11) and (5.12) are denoted by $\mathcal{S}_1$ and $\mathcal{S}_2$, respectively, we have

$$\mathcal{F}_2 \subseteq \mathcal{F}_1, \quad \text{and} \quad D_1 \subseteq D_2, \quad \Rightarrow \quad \mathcal{S}_2 \subseteq \mathcal{S}_1. \tag{5.13}$$

These implications are obvious because, on the one hand, an enlargement of the admissible functions allows us an enlargement of the set of all solutions but never a reduction. On the other hand, an enlargement of the equation domain implies a more restrictive equation because this implies more restrictions on the unknown functions (conditions at more points); hence, the set of all solutions may be reduced.

To continue solving the problem we have several methods, based in three steeps:

1. Enlarge the domain og the functional equation.
2. Find its general solution on the enlarged domain.
3. The last steep can be:
   - a.- Use the obtained solutions as particular solutions of the equation on the initial domain.
   - b.- Use the obtained solutions as particular solutions of the equation in the unrestricted class.
   - c.- Find which of the solutions of (5.11) are true solutions of the equation with the initial or unrestricted domain.
   - d.- Determine which of the solutions of (5.11) belong to the initial class.

Of course, many other methods can be used, too. A description of the main methods for solving functional equations will be given in section 5.4.

Note that methods (a) and (b) lead to *particular solutions* of the given functional equation for the initial domain and class. On the contrary, methods (c) and (d) allow the general solution to be obtained in a more restrictive situation. So, the obtained solution may not actually be a solution for the specified domain and class and an additional test is required. In such a case, we shall refer to them as *candidate solutions*. These concepts of general, particular and candidate solutions can be used to obtain computer solutions, even under changes in the domain and/or class of the equation.

Given a functional Equation $(E, D, \mathcal{F})$, it is interesting to find triplets $(E, D_1, \mathcal{F}_1)$ and $(E, D_2, \mathcal{F}_2)$ with $D_1 \subset D \subset D_2$ and $\mathcal{F}_2 \subset \mathcal{F} \subset \mathcal{F}_1$, such that they have the same general solution as the initial equation. In particular, one of the most interesting results is obtained when the sets $D_1, D_2, \mathcal{F}_1$ and $\mathcal{F}_2$ cannot be improved; that is, when they lead to an optimum (a minimum of restrictions) characterization of the general solution set.

**Definition 5.6** ***Equivalent functional equations.*** *Let*

$$E_1[\mathbf{f}, \mathbf{x}] = 0, \quad \forall\, \mathbf{x} \in D, \quad \mathbf{f} \in \mathcal{F}_1 \tag{5.14}$$

$$E_2[\mathbf{f}, \mathbf{x}] = 0, \quad \forall\, \mathbf{x} \in D, \quad \mathbf{f} \in \mathcal{F}_2 \tag{5.15}$$

*be two functional equations. We say that equations (5.14) and (5.15) are equivalent if and only if their general solutions coincide.*

For a detailed treatment of restricted domains see [13], [55] and [87].

## 5.4 Some methods for solving functional equations

There exist several methods to solve functional equations. Now, in this section, a sumary of these methods are given.

Unlike the field of differential equations, where a clear methodology to solve them exists, in functional equations such a methodology does not exist. In fact, in many cases "ad hoc" methods are required. This represents a great shortcoming and perhaps one of the reasons explaining why engineers and applied scientists have not incorporated functional equations into their daily work. To facilitate the use of functional equations we can:

- Elaborate a list including the main functional equations and their corresponding solutions.
- Identify the sets of equations which can be solved using the same methods.

The main methods for solving functional equations to be analyzed are [46]:

1. Replacement of variables by given values
2. Transforming one or several variables
3. Transforming one or several functions
4. Using a more general equation
5. Treating some variables as constants
6. Inductive methods
7. Iterative methods
8. Separation of variables
9. Reduction by means of analytical techniques (differentiation, integration, etc.)
10. Mixed methods

### 5.4.1 Replacement of variables by given values

If we replace one or several variables appearing in the functional equation by carefully selected values, some mathematical relations that give some of the unknown functions or simpler functional equations can be obtained. This method requires a final check of the resulting solutions because the previous replacement leads to equations associated with a set of necessary, but not sufficient, conditions for the functions to be solutions of the initial equation.

Section 5.5.6 Euler's equation represent a similar way to solve the functional equation [120].

**Theorem 5.1** ***Homogeneous equations:*** *The most general solution of the equation*

$$f(yx) = y^k f(x); \quad x, y \in \mathbf{R}_+, \tag{5.16}$$

*where $f$ is a real function of a real variable and $k$ is a given constant, is*

$$f(x) = cx^k, \tag{5.17}$$

*where $c$ is an arbitrary constant.*

With $x = 1$ in (5.16) we get $f(y) = cy^k$, where $c = f(1)$. This solution, taking into account the commutativity of the product of real numbers, satisfies (5.16) and then (5.17) is proved. Note that this proof only requires the existence of a unit element and the commutativity of the product. Thus, the same solution is valid for many other domains and classes of functions [46].

### 5.4.2 Transforming one or several variables

By transforming one or several of the variables appearing in the functional equation we can transform the given equations in others, the solutions of which are known.

Section 5.5.3 shown the Cauchy's exponential equation, clear example of transformation of several variables to solve a functional equation.

### 5.4.3 Transforming one or several functions

Similarly, we can transform one or several functions and get some equations with known solutions [46].

### 5.4.4 Using a more general equation

Assume that we know the general solution of a functional equation with say $n$ unknown functions. Assume also that we are asked about the general solution of an equation which is a particular case of the initial equation where some of the n functions are known. The general solution of this new equation can be easily obtained by forcing the known functions to fit into the general format solution of the starting equation. Some useful equations to be used in this group of methods are

$$\sum_{k=1}^{n} f_k(x)g_k(y) = 0, \tag{5.18}$$

$$F[G(x,y), H(u,v)] = K[M(x,u), N(y,v)], \tag{5.19}$$

$$G(x,y) = H[M(x,z), N(y,z)]. \tag{5.20}$$

For more information about how can solve functional equation using this method see [46].

### 5.4.5 Treating some variables as constants

If, after considering as constants some of the variables appearing in a functional equation, we are able to solve the resulting functional equation, then, by making the arbitrary constants and/or the functions in the resulting general solution depend on those variables, we obtain the general solution of the initial problem.

### 5.4.6 Inductive methods

The induction method allows us to solve some functional equations.

### 5.4.7 Iterative methods

Some techniques related to iterative methods are also useful to solve some functional equations.

### 5.4.8 Separation of variables

If we can force some variables to appear on the right hand side of the equation and some others on its left hand side, then neither side must depend on the non common variables. This leads to new and normally simpler functional equations.

These methods (Inductive and iterative method and separation of variable method) are explained with more details in the bibliography (see [46], [120], [121] and [17]).

### 5.4.9 Reduction by means of analytical techniques

Some other useful techniques are [46]:

- Transformation of a functional equation into a differential equation.
- Transformation of a functional equation into an integral equation.
- Finding the solution over dense sets and extrapolating solutions by continuity.
- Use of characteristic mappings and invariants.

An example of this type of functional equation is presented in section 5.5.7, with d'Alambert equation.

### 5.4.10 Mixed methods

By mixed methods we understand a combination of the previous methods, as for example:

1. Multiple replacements.
2. Transforming variables and functions.
3. Replacements and changes of variables.
4. Replacements and changes of functions.

**Theorem 5.2** ***Cauchy's equation III:*** *The most general solutions, which are continuous-at-a-point, of the functional equation [46]*

$$f(xy) = f(x) + f(y); \quad x, y \in \mathbf{T} \tag{5.21}$$

*are*

$$f(x) = \begin{cases} c\log(x) & \text{if} \quad \mathbf{T} = \mathbb{R}_{++}, \\ c\log(|x|) & \text{if} \quad \mathbf{T} = \mathbb{R} - \{0\}, \\ 0 & \text{if} \quad \mathbf{T} = \mathbb{R}. \end{cases} \tag{5.22}$$

For positive $x$ and $y$, we can make the following change of variables

$$\begin{cases} u = \log(x) & \Leftrightarrow \quad x = \exp(u), \\ v = \log(y) & \Leftrightarrow \quad y = \exp(v), \end{cases} \tag{5.23}$$

and get

$$f(e^u e^v) = f(e^{u+v}) = f(e^u) + f(e^v), \tag{5.24}$$

which is equivalent to

$$g(u + v) = g(u) + g(v), \tag{5.25}$$

where $g(x) = f[\exp(x)]$.

Thus, we obtain again a Cauchy's equation (see section 5.5.1). So, under some mild regularity conditions, we can write

$$g(x) = cx \;\Rightarrow\; f(x) = c\log(x);\;\; x \in \mathbb{R}_{++}. \tag{5.26}$$

If Equation (5.21) is satisfied for $y = 0$, then $f(0) = f(x) + f(0)$, which implies $f(x) = 0$ for all $x$.

Finally, if Equation (5.21) is satisfied for all $x \neq 0$ and $y \neq 0$, then we have $2f(t) = f(t^2) = 2f(-t)$ and then $f(x) = f(-x) = c\log(|x|)$.

## 5.5 Functional equations with two variables

In this section diverse functional equation with two variables are defined [120].

### 5.5.1 Cauchy's equation

Let us begin by restating and solving Cauchy's equation. Let $f : \mathbf{R} \to \mathbf{R}$ be a continuous function satisfying

$$f(x + y) = f(x) + f(y), \tag{5.27}$$

for a real $x$ and $y$. We show that there exists a real number $a$ such that $f(x) = ax$ for all $x \in \mathbf{R}$ (see [121] and [46]).

A special case of this is found by setting $x_1 = ... = x_n = x$, then becomes

$$f(nx) = nf(x), \tag{5.28}$$

for all positive integers $n$ and for all real number $x$.

But what happen when $a = 0$?, in this case

$$\begin{aligned} f(y) &= f(y + 0) \\ &= f(y) + f(0). \end{aligned} \tag{5.29}$$

So $f(0) = 0$. Similarly, the case of $a < 0$ gives like a solution

$$\begin{aligned} 0 &= f(0) \\ &= f(a + (-a)) \\ &= f(a) + f(-a) \\ f(ax) &= f(-(-a)x) \\ &= af(x), \end{aligned} \tag{5.30}$$

for all real values of $x$ and rational values of $a$.

We can summarize all these informations in two propositions:

**Proposition 1** Let $f : \mathbf{R} \to \mathbf{R}$ satisfy Cauchy's equation

$$f(x + y) = f(x) + f(y)$$

for all real values $x$ and $y$. Then there exists a real number $a$ such that

$$f(q) = aq$$

for all rational numbers $q$.

**Proposition 2** Suppose that $f : \mathbf{R} \to \mathbf{R}$ and $g : \mathbf{R} \to \mathbf{R}$ are continuos functions such that $f(q) = g(q)$ for all rational numbers $q$. Then $f(x) = g(x)$ for all real number $x$.

### 5.5.2 Jensen's equation

Jensen's equation is of the form:

$$f\left(\frac{x+y}{2}\right) = \frac{f(x)+f(y)}{2}, \tag{5.31}$$

that is a version of the Cauchy's equation using averages [121].

The solution to the equation is easy to obtain. Let $g(x) = f(x) - f(0)$, that is

$$g\left(\frac{x+y}{2}\right) = \frac{g(x)+g(y)}{2}. \tag{5.32}$$

If $y = 0$, knowing that Equation (5.32) is continuous, and substituting $x$ by $x + y$ we obtain

$$g\left(\frac{x+y}{2}\right) = \frac{g(x+y)}{2}. \tag{5.33}$$

Substituting this equation in Equation (5.32) and working in the simplification of the equation obtained, the result is

$$g(x+y) = g(x) + y(y), \tag{5.34}$$

which is Cauchy's equation (section 5.5.1).

### 5.5.3 Cauchy's exponential equation

This equation has the form

$$f(x+y) = f(x)f(y), \tag{5.35}$$

where $f : \mathbf{R} \to \mathbf{R}$, satisfiying

$$f(x) = \exp(cx) \text{ and } f(x) = 0, \tag{5.36}$$

where $c$ is an arbitrary constant.

Replacing $x$ and $y$ by $t/2$ in (5.36) we obtain

$$f(t) = f\left(\frac{t}{2}\right)^2 \quad \Rightarrow \quad f(t) \geq 0, \ \ \forall t.$$

Now, if $f(t_0) = 0$ for some $t_0$ then $f(t) = f(t - t_0 + t_0) = f(t - t_0)f(t_0) = 0$ for all $t$. Thus, either $f(t) > 0$ for all $t$, or $f(t) \equiv 0$.
If $f(t) > 0$ for all t, then we can take logarithms on both sides in (5.35) and get

$$\log f(x+y) = \log\left[f(x)f(y)\right] = \log f(x) + \log f(y),$$

which, using the notation $g(x) = \log f(x)$, leads to

$$g(x+y) = g(x) + g(y),$$

which is Cauchy's equation with solution

$$g(x) = cx.$$

Thus, we finally get

$$f(x) = \exp(cx).$$

Following the steps realized in [121], the conclusion is that there exist a real number $b < 0$ such that $f(x) = b^x$ for all real $x$.

### 5.5.4 Pexider's equation

Pexider's equation has the form

$$f(x+y) = g(x) + h(y). \tag{5.37}$$

We need to discover the solutions for all the functions, $f, g, h : \mathbf{R} \to \mathbf{R}$ satisfying Equation (5.37) for all real number $x$ and $y$ [121].

This equation is a generalization of Cauchy's equation. Putting $y = 0$ and setting $h(0) = b$, similarly putting $x = 0$ and $g(0) = a$, we have

$$f(x+y) = f(x) + f(y) - a - b. \tag{5.38}$$

Let $f_0(z) = f(z) - a - b$ for all real $z$, $f_0$ satisfies $f_0(x+y) = f_0(x) + f_0(y)$, which is Cauchy's equation. So, the solution for $f_0$ is $f_0(z) = cz$, and the solution to Pexider's equation is

$$\begin{aligned} f(z) &= cz + a + b \\ g(x) &= cx + a \\ h(y) &= cy + b. \end{aligned} \tag{5.39}$$

### 5.5.5 Vincze's equation

This equation is considered a generalization of *Pexider's equation*. Consider the function $f, g, h$

$$f(x+y) = g(x)k(y) + y(y) \tag{5.40}$$

for a real $x$ and $y$ [121].

Taking $k(0) = a$ and $h(0) = b$. If $a = 0$, $f$ is a constant function, but in this case consider $a \neq 0$. Putting $y = 0$ in Equation (5.40) we get

$$g(x) = \frac{f(x) - b}{a}. \tag{5.41}$$

Defining $\phi(y) = k(y)/a$ and $\varphi(y) = h(y) - bk(y)/a$, and substitutions of $\phi(0) = 1$ and $\varphi(0) = 0$, leads to the final equation

$$(\phi(y) - 1)\chi(x) = (\phi(x) - 1)\chi(y), \tag{5.42}$$

where $\chi(y) = f(y) - f(0)$.

For the complete analysis of Vincze's equation see [121].

### 5.5.6 Euler's equation

The Euler's equation is characteristic for its property of homogeneity (see [121] and [46]). Let $k$ be a real number, the equation is

$$f(tx, ty) = t^k f(x, y) \tag{5.43}$$

A function $f(x)$ satisfying a Euler's equation is called *homogeneous function of degree k*. In table 5.1 some examples of these type of equations are shown.

Table 5.1: Some example of homogeneous functions.

| Function | Degree |
|---|---|
| $f(x,y) = (x+y)/2$ | 1 |
| $f(x,y) = x/y$ | 0 |

### 5.5.7 D'Alambert's equation

D'Alamber's equation is:

$$f(x+y) + f(x-y) = 2f(x)g(y), \tag{5.44}$$

where

$$f(x) = 1, \;\; f(x) = 0, \;\; f(x) = \cosh(Bx), \;\; f(x) = \cos(Bx), \tag{5.45}$$

and $B$ is an arbitrary constant.

To solve D'Alembert's equation we initially set $y = 0$ and then $x = 0$ to obtain

$$f(0) = 1 \;\text{ or }\; f(x) = 0 \;\text{ and }\; f(y) = f(-y). \tag{5.46}$$

Then we differentiate twice with respect to $y$ and set $y = 0$ and we get

$$f''(x) = kf(x) \Rightarrow f(x) = \begin{cases} a\cosh\left(\sqrt{k}x\right) + b\sinh(\sqrt{k}x) & \text{if} \quad k > 0, \\ a + bx & \text{if} \quad k = 0, \\ a\cos\left(\sqrt{-k}x\right) + b\sin(\sqrt{-k}x) & \text{if} \quad k < 0, \end{cases} \tag{5.47}$$

where we have made $k = f''(0)$. Using now (5.46) we get $a = 1$ and $b = 0$. Thus, the general differentiable solution of (5.47) becomes

$$f(x) = \begin{cases} \cosh(\sqrt{k}x) & \text{if} \quad k > 0, \\ 1 & \text{if} \quad k = 0, \\ 0 & \\ \cos(\sqrt{-k}x) & \text{if} \quad k < 0. \end{cases} \tag{5.48}$$

The derivation of this equation is complex, we can find the solution in books such as [121]. figure 5.4 shows some of the functions that can be found as a solutions to d'Alambert's equations in this section. The example corresponds to $\cos nx$ and $\cosh nx$ for $n = 1, 2, 3$.

### 5.5.8 Equations involving functions of two variables

One way to extend Cauchy's equation is to consider functions of two or more variables [121].

Suppose $f(x,y)$ is a real function dependent of two variables $x$ and $y$, which satisfies

$$f(x_1 + x_2, y) = f(x_1, y) + f(x_2, y); \tag{5.49}$$

$$f(x, y_1 + y_2) = f(x, y_1) + f(x, y_2); \tag{5.50}$$

where $x_1, x_2, y_1$ and $y_2$ are real values. If $f$ is also a continuous function, when $y$ is fixed, the function $f$ can be written in the form

$$f(x,y) = c(y)x, \tag{5.51}$$

Entering in Equation (5.50), we get

$$c(y_1 + y_2)x = c(y_1)x + c(y_2)x, \tag{5.52}$$

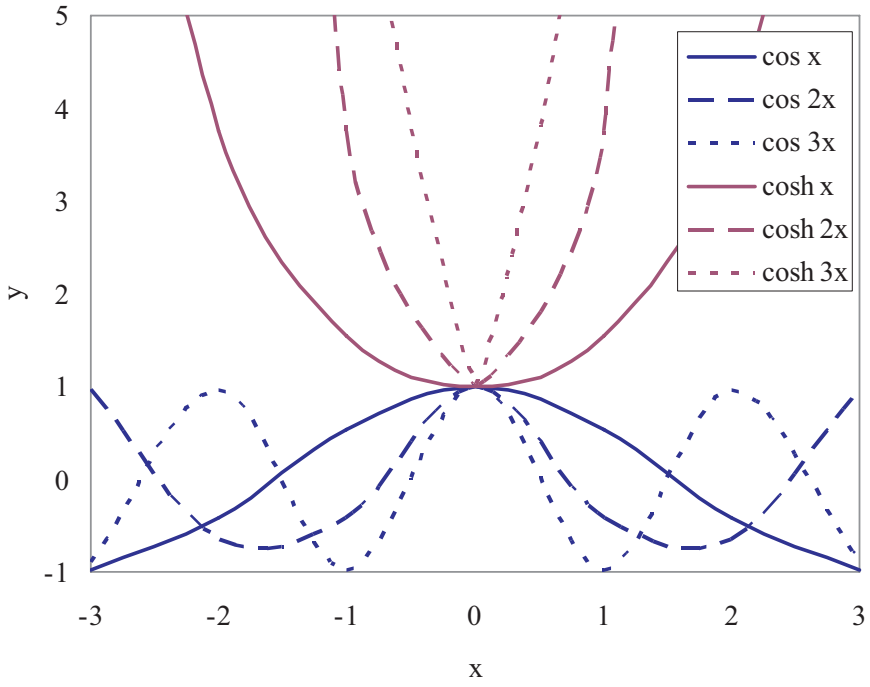


Figure 5.4: Some solutions of D'Alambert's equation. The functions presented are $\cos nx$ and $\cosh nx$ for $n = 1, 2, 3$ [121].

Making $x = 1$ we obtain the Cauchy's equation. So, the conclusion is that *"there exists some real number $c_0$ such that $c(y) = c_0 y$ for all $y$"* [121]

$$f(x, y) = c_0 xy. \tag{5.53}$$

for a real $x$ and $y$.

## 5.6 Functional equations with one variable

### 5.6.1 Basic families of equations

The simplest families of functional equations with one variable that we can write has the form

$$f(x) = f(\alpha(x)), \tag{5.54}$$

for real $x$ values, where $\alpha : \mathbf{R} \rightarrow \mathbf{R}$ is a specified function [121].

There exist two different ways of analyzing this equation, assuming that $f$ is a continuous function or not. If we do not assume that $f$ is continuous, the solution for the equation is the family of funtions

$$\alpha^1 = \alpha; \alpha^{n+1}(x) = \alpha(\alpha^n(x)), \tag{5.55}$$

for $n = 1, 2, ....$ Assuming that $\alpha^0(x) = x$, the solution of the problem is the sequence

$$f(x) = f(\alpha^n(x)). \tag{5.56}$$

However, if $f$ is continuous function, the limit of the equation gives us

$$\begin{aligned} f(x_0) &= f(\lim_{n\to\infty} \alpha^n(x)) \\ &= \lim_{n\to\infty} \alpha^n(x) \\ &= f(x) \end{aligned} \tag{5.57}$$

for all $x$. The conclusion is that $f$ must be constant, and to avoid problems, $x_0$ must to be in the domain of $f$.

For the complete derivation of this equation see [121].

### 5.6.2 Conjugate equations

As Equation (5.54) there are one-to-one functions which are solutions to it. In this subsection some examples are presented.

The equation

$$f(\alpha(x)) = sf(x), \tag{5.58}$$

is called *Schröder's* ***equation***. We assume that $\alpha(x) = x$ has not solutions on some interval on which the function $f(x)$ is to be constructed. With this, we avoid the problem about the domain of definition of any solution in Equation (5.58). To solve the problem we can use different methods, but here we present a kind of inverse equation to *Schöder's* equation.

Let $f$ be a solution to Equation (5.58), $g = f^{-1}$ such that $f(x) = y$ if and only if $g(y) = x$.

$$g(sx) = \alpha(g(x)). \tag{5.59}$$

Equation (5.59) is known as ***Poincare's equation***.

The equation

$$f(\alpha(x)) = f(x) + a, \tag{5.60}$$

where $a$ is a real number (nonzero), is called ***Abel's equation***. As in *Schöder's* equation, we need to define the domain of $f$ very carefully.

The equation

$$f(\alpha(x)) = (f(x))^p, \tag{5.61}$$

is called *Böttcher's* ***equation***. The value of $p \neq 1$. This equation is used to analyze nonnegative functions of $f(x)$.

### 5.6.3 Functional equations and nested radicals

A nested radical function,

$$f(s) = \sqrt{1 + x\sqrt{1 + (x+1)\sqrt{\ldots}}}, \tag{5.62}$$

can be solved squaring both sides

$$(f(x))^2 = 1 + xf(x+1), \tag{5.63}$$

where $f(x) \geq 0$.

This equation does not fit into any family of equations studied above. To determine the solution we need to guess it. If we define $f(x)$ which a polynomial equation, that is $f(x) = ax+b$, we get

$$(ax + b)^2 = 1 + x(ax + a + b), \tag{5.64}$$

that is true for all $x$. Taking $f(x) = x+1$, $a = 1, b = 1$, and bounding both sides of the equations [121], we have

$$\frac{x+1}{2} \leq f(x) \leq 2(x+1). \tag{5.65}$$

## 5.7 Functional equations in probability theory

The analysis of functional equations in probability theory is an important subject in engineer problems. In this section several results on the Cauchy functional equation and on distribution functions are analyzed [17].

### 5.7.1 Integrated Cauchy functional equations on $\mathbf{R}_+$

An extension of the classical Cauchy's equation is the integral equation

$$\int_S (f(x+y) - f(x)f(y))d\upsilon(y) = 0, \quad \forall \quad x \in S, \tag{5.66}$$

where $f : s \to R$, $S$ is a semigroup of $\mathbf{R}$, and $\upsilon$ is a positive measure of $S$. If $\int_S (f(y)d\upsilon(y))$ is nonzero and finite, the Equation (5.67) reduces to

$$f(x) = \int_S f(x+y)d\sigma(y) = 0, \quad \forall \quad x \in S, \tag{5.67}$$

where $\sigma$ is related to $\upsilon$. This equation, with $f$ and $\sigma$ positive, appear repeatedly in analytical probability theory. We call these type of equations as *integrated Cauchy functional equation (ICFE)*, and normally are written as $f = f \bullet \sigma$ on $S$ for simplicity. The aim of this subsection is to shown some applications of the solution of the ICFE.

#### The lack of memory property of the exponential and geometric laws

Consider a real variable $X$ with an exponential distribution function, the lack of memory property is

$$P[X > y + x | X > y] = P[X > x], \quad \forall x, y \geq 0. \tag{5.68}$$

In the same way, if this property holds, let $T = 1 - F$, where $F$ is the distribution function of $X$. $T$ satisfies the Cauchy's equation, so $F$ is a exponential distribution function. If we replace $y > 0$ in the Equation (5.68) by a real variable $Y > 0$, assuming that $P[X > Y] > 0$, we obtain

$$P[X > Y + x | X > Y] = P[X > x], \quad for \quad x \geq 0. \tag{5.69}$$

If $G$ is the distribution function of $Y$, then

$$cT(x) = \int_{[0,\infty)} T(x+y)dG(y), \quad \forall x \geq 0, \tag{5.70}$$

where $c = PX > Y$.

### 5.7.2 Integrated Cauchy functional equation with error terms on $\mathbf{R}_+$

Similarly to Equation (5.68), the $\epsilon - ICFE(\sigma, S)$ equations are defined by

$$f(x) = \int_0^\infty f(x+y)d\sigma(y) + S(x), \quad \forall x \geq 0, \tag{5.71}$$

where the error is $S$ and is such that $|S(x)| \leq Ce^{-\epsilon x}$ for all $x \geq 0$.

**Characterization of the Weibull distribution**

In this subsection we want to present the steps to obtain the Weibull distribution and its characterization.

Consider $g$ be a bounded, real value, continuous function on $[0, \infty)$, that satisfy the next relation for some values of $\alpha > 0$

$$\exp e^{-\alpha x} g(x) = \int_{\omega} \exp[e^{-\alpha x} \int_0^{\infty} g(x+y) u(dy, w)] dP(w), \tag{5.72}$$

where $(\omega, \mathbf{B}, P)$ is a probability space in $\mathbf{R}$, and $g$ is inside of the bounds.

For more information about this type of equations see [17].

## 5.8 Applications to science and engineering

In this section some examples of application of functional equations to science and engineering are shown. These applications solve problems of different fields of science, like traffic, network, fatigue, etc.

### 5.8.1 A statistical model for lifetime analysis

In many practical engineering situations, the lifetime variable, $T$, appears as a random variable which depends on one regressor variable, $X$. This is, for example, the case of the fatigue life of wires, strands or tendons, the time up to breakdown in solid dielectrics or the time up to failure of marine breakwaters, which depend on the regressor variables stress range, voltage stress or wave height, respectively [46].

As a consequence, a regression model as shown in figure 5.5, could be a convenient approach to the problem. The model is completely established as soon as the cumulative conditional distribution function of lifetime, $F(t, x)$, is defined for every value $x$ of $X$.

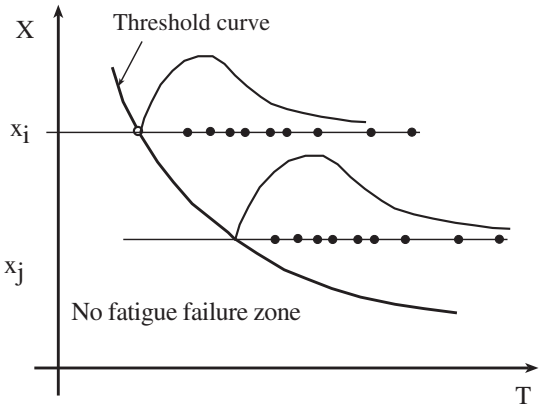


Figure 5.5: Regression model. figure from [46]

Two different ways in which the engineer can tackle the problem are:

1. Using standard linear regression models in order to fit the experimental data.

2. Creating adequate models not only to fit the experimental data but also to satisfy physical and theoretical considerations.

By the first approach we mean the use of ready-made regression models, i.e., models not specially designed for the problem under consideration, but very well recognized by statisticians and experienced engineers. This is the most generally accepted approach because of its simplicity, its widespread use and the possibility of performing many standard and simple analysis, such as confidence limit analysis for example.

In the cases in which the application of the first approach is not satisfactory, the engineer tries to develop tailor–made regression models. These models can either reflect his experience and feeling about the problem or be based on physical and theoretical considerations.

In the following paragraphs, we derive a statistical model for lifetime analysis related to the weakest link principle with a wide applicability to engineering problems.

This division into two approaches can sound artificial to the reader and in some way it is artificial, in the sense that methods in the second group can go into the first as soon as they are investigated, experimented and widely recognized. This makes it difficult to define a clear cut between the two groups. However, the main distinction between the two groups is that in the first case the engineer only wants to adjust the trend of the experimental data but in the second, he also wants to satisfy some extra physical conditions such as compatibility, feasible range, stability, etc., which must hold for the problem under consideration.

In the following paragraphs, the second approach will be used to derive a statistical model for lifetime analysis related to the weakest link principle with a wide applicability to engineering problems.

**Derivation of the fatigue model:** The following assumptions are made [37]:

1. **Weakest link principle**: This principle establishes that the fatigue lifetime of a longitudinal element is the minimum fatigue life of its constituent pieces.

2. **Stability**: The selected distribution function type must hold (be valid) for different specimen lengths.

3. **Limit behavior**: To include the extreme case of the size of the supposed pieces constituting the element going to zero, or the number of pieces going to infinity, it is convenient for the distribution function family to be an asymptotic family (see [70] and [33]).

4. **Limited range**: Experience shows that the lifetime $T$ and the stress range $X$, have a finite lower end, which must coincide with the theoretical lower end of the selected cdf. This implies that the Weibull distribution is the only one satisfying requirements 1 to 4.

5. **Compatibility**: In the X–T field, the cumulative distribution function of the lifetime given stress range, $F(t;x)$, should be compatible with the cumulative distribution function of the stress range given lifetime, $E(x;t)$.

These conditions lead to the following functional equation

$$\begin{aligned} F(t,x) &= 1-\exp\left\{-\left[\frac{t-\gamma_t(x)}{\alpha_t(x)}\right]^{\beta_t(x)}\right\} \\ &= 1-\exp\left\{-\left[\frac{x-\gamma_x(t)}{\alpha_x(t)}\right]^{\beta_x(t)}\right\} = E(x;t), \end{aligned} \tag{5.73}$$

where $\gamma_t(x)$, $\alpha_t(x)$ and $\beta_t(x)$ are the location, scale and shape parameters of the Weibull laws for given $x$, and $\gamma_x(t)$, $\alpha_x(t)$ and $\beta_x(t)$ are the location, scale and shape parameters of the Weibull laws for given $t$.

Expression (5.73) is equivalent to the functional equation

$$\left[\frac{t-\gamma_t(x)}{\alpha_t(x)}\right]^{\beta_t(x)} = \left[\frac{x-\gamma_x(t)}{\alpha_x(t)}\right]^{\beta_x(t)}. \tag{5.74}$$

[43] have shown that the only feasible solutions of Equation (5.73) are the three models:

- **Model 1** (see figure 5.6):

$$F(t,x) = 1 - e^{-[(t-A)(x-B)/C+D]^E}. \tag{5.75}$$

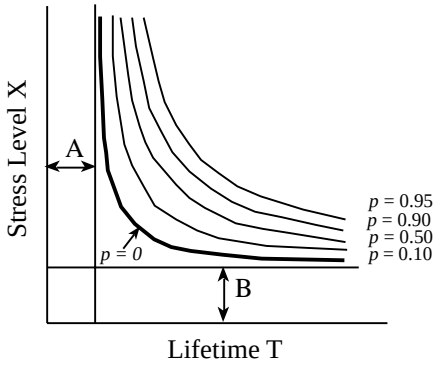


Figure 5.6: Wöhler field of model 1. figure from [46]

- **Model 2** (see figure 5.7):

$$F(t,x) = 1 - e^{-\left[C(t-A)^E(x-B)^D\right]}. \tag{5.76}$$

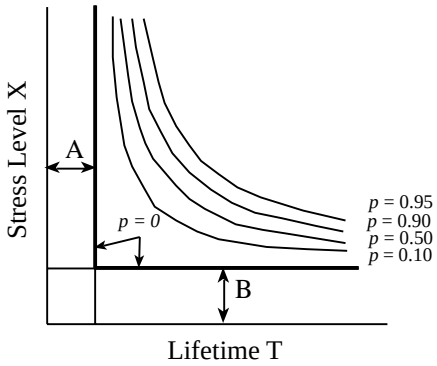


Figure 5.7: Wöhler field of model 2. figure from [46]

- **Model 3**:

$$F(t,x) = 1 - e^{-\left[C(t-A)^E(x-B)^D e^{F\log(t-A)\log(x-B)}\right]}, \tag{5.77}$$

where $A$,$B$, $C, E > 0$, $D$ and $F$ are arbitrary constants.

### 5.8.2 Statistical models for fatigue life of longitudinal elements

One of the most important problems when dealing with the statistical analysis of the fatigue life of longitudinal elements is the size effect; that is, the influence of length on the survivor function [46].

By longitudinal element we understand an element satisfying the following two conditions:

- only one dimension is important in the behavior of the element and
- if the element is longitudinally divided into imaginary pieces (see figure 5.8) all pieces are subject to the same external action (stress, force, etc.)

Several models have been given in the past to solve this problem, but, unfortunately, most of them are based on the assumption of independence of the fatigue life of non-overlapping pieces. This assumption states that if an element of length $s$, such as that shown in figure 5.8, is hypothetically divided into several pieces of lengths $s_1, s_2, ..., s_n$, then the survivor function of the element $S(s,z)$ must satisfy the equation

$$S(s,z) = \prod_{i=1}^{n} S(s_i, z).$$


Figure 5.8: Illustration of the hypothesis of independence. figure from [46]

Here we shall abandon the independence assumption and, making use of the functional equations theory, we shall state the problem in a very different way.

We shall assume here that a team of three members is required to design a consensus model for the analysis of the fatigue life of longitudinal elements. However, they are required to give separate proposals before joining together and reaching a consensus. The three proposals associated with the three members will be denoted by models 1, 2 and 3, respectively.

#### Model 1

For the sake of simplicity we assume $n = 2$, that is, the element of length $x + y$ is divided into two non-overlapping pieces of lengths $x$ and $y$. We also assume that there exists a function $S(x,z)$ that gives the survivor function of a piece of length $x$ and that the survivor function of

the element can be calculated in terms of that of the two pieces. In other words, $S(x,z)$ must satisfy the following functional equation

$$S(x+y,z) = H[S(x,z), S(y,z)], \tag{5.78}$$

where the function $H$ indicates how the survivor function of the element can be obtained from those of the pieces [46].

It is worthwhile mentioning that Equation (5.78) implies the associativity and commutativity character of the $H$ function and the dependence of the survivor function $S$ on the total length of the element. In fact we can write

$$\begin{aligned} S(x+y+z,t) &= H[S(x+y,t), S(z,t)] \\ &= H[H[S(x,t), S(y,t)], S(z,t)] \\ &= H[S(x,t), S(y+z,t)] \\ &= H[S(x,t), H[S(y,t), S(z,t)]] \end{aligned}$$

and

$$S(x+y,t) = H[S(x,t), S(y,t)] = S(y+x,t) = H[S(y,t), S(x,t)].$$

Thus, the survivor function of an element of length $s$ is independent of the number and size of the sub-elements into which it is divided in order to calculate it, using (5.78).

In the following paragraphs we solve functional Equation (5.78) in two different forms.

The functional Equation (5.78) is a particular case of the functional equation

$$S[G(x,y),z] = H[M(x,z), N(y,z)], \tag{5.79}$$

with $M = N = S$ and $G(x,y) = x+y$.

Is easily satisfy all regularity conditions, because $S(x,0) = 1$ and we can choose families of survivor functions such that $S_1(x,c) \neq 0$ and functions $H$ such that $H_1 \neq 0$ and $H_2 \neq 0$. The general solution of (5.79) is

$$\begin{aligned} S(x,z) &= l[f(z)g^{-1}(x) + \alpha(z) + \beta(z)], \\ G(x,y) &= g[h(x) + k(y)], \\ H(x,y) &= l[m(x) + n(y)], \\ M(x,z) &= m^{-1}[f(z)h(x) + \alpha(z)] \\ N(x,z) &= n^{-1}[f(z)k(x) + \beta(z)] \end{aligned} \tag{5.80}$$

where $g, h, k, l, m$ and $n$ are arbitrary strictly monotonic continuously differentiable functions and $f, \alpha$ and $\beta$ are arbitrary continuously differentiable functions.

Thus, for Equation (5.78) we have

$$\begin{aligned} S(x,z) &= l[f(z)g^{-1}(x) + \alpha(z) + \beta(z)] \\ &= m^{-1}[f(z)h(x) + \alpha(z)] \\ &= n^{-1}[f(z)k(x) + \beta(z)] \\ g[h(x) + k(y)] &= x + y, \end{aligned} \tag{5.81}$$

from which

$$g^{-1}(x+y) = h(x) + k(y),$$

which is Pexider's equation I with the general continuous-at-a-point solution (see [46] chapter 4)

$$g^{-1}(x) = Ax + B + C; \;\; h(x) = Ax + B; \;\; k(x) = Ax + C.$$

With this, expressions (5.81) become

$$\begin{aligned} S(x,z) &= l[f(z)(Ax+B+C)+\alpha(z)+\beta(z)] \\ &= m^{-1}[f(z)[Ax+B]+\alpha(z)] \\ &= n^{-1}[f(z)[Ax+C]+\beta(z)], \end{aligned}$$

and making $Af(z)x = u$ we obtain

$$\begin{aligned} S(x,z) &= l[u+(B+C)f(z)+\alpha(z)+\beta(z)] \\ &= m^{-1}[u+Bf(z)+\alpha(z)] \\ &= n^{-1}[u+Cf(z)+\beta(z)], \end{aligned} \tag{5.82}$$

and, we get

$$\begin{aligned} u &= cu+a \quad \Rightarrow \quad c=1, \;\; a=0, \\ l(x) &= m^{-1}\left(\frac{x-a-b}{c}\right) \\ &= m^{-1}(x-b) \\ (B+C)f(z)+\alpha(z)+\beta(z) &= Bf(z)+\alpha(z)+b \Rightarrow \beta(z) = b-Cf(z). \end{aligned}$$

Then, (5.82) becomes

$$S(x,z) = m^{-1}[u+Bf(z)+\alpha(z)] = n^{-1}(u+b),$$

which implies

$$\begin{aligned} u &= c_1u+a_1 \quad \Rightarrow \quad c_1=1, \;\; a_1=0, \\ m^{-1}(x) &= n^{-1}\left(\frac{x-a_1-b_1}{c_1}\right) = n^{-1}(x-b_1), \\ Bf(z)+\alpha(z) &= c_1b+b_1 = b+b_1 \quad \Rightarrow \quad \alpha(z) = b+b_1-Bf(z), \end{aligned}$$

and finally we get the desired solution

**Model 1:** The general solution of (5.78) is:

$$S(x,z) = w[f(z)x]; \;\; H(x,y) = w[w^{-1}(x)+w^{-1}(y)],$$

where we have made $w^{-1}(x) = \dfrac{[n(x)-b]}{A}$.

Due to the weakest link principle and because $S(x,z)$ is a survivor function, it must be non-increasing in $z$ and $x$. Then, in addition, we must have

$$S(x,0)=1 \;\Rightarrow\; w[f(0)x]=1 \;\Rightarrow\; \begin{cases} [f(0)=0 \;;\; w(0)=1], \;\text{ or} \\ [f(0)=\infty \;;\; w(\infty)=1], \;\text{ or}. \\ [f(0)=-\infty \;;\; w(-\infty)=1] \end{cases}$$

$$S(x,\infty)=0 \;\Rightarrow\; w[f(\infty)x]=0 \;\Rightarrow\; \begin{cases} [f(\infty)=0 \;;\; w(0)=0], \;\text{ or} \\ [f(\infty)=\infty \;;\; w(\infty)=0], \;\text{ or}. \\ [f(\infty)=-\infty \;;\; w(-\infty)=0] \end{cases}$$

If $w(x) = \exp(Dx)$ we get the model of independence.

The structure of the function $H$ reveals its above mentioned associative and commutative character.

We can solve (5.78) in a much easier way if we observe that the variable $z$ plays the role of one parameter, i.e., for any fixed value of $z$, Equation (5.78) can be written in the form

$$S(x+y) = H[S(x), S(y)],$$

and due to the associative character of $H$ we can write

$$H(x,y) = w[w^{-1}(x) + w^{-1}(y)],$$

and its substitution into (5.78) leads to

$$\begin{array}{rcl} S(x+y,z) & = & w\{w^{-1}[S(x,z)] + w^{-1}[S(y,z)]\} \Rightarrow \\ & \Rightarrow & G(x+y,z) = G(x,z) + G(y,z), \end{array}$$

with $G(x,z) = w^{-1}S(x,z)$, which, for $z$ held constant, is Cauchy's Equation (4.7) and then:

$$G(x,z) = f(z)x \;\Rightarrow\; S(x,z) = w[f(z)x].$$

**Model 2**

Member 2 in the team wants to start from the following result : [26] based on some experimental results of [108], suggest the following model for the survivor function

$$S(x,z) = S(y,z)^{N(y,x)}, \tag{5.83}$$

where $S(x,z)$ and $S(y,z)$ are the survivor functions associated with two elements of lengths $x$ and $y$, respectively, and $N(y,x)$ is an unknown function.

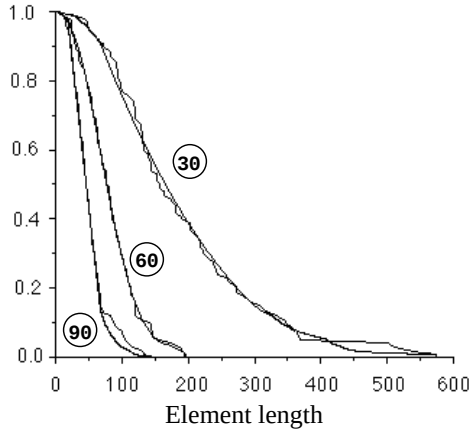


Figure 5.9: Experimental and theoretical survivor functions for lengths 30, 60 and 90 cm. (from [26]).

figure 5.9 shows the experimental survivor functions and those obtained using model (5.83) (see [26]).

Note that (5.83) is an implicit function of $S(x,z)$, or in other words, it is a functional equation. Thus, it must be solved to know what the Bogdanoff and Kozin proposal is. [34] showed that the only compatible functions for $N(y,x)$ are those of the form $N(y,x) = \dfrac{q(x)}{q(y)}$ [46].

We know

$$S(x,z) = p(z)^{q(x)}; \quad N(y,x) = \frac{q(x)}{q(y)}. \tag{5.84}$$

For $S(x,z)$ to be a survivor function it must be non-increasing in $z$ and we must have

$$\begin{array}{rcrcl} S(x,0) = 1 & \Rightarrow & p(0)^{q(x)} = 1 & \Rightarrow & p(0) = 1, \\ S(x,\infty) = 0 & \Rightarrow & p(\infty)^{q(x)} = 0 & \Rightarrow & p(\infty) = 0. \end{array}$$

If $q(x) = x$ we get the model of independence.

The hazard function associated with $S(x,z)$ is

$$h(x,z) = \frac{-p'(z)}{p(z)} q(x) = -[\log p(z)]' q(x) = s(z)q(x),$$

which shows that Model 2 is the Cox–proportional hazards model (see [54]). Thus, functional Equation (5.83) characterizes the proportional hazards Cox-model.

**Model 3**

Member 3, based on expression (5.83), assumes that the survivor function of one element of length $x$ can be obtained from the survivor function of one element of length $y$ and a given, but unknown, function of $x$ and $y$. In other words he assumes that the survivor function must satisfy the functional equation

$$S(x,z) = K[S(y,z), N(x,y)], \tag{5.85}$$

which is a particular case of

$$G(x,y) = K[M(x,z), N(y,z)],$$

with $S(x,y) = G(y,x) = M(y,x)$.

If we choose $F$ and $N$ to be invertible with respect to their first argument and $K$ invertible with respect to its first argument for a fixed value of the second, then the regularity conditions hold and the general solution of the last equation is:

$$\begin{array}{rclrcl} G(x,y) & = & f^{-1}[p(x) + q(y)]; & K(x,y) & = & f^{-1}[l(x) + n(y)]; \\ M(x,y) & = & l^{-1}[p(x) + r(y)]; & N(x,y) & = & n^{-1}[q(x) - r(y)], \end{array} \tag{5.86}$$

and then, for (5.85) we must have

$$\begin{array}{rcl} S(x,z) & = & f^{-1}[p(z) + q(x)] \\ & = & l^{-1}[p(z) + r(x)], \\ K(x,y) & = & f^{-1}[l(x) + n(y)], \\ N(y,z) & = & n^{-1}[q(y) - r(z)], \end{array} \tag{5.87}$$

implies

$$\begin{array}{rcl} p(z) & = & cp(z) + a \;\Rightarrow\; c = 1, \;\; a = 0, \\ f^{-1}(x) & = & l^{-1}\left(\dfrac{x - a - b}{c}\right) = l^{-1}(x - b), \\ q(x) & = & cr(x) + b = r(x) + b, \end{array}$$

and then, from Expression (5.87), model 3 becomes

$$\begin{array}{rrcl} \textbf{Model 3}: & S(x,z) & = & l^{-1}[p(z)+r(x)], \\ & K(x,y) & = & l^{-1}[l(x)+m(y)], \\ & N(x,y) & = & m^{-1}[r(x)-r(y)], \end{array} \tag{5.88}$$

where we have made $m(x) = n(x) - b$.

For $S(x,z)$ to be a survivor function it must be non-increasing in $z$ and we must have

$$S(x,0) = l^{-1}[p(0)+r(x)] = 1 \;\Rightarrow \begin{cases} [l(1) = p(0) = -\infty], & \text{or} \\ [l(1) = p(0) = \infty], & \text{or} \\ [r(x) = l(1) - p(0)] & \end{cases}.$$

$$S(x,\infty) = l^{-1}[p(\infty)+r(x)] = 0 \;\Rightarrow \begin{cases} [l(0) = p(\infty) = \infty], & \text{or} \\ [l(0) = p(\infty) = -\infty], & \text{or}. \\ [r(x) = l(0) - p(\infty)] & \end{cases}$$

If $l^{-1}(x) = \exp[D\exp(Cx)]$ we get the model of independence.

One important aspect to point out here is that Equation (5.85) is more than a simple generalization of Equation (5.83). In fact, it includes some extra compatibility conditions, in the sense that no arbitrary $N(y,x)$ is admissible in Model 3, even though, initially, the function $N(y,x)$ seems to be arbitrary. In order to prove this, we show that the only admissible $N$ functions are those appearing in Model 2 (Expression (5.84)) [46].

Let us assume that function $K$ is that implied from Equation (5.88), that is

$$K(x,y) = x^y = l^{-1}[l(x)+m(y)] \;\Rightarrow\; l(x^y) = l(x) + m(y),$$

which, by making the change of variable $u = \log(x)$, can be written

$$l[\exp(uy)] = l[\exp(u)] + m(y).$$

This is a Pexider functional equation with solution

$$l(x) = c\log[\alpha\log(x)];\;\; m(y) = c\log(y).$$

Thus, we finally get

$$\begin{aligned} N(x,y) &= m^{-1}[r(x)-r(y)] = \exp\left[\frac{r(x)-r(y)}{c}\right] = \frac{q(x)}{q(y)}, \\ q(x) &= \exp\left[\frac{r(x)}{c}\right], \end{aligned}$$

which is model 2.

**Reaching a consensus**

In the second and final step the team is required to join and reach a consensus.

Normally, a consensus solution is understood as a linear combination of the quantitative judgments of several individuals. However, in many cases the consensual solution reached does not satisfy many of the properties that were satisfied by the solutions in the proposals given by the different individuals (see [72]). This fact is irrelevant when one tries to use the consensus model to make some evaluations, such as to calculate some probabilities, for example, but becomes a very serious inconvenience when one tries to model a physical system. In fact, the functional equations (5.78), (5.83) and (5.85) state some properties, which the different members

understand the physical system must satisfy. Thus, any member would not accept models violating his/her associated functional equation. Thus, in the following, we shall understand consensus as the intersection of the three families of models, if it exists, i.e., as models satisfying all the requirements. We start by analyzing the common part of Models 1 and 2 (see the corresponding equations).

$$S(x,z) \quad = \quad w[f(z)x] = p(z)^{q(x)},$$

which implies

$$\log[S(x,z)] = \log\{w[f(z)x]\} = q(x)\log[p(z)],$$

and making the change of variable $u = f(z)$ we get

$$\log\{w[ux]\} = q(x)\log\{p[f^{-1}(u)]\},$$

which is Pexider's functional Equation with the general continuous-at-a-point solution (see [46], chapter 4)

$$\log\{[w(x)]\} = ABx^C, \;\; q(x) = Ax^C, \;\; \log\{p[f^{-1}(x)]\} = Bx^C.$$

Thus,

$$\begin{array}{lllllll} S(x,z) & = & \exp\left\{AB[f(z)x]^C\right\}; & & w(x) & = & \exp\left(ABx^C\right); \\ p(z) & = & \exp[Bf^C(z)]; & & q(x) & = & Ax^C, \end{array} \tag{5.89}$$

which shows that Models 1 and 2 are not coincident but they share the common model

$$S(x,z) = \exp\left\{AB[f(z)x]^C\right\} \;\equiv\; S(x,z) = \exp[f(z)x]^C = \beta(z)^{x^C}, \tag{5.90}$$

where $\beta(z)$ is an arbitrary positive function.

Model (5.90) for $C = 1$ becomes the model of independence.

The hazard function for this model is

$$h(x,z) = \frac{\dfrac{d\beta(z)}{dz}}{\beta(z)}x^c = -\frac{d\{\log[\beta(z)]\}}{dz}x^c = s(z)x^c.$$

If now we look for the common part of Models 1 and 3 we get the functional equation

$$S(x,z) = l^{-1}[p(z) + r(x)] = w[f(z)x],$$

which, by making the change of variable $u = f(z)$, becomes Pexider's Equation (5.37)

$$l[w(ux)] = p[f^{-1}(u)] + r(x),$$

with the general continuous-at-a-point solution

$$l[w(x)] = A\log(BCx); \;\; p[f^{-1}(x)] = A\log(Bx); \;\; r(x) = A\log(Cx),$$

and then we finally get

$$w(x) = l^{-1}[A\log(BCx)]; \;\; f^{-1}(x) = p^{-1}[A\log(Bx)]; \;\; r(x) = A\log(Cx),$$

which shows that Model 1 is a particular case of Model 3.

Finally, we compare Models 2 and 3. For the coincidence we must have

$$S(x,z) = l^{-1}[p_1(z) + r(x)] = p(z)^{q(x)},$$

and taking logarithms we get

$$q(x)\log p(z) = \log\{l^{-1}[p_1(z) + r(x)]\}$$

which implies

$$l\{\exp[q(x)\log p(z)]\} = p_1(z) + r(x),$$

which is Pexider's Equation. Thus, we have

$$\begin{aligned} l[\exp(x)] &= A\log(BCx), \\ r[q^{-1}(x)] &= A\log(Bx), \\ p_1\{p^{-1}[\exp(x)]\} &= A\log(Cx), \end{aligned}$$

and then

$$\begin{aligned} l^{-1}(x) &= \exp\left[\exp(x/A)/(BC)\right], \\ q(x) &= \exp\left(r(x)/A\right)/B, \\ p(z) &= \exp\left[\exp\left(p_1(z)/A\right)/C\right], \end{aligned}$$

which shows that Model 2 is a particular case of Model 3.

Thus, we can conclude that a consensus model could be model (5.90), which is the family of models common to all three members of the team.

figure 5.10 shows the required separate and consensus proposals as well as the common proposals associated with all three groups of only two members.

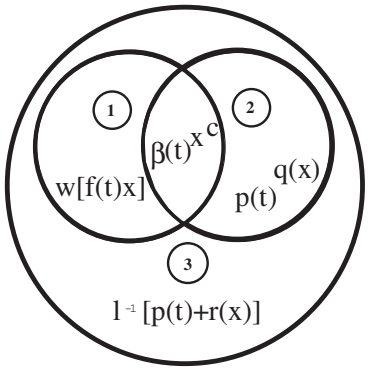


Figure 5.10: Illustration of separate and consensus proposals. Image from [46]

As a final conclusion, we can add that functional equations can prove themselves to be a very powerful tool to be used in model design. As a matter of fact, the engineer can state all the conditions to be satisfied by the desired model in terms of functional equations. Then, by first solving the resulting system and then in terms of its general solution, one can make the selection by playing with the remaining degrees of freedom.

# Part III

# Theoretical Contributions. Proposed Model

# Chapter 6

# The Weibull and Gumbel S–N Field Stress Based Fatigue Models

In this Chapter, the model which gives title to this doctoral thesis is presented.
Its derivation is based on the application of functional equations, studied in the previous chapter, and in the analysis of compatibility, statistical and physical conditions.

## 6.1 Introduction

The limitations of the models currently used in the fatigue design based on Wöhler curves (see Section 4.2 and table 4.1) are derived by the problem of characterizing to fatigue the material carrying out tests under constant stress levels.

These models are applicable for a given constant stress level but fail to predict the fatigue behavior when different stress levels are considered. Empirical mean stress equations, as those of Goodmann [75], modified Goodman (see Smith [122]), Soderberg [125], Morrow [96] and [98], Haibach ([77], Smith-Watson-Topper [123] and Walker [129], are currently applied for this transformation [59]. All of them refer lastly to the fatigue material properties related to tests performed for a reference stress range or stress level, and different quality fittings to the experimental results have been achieved according to the material and the state, notched or un-notched, of the structural member.

The author of this doctoral thesis and her supervisors, based on the compatibility conditions of the Wöhler field together with statistical and physical conditions and solving a system of functional equations, proposed for the first time a general fatigue regression model that includes the consideration of the mean effect, without the need of resorting to empirical relations, firstly in a simple 6-parameter Weibull model version [36], and later in an extended 9-parameter Weibull model version [42], which parameter evaluation required a relatively simple test strategy. Even if these two models represented a relevant advance in understanding the effect of the mean stress, its application was limited only to positive stress ranges $R$, a case frequently present in some structural elements. However, since load spectra, to which mechanical and structural elements are generally subject in practice, can include a significant portion of cycles under compressive

minimum stress, it implies an important limitation for the practical application of this model. Particularly, the consideration of testing under fully reversed stress, a standard choice for many laboratories, remained excluded.

In this work, a Weibull regression model for statistical analysis of stress life data for any possible loading situations in tension and compression is developed that is later transformed in a Gumbel model, as a revision of the previous version of the fatigue model, thus facilitating its application to real loading spectra. The model enforces the compatibility condition of the Wöhler fields associated with constant $\sigma_{min}$ and constant $\sigma_{max}$, that leads to a system of functional equations, which solution provides a model with the desired requirements.

The model depends on 8 parameters that can be estimated by maximum likelihood or non-linear regression methods, and supplies all the material basic probabilistic fatigue information to be used in a damage accumulation assessment for fatigue life prediction using practical load spectra.

The main achievements of the model proposed are:

- According to the Buckingham's theorem [31], only dimensionless variables are used in the model and the corresponding regression equation. This implies on one hand less variables involved in the problem, i.e., a simpler but not less powerful model and, on the other hand, that the parameters or constants resulting in the model are also dimensionless, that is, their values are independent of the units being used.

- The model is not based on arbitrary assumptions, but on sound physical and statistical properties exigeable to any fatigue model. Thus the model is the only one resulting from the selected constraints.

- The model provides useful statistical information including not only mean values but also variability of the model, and permits calculating probabilities.

Concerning the testing strategy, in the experimental common practice, material fatigue characterization consists of selecting several characteristic stress ratios $R$, ranging from $-1$ to 0.50 or even higher positive ratios, covering the region of interest. This ensures the applicability of the empirical stress level equation fitted to the data, that is obtained, for instance, by regression [2]. The model proposed enables us the consideration of other possible testing strategies due to its capability of evaluating data resulting from tests carried out for any constant $\sigma_{max}$, $\sigma_{min}$, $\sigma_{mean}$ or stress ratio $R$. In fact, tests can be repeated for a certain set of fixed stress levels, the only requirement being to cover a sufficient broad range of stress levels in order to guarantee reliability in the parameter estimation.

Once the basic material fatigue information related to the Wöhler field is supplied for any possible combinations of $\sigma_{max}$ and $\sigma_{min}$, a model is needed to perform a damage assessment allowing for life prediction. In this case, the model provides probabilistic bases for calculating the damage accumulation for any type of loading being considered. In fact, due to the possible identification of the probability of failure, represented by the percentile curves in the Wöhler field for any $\sigma_{max}$ and $\sigma_{min}$ with the damage state [42] the model can be used in cumulative damage calculations for fatigue life prediction of components subject to even complex loading histories. This issue is being the main objective of a joint research program launched presently at the Empa - Dübendorf, Switzerland. The experimental validation of the model (see Chapter 7) is based on data obtained from a set of experiments realized in this research institute.

The model is based in the works developed by Castillo (see [34] and [44]), Fernández–Canteli (see [64], [65] and [66]) and Castillo and Fernández–Canteli (see [37], [35], [39] and [36]).

## 6.2 Derivation of the model

Consider a fatigue test conducted at constant minimum and maximum stresses denoted for simplicity $\sigma_m$ and $\sigma_M$, respectively, and let $N$ be the random number of cycles to failure associated with the test. Then, one is interested in determining the probability of failure $p$ of a randomly chosen specimen when subject to such a test.

In this section a formula for $p$ in terms of $N, \sigma_m$ and $\sigma_M$ is derived, using as few arbitrary assumptions as possible. To this end, we use the Buckingham $\Pi$ theorem [31], some knowledge from fatigue and extreme value theory, and some compatibility assumptions.

The Buckingham $\Pi$ theorem states that if we have a physically meaningful equation involving a certain number, $n$, of physical variables, and these variables are expressible in terms of $k$ independent fundamental physical quantities, then the original expression is equivalent to an equation involving a set of $v = n - k$ dimensionless variables constructed from the original variables. This theorem states that in fact a set of less variables is sufficient to analyze the problem under consideration.

From fatigue knowledge, we introduce two new variables: a stress $\sigma_0$, which can be the fatigue limit or any other equivalent variable, and $N_0$ (cycles), which are used to obtain the required dimensionless variables. Thus, we conclude that our problem depends on the following 6 variables:

$$p, \sigma_m, \sigma_M, \sigma_0, N, N_0.$$

If we assume that there is a relationship among these variables

$$r(p, \sigma_m, \sigma_M, \sigma_0, N, N_0) = 0, \tag{6.1}$$

using the Buckingham $\Pi$ theorem, we can select the dimensionless variables $\sigma_m^* = \sigma_m/\sigma_0$, $\sigma_M^* = \sigma_M/\sigma_0$ and $N^* = N/N_0$ and $p$, already dimensionless, and then the relationship

$$g(p, N^*, \sigma_m^*, \sigma_M^*) = 0, \tag{6.2}$$

or

$$p = h(N^*, \sigma_m^*, \sigma_M^*), \tag{6.3}$$

is equivalent to (6.1). So, one of our aims is to obtain the function $h(N^*, \sigma_m^*, \sigma_M^*)$.

With this purpose in mind, we proceed as follows: First, we apply the fatigue model presented by Castillo et al. [39] for constant maximum stress $\sigma_M$ to the dimensionless variable

$$\Delta\sigma^* = \sigma_M^* - \sigma_m^* = \frac{\sigma_M - \sigma_m}{\sigma_0}. \tag{6.4}$$

Natural scale instead of a logarithmic scale for the stress amplitude arises as a natural requirement from the model. Otherwise inconsistencies arise in the solution of the functional equation when null or negative values for the stress range, i.e., compression in the $\sigma_{min}$, are considered.

According to these authors ([37], [43]) , the only possible model satisfying several physical conditions (weakest link principle and limited range), compatibility conditions (of life and stress range), statistical conditions (stability, limit behavior) and extreme value analysis properties ([33], [39], [36] and [70]) is the model

$$p = 1 - \exp\left\{ - \left[ \frac{(\log N^* - B)\,(\sigma_M^* - \sigma_m^* - C) - E}{D} \right]^A \right\}. \tag{6.5}$$

The physical meanings of the parameters are:

$A$: Weibull shape parameter of the cumulative distribution function (cdf) in the S–N field.

$B$: Threshold value of log-lifetime (see figure 6.1).

$C$: Endurance limit ($\Delta\sigma^*$) (see figure 6.1).

$E$: Parameter defining the position of the corresponding zero-percentile hyperbola.

$D$: Weibull scale factor.

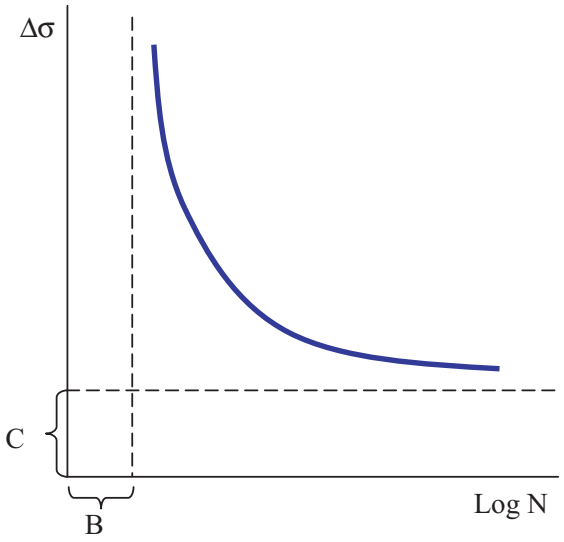


Figure 6.1: Schematic representation of the physical meanings of $B$ and $C$ model parameters.

We note that this model has not been arbitrarily chosen, but derived from a set of conditions that a reasonable model must satisfy. Finally, the use of functional equations ([11], [46] and [49]) guarantees that the resulting model in (6.6) is the unique solution.

An interesting limiting case of this model for $A \to \infty$ is the Gumbel model

$$p = 1 - \exp\left\{-\exp\left[\frac{(\log N^* - B)\,(\sigma_M^* - \sigma_m^* - C) - E}{D}\right]\right\}, \tag{6.6}$$

which also satisfies the previous conditions and will be used in this paper.

Assuming that the model is valid for any fixed values of $\sigma_m$ and $\sigma_M$, and since for different constant values of $\sigma_M$ one must have different models of the form (6.6), the parameters $A, B, C, D$ and $E$ must be functions of $\sigma_M$ [42].

Similarly, if the constant load fatigue tests are run for constant values of $\sigma_m$, one has another family of models, where now the parameters $A, B, C, D$ and $E$ are functions of $\sigma_m$. Our next goal is to obtain these functions using the following compatibility condition:

*If we run a constant load fatigue test oscillating from $\sigma_m$ to $\sigma_M$, we can derive the model as a particular case of (a) constant $\sigma_m$ or (b) constant $\sigma_M$, but both models must be the same (compatibility condition), that is:*

$$\left[\frac{(\log N^* - B_m(\sigma_m^*))(\Delta\sigma^* - C_m(\sigma_m^*)) - E_m(\sigma_m^*)}{D_m(\sigma_m^*)}\right]^{A_m} = \left[\frac{(\log N^* - B_M(\sigma_M^*))(\Delta\sigma^* - C_M(\sigma_M^*)) - E_M(\sigma_M^*)}{D_M(\sigma_M^*)}\right]^{A_M}. \tag{6.7}$$

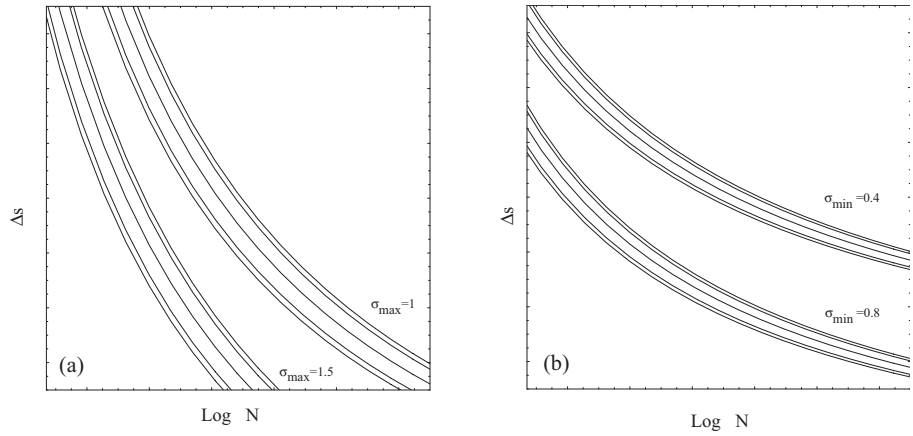


Figure 6.2: Wöhler curves for different percentiles: (a) for constant $\sigma_{max}$, (b) for constant $\sigma_{min}$. Image from [42]

The compatibility condition is represented at the intersection of both different families of curves $(\sigma_m, \sigma_M)$. Consider a situation, in which $R^*$ and $N$ of failure is known. If the load ratio $R^* = R_f$ is fixed, the probability of failure, defined by the area inside the probability density function (pdf), for a number of cycles $N_f$, will be $p(N, R^*) = p_{f1}$. On other hand, if the number of cycles is fixed $N = N_f$, the new probability of failure for a stress ratio $R^*$ will be $p(R^*, N) = p_{f2}$. The compatibility condition define that these two different probabilities $p_{f1}$ and $p_{f2}$ are equal (see figure 6.3).

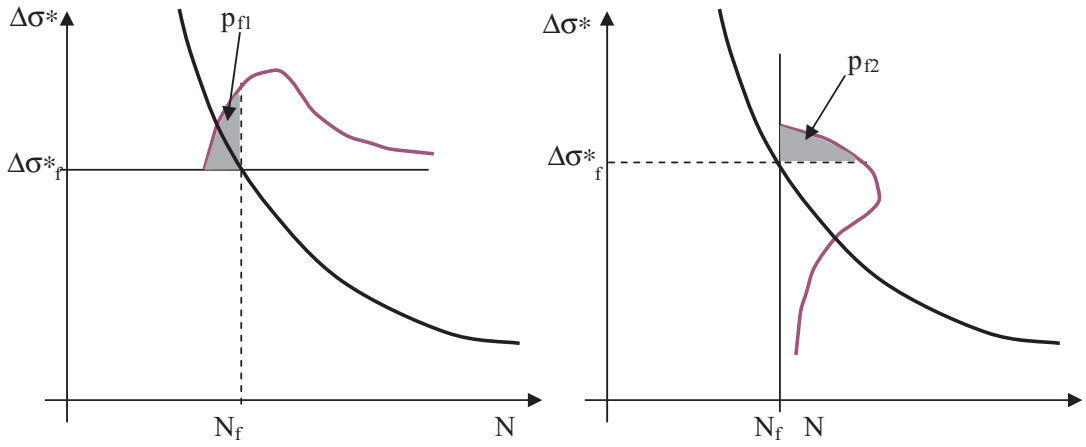


Figure 6.3: Schematic representation about the compatibility in Castillo's models (see [42], [40]).

This compatibility was shown in figure 8.1, where the compatibility states that the set of percentiles must intersect at horizontally aligned points.

Equation (6.7) is a functional equation, in which the unknowns are the 8 functions $B_m(\sigma_m^*)$, $C_m(\sigma_m^*)$, $D_m(\sigma_m^*)$, $E_m(\sigma_m^*)$, $B_M(\sigma_M^*)$, $C_M(\sigma_M^*)$, $D_M(\sigma_M^*)$ and $E_M(\sigma_M^*)$. The beauty of functional equations is that a single equation allows us determining the solution for all the unknown functions involved. The complete derivation of the model is made in Appendix A: Model

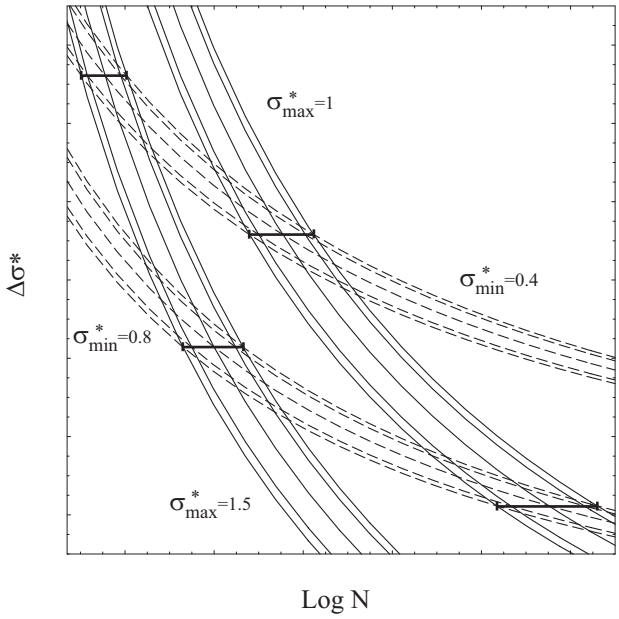


Figure 6.4: Schematic Wöhler curves for percentiles $\{0.01, 0.05, 0.5, 0.95, 0.99\}$ for $\sigma^*_{max} = 1$ and $\sigma^*_{max} = 1.5$, and $\sigma^*_{min} = 0.4$ and $\sigma^*_{min} = 0.8$, illustrating the compatibility condition. Dashed lines refer to Wöhler curves for constant $\sigma^*_{min}$, and continuous lines refer to Wöhler curves for constant $\sigma^*_{max}$. Image from [42].

Derivation.

For the functional equation (6.7) to be satisfied for any $N^*$, $\sigma^*_m$ and $\sigma^*_M$, both models must have the same parameters. Writing the model in (6.7) as

$$\left[\frac{\log N^* - \left[B_m(\sigma^*_m) + \frac{E_m(\sigma^*_m)}{\Delta\sigma^* - C_m(\sigma^*_m)}\right]}{\frac{D_m(\sigma^*_m)}{\Delta\sigma^* - C_m(\sigma^*_m)}}\right]^{A_m} = \left[\frac{\log N^* - \left[B_M(\sigma^*_M) + \frac{E_M(\sigma^*_M)}{\Delta\sigma^* - C_M(\sigma^*_M)}\right]}{\frac{D_M(\sigma^*_M)}{\Delta\sigma^* - C_M(\sigma^*_M)}}\right]^{A_M} \quad ; \quad \forall N^* \tag{6.8}$$

and forcing the Weibull parameters to coincide one gets:

$$A_m(\sigma^*_m) = A_M(\sigma^*_M); \quad \forall\sigma^*_m, \sigma^*_M \tag{6.9}$$

$$\frac{D_m(\sigma^*_m)}{D_M(\sigma^*_M)} = \frac{\Delta\sigma^* - C_m(\sigma^*_m)}{\Delta\sigma^* - C_M(\sigma^*_M)} = \frac{(\sigma^*_M - \sigma^*_m) - C_m(\sigma^*_m)}{(\sigma^*_M - \sigma^*_m) - C_M(\sigma^*_M)}; \quad \forall\sigma^*_m, \sigma^*_M \tag{6.10}$$

$$\begin{aligned} B_M(\sigma^*_M) &= B_m(\sigma^*_m) - \frac{E_M(\sigma^*_M)}{\Delta\sigma^* - C_M(\sigma^*_M)} + \frac{E_m(\sigma^*_m)}{\Delta\sigma^* - C_m(\sigma^*_m)} \\ &= B_m(\sigma^*_m) - \frac{E_M(\sigma^*_M)}{(\sigma^*_M - \sigma^*_m) - C_M(\sigma^*_M)} + \frac{E_m(\sigma^*_m)}{(\sigma^*_M - \sigma^*_m) - C_m(\sigma^*_m)}; \quad \forall\sigma^*_m, \sigma^*_M. \end{aligned} \tag{6.11}$$

The system of functional equations (6.9) to (6.11) deserve a careful attention because they involve a deep knowledge about our problem. In particular, they are not simple equalities, but each a full collection of equalities, because they must hold for any feasible pair $\sigma^*_m, \sigma^*_M$.

Solving the system of functional equations (6.9) to (6.11) (see appendix) one gets the Weibull model:

$$p = 1 - \exp\left\{-\left[C_0 + C_1\sigma^*_m + C_2\sigma^*_M + C_3\sigma^*_m\sigma^*_M + (C_4 + C_5\sigma^*_m + C_6\sigma^*_M + C_7\sigma^*_m\sigma^*_M)\log N^*\right]^A\right\}, \tag{6.12}$$

which depends on nine parameters supplying a complete probabilistic information for any Wöhler curves of the material related to whichever given stress level, and where $p = F(N; \sigma_m^*, \sigma_M^*)$. We note that (6.12) is the function $h(N^*, \sigma_m^*, \sigma_M^*)$ in (6.3) sought after.

We note that an important limiting case of the Weibull model is the Gumbel model which results for $A \to \infty$ [37]. In addition, if all the arguments used to obtain the Weibull model are derived for the Gumbel model we obtain exactly the same functional equations. This implies that a valid fatigue model is the following Gumbel model:

$$p = 1 - \exp\left\{-\exp\left[C_0 + C_1\sigma_m^* + C_2\sigma_M^* + C_3\sigma_m^*\sigma_M^* + (C_4 + C_5\sigma_m^* + C_6\sigma_M^* + C_7\sigma_m^*\sigma_M^*)\log N^*\right]\right\}, \tag{6.13}$$

which has the advantage of having one parameter less, and even more important, that the range of definition for $\log N$ includes the range $(-\infty, \infty)$. This avoids deciding whether or not we are in the allowable region.

## 6.3 Some properties of the model

The graphs $(\log N, \Delta\sigma)$ of the percentiles for fixed $\sigma_{max}$ or $\sigma_{min}$ are hyperbolas. We note that the hyperbolas arise not because of a reasonable, though nevertheless arbitrary assumption, but as the only possible solution to the functional equation (see Appendix A).

The two asymptotes of the hyperbolas can be calculated as follows.

- The asymptotic value of $\Delta\sigma$ for large $\log N$ keeping $\sigma_{min} = \sigma_m$ constant is

$$\Delta\sigma_{m0} = \lim_{N\to\infty} \Delta\sigma = -\frac{C_4 + \sigma_m(C_5 + C_6 + C_7\sigma_m)}{C_6 + C_7\sigma_m} \tag{6.14}$$

  and the asymptotic value of $\Delta\sigma$ for constant $\sigma_{max} = \sigma_M$ is

$$\Delta\sigma_{M0} = \lim_{N\to\infty} \Delta\sigma = \frac{C_4 + \sigma_M(C_5 + C_6 + C_7\sigma_M)}{C_5 + C_7\sigma_M}. \tag{6.15}$$

- Similarly, the asymptotic value of $\log N$ for large $\Delta\sigma$ keeping $\sigma_{min} = \sigma_m$ constant is

$$\log N_{m0} = \lim_{\Delta\sigma\to\infty} \log N = -\frac{C_2 + C_3\sigma_m}{C_6 + C_7\sigma_m}, \tag{6.16}$$

  and the asymptotic value of $\log N$ for constant $\sigma_{max} = \sigma_M$ is

$$\log N_{M0} = \lim_{\Delta\sigma\to\infty} \log N = -\frac{C_1 + C_3\sigma_M}{C_5 + C_7\sigma_M}. \tag{6.17}$$

It is interesting to see, that the general model allows the asymptotes to be dependent on the constant $\sigma_{min}$ and $\sigma_{max}$ levels being considered.

### 6.3.1 The regression equation for $\sigma_{max}$-$\log N$ for different stress ratios $R$

Since the common practice consists of using a regression equation to fit the $\sigma_{max}$-$\log N$ field, in this subsection the regression model resulting from the Weibull and Gumbel models are derived.

As an illustrative example, in the evaluation of fatigue results for different materials proposed by the MIL-HDBK-5G [2], a regression model of the form

$$\log N = A_1 + A_2 \log_{10}(S_{max}(1 - R)^{A_3} - A_4), \tag{6.18}$$

is considered, where $A_1, A_2, A_3$ and $A_4$ are constants with dimensions, except the dimensionless constant $A_3$. However, the bases for selecting this model are not given.

Alternatively, a regression model based on physical and statistical grounds is presented below.

According to the model (6.12), the $p$ percentile of $\log N$ for a given $\sigma_{max}$ and stress ratio $R$ can be derived from expression (6.12) by replacing $\sigma_{min}$ by $\sigma_{max} - \Delta\sigma$, to obtain

$$\log N = \frac{C_0 + C_2\sigma_{max} + C_1 R\sigma_{max} + C_3 R\sigma_{max}^2 - (-\log[1-p])^{1/A}}{C_4 + C_6\sigma_{max} + C_5 R\sigma_{max} + C_7 R\sigma_{max}^2}, \tag{6.19}$$

and the regression equation for $\sigma_{max}$-$\log N$ for different stress ratios $R$, taking into account that the mean is a percentile dependent on $A$, can be obtained replacing $(-\log(1-p))^A$ by $\Gamma\left(1+1/A\right)$, where $\Gamma$ is the gamma function, which is the mean for the Weibull $W(0,1,A)$ model, leading to the expression

$$\log N = \frac{C_0 + C_2\sigma_{max} + C_1 R\sigma_{max} + C_3 R\sigma_{max}^2 - \Gamma\left(1+\frac{1}{A}\right)}{C_4 + C_6\sigma_{max} + C_5 R\sigma_{max} + C_7 R\sigma_{max}^2}, \tag{6.20}$$

which for the Gumbel model becomes

$$\log N = \frac{C_0 + C_2\sigma_{max} + C_1 R\sigma_{max} + C_3 R\sigma_{max}^2 + \gamma}{C_4 + C_6\sigma_{max} + C_5 R\sigma_{max} + C_7 R\sigma_{max}^2}, \tag{6.21}$$

where $\gamma = 0.57772$ is the Euler-Mascheroni number.

The relevant issue of Equations (6.20) and (6.21) is that they have been derived from all the indicated properties, and not arbitrarily chosen. Thus, this regression model will be selected to fit the experimental data.

## 6.4 Restrictions

For the model to be physically and statistically valid its parameters must satisfy the following constraints:

### 6.4.1 Physical restrictions

1. The asymptotic value $\Delta\sigma_{m0}$ must be non-negative, i.e.

$$\Delta\sigma_{m0} = -\frac{C_4 + \sigma_m(C_5 + C_6 + C_7\sigma_m)}{C_6 + C_7\sigma_m} \geq 0. \tag{6.22}$$

2. The asymptotic value $\Delta\sigma_{m0}$, due to physical reasons, must be non-increasing in $\sigma_m$, that is,

$$(C_6 + C_7\sigma_m)^2 + C_5C_6 - C_4C_7 \geq 0. \tag{6.23}$$

3. The asymptotic value $\Delta\sigma_{M0}$ must be non-negative, i.e.

$$\Delta\sigma_{M0} = \frac{C_4 + \sigma_M(C_5 + C_6 + C_7\sigma_M)}{C_5 + C_7\sigma_M} \geq 0. \tag{6.24}$$

4. The asymptotic value $\Delta\sigma_{M0}$ must also be non-increasing in $\sigma_M$, that is,

$$(C_5 + C_7\sigma_M)^2 + C_5C_6 - C_4C_7 \leq 0. \tag{6.25}$$

5. The asymptotic value $\log N_{m0}$ must be non-increasing in $\sigma_m$:

$$C_3C_6 - C_2C_7 \geq 0. \tag{6.26}$$

6. The asymptotic value of $\log N_{M0}$ must be non-increasing in $\sigma_M$:

$$C_3C_5 - C_1C_7 \geq 0. \tag{6.27}$$

### 6.4.2 Statistical restrictions

1. The cdf in (6.12) must be non-decreasing in $\log N$:

$$C_4 + C_5\sigma_m + C_6\sigma_M + C_7\sigma_m\sigma_M > 0; \quad \sigma_{m0} \leq \sigma_m \leq \sigma_M \leq \sigma_{M0}, \tag{6.28}$$

which implies:

$$\begin{aligned} C_4 + C_5\sigma_{m0} + C_6\sigma_{M0} + C_7\sigma_{m0}\sigma_{M0} &> 0 && (6.29)\\ C_4 + C_5\sigma_{m0} + C_6\sigma_{m0} + C_7\sigma_{m0}\sigma_{m0} &> 0 && (6.30)\\ C_4 + C_5\sigma_{M0} + C_6\sigma_{M0} + C_7\sigma_{M0}\sigma_{M0} &> 0. && (6.31) \end{aligned}$$

2. The cdf in (6.12) must be non-increasing in $\sigma_m$:

$$C_1 + C_3\sigma_M + (C_5 + C_7\sigma_M)\log N \leq 0; \quad N_0 \leq N; \quad \sigma_{m0} \leq \sigma_M \geq \sigma_{M0}, \tag{6.32}$$

3. The cdf in (6.12) must be non-decreasing in $\sigma_M$:

$$C_2 + C_3\sigma_m + (C_6 + C_7\sigma_m)\log N \geq 0; \quad N_0 \leq N; \quad \sigma_{m0} \leq \sigma_m \leq \sigma_{M0}, \tag{6.33}$$

4. The curvature of the zero-percentile of $(\log N, \Delta\sigma)$ for constant $\sigma_{min}$ must be non-negative, that is, $\dfrac{\partial^2\Delta\sigma}{\partial(\log N)^2} \geq 0$, which leads to:

$$\begin{aligned} (C_6 + C_7\sigma_m)\left(\sigma_m(C_1C_6 - C_3C_4) + (C_1C_7 - C_3C_5)\sigma_m^2 - C_2(C_4 + C_5\sigma_m)\right) & \\ +(C_0 - (-\log(1-p))^{1/A})(C_6 + C_7\sigma_m)^2 &\leq 0 \end{aligned} \tag{6.34}$$

It is sufficient to force the positivity at one point, as for example, $p = 0.5$.

5. The curvature of the zero-percentile of $(\log N, \Delta\sigma)$ for constant $\sigma_{max}$ must be non-negative, that is, $\dfrac{\partial^2\Delta\sigma}{\partial(\log N)^2} \geq 0$, leading to:

$$\begin{aligned} (C_5 + C_7\sigma_M)\left(\sigma_M(C_2C_5 - C_3C_4) + (C_2C_7 - C_3C_6)\sigma_M^2 - C_1(C_4 + C_6\sigma_M)\right) & \\ +(C_0 - (-\log(1-p))^{1/A})(C_5 + C_7\sigma_M)^2 &\leq 0, \end{aligned} \tag{6.35}$$

Inclusion of these constraints into the estimation method leads to valid models. This is an important fact to be taken into consideration, because alternative methods do not take this into account sufficiently, and lack generality.

### 6.4.3 Range of the problem. Simplifications of constraints

In order to make the application of these restriction (Equations (6.28)-(6.35)) easy, an analysis of the ranges of application of the model can be made. The ranges are:

- The ranges of $\sigma^*_{min}$ and $\sigma^*_{max}$ are

$$\sigma^*_{min} \in [-1, 1]; \quad \sigma^*_{max} \in [0, 1] \qquad \forall \quad \sigma_{min} \leq \sigma_{max}, \tag{6.36}$$

  so, the range of $\Delta\sigma$ is

$$\Delta\sigma^* = \sigma^*_{max} - \sigma^*_{min} \quad \rightarrow \quad \in [-1, 2], \tag{6.37}$$

  But, knowing that $\sigma_{max}$ must be greater than $\sigma_{min}$, the range of $\Delta\sigma$ is finally $\Delta\sigma \in [0, 2]$ (see figure 6.5).

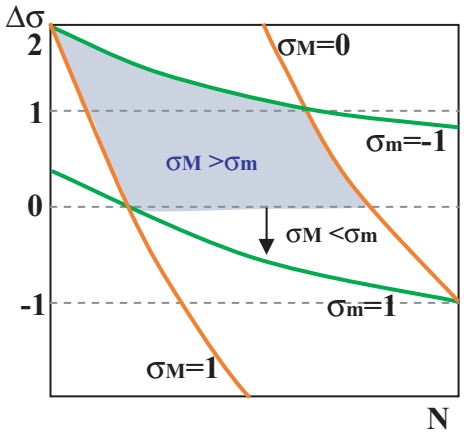


Figure 6.5: Schematic representation of the range of the problem.

- The range for the number of cycles, $N$, goes from $N = 1 \rightarrow \log N = 0$, to $N = \infty \rightarrow \log N = \infty$.

But this last hypothesi about the range of number of cycles, doesn't give a useful information about the simplification of the constraints because almost all these constraints are defined in the range of load. So, according to this, the final constraints are:

1. The cdf constraints (Equations (6.29) to (6.31)) are transformed in

$$C_4 \geq 0 \tag{6.38}$$
$$C_4 - C_5 \geq 0 \tag{6.39}$$
$$C_4 + C_5 \geq 0 \tag{6.40}$$
$$C_4 - C_5 + C_6 - C_7 \geq 0 \tag{6.41}$$
$$C_4 + C_5 + C_6 + C_7 \geq 0. \tag{6.42}$$

2. The curvature of the zero-percentile of $(\log N, \Delta\sigma)$ for constant $\sigma_{min}$ (Equation (6.34)) leads to:

$$(C_6 - C_7)[(C_0 + \gamma)(C_6 - C_7) + C_3(C_4 - C_5) + C_1(C_7 - C_6) + C_2(C_5 - C_4)] \leq 0 \tag{6.43}$$
$$(C_6 + C_7)[(C_0 + \gamma)(C_6 + C_7) + C_1(C_6 - +C_7) - (C_2 + C_3)(C_4 + C_5)] \leq 0. \tag{6.44}$$

3. The curvature of the zero-percentile of $(\log N, \Delta\sigma)$ for constant $\sigma_{max}$ (Equaton (6.35)) is now:

$$C_5[C_5(C_0+\gamma) - C_1C_4] \leq 0 \quad (6.45)$$
$$(C_5+C_7)[(C_0+C_2+\gamma)(C_5+C_7) - (C_4+C_6)(C_1+C_3)] \leq 0. \quad (6.46)$$

4. The asymptotic value $\Delta\sigma_{m0}$ (Equation (6.23)) is:

$$(C_6-C_7)^2 + C_5C_6 - C_4C_7 \geq 0 \quad (6.47)$$
$$(C_6+C_7)^2 + C_5C_6 - C_4C_7 \geq 0. \quad (6.48)$$

5. The asymptotic value $\Delta\sigma_{M0}$ (Equation (6.25)) is transformed now to:

$$C_5^2 + C_5C_6 - C_4C_7 \leq 0 \quad (6.49)$$
$$(C_5+C_7)^2 + C_5C_6 - C_4C_7 \leq 0. \quad (6.50)$$

## 6.5 Resulting models and submodels

In this section, we discuss some particular and interesting submodels of the general Gumbel model (6.13).

### 6.5.1 General model

The general model with $\Delta\sigma$ and $\log N$ asymptotes dependent on $\sigma_m$ and $\sigma_M$ was defined in Equation (6.13):

$$p = 1 - \exp\left\{-\exp\left[C_0 + C_1\sigma_m^* + C_2\sigma_M^* + C_3\sigma_m^*\sigma_M^* + (C_4 + C_5\sigma_m^* + C_6\sigma_M^* + C_7\sigma_m^*\sigma_M^*)\log N^*\right]\right\}, \quad (6.51)$$

subject to constraints (6.22) to (6.35), Equations (6.38)-(6.50).

### 6.5.2 Submodel Nr.1

The first submodel is the linear model of (6.13). To have a linear submodel it is necessary to have no asymptotes and any product between variables (load and number of cycles), because these products transform the problem from a linear to a nonlinear problem. The variables affected are $C_5, C_6$ and $C_7$ that must be equal to zero.

The simplest model is:

$$p = 1 - \exp\left\{-\exp\left[C_0 + C_1\sigma_m^* + C_2\sigma_M^* + C_3\sigma_m^*\sigma_M^* + C_4\log N^*\right]\right\} \quad C_4 \geq 0, \quad (6.52)$$

Note that this submodel in a semilog scale leads to a Wöhler field made of straight lines (see figure 6.6 (a)).

### 6.5.3 Submodel Nr. 2

This submodel has a fixed vertical asymptote. The model with $\log N$ asymptote independent on $\sigma_m$ and $\sigma_M$:

$$p = 1 - \exp\left\{-\exp\left[C_0 + C_2(\tfrac{C_5}{C_6}\sigma_m^* + \sigma_M^* + \tfrac{C_7}{C_6}\sigma_m^*\sigma_M^*) + (C_4 + C_5\sigma_m^* + C_6\sigma_M^* + C_7\sigma_m^*\sigma_M^*)\log N^*\right]\right\}, \quad (6.53)$$

which is obtained for $C_1 = \frac{C_2 C_5}{C_6}; C_3 = \frac{C_2 C_7}{C_6}$, subject to constraints (6.22) to (6.35). Replacing $C_3 = C_7 = 0$ into these constraints, and taking into account the range of load (Equations (6.38)-(6.50)) one concludes that they are equivalent to the set of constraints:

$$\begin{aligned}
C_4 &\geq 0 \\
C_4 - C_5 &\geq 0 \\
C_4 + C_5 &\geq 0 \\
C_4 - C_5 + C_6 - C_7 &\geq 0 \\
C_4 + C_5 + C_6 + C_7 &\geq 0 \\
(C_6 - C_7)[(C_0 + \gamma)(C_6 - C_7) + C_2(C_4 - C_5 + \frac{1}{C_6}(C_4 C_7 - C_5 C_6 - 2C_5 C_7))] &\leq 0 \\
(C_6 + C_7)[(C_0 + \gamma)(C_6 + C_7) - C_2 C_4(1 + \frac{C_7}{C_6})] &\leq 0 \\
C_5^2[C_0 + \gamma - \frac{C_2 C_4}{C_6}] &\leq 0 \\
(C_5 + C_7)[(C_0 + \gamma)(C_5 + C_7) + C_2(C_5 - C_7 - 2\frac{C_5 C_4}{C_6} - 2C_2 C_5)] &\leq 0 \\
(C_6 - C_7)^2 + C_5 C_6 - C_4 C_7 &\geq 0 \\
(C_6 + C_7)^2 + C_5 C_6 - C_4 C_7 &\geq 0 \\
C_5^2 + C_5 C_6 - C_4 C_7 &\leq 0 \\
(C_5 + C_7)^2 + C_5 C_6 - C_4 C_7 &\leq 0. \qquad (6.54)
\end{aligned}$$

This model is represented in figure 6.6 (b).

### 6.5.4 Submodel Nr. 3

The third submodel has a fixed horizontal asymptote. The model with $\Delta\sigma$ asymptote independent on $\sigma_m$ and $\sigma_M$ (figure 6.6 (c)) is:

$$p = 1 - \exp\left\{-\exp\left[C_0 + C_1\sigma_m^* + C_2\sigma_M^* + C_3\sigma_m^*\sigma_M^* + \log N^*\left(C_4 + C_5\sigma_m^* + C_6\sigma_M^* + \tfrac{C_5 - C_6}{\sigma_m^* - \sigma_M^*}\sigma_m^*\sigma_M^*)\right)\right]\right\}, \qquad (6.55)$$

which is obtained for $C_7 = \frac{C_5 C_6}{\sigma_m^* - \sigma_M^*}$, that taking into account the range of load transform $C_5 = C_6$ and $C_7 = 0$. The final constraints of this submodel are:

$$\begin{aligned}
C_4 &\geq 0 \\
C_4 - C_5 &\geq 0 \\
C_4 + C_5 &\geq 0 \\
C_4 - 2C_5 &\geq 0 \\
C_4 + 2C_5 &\geq 0 \\
C_5[C_5(C_0 + \gamma - C_1 + C_2 - C_3) + C_4(C_3 - C_2)] &\leq 0 \\
C_5[C_5(C_0 + \gamma + C_1 - C_2 + C_3) + C_4(C_3 - C_2)] &\leq 0 \\
C_5[C_5(C_0 + \gamma) - C_1 C_4] &\leq 0 \\
C_5[C_5(C_0 + \gamma + C_2 - C_1 - C_3) - C_4(C_1 + C_3)] &\leq 0. \qquad (6.56)
\end{aligned}$$

But, from Equations (6.47)-(6.50), the model leads to $C_5 = C_6 = 0$ that, in addition with $C_7 = 0$ transform this submodel in the linear submodel.

### 6.5.5 Submodel Nr. 4

This submodel with both fixed asymptotes, is derived from the two previous models, Equations (6.53) and (6.55). So, with $C_5 = C_6 = C_7 = 0$ the model leads to $C_3 = 0$ and $C_1 = C_2$. Finally, the model with $\Delta\sigma$ and $\log N$ asymptotes independent on $\sigma_m$ and $\sigma_M$ (see figure 6.6 (d)) is a model with only three parameters:

$$p = 1 - \exp\left\{-\exp\left[C_0 + C_1(\sigma_m^* + \sigma_M^*) + C_4 \log N^*\right]\right\}, \quad C_4 \geq 0. \tag{6.57}$$

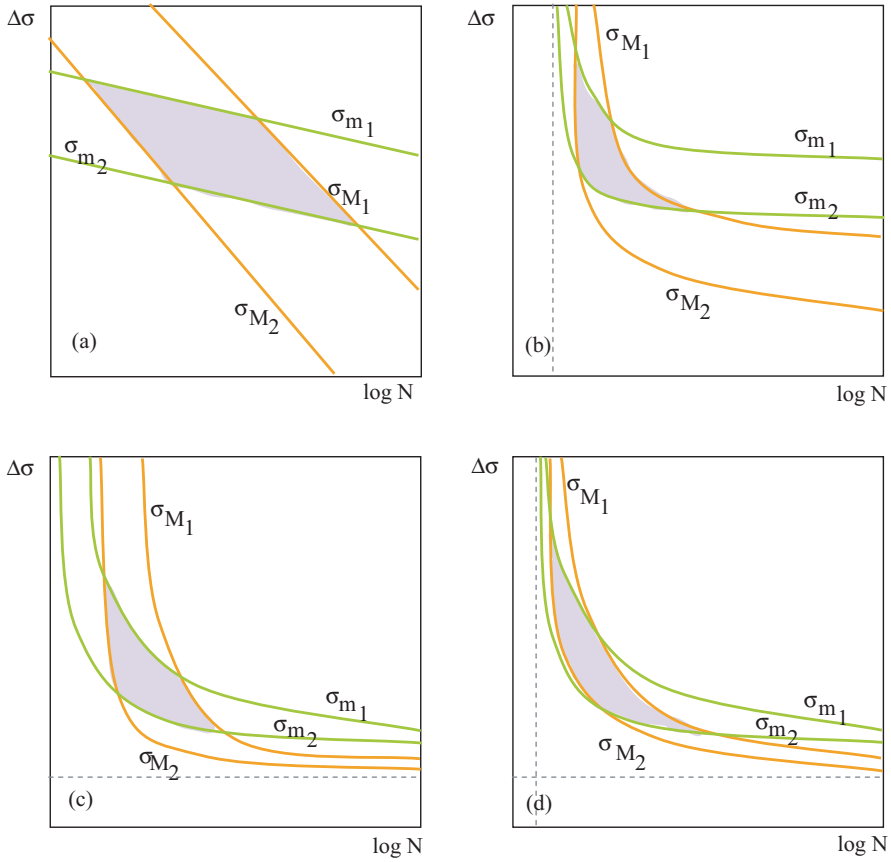


Figure 6.6: Schematic representation of different sub-models.

### 6.5.6 Submodel Nr. 5

The last submodel presented in this section is obtained analyzing the situation of the asymptotes and the cdf function:

$$p = 1 - \exp\left\{-\exp\left[C_0 + C_1\sigma_m^* + C_2\sigma_M^* + \log N^*[C_5(\sigma_m^* - \sigma_M^*])\right]\right\}, \tag{6.58}$$

which is obtained for $C_3 = C_4 = C_7 = 0$, that operating become in $C_6 = -C_5$. that taking into account the range of load transform $C_5 = C_6$ and $C_7 = 0$. The final constraints of this

sub-model are:

$$\begin{aligned} C_1 &\leq 0 \\ C_5 &\leq 0 \\ \log N &\geq -\frac{C_1}{C_5}. \end{aligned} \tag{6.59}$$

This submodel is used in the appendix D, where an informatic tool (SISIFO program) is presented.

## 6.6 Parameter estimation

The parameter estimation of the model can be done by several methods. The two most useful are described below.

### 6.6.1 Maximum likelihood estimation

The most well known method for estimating the parameters of a statistical model is the maximum likelihood method, which shows good statistical properties. Thus, it is one of the first possibilities to be considered.

The log-likelihood function of the Weibull model (6.13) is

$$L = \sum_{i \in I_1} \left[ \log(A) + (A-1)\log(H(N_i^*)) + \log\left(C_4 + C_5\sigma^*_{m_i} + C_6\sigma^*_{M_i} + C_7\sigma^*_{m_i}\sigma^*_{M_i}\right) - \log(N_i^*) \right] - \sum_{i \in I_1 \cup I_0} H^A(N_i^*), \tag{6.60}$$

where $I_1$ and $I_0$ are the set of non-runouts and runouts, respectively, $N_i$ refers to the actual value of the fatigue life in number of cycles, or the limit number of cycles for runouts, and

$$H(N_i) = C_0 + C_1\sigma^*_{m_i} + C_2\sigma^*_{M_i} + C_3\sigma^*_{m_i}\sigma^*_{M_i} + \left(C_4 + C_5\sigma^*_{m_i} + C_6\sigma^*_{M_i} + C_7\sigma^*_{m_i}\sigma^*_{M_i}\right)\log N_i^*. \tag{6.61}$$

Similarly, for the Gumbel model (6.13), the log-likelihood becomes:

$$L = \sum_{i \in I_1} \left[ H(N_i^*) + \log\left(C_4 + C_5\sigma^*_{m_i} + C_6\sigma^*_{M_i} + C_7\sigma^*_{m_i}\sigma^*_{M_i}\right) - \log(N_i^*) \right] - \sum_{i \in I_1 \cup I_0} \exp(H(N_i^*)). \tag{6.62}$$

Thus, to estimate the parameters of the model we can maximize (6.60) or (6.62) with respect to the parameters, but subject to the set of constraints (6.38) to (6.50) or the equivalent ones for simpler models. For the Weibull models one must add the condition $H(N_i) \geq 0; \forall i$, which is a very disturbing set of constraints, because the $C$'s are unknown. Thus, when possible, it is recommendable to use the Gumbel model instead of the Weibull model because of its simplicity and due to the fact that estimation is much easier. If the values of the $A$ parameter are high, as it happens to be with many materials, the Gumbel model is the most convenient option to choose.

If the optimum value is not on the boundary of the feasible region, the asymptotic covariance matrix of the estimates $C_0, C_1, C_2, C_3, C_4, C_5, C_6, C_7$ can be calculated using the well known formula

$$Covar = \left( -\frac{\partial L^2}{\partial C_i \partial C_j} \right)\Bigg|_{\mathbf{C}}^{-1} \tag{6.63}$$

where $\mathbf{C}$ are the maximum likelihood parameter estimates. This matrix is the basic tool to determine confidence intervals of other related variables, as percentiles for example.

If the optimum value is on the boundary of the feasible region, the covariance matrix must be obtained by the bootstrap method (see [63], [99]).

### 6.6.2 Parameter estimation by regression

Another possibility consists of using a regression model, i.e., minimize the following sum of squares for the Weibull model

$$Q = \sum_{i=1}^{n} \left( \log N + \frac{C_0 + C_2\sigma^*_{max} + C_1 R\sigma^*_{max} + C_3 R{\sigma^*_{max}}^2 - \Gamma\left(1 + \frac{1}{A}\right)}{C_4 + C_6\sigma^*_{max} + C_5 R\sigma^*_{max} + C_7 R{\sigma^*_{max}}^2} \right)^2, \tag{6.64}$$

based on (6.20), where the parameter $A$ must be estimated using other methods, or for the Gumbel model

$$Q = \sum_{i=1}^{n} \left( \log N + \frac{C_0 + C_2\sigma^*_{max} + C_1 R\sigma^*_{max} + C_3 R{\sigma^*_{max}}^2 + \gamma}{C_4 + C_6\sigma^*_{max} + C_5 R\sigma^*_{max} + C_7 R{\sigma^*_{max}}^2} \right)^2, \tag{6.65}$$

subject to the constraints (6.38) to (6.50).

To estimate the shape Weibull parameter $A$ one can use a sample with constant $\sigma_{max}$, $\sigma_{min}$ or $R = \sigma_{min}/\sigma_{max}$, because the corresponding distribution is Weibull with the same $A$ parameter. Once this has been estimated, one can minimize (6.64) to estimate the remaining parameters.

For large sample sizes one could avoid the constraints, and assume that the data already contain the necessary information about the constraints. However, this is very risky, and one can face problems depending on the posterior use of the model

There are other methods to estimate the parameters of the model (see [38] and [44]).

## 6.7 Use of the model in practise

The general expression of the model is presented in Equation (6.13), based on the three variables defined in Section 6.2, $\sigma^*_m = \sigma_m/\sigma_0$, $\sigma^*_M = \sigma_M/\sigma_0$ and $N^* = N/N_0$. These equations show that the model in (6.13) really depends on 8 parameters, and that $\sigma_0$ and $N_0$ can be chosen arbitrarily to obtain dimensionless stress ratios close to one to avoid numerical difficulties.

The proceeding steps in practice are:

**Step 1:** *Design of the testing strategy.* A set of testing cases encompassing several stress level conditions, i.e., varying $\sigma_M$ and $\sigma_m$ is selected, for example, the set of pairs

$$\{(\sigma_{m_i}, \sigma_{M_i}) \mid i = 1, 2, \ldots, n\},$$

which cover the desired region, where the regression equation is to be used.

**Step 2:** *Choose the normalizing variables* $\log N_0$ *and* $\sigma_0$*.* Choose $\log N_0$ and $\sigma_0$ and normalize the data to dimensionless form.

**Step 3:** *Estimate the model parameters.* Use one of the estimation methods discussed in Section 6.6 to estimate the parameters $C_0, C_1, C_2, C_3, C_4, C_5, C_6, C_7$ in (6.13).

**Step 4:** *Extrapolate to other testing conditions.* Use the model (6.13) and the parameters $C_1, C_2, C_3, C_4, C_5, C_7$ and $\log N_0$ and $\sigma_0$ for any other testing condition (see Section 6.7.1).

### 6.7.1 Some different representations of the Gumbel model

There are, different parametric forms for the Wöhler field, as required by the user. In the next lines a representation of the most useful forms are defined.

1. $\Delta\sigma$-$\log N$ for constant $\sigma_M$:

$$\log N = \frac{-C_0 + C_1\Delta\sigma - C_1\sigma_M - C_2\sigma_M + C_3\Delta\sigma\sigma_M - C_3\sigma_M^2 + \log(-\log(1-p))}{C_4 - C_5\Delta\sigma + C_5\sigma_M + C_6\sigma_M - C_7\Delta\sigma\sigma_M + C_7\sigma_M^2} \tag{6.66}$$

2. $\Delta\sigma$-$\log N$ for constant $\sigma_m$:

$$\log N = \frac{-C_0 - C_2\Delta\sigma - C_1\sigma_m - C_2\sigma_m - C_3\Delta\sigma\sigma_m - C_3\sigma_m^2 + \log(-\log(1-p))}{C_4 + C_6\Delta\sigma + C_5\sigma_m + C_6\sigma_m + C_7\Delta\sigma\sigma_m + C_7\sigma_m^2} \tag{6.67}$$

3. $\Delta\sigma$-$\log N$ for constant $\sigma_{mean}$:

$$\log N = \frac{-4C_0 + 2C_1\Delta\sigma - 2C_2\Delta\sigma + C_3\Delta\sigma^2 - 4\sigma_{mean}(C_1 + C_2 + C_3\sigma_{mean}) + 4\log(-\log(1-p))}{4C_4 - 2C_5\Delta\sigma + 2C_6\Delta\sigma - C_7\Delta\sigma^2 + 4\sigma_{mean}(C_5 + C_6 + C_7\sigma_{mean})} \tag{6.68}$$

4. $\Delta\sigma$-$\log N$ for constant $R$:

$$\log N = \frac{-C_0(R-1)^2 - \Delta\sigma(C_2(1-R) + R(C_1 + C_3\Delta\sigma - C_1R)) + (R-1)^2\log(-\log(1-p))}{C_4(R-1)^2 + \Delta\sigma(C_6(1-R) + R(C_5 + C_7\Delta\sigma - C_5R))} \tag{6.69}$$

## 6.8 Example of application

### 6.8.1 Validation using data in the existing literature

To check the model performance and to illustrate its application to practical cases, the model is applied in this section to a real example [40].

This example, uses some data published in the existing literature. The data correspond to fatigue results from the MIL-HDBK-5G [2]. In particular, fatigue sample data from specimens made of notched Inconel 718 bars including three stress ratios ($R = -0.50, 0.10, 0.50$).

Since in Section 6.7 a methodology has been proposed to deal with practical cases, it is applied here step by step, as follows:

**Step 1:** *Design of the testing strategy.* In this example, data is derived from published data, so there isn't a testing strategy. In Chapter 7 a real strategy will be presented.

**Step 2:** *Choose the normalizing variables* $\log N_0$ *and* $\sigma_0$. As indicated, we have chosen $\log N_0 = 0$ ($N_0 = 1$ cycle) and $\sigma_0 = 1000$ MPa. and normalized the data to dimensionless form by dividing the lifetime and stresses by 1 cycle and 1000 MPa, respectively.

**Step 3:** *Estimate the model parameters.* We have used the maximum likelihood method for the Gumbel models as discussed in Section 6.6.1 to estimate the parameters $C_0, C_1, C_2, C_3, C_4, C_5, C_6$ and $C_7$ in the Gumbel model (6.13) and the resulting parameter estimates are shown in table 6.1.

The following cases have been considered:

Table 6.1: Parameter estimates cases 1 to 4.

| Case | Parameters | | | | | | | |
|---|---|---|---|---|---|---|---|---|
| | $C_0$ | $C_1$ | $C_2$ | $C_3$ | $C_4$ | $C_5$ | $C_6$ | $C_7$ |
| 1 | -46748.8 | 11631.7 | -20502.9 | -10430.8 | 2457.73 | -5134. | 5737.14 | 3070.4 |
| 2 | -10.1959 | 44.7721 | -39.1862 | 0 | 0 | -5.66951 | 5.66951 | 0 |
| 3 | -10.8552 | 42.8311 | -36.9141 | 0 | 0 | -5.56015 | 5.56015 | 0 |
| 4 | -12.1504 | 49.975 | -42.9144 | 0 | 0 | -6.34962 | 6.34962 | 0 |

**Case 0.** It corresponds to the regression model (6.18) without constraints fitted to all data excluding runouts. The data and the corresponding curves provided in the MIL-HDBK-5G are plotted in the top graph of figure 6.7. The fit is reasonably good, but the quality of extrapolations based on this model is not guaranteed by a physically justified regression equation.

**Case 1.** It corresponds to the general 8 parameter regression model (6.13) without constraints fitted to all data excluding runouts. The intermediate graph of figure 6.7 shows the real data classified by $R$ values, together with the estimated (regression) curves. The fit is better than in the previous case, especially in the lower region. In adition, since the regression model has been derived based on physical and statistical bases, the extrapolation can be done with a higher reliability. However, taking into account that the constraints were not imposed and normally not all will be satisfied, extrapolation must be done with care.

**Case 2.** It corresponds to the Gumbel version of the model (6.57) with fixed asymptotes including all the constraints and fitted with all data excluding the runouts. The corresponding model is plotted in the lower part of figure 6.7. Since the model used has been constrained by a high number of constraints or conditions, the fit of the model to the data is not as good as in the previous case. However, this is not a shortcoming but on the contrary can be considered as an advantage. In fact, the plot reveals that the data point with the smallest number of cycles to failure appears to be an outlier, and in fact it corresponds to the low cycle fatigue region. In addition, the curvature of the data points for $R = -0.5$ points out to the possibility of a plastic failure. Note that the outlier character of this point was hidden in the two previous cases.

**Case 3.** It corresponds to the Gumbel version of the model (6.13) with fixed asymptotes including all the constraints and fitted with all data including the runouts. The model appears in the upper part of figure 6.8. In this case the runouts were not removed, but taken into consideration in the estimation process, using expression (6.62). Note that the runouts do not contain exact information about the lifetime, but contain some information, which is also valuable, and must not be neglected. A comparison of the plots of cases 2 and 3 show that they are very similar, and that the main differences occur in the lower right region, as expected. Note that again the data point with the least lifetime appears as a clear outlier, which was not the case for cases 0 and 1.

**Case 4.** It corresponds to the Gumbel version of the model (6.13) with fixed asymptotes including all the constraints and fitted with all data but the outlier and including the runouts. The model appears in the lower part of figure 6.8. Since the data point with the smallest lifetime appears as an outlier and there are physical reasons to justify it, in this

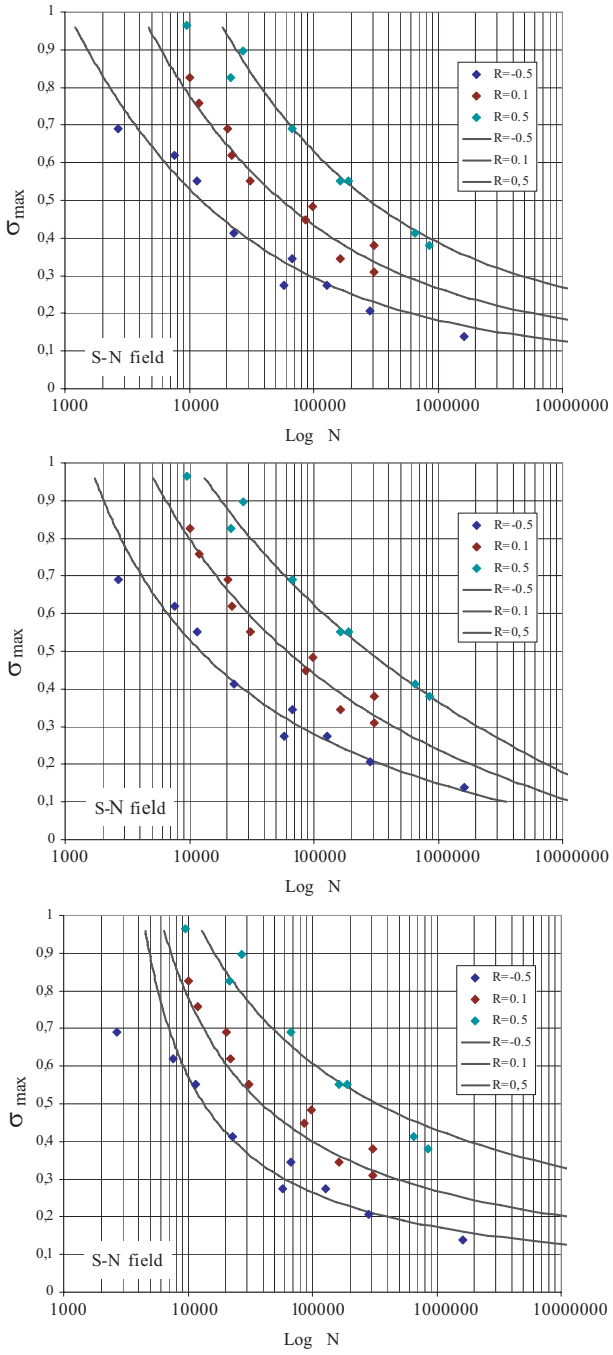


Figure 6.7: S–N curves for notched $K_t = 3.3$, AISI 4340 Alloy steel bar fitted by three different methods. The upper corresponds to the MIL-HDBK-5G, the intermediate to the proposed model without constraints and the lower to the proposed model including all the constraints.

case this data point has been removed and the model re-estimated. A comparison with the plots of case 3 reveals that the resulting models are very similar, and then one can conclude that the outlier has a negligible influence due to the strong constraints imposed to the model. So, the robustness of the proposed estimation regression method has been

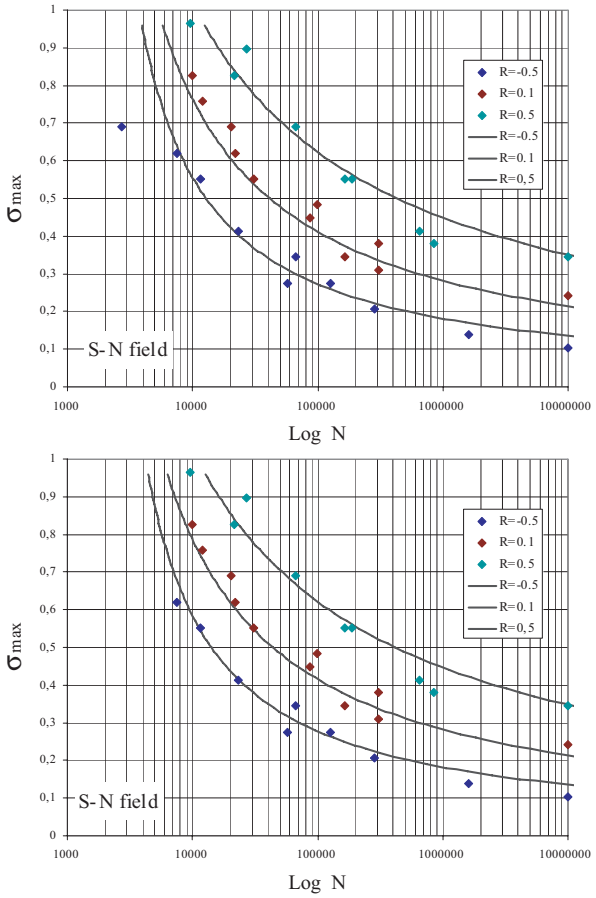


Figure 6.8: S–N curves for notched $K_t = 3.3$, AISI 4340 Alloy steel bar fitted using the proposed regression model with constraints and including the runouts. In the lower figure the outlier has been removed.

shown comparing the results obtained when removing one outlier suspected to belong to low-cycle fatigue, as shown in figure 6.8, which shows practically the same resulting evaluation results.

It seems reasonable to use this model as the most adequate to represent the material fatigue strength corresponding to the given data. Then, the variance matrix of the Gumbel parameter estimates $C_0, C_1, C_2, C_5, C_6)$ has been calculated using formula (6.63) and the following matrix has been obtained

$$\begin{pmatrix} 3.302 & -9.247 & 8.892 & 1.296 & -1.446 \\ -9.247 & 122.453 & -41.208 & -12.863 & 5.636 \\ 8.892 & -41.208 & 33.956 & 5.071 & -4.851 \\ 1.296 & -12.863 & 5.071 & 1.403 & -0.723 \\ -1.446 & 5.636 & -4.851 & -0.723 & 0.726 \end{pmatrix}$$

**Step 4:** *Extrapolate to other testing conditions.* Once the parameter estimates are available, the model (6.12) can be used to extrapolate to other testing conditions. For example, one can predict the expected lifetimes associated with other $R$ values, plot the percentiles curves, etc. For example, in table 6.2 the estimated percentile values associated with the different data

| Data | $p$ | Data | $p$ | Data | $p$ | Data | $p$ | Data | $p$ | Data | $p$ |
|---|---|---|---|---|---|---|---|---|---|---|---|
| 1 | 0.004 | 6 | 0.161 | 11 | 0.734 | 16 | 0.959 | 21 | 0.860 | 26 | 0.312 |
| 2 | 0.356 | 7 | 0.664 | 12 | 0.638 | 17 | 0.639 | 22 | 0.259 | 27 | 0.369 |
| 3 | 0.632 | 8 | 0.249 | 13 | 0.912 | 18 | 0.874 | 23 | 0.876 | 28 | 0.144 |
| 4 | 0.512 | 9 | 0.082 | 14 | 0.618 | 19 | 0.220 | 24 | 0.385 | 29 | 0.092 |
| 5 | 0.933 | 10 | 0.049 | 15 | 0.516 | 20 | 0.223 | 25 | 0.547 | 30 | 0.376 |

Table 6.2: Estimated percentile values associated with the different data points using the Gumbel fitted model.

points in figure 6.9 are shown. They have been determined using the Gumbel fitted model. It is interesting to see that the first data point has an associated value of 0.004, which reveals its outlier character.

Further, the model can supply all the desired information corresponding to any possible testing condition alternative. For example, in figure 6.9 the S/N curves for constant $R = 0.5, 0.1, -0.5$ and $-1$ (From top to bottom and left to right) including the percentiles 0.01, 0.05, 0.50, 0.95 and 0.99 are represented.

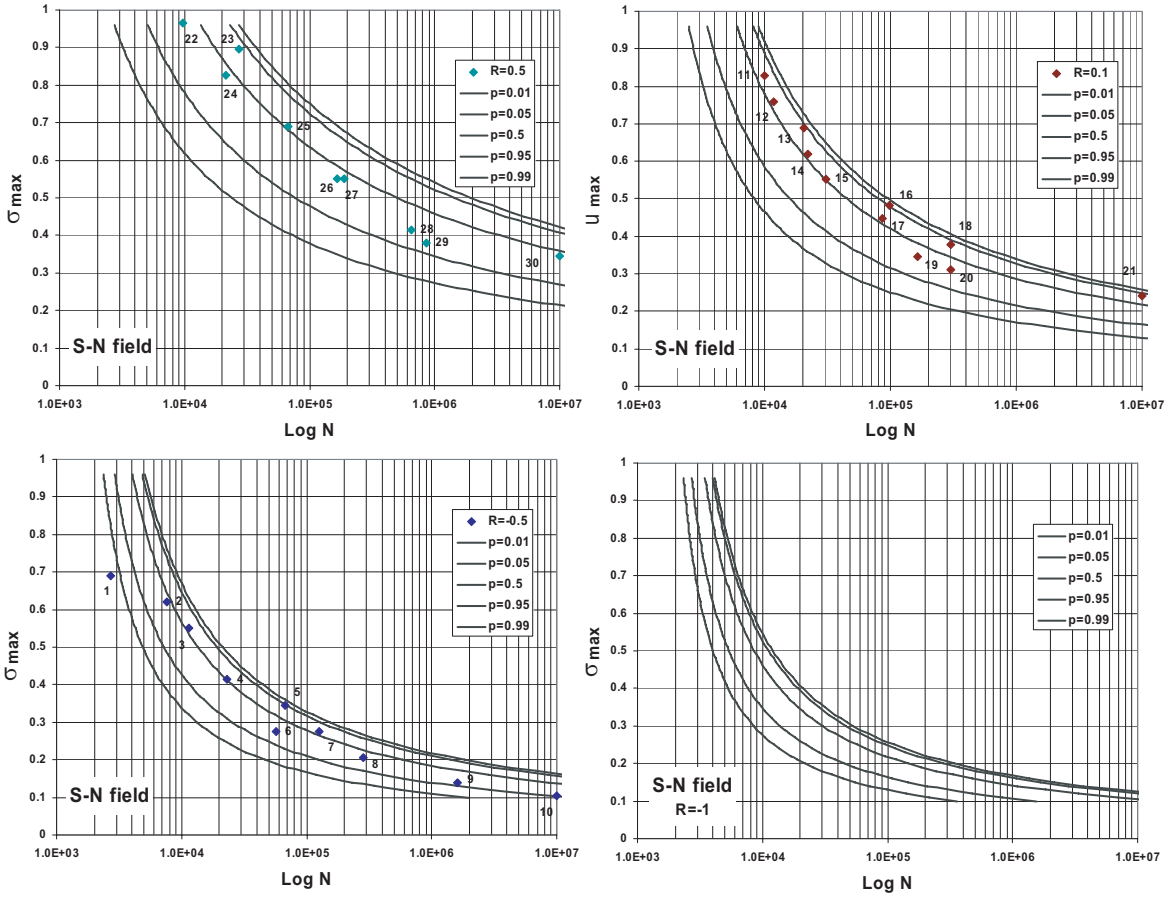


Figure 6.9: S–N curves for constant $R = 0.5, 0.1, -0.5$ and $-1$ (From top to bottom and left to right). The percentiles 0.01, 0.05, 0.50, 0.95 and 0.99 are represented.

Similarly, in figure 6.10 the $\Delta\sigma$-$\log N$ Wöhler fields for $\sigma_M = 0.8$, $\sigma_m = 0$, $R = -1$ and $\sigma_{mean} = -0.20$ are shown. They have been plotted using equations (6.66) to (6.69), respectively.

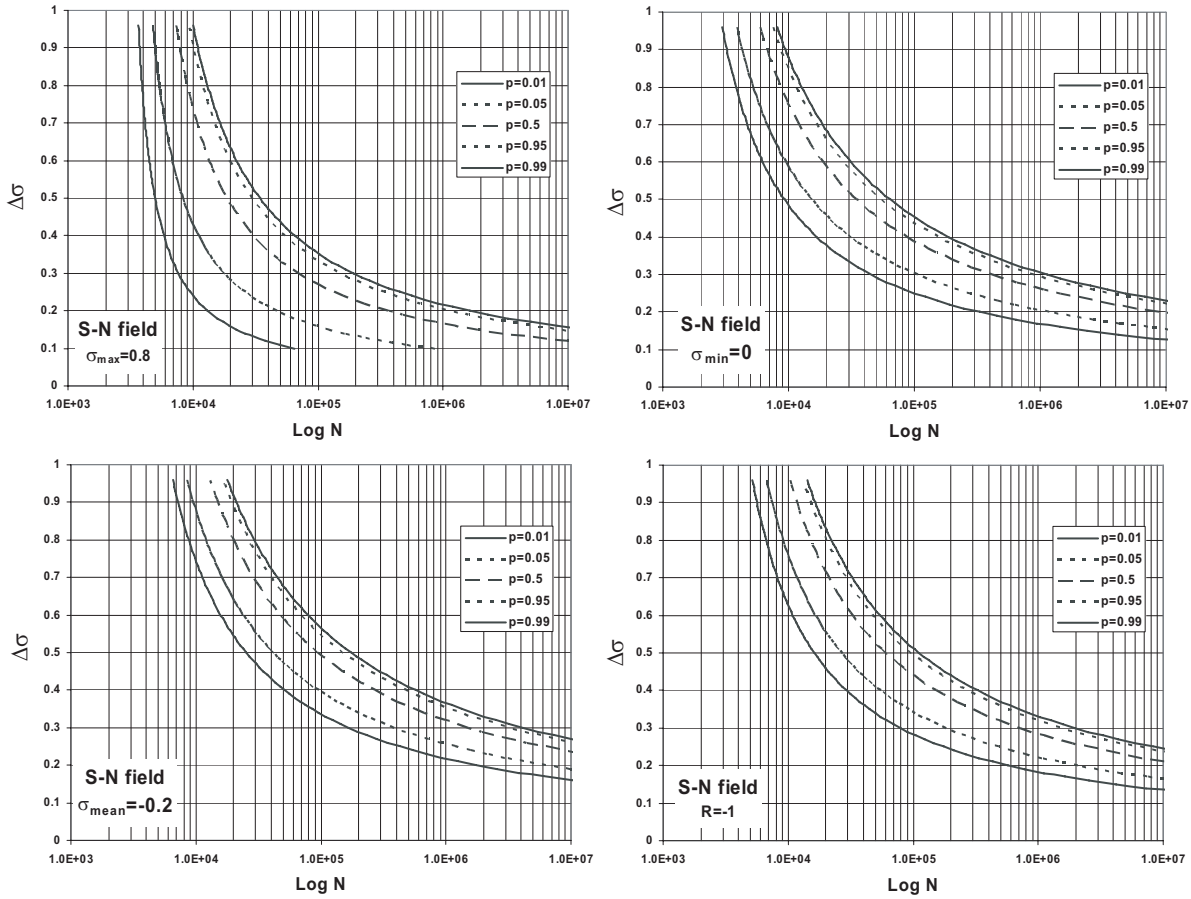


Figure 6.10: S–N curves for constant $\sigma_M = 0.8$, $\sigma_m = 0$, $\sigma_{mean} = 0$ and $R = -1$ (From top to bottom and left to right). The percentiles 0.01, 0.05, 0.50, 0.95 and 0.99 are represented.

## 6.9 Conclusions

The main conclusions obtained from this chapter are:

- A general Weibull regression model for statistical analysis of stress life data for the case of $\sigma_{max}$ being tension has been developed. The model is based on statistical and physical considerations, in particular, on compatibility conditions in the Wöhler field that leads to a system of functional equations.

- The model depends on 8 parameters that can be estimated by maximum likelihood and also by non-linear regression. It supplies all the material basic probabilistic fatigue information to be used in a damage accumulation assessment for fatigue life prediction of structural and mechanical components under real loading spectra.

- The model was satisfactorily applied to the evaluation of fatigue results from an external experimental program. In particular, in the example presented in Section 6.8.1, the method allows us detecting some data points corresponding presumably to low-cycle fatigue, so that when removed, the resulting model remains practically unaltered as the original one. This is due to the large number of constraints that have been observed in order to obtain only physically and statistically valid models. This is not the case of other models commonly used in practice.

- Once the parameters of the model have been estimated, the model allows us obtaining any kind of Wöhler field according to the testing condition chosen, as it has been demonstrated in the example of application.

- Finally, it is worthwhile mentioning that the model is the basic tool to develop a damage accumulation tool involving any load spectrum.

# Part IV

# Experimental Validation of the Models

# Chapter 7

# Experimental Validation of the Model

In this Chapter, the experimental validation of the model proposed in chapter 6 is made. Two different materials, low-alloy steel and aluminum alloy are tested.
The aim of this Chapter is to show that the results seem to confirm the applicability of the model showing its capability to provide linear and nonlinear trends for the S–N curves and, furthermore the P–S–N field.

## 7.1 Introduction

Some of the problems faced when searching for a model able to predict adequately the material lifetime have been shown in the previous chapters (see chapters 2 and 4). Real structures, equipment, vehicles and machines are subjected to fatigue load histories involving complex varying stress ranges and levels, which can cause their failure after a certain time period. Due to the recent advances in mechanical and structural design methods, as for example, in finite element techniques, and to market pressure in reducing material consumption, in order to optimize production costs, fatigue is becoming a determinant failure criterion for an increasing number of structural members and mechanical components in real practice. Fatigue design demands a cumulative damage model that requires a basic material fatigue characterization with consideration of stress range and mean stress level. These are considered the main and secondary parameters, respectively, governing the fatigue process.

The fundamental information is provided by means of laboratory tests, usually carried out under different constant stress ranges, while the stress ratio is maintained throughout unchanged, (S–N curves) or under a particular accelerated load history (ASTM E606 [5]). Thus, the evaluation of both (a) the standard fatigue data results, and (b) the damage model to be applied, become crucial to the lifetime prediction.

Concerning the testing strategy, the common practice in material fatigue characterization consists of selecting several data series with a reference constant stress level covering the region of interest: commonly, constant $\sigma_M$ or constant $\sigma_m$ in structural design and constant $\sigma_{mean}$ or stress ratio $R = \sigma_m/\sigma_M$ in mechanical design. This information is insufficient for the calculation of the damage accumulation in real load cases in which varying mean stress levels are present. For this reason, empirical transformation rules, not always sufficiently supported by experimentation,

are currently applied. Researchers try to transform stress ranges at a certain mean stress level, corresponding to the real load, to presumably "equivalent" stress ranges related to those provided by the Wöhler curves obtained in the laboratory.

In this chapter, the general Gumbel fatigue model for assessment of the Wöhler field developed by the authors in the previous Chapter, that includes the consideration of the mean stress effect, is applied to two different materials to show that it is valid for some practical applications.

Continuing with the research in this doctoral thesis, the next step consists of making the experimental validation of the proposed model (one example to validate the model theoretically was presented in Chapter 6, Section 6.8.1). The experimental validation was made with two sets of fatigue data corresponding to two different materials, low-alloy steel 42CrMo4 and aluminum alloy AlMgSi1 [110].

The chapter is organized as follows: In section 7.2 the material is presented, then in section 7.3 a description of specimens is made, section 7.4 and 7.5 define the experimental program and the testing strategy, respectively. Section 7.6 gives the parameter estimates and uses different methods for checking the validity of the model (Section 7.7). Finally, Section 7.8 provides some conclusions about the model and the materials.

## 7.2 Materials

For the validation of the model two different materials will be analyzed. These materials were considered in an experimental fatigue program launched at Empa (Swiss Federal Laboratories for Testing and Research at Dübendorf (Switzerland)).

The materials chosen (a low alloy steel and an aluminum alloy) have a very different behavior under cyclic and static load, so we can characterize the model for different states of load:

- A low–alloy steel 42CrMo4 (material number coded DIN-1.7225) with a nominal value of the ultimate strength $R_m = 1067MPa$ and of the yield strength, $R_y = 975.3MPa$.

- An aluminium alloy AlMgSi1 (material number coded DIN-3.2315) with a nominal value of the ultimate strength $R_m = 391.7MPa$ and of the yield strength, $R_{p_{0.2}} = 364.3MPa$.

Both materials were tested to know the static properties based on the ASTM E8M-04 norm [7]. The results are shown in table 7.1 and in Appendix B. Furthermore, a metallographic test (following the standard ASTM E7-03 [4]) was realized to each material to validate that the chemical properties are the corrects one (see table 7.2 and Appendix B). More properties of these materials are presented in [27] and [28].

These materials are used in structural construction because of its satisfactory service mechanical behavior and fatigue life. In addition, the AlMgSi1 shows good weather resistance, lightweight and minimum thermal expansion properties.

Table 7.1: Static characteristics of the metallic alloys used.

| Material | $R_y$ [MPa] | $R_{p_{0.2}}$ [MPa] | $R_m$ [MPa] | E modulus [MPa] |
|---|---|---|---|---|
| 42CrMo4 | 975.3 | 967.3 | 1067 | 204870 |
| AlMgSi1 | – | 364.3 | 391.7 | 72080 |

Table 7.2: Chemical compositions of 42CrMo4 steel according to DIN EN 10083-3:2007-01 and AlMgSi1 alloy according with DIN EN 573-3 respectively.

| 42CrMo4 | C | Si | Mn | S | P | Cr | Mo | Fe | | | |
|---|---|---|---|---|---|---|---|---|---|---|---|
| g/100g | 0.38-0.45 | ≤ 0.40 | 0.60-0.90 | ≤ 0.035 | ≤0.025 | 0.90-1.20 | 0.15-0.30 | remains | | | |
| AlMgSi1 | Si | Fe | Cu | Mn | Mg | Cr | Ni | Zn | various | Ti | Al |
| g/100g | 0.70-1.30 | 0.50 | 0.10 | 0.40-1.0 | 0.60-1.20 | 0.25 | - | 0.20 | 0.15 | 0.10 | remains |

## 7.3 Specimens

The definition of the geometric characteristics of the specimens depends on the test to be run. All these specimens are cylindric, but with different useful lengths. For example, Wolf, Fleck and Eifler [133], define the geometric characteristics (see figure 7.1 (b)) for temperature measures in the fatigue behavior. Starke, Walther and Eifler [127], define the geometric characteristics of the specimens to analyze fatigue behavior based on strain, temperature and electrical measures (see figure 7.1 (a)).

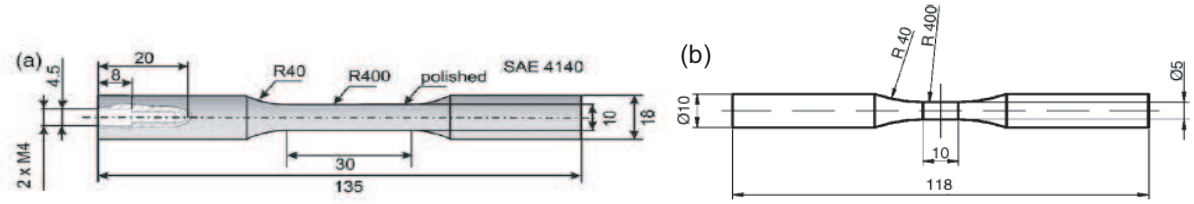


Figure 7.1: Different geometries for fatigue tests: (a) Starke et al. specimen [127], (b) Wolf et al. specimen [133].

One aspect to be taken into account is the length effect that occurs in fatigue tests. Castillo et al. [47] defines a new model of fatigue, that can analyze the lifetime of a component based on test specimens shorter than the real components. This model is in accordance with the weakest link concept in the way as: *an element of length L can be considered to be divided into a series of n fictitious sub-elements of small length* $L_0$*, i.e.* $L = nL_0$*, and the failure occurs when the weakest subelement fails* [35].

The final specimens shown in figure 7.2, are cylindrical and the test length of the specimens was $L_2$ mm, with 8 mm in diameter. The total length was $L_1$ mm and the radius of transition to the test section of the specimen was 55 mm. The different lengths used for each material are shown in table 7.3.

Table 7.3: Specimen's dimensions for each material.

| Material | $L_1$ (mm) | $L_2$ (mm) | d (mm) | r (mm) |
|---|---|---|---|---|
| 42CrMo4 | 130 | 30 | 8 | 55 |
| AlMgSi1 | 110 | 10 | 8 | 55 |

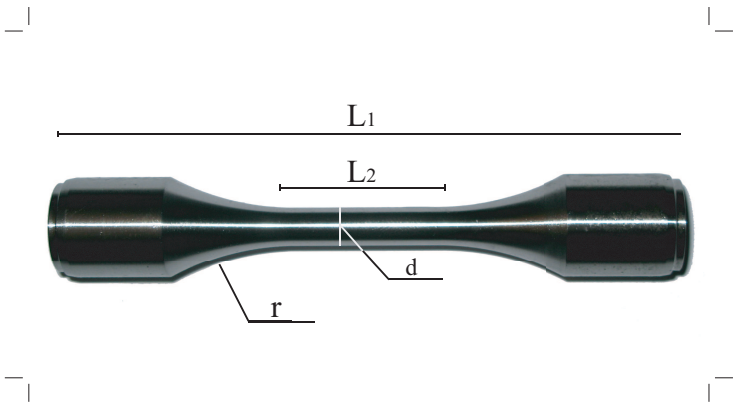


Figure 7.2: Geometry of the testing specimen.

## 7.4 Experimental procedure

The testing machines used for the validation were two: a servo hydraulic testing machine, 160 kN load capacity with a steel alloy grip based on ASTM E606 [5] (see figure 7.3), and a high frequency vibrophore machine with capacity of 150 Hz of frequency (see figure 7.4).

(a)

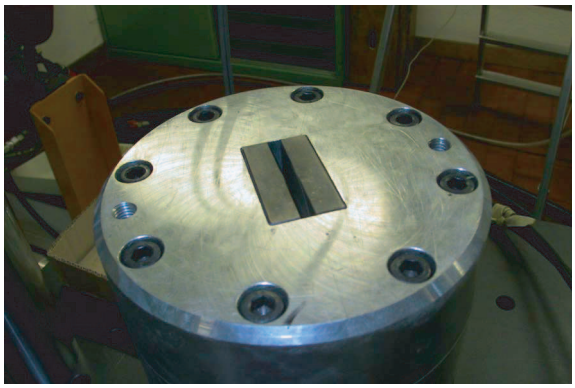

(b)

Figure 7.3: Schenk Machine, used for 42CrMo4 tests. (a) General sight of the machine, (b) detail of the machine, specimen's grips.

In the case of the 42CrMo4 steel, all the tests were conducted using the servo hydraulic testing machine at frequencies ranging from 1 to 10 Hz. For the AlMgSi1 alloy, the high frequency vibrophore machine was be run at a maximum frequency of 80 Hz. In this way, only 34.7 hours were needed to complete a test with a limit number of cycles of 10 millions.

In the case of 42CrMo4 steel a machine slower than that used for aluminum alloy was used

(a)

(b)

Figure 7.4: Rumul Machine, used for AlMgSi1 tests. (a) General sight of the machine, (b) detail of the machine, specimen testing.

to avoid the temperature effect created by the high frequencies. The specimen temperature was continuously monitored to keep it sufficiently low in order not to influence the failure mechanism during testing. All the tests were run at 25°C degrees.

## 7.5 Type of load and testing strategy

In this section the testing strategy and the type of load are analyzed. The aim of any testing strategy is to generate the most adequate test samples to estimate the model parameters in (6.13).

The type of load proposed consists of testing specimens subject to alternating fatigue loads from a value of $\sigma_m^*$ to a value $\sigma_M^*$, which can change from test to test. Normally, a minimum, of 8 to 12 tests with the same $\sigma_M^*$ and different $\sigma_m^*$ are sufficient to predict Wöhler curves for the associated constant $\sigma_M^*$, but not for other possible combinations of $\sigma_m^*$ and $\sigma_M^*$. Since we aim at predicting fatigue life for a stress history of any combination of stresses, more tests are needed by combining groups of tests run for constant $\sigma_M^*$ and varying $\sigma_m^*$ with groups of tests run for constant $\sigma_m^*$ and varying $\sigma_M^*$.

In our case, a seemingly efficient testing strategy would consist of carrying out four groups of tests, in which $\sigma_M^*$ are constant for each group of test. Then, different levels of $\sigma_m^*$ are chosen to test a large range of load. In figure 6.7 the distribution of these tests is shown schematically.

To this goal, in both materials all tests were conducted under four constant $\sigma_M^*$ levels corresponding to given percentages of the yield strength and different values of $\sigma_m^*$ [110]. In the case of the 42CrMo4 steel, the values of these levels correspond to the 0.98, 0.9, 0.8 and 0.7 of the yield strength. For the AlMgSi1 alloy, the values of these levels correspond to the 0.9, 0.8, 0.7 and 0.6 of the yield strength (See figure 7.5).

Due to the lack of an exact knowledge of the fatigue limit for both materials, the minimum testing amplitudes of these materials were estimated from the literature (see Boller and Seeger [27, 28]) 450 MPa for the steel alloy and 80 MPa for the aluminium alloy. The different levels were chosen to optimize the test times trying to avoid run-outs.

The distributions of the different test loads are shown in figure 7.5. In addition, five and ten million of cycles were fixed as run-out values, respectively, for the 42CrMo4 and AlMgSi1 alloys. The resulting lifetimes are shown in table 7.4.

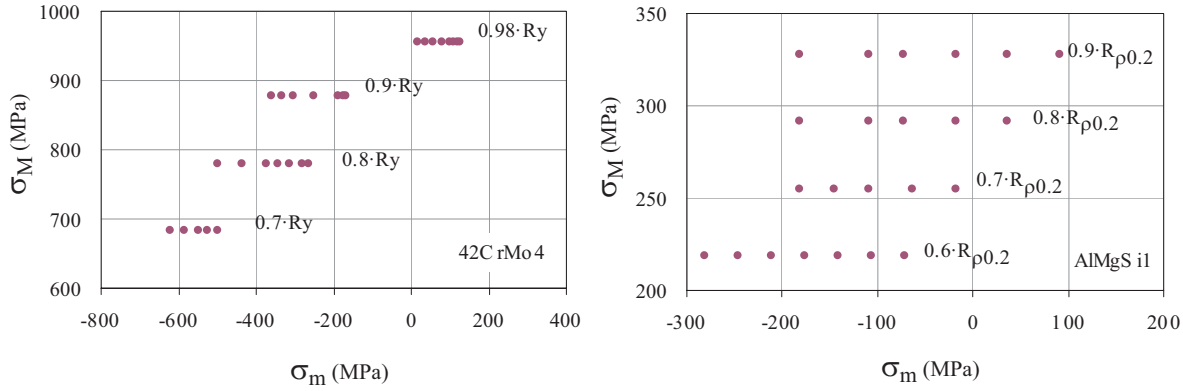


Figure 7.5: Distribution of the different tests loads. The left figure corresponds to the 42CrMo4 steel, and the right figure to the AlMgSi1 alloy.

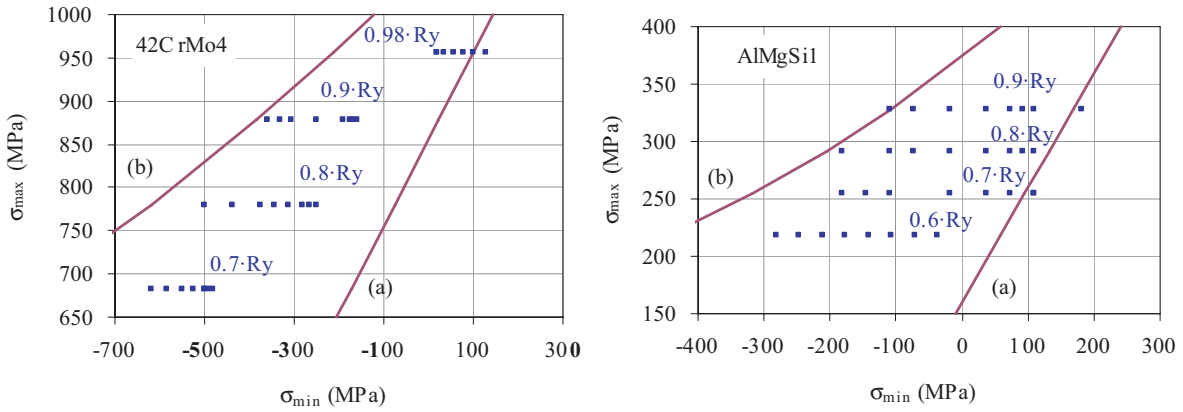


Figure 7.6: Schematic representation of the different between both distributions of the different tests loads. The left figure corresponds to the 42CrMo4 steel, and the right figure to the AlMgSi1 alloy.

In figure 7.6 we can observe that there is a big difference between both distributions. Furthermore, in this figure we can observe the limits in the test distributions: Line (a) represents the lower bound, defined by the endurance limit; line (b) represents the higher bound, defined by the yield stress. Almost all the test results are between both lines, only four points are outside this region. The aim of this is to know exactly the exact situation of the bounds.

Table 7.4: Resulting lifetimes for 42CrMo4 and AlMgSi1.

| Material | 42CrMo4 | | | AlMgSi1 | | |
|---|---|---|---|---|---|---|
| Nr. Test | $\sigma_{min}$ | $\sigma_{max}$ | Ncycles | $\sigma_{min}$ | $\sigma_{max}$ | Ncycles |
| 1 | 17.51 | 955.50 | 65277 | -182.15 | 327.87 | 19100 |
| 2 | 35.24 | 955.50 | 23700 | -109.29 | 327.87 | 34000 |
| 3 | 55.27 | 955.50 | 52700 | -72.86 | 327.87 | 42800 |
| 4 | 78.43 | 955.50 | 40900 | 36.43 | 327.87 | 153100 |
| 5 | 119.11 | 955.50 | 85900 | -18.22 | 327.87 | 63800 |
| 6 | 108.91 | 955.50 | 124300 | 91.08 | 327.87 | 360400 |
| 7 | 124.21 | 955.50 | 222900 | -182.15 | 291.44 | 28700 |
| 8 | 98.71 | 955.50 | 93500 | -72.86 | 291.44 | 71700 |
| 9 | -250.00 | 877.80 | 17281 | -109.29 | 291.44 | 59900 |
| 10 | -190.00 | 877.80 | 48787 | -18.22 | 291.44 | 143500 |
| 11 | -175.00 | 877.80 | 81244 | 36.43 | 291.44 | 326400 |
| 12 | -360.00 | 877.80 | 3373 | -182.15 | 255.01 | 48000 |
| 13 | -305.00 | 877.80 | 21812 | -145.72 | 255.01 | 57900 |
| 14 | -332.50 | 877.80 | 7265 | -109.29 | 255.01 | 113100 |
| 15 | -167.50 | 877.80 | 125800 | -18.22 | 255.01 | 348300 |
| 16 | -500.00 | 780.23 | 11439 | -63.75 | 255.01 | 172500 |
| 17 | -437.50 | 780.23 | 14973 | -71.42 | 218.58 | 526500 |
| 18 | -375.00 | 780.23 | 32055 | -281.42 | 218.58 | 37100 |
| 19 | -312.50 | 780.23 | 483000 | -246.42 | 218.58 | 54400 |
| 20 | -343.75 | 780.23 | 36708 | -211.42 | 218.58 | 80300 |
| 21 | -265.63 | 780.23 | 532200 | -176.42 | 218.58 | 96300 |
| 22 | -281.25 | 780.23 | 123100 | -141.42 | 218.58 | 175500 |
| 23 | -550.00 | 682.73 | 183024 | -106.42 | 218.58 | 172800 |
| 24 | -620.00 | 682.73 | 19331 | | | |
| 25 | -525.00 | 682.73 | 347102 | | | |
| 26 | -585.00 | 682.73 | 33925 | | | |
| 27 | -500.00 | 682.73 | 381543 | | | |

## 7.6 Parameter estimation

The parameter estimation is made in this section. For this, we cannot use simple software tools, such Excel, but exists other specialized optimization softwares, as Mathematica or GAMS (CONOPT solver), that make easier the job, specially with the implementation of the constraints.

### 7.6.1 General information

In Section 6.7 the steps proposed for the parameter estimation [40] were presented. A set $\{(\sigma^*_{m_i}, \sigma^*_{M_i}) \mid i = 1, 2, \ldots, n\}$, of testing cases encompassing several stress level conditions varying $\sigma^*_M$ and $\sigma^*_m$ was selected to cover the desired region (**Step 1**).

**Step 2:** *Choose the normalizing variables* $\log N^*_0$ *and* $\sigma^*_0$. Choose $\log N_0$ and $\sigma_0$ and normalize the data to dimensionless form. In both cases, the maximum stress was chosen as $\sigma_0$, $\sigma_0 = 0.98R_y$ MPa for 42CrMo4 and $\sigma^*_0 = 0.9R_{p0.2}$ MPa for AlMgSi1. To define $N_0$, the maximum number

of cycles were selected, that is, $N_0 = 532000$ and $N_0 = 526500$ cycles, respectively (see table 7.4).

**Step 3:** *Estimate the model parameters.* Use one of the estimation methods discussed in Section 6.6 to estimate the parameters $C_0$ to $C_7$ in the Gumbel model (6.13).

The implementation of the proposed estimation methods such as those described in Section 6.6 is not difficult but cannot be easily implemented in simple software tools, such as Excel. The use of a specialized optimization software, as Mathematica or GAMS for example, facilitates the estimation job, and specially the implementation of constraints presented in Equations (6.22)–(6.35).

We have used the two different estimation methods, maximization of the loglikelihood (6.62) and minimization of the regression equation (6.65). The parameter estimation will be developed in the next subsections.

**Step 3:** *Extrapolate to other testing conditions.* Use the model (6.13) and the parameters $C_0$ to $C_7$ and $\log N_0$ and $\sigma_0$ for any other testing condition. This is illustrated in Section 7.7.

### 7.6.2 Parameter estimation for the 42CrMo4 steel

The parameters of all the cases considered have been estimated and the results are shown in tables 7.5 for the 42CrMo4 steel.

Table 7.5: Parameter estimates for different estimation methods for the 42CrMo4 steel.

| Case | $C_0$ | $C_1$ | $C_2$ | $C_3$ | $C_4$ | $C_5$ | $C_6$ | $C_7$ |
|---|---|---|---|---|---|---|---|---|
| Max.Lik. | -79.066 | -63.141 | 85.309 | 38.297 | 0.000 | 0.000 | 2.394 | 0.000 |
| L.Squares | -77.338 | -53.530 | 83.913 | 26.824 | 0.000 | 0.000 | 2.570 | 0.000 |

Figure 7.7 shows the experimental data and the resulting median curves according to the fitted model. We can observe a reasonable fit [110].

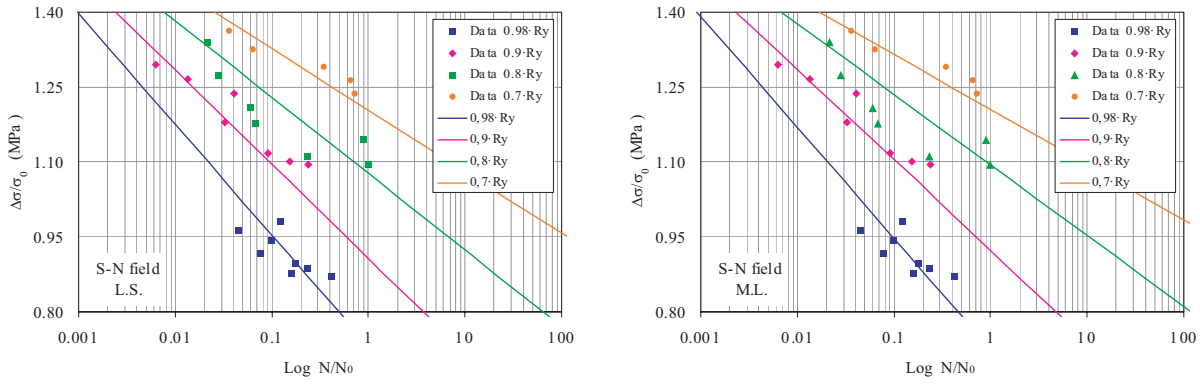


Figure 7.7: S–N curves for constant $\sigma_M^*$ for Gumbel model with constraints for the 42CrMo4 steel using different methods: least squares (left side) and maximum likelihood (right side).

The variance-covariance matrix of the Gumbel parameter estimates $C_0$ to $C_7$ has been cal-

culated using formula (6.63) and the following matrix has been obtained for the 42CrMo4 steel:

$$\begin{pmatrix} 423.723 & -386.651 & -334.520 & -5.221 & 1.930 & -0.627 & 0.602 & 367.882 \\ -386.651 & 435.239 & 268.816 & 2.983 & -0.227 & 5.301 & -2.083 & -411.034 \\ -334.520 & 268.816 & 283.325 & 4.445 & -1.889 & -0.974 & 0.451 & -256.652 \\ -5.221 & 2.983 & 4.445 & 0.676 & -0.028 & -0.695 & 0.041 & -2.945 \\ 1.930 & -0.227 & -1.889 & -0.028 & 0.487 & 0.073 & -0.415 & 0.298 \\ -0.627 & 5.301 & -0.974 & -0.695 & 0.073 & 0.966 & -0.042 & -4.726 \\ 0.602 & -2.083 & 0.451 & 0.041 & -0.415 & -0.042 & 0.672 & 2.012 \\ 367.882 & -411.034 & -256.652 & -2.945 & 0.298 & -4.726 & 2.012 & 388.523 \end{pmatrix}.$$

### 7.6.3 Parameter estimation for the AlMgSi1 alloy

Similarly at 42CrMo4, the parameters of all the cases considered have been estimated and presented in table 7.6 for the AlMgSi1 alloy. The graphical results are shown in figure 7.8, where we can observe a better fit than chromo [110].

Table 7.6: Parameter estimates for different estimation methods for the AlMgSi1 alloy.

| Case | $C_0$ | $C_1$ | $C_2$ | $C_3$ | $C_4$ | $C_5$ | $C_6$ | $C_7$ |
|---|---|---|---|---|---|---|---|---|
| Max. Lik. | -78.507 | -31.357 | 101.460 | -34.960 | 0.000 | 0.000 | 13.302 | -8.642 |
| L.Squares | -24.737 | -16.091 | 31.803 | -4.569 | 1.619 | -1.619 | 2.837 | -0.377 |

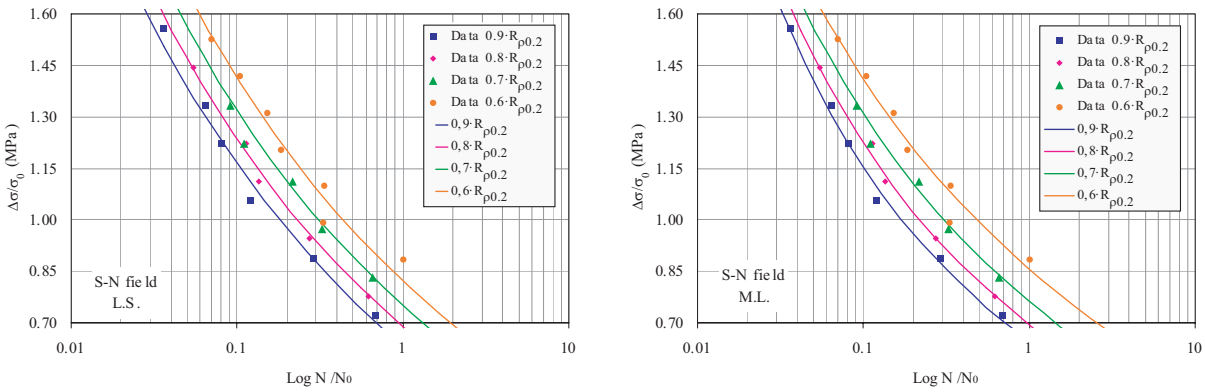


Figure 7.8: S–N curves for constant $\sigma_M^*$ for Gumbel model with constraints for the AlMgSi1 alloy using different methods: least squares (left side) and maximum likelihood (right side).

Finally, the variance-covariance matrix of the Gumbel parameter estimates $C_0$ to $C_7$ has been calculated using formula (6.63) and the following matrix has been obtained for the AlMgSi1 alloy:

$$\begin{pmatrix} 206.358 & -247.932 & -69.555 & -17.021 & 12.080 & -10.425 & 8.345 & 196.913 \\ -247.932 & 648.066 & -152.432 & 6.427 & -1.471 & 75.313 & -50.212 & -505.132 \\ -69.555 & -152.432 & 195.600 & 13.421 & -11.664 & -36.919 & 27.165 & 115.082 \\ -17.021 & 6.427 & 13.421 & 4.309 & -1.204 & -3.470 & 1.069 & -4.833 \\ 12.080 & -1.471 & -11.664 & -1.204 & 3.408 & 1.236 & -3.365 & 1.391 \\ -10.425 & 75.313 & -36.919 & -3.470 & 1.236 & 13.511 & -6.889 & -58.325 \\ 8.345 & -50.212 & 27.165 & 1.069 & -3.365 & -6.889 & 10.118 & 39.604 \\ 196.913 & -505.132 & 115.082 & -4.833 & 1.391 & -58.325 & 39.604 & 394.455 \end{pmatrix}.$$

## 7.7 Parameter validation

After performing the parameter estimation, the quality of the fitted models were assessed. Some methods for checking whether a fitted model is in agreement with the data were used.

This validation was done using the PP–plot and QQ–plot and the Kolmogorov-Smirnov and Chi-square tests. For other treatment of the validation problem, see Drees, de Haan and Li [61] and Fei, Lu and Xu [80].

Let $x_1, x_2, ..., x_n$ be a sample from a given population with cdf $F(x)$. Let $x_{1:n}, x_{2:n}, ..., x_{n:n}$ be the corresponding order statistics and $p_{1:n}, p_{2:n}, ..., p_{n:n}$ be plotting positions such as $p_{i:n} = i/(n+1)$. If $\hat{F}(x)$ is an estimate of $F(x)$ based on $x_1, x_2, ..., x_n$, then $\hat{F}(x_{i:n})$ is the estimated probability corresponding to $x_{i:n}$. The difference between $\hat{F}(x_{i:n})$ and $p_{i:n}$ is an indication of the quality of fit. The scatter plot of $\hat{F}(x_{i:n})$ versus $p_{i:n}$; $i = 1; 2; ...; n$; is called a PP–plot, which is very useful for model validation. If the model fits the data well, the graph will be close to the $45^o$ line. Note that all the points in the PP–plot are inside the unit square $[0, 1] \times [0, 1]$. An alternative and good complement to PP–plots are the QQ–plots, which represent the scatter plot of the points $x_{i:n}$ versus $\hat{F}(x_{i:n})$. Figures 7.9 and 7.10 show these plots and the good agreement between data and model.

A quantitative alternative to this model validation methods is the Kolmogorov-Smirnov test, which can be used to test the log-Gumbel model 6.13, and uses the well known statistic:

$$D = \max_{1 \le i \le n} \left( F(H(N_i^*)) - \frac{i-1}{n}, \frac{1}{n} - F(H(N_i^*)) \right), \tag{7.1}$$

where $F$ is the Gumbel cdf and $H(N_i^*)$ is the sample order statistics (see Equation (6.61)). A large value of $D$ indicates that the model must be rejected as a valid model. We have calculated the statistic in Equation (7.1) for the real sample and the corresponding estimated model (see tables 7.5 and 7.6). In addition, to obtain a more precise critical value, we have simulated 1000 samples from the estimated model, and calculated the statistic in (7.1) using the simulated samples and their resulting parameters estimates, obtaining a simulated sample of the statistic in Equation (6.61), and the corresponding critical values, which are shown in tables 7.7 and 7.8, where the significance levels are also shown in parentheses. These tests reveal that the models are far from being rejected at a significant level of 0.05 for both materials.

The qualities of the fitted models (least squares and maximum likelihood) were also tested using the Chi-square goodness of fit test, using 10 cells of the same probability. Since some parameters were estimated, we have obtained the corresponding critical points for the Chi-square tests by simulating 1000 samples and estimating the model parameters with the proposed methods, following exactly the same process as the one indicated for the Kolmogoronov-Smirnov test. The values of the Chi-square statistics and the corresponding critical values are indicated in tables 7.7 and 7.8. Again, the models are far from being rejected at a significance level of 0.05 for both materials.

In summary, the PP–plot and QQ–plot in figures 7.9 and 7.10 and the Kolmogoronov-Smirnov tests together with the Chi-Square tests indicate that the maximum likelihood and the least squares based model provide from a practical point of view good and similar fits for the 42CrMo4 steel alloy and the AlMgSi1 aluminum alloy.

Thus, from all the above tests we can conclude that the log-Gumbel model is a good model for both materials (42CrMo4 and AlMgSi1) [110].

One final conclusion that can be drawn from this example is that the constraints really help when the sample size is small, because they reduce the effect of outliers. The data in this example really indicate that the sample sizes used are not as small as they could appear as a first

Table 7.7: Goodness of fit tests for the 42CrMo4 steel (in parenthesis the $p$ value).

| Case | Nr. | Kolmogoronov-Smirnov test | | | Chi-Square test | | |
|---|---|---|---|---|---|---|---|
| | tests | Max. Diff. | Critical Value | Uniformity? | $\chi^2$ | Critical Value | Ok? |
| M.L. | 27 | 0.114 (0.36) | 0.161 | Yes | 5.222 (0.86) | 14.111 | Yes |
| L.S. | 27 | 0.099 (0.70) | 0.556 | Yes | 5.222 (0.92) | 56.333 | Yes |

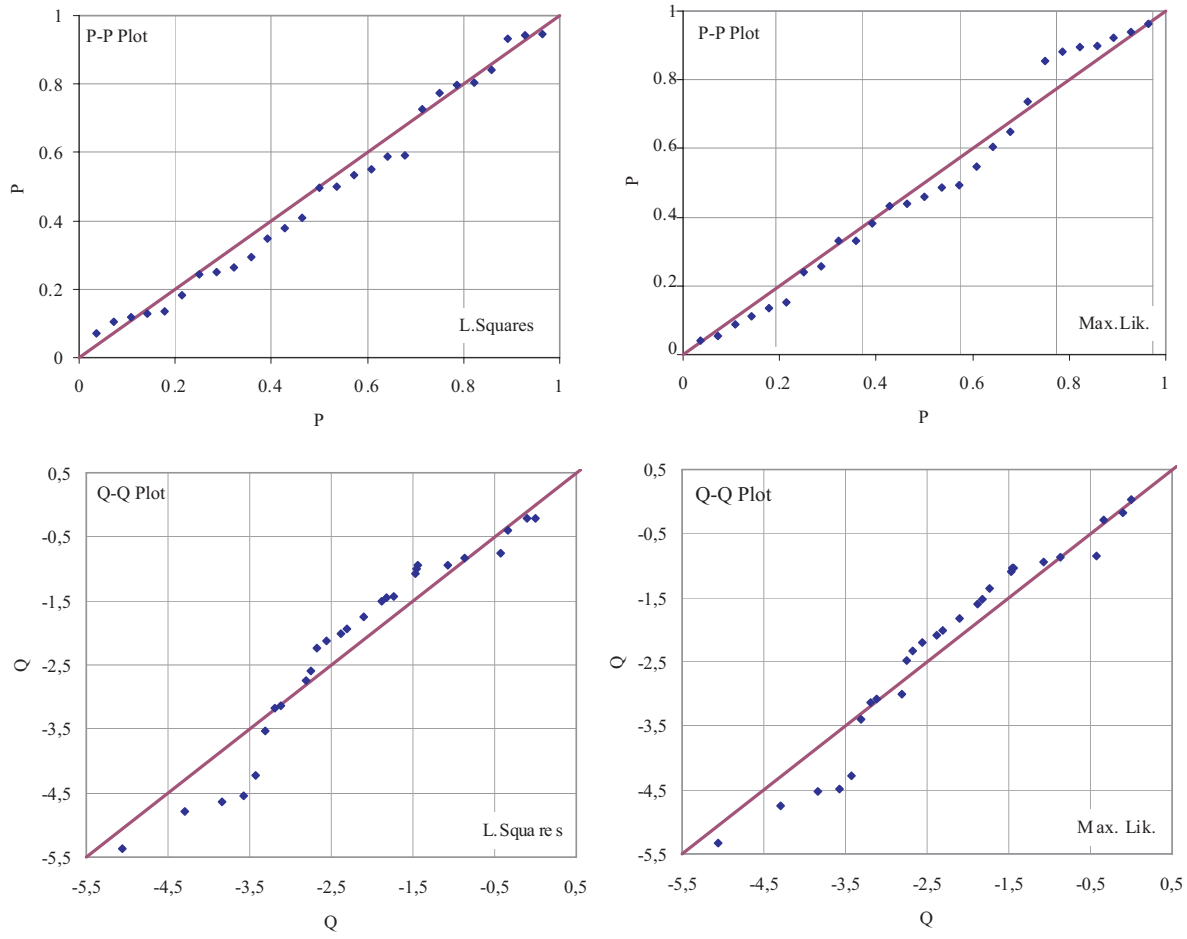


Figure 7.9: PP–plot for different analysis cases of the 42CrMo4 steel: least squares (left side), maximum likelihood (right side).

look. The main reason is that important physical conditions and knowledge about the fatigue problem has been used in deriving the model. As indicated, the model was not based on an arbitrary selection of its functional form, but based on constraints of physical nature.

### 7.7.1 Validation of the theoretical example

Here, the validation of theoretical example presented in Section 6.8.1 is made. The methods and steps used are the same than those for the experimental validation of chromo and aluminum alloy.

Table 7.8: Goodness of fit tests for the AlMgSi1 alloy (in parenthesis the $p$ value).

| Case | Nr. | Kolmogoronov-Smirnov test | | | Chi-Square test | | |
|---|---|---|---|---|---|---|---|
| | tests | Max. Diff. | Critical Value | Uniformity? | $\chi^2$ | Critical Value | Ok? |
| M.L. | 23 | 0.111 (0.54) | 0.183 | Yes | 7.000 (0.52) | 14.826 | Yes |
| L.S. | 23 | 0.157 (0.51) | 0.522 | Yes | 16.565 (0.37) | 46.478 | Yes |

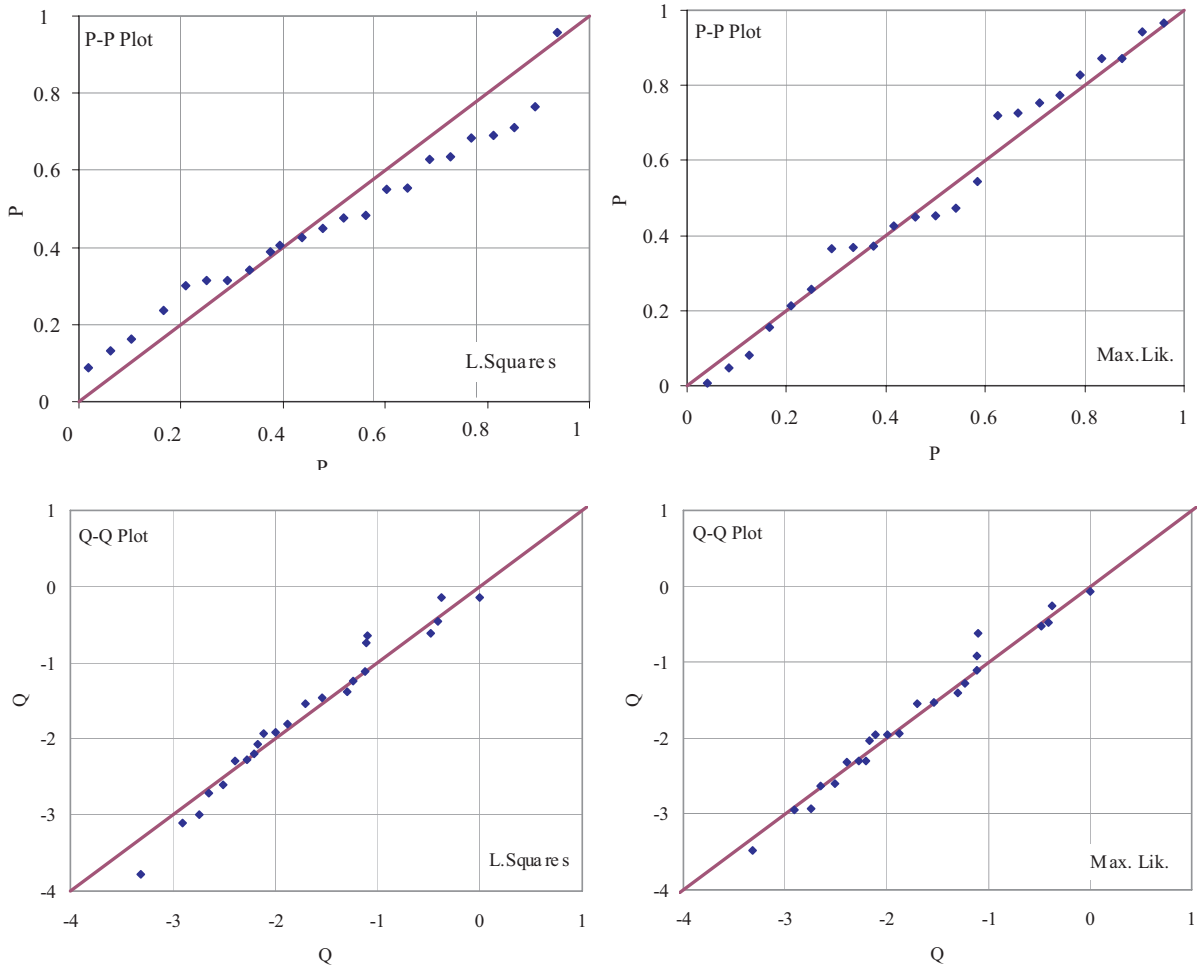


Figure 7.10: PP–plot for different analysis cases of the AlMgSi1 alloy: least squares (left side), maximum likelihood (right side).

The analysis of PP–plot (see figure 7.11 (right side)) shows that relationship between model probability and theoretical probability is almost a 45° line, so the fit of the model, with the parameter estimated in section 6.8.1 were good.

The results of the Kolmogoronov-Smirnov and Chi-Square are shown in table 7.9. Note that the results are better than those for the experimental validation model.

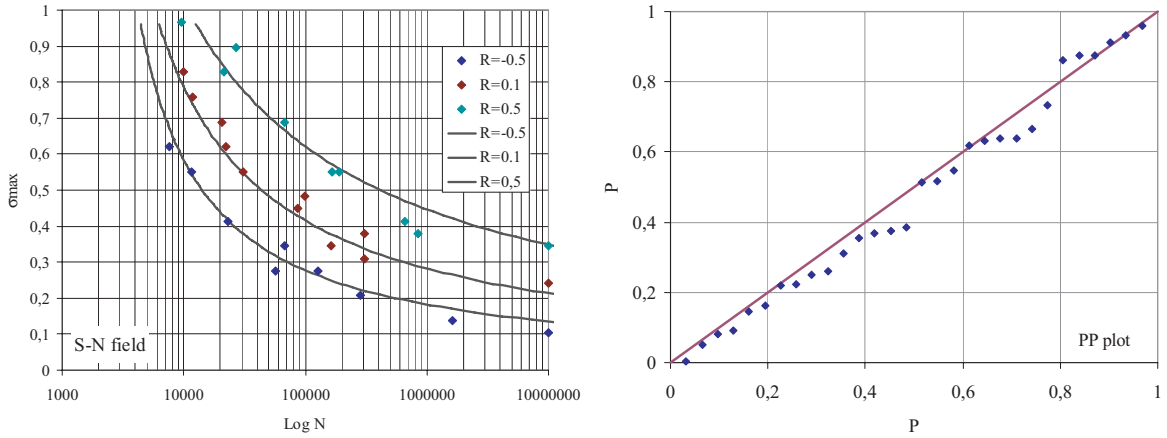


Figure 7.11: Representation of the Gumbel Model obtained in the example analyzed in section 6.8.1 (left side) and its PP–plot (right side).

Table 7.9: Goodness of fit tests for the theoretical example shown in section 6.8.1.

| Nr. | Kolmogoronov-Smirnov test | | | Chi-Square test | | |
|---|---|---|---|---|---|---|
| tests | Max. Diff. | Critical Value | Uniformity? | $\chi^2$ | Critical Value | Ok? |
| 30 | 0.067 | 0.242 | Yes | 1.333 | 11.071 | Yes |

### 7.7.2 Extrapolation

Once the parameter estimates are available, the model (6.13) can be used to extrapolate to other testing conditions. For example, one can predict the expected lifetimes associated with other constant values of $\sigma_M^*$, plot the percentile curves, etc.

In table 7.10 the estimated percentile values associated with the different data points in figure 7.12 for the 42CrMo4 steel are shown. Similarly, in table 7.11, the percentile values associated with the different data points in figure 7.13 for the AlMgSi1 alloy are shown [110].

Table 7.10: Estimated percentile values associated with the different data points using the Gumbel fitted model for the 42CrMo4 steel.

| Data | p | Data | p | Data | p | Data | p |
|---|---|---|---|---|---|---|---|
| 1 | 0.883 | 8 | 0.921 | 15 | 0.940 | 22 | 0.441 |
| 2 | 0.113 | 9 | 0.241 | 16 | 0.547 | 23 | 0.433 |
| 3 | 0.383 | 10 | 0.485 | 17 | 0.154 | 24 | 0.330 |
| 4 | 0.134 | 11 | 0.964 | 18 | 0.087 | 25 | 0.855 |
| 5 | 0.459 | 12 | 0.329 | 19 | 0.041 | 26 | 0.896 |
| 6 | 0.606 | 13 | 0.492 | 20 | 0.899 | 27 | 0.647 |
| 7 | 0.256 | 14 | 0.738 | 21 | 0.054 | | |

But, how can we know that really the model can be extrapolated to other load conditions? We can answer to this question easily. If we know the parameter of one material, estimated

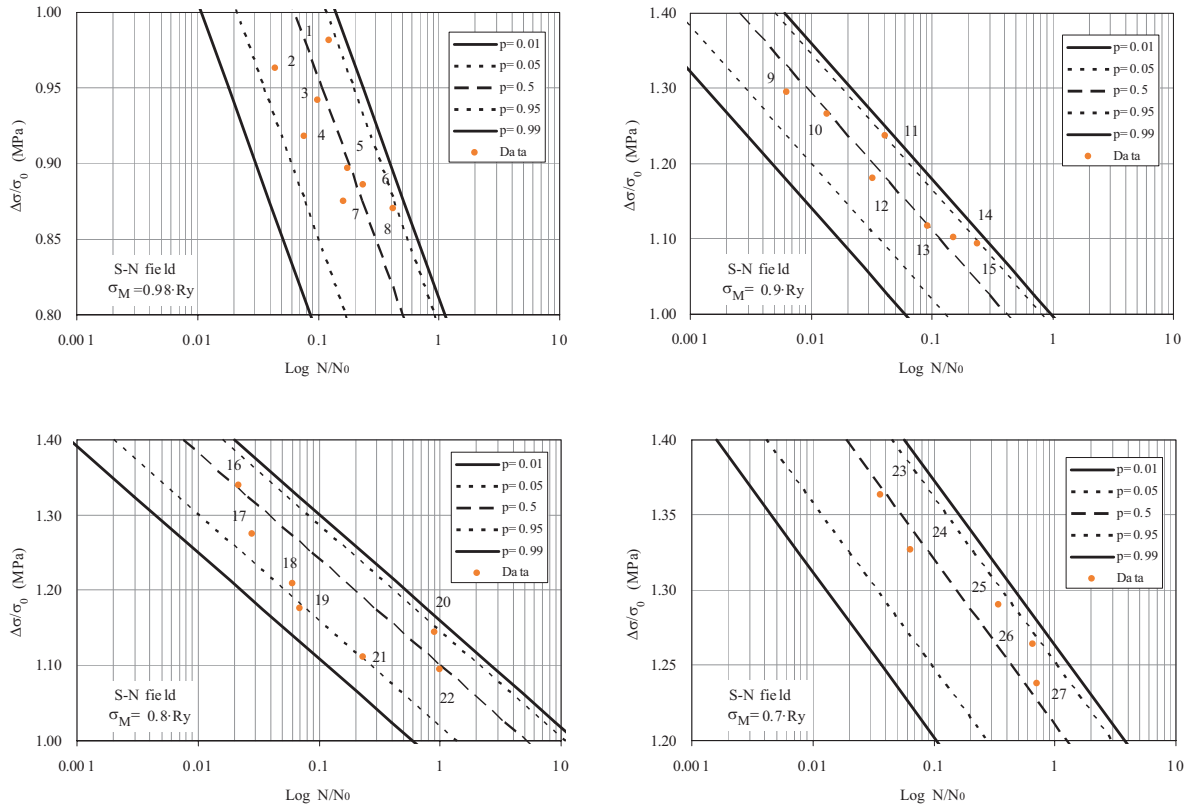


Figure 7.12: S–N curves representing constant $\sigma_M^* = 0.98, 0.9, 0.8$ and $0.7R_y$ for the 42CrMo4 steel (from top to bottom and left to right). The percentiles 0.01, 0.05, 0.50, 0.95 and 0.99 are represented.

Table 7.11: Estimated percentile values associated with the different data points using the Gumbel fitted model for the AlMgSi1 alloy.

| Data | p | Data | p | Data | p | Data | p |
|---|---|---|---|---|---|---|---|
| 1 | 0.544 | 7 | 0.472 | 13 | 0.048 | 19 | 0.873 |
| 2 | 0.872 | 8 | 0.967 | 14 | 0.828 | 20 | 0.155 |
| 3 | 0.451 | 9 | 0.214 | 15 | 0.371 | 21 | 0.720 |
| 4 | 0.083 | 10 | 0.369 | 16 | 0.258 | 22 | 0.006 |
| 5 | 0.754 | 11 | 0.454 | 17 | 0.427 | 23 | 0.941 |
| 6 | 0.774 | 12 | 0.366 | 18 | 0.728 | | |

with different series, and using the Gumbel model (6.13), we can delete one of these series and estimate again the parameter for the model. Then, make the extrapolation of the model to the deletes series and validate the fit of the curve.

All these processes are shown in the next figures. The extrapolation has been done for the AlMgSi1 alloy, described in Section 7.2, with the estimated parameter in Section 7.6.3. Figures 7.14, 7.15, 7.16 and 7.17 represent the re-estimation of the model without one of the initial series. The parameters obtained after these new estimations are presented in table 7.12, all of

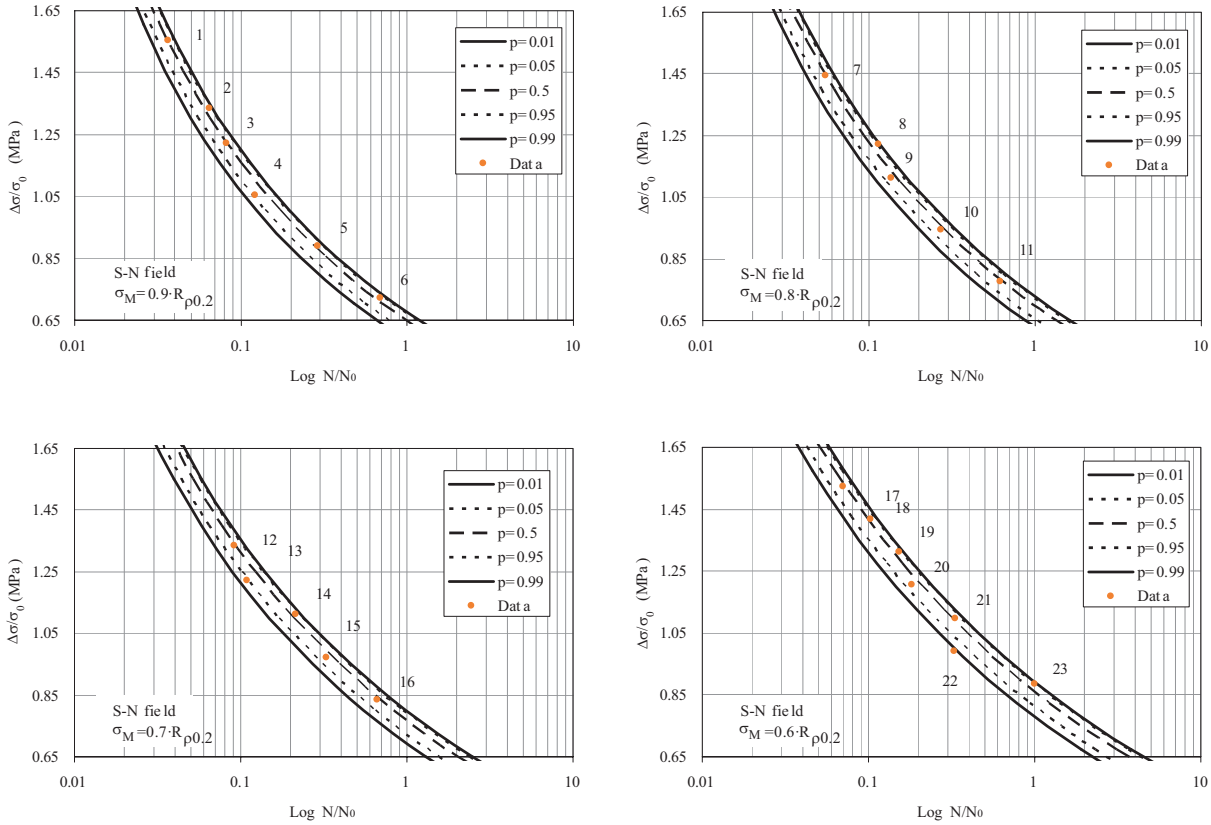


Figure 7.13: S–N curves representing constant $\sigma_M^* = 0.9, 0.8, 0.7$ and $0.6R_{p0.2}$ for the AlMgSi1 alloy (from top to bottom and left to right). The percentiles 0.01, 0.05, 0.50, 0.95 and 0.99 are represented.

them have been estimated with maximum likelihood method (see Section 6.7.1). The PP–plot of each new estimation (see figure 7.18) shows the goodness of each estimation and, furthermore, in table 7.13 uniformity test results are analyzed.

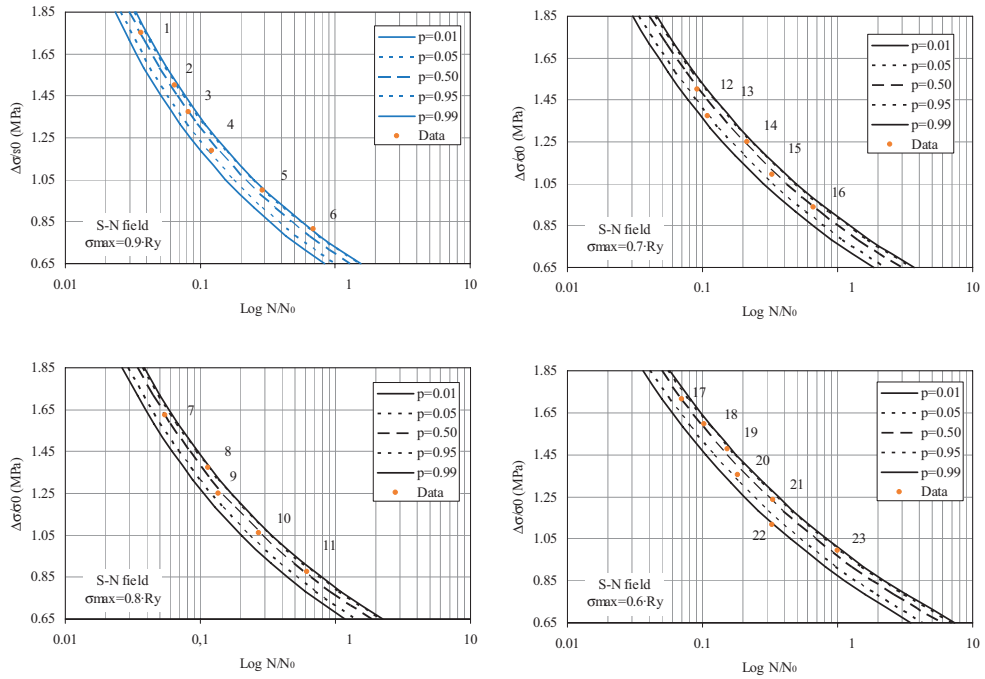


Figure 7.14: S–N field extrapolated to $\sigma_M = 0.9R_y$ (blue lines). The other S–N fields represent the curves obtained with the $0.8, 0.7$ and $0.6R_y$ series data.

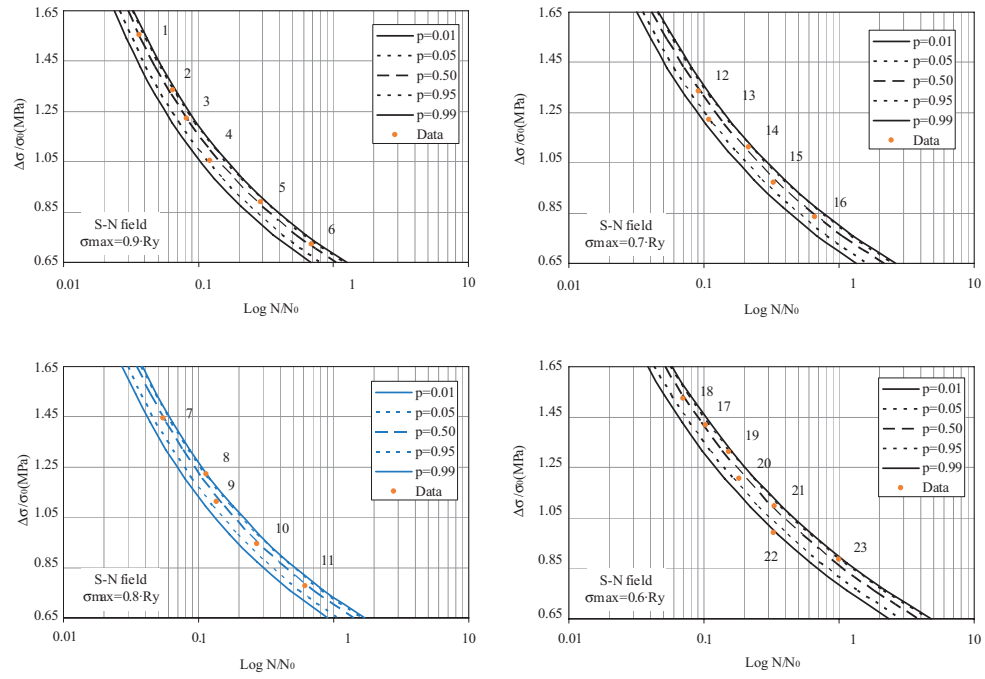


Figure 7.15: S–N field extrapolated to $\sigma_M = 0.8R_y$ (blue lines). The other S–N fields represent the curves obtained with the $0.9, 0.7$ and $0.6R_y$ series data.

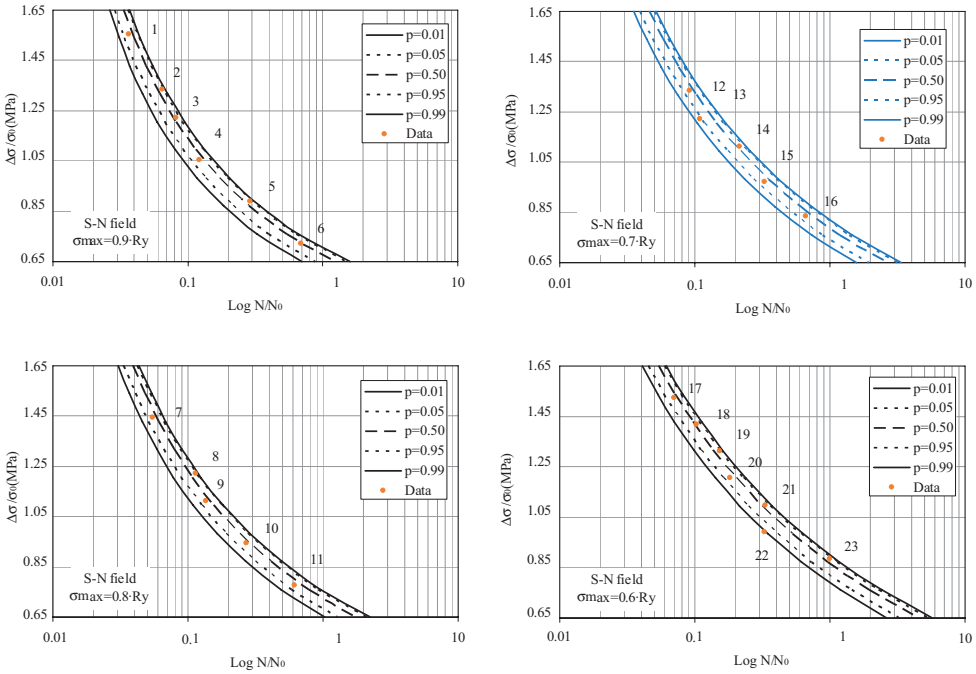


Figure 7.16: S–N field extrapolated to $\sigma_M = 0.7R_y$ (blue lines). The other S–N fields represent the curves obtained with the $0.9, 0.8$ and $0.6R_y$ series data.

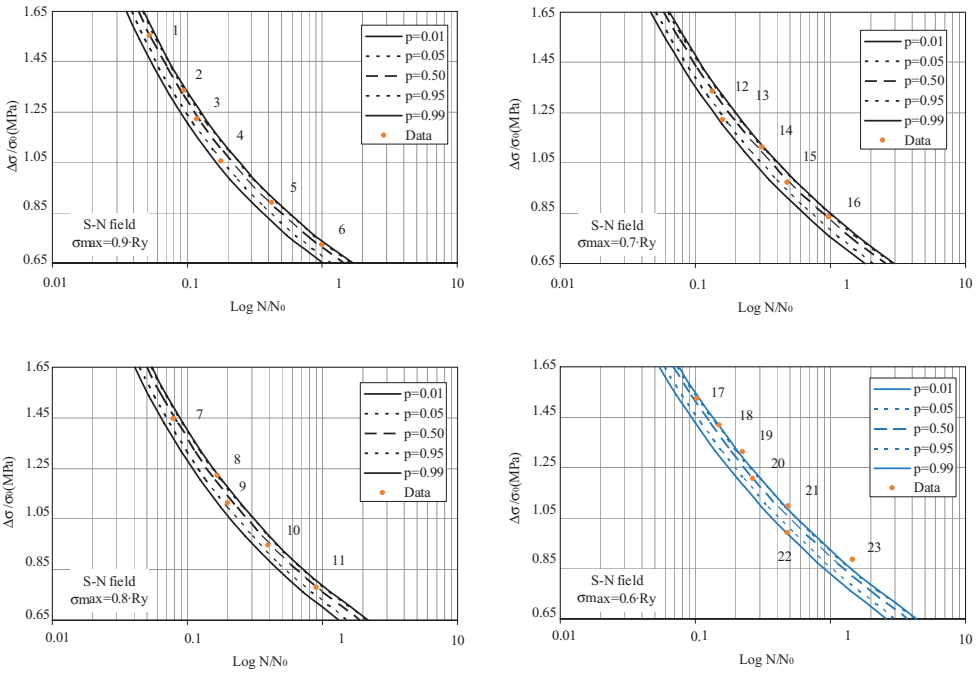


Figure 7.17: S–N field extrapolated to $\sigma_M = 0.6R_y$ (blue lines). The other S–N fields represent the curves obtained with the $0.9, 0.8$ and $0.7R_y$ series data.

Table 7.12: Estimated parameter for different cases of study.

| Serie deleted | Parameters | | | | | | | |
|---|---|---|---|---|---|---|---|---|
| | $C_0$ | $C_1$ | $C_2$ | $C_3$ | $C_4$ | $C_5$ | $C_6$ | $C_7$ |
| Original | -78.5072 | -31.3573 | 101.4600 | -34.9600 | 0.0000 | 0.0000 | 13.3021 | -8.6420 |
| $0.9R_y$ | -76.1105 | -29.1199 | 87.8549 | -21.9324 | 0.0000 | 0.0000 | 11.4951 | -5.8264 |
| $0.8R_y$ | -78.4884 | -31.6460 | 101.1503 | -35.2517 | 0.0000 | 0.0000 | 13.0518 | -9.0942 |
| $0.7R_y$ | -74.4392 | -40.7260 | 94.5836 | -22.3054 | 1.8062 | 0.0000 | 9.3937 | -10.5329 |
| $0.7R_y$ | -85.0225 | -50.3607 | 105.2599 | -20.9113 | 5.5017 | 0.0000 | 9.6941 | -9.4481 |

Table 7.13: Goodness of fit test for the different cases of study.

| Serie deleted | Nr. Test | Kolmogoronov-Smirnov | | | Chi-Square Test | | |
|---|---|---|---|---|---|---|---|
| | | Max. Dif. | Limit | Uniformity? | $\chi^2$ | Critical Value | ok? |
| Original | 23 | 0.141 | 0.275 | Yes | 5.696 | 7.815 | Ok |
| $0.9R_y$ | 17 | 0.074 | 0.318 | Yes | 1.588 | 7.815 | Ok |
| $0.8R_y$ | 18 | 0.167 | 0.309 | Yes | 2.444 | 7.815 | Ok |
| $0.7R_y$ | 18 | 0.194 | 0.309 | Yes | 4.222 | 7.815 | Ok |
| $0.6R_y$ | 16 | 0.125 | 0.327 | Yes | 3.500 | 9.488 | Ok |

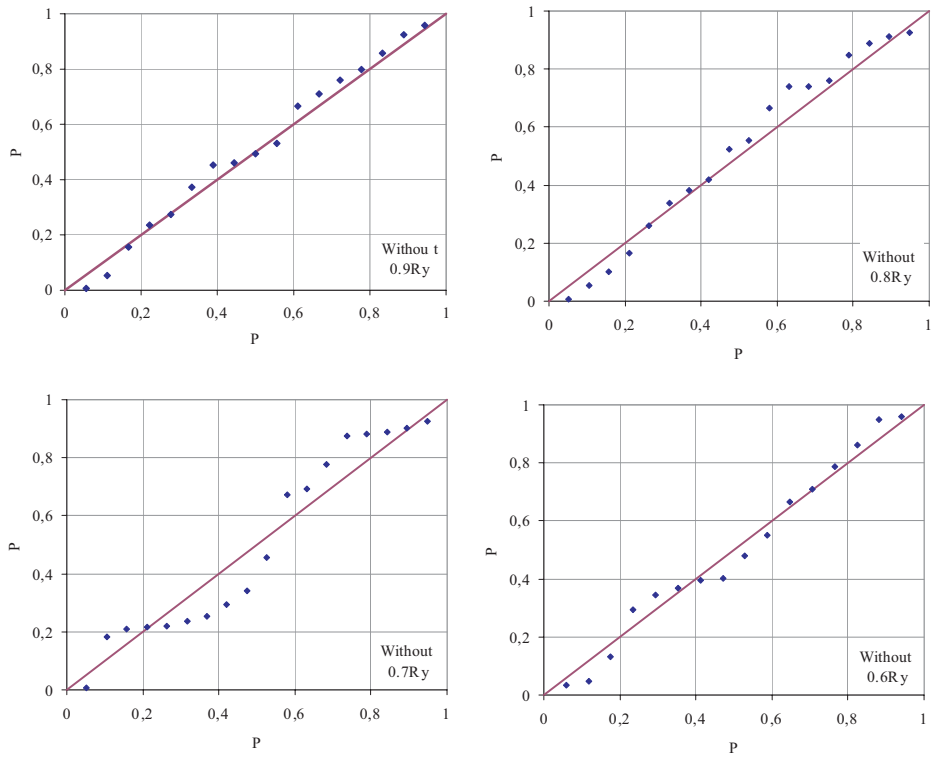


Figure 7.18: Representation of the PP–plot obtained for different estimations. From the top to bottom, and left to right: without $0.9R_y$, without $0.8R_y$, without $0.7R_y$ and $0.6R_y$ original series data.

## 7.8 Conclusions

The main conclusions drawn from this chapter are:

- Two different materials (a low–alloy steel and an aluminum alloy) have been analyzed and their model parameters obtained. The behaviors of these materials are different. The results show less dispersion for the AlMgSi1 alloy than for the 42CrMo4 steel.
- The 42CrMo4 material shows linear or almost linear trend of the Wöhler field, while the AlMgSi1 material shows the typical curvature of S–N fields.
- Different models have been obtained without parameter fixed. The model has the capacity of choosing the best parameter for each material.
- The distribution of the points doesn't affect the parameter estimation, but a wide range of data is necessary for a good estimation.
- Model validation have been made for both materials and, furthermore, for the theoretical example presented. The results show the goodness fit of the models for different constant ratios, i.e. $R$ ratio or $\sigma_M$.
- The capacity of the model to be extrapolated has been presented. Two different extrapolation have been made: first, the P-S–N field for both materials, second re-estimation of the model without some of the original data to validate the extrapolation.
- The extrapolation of the model can be done for any range of load, but better results are obtained if the extrapolation is made when one of the middle series is deleted (see figure 7.14 to figure 7.17).

# Chapter 8

# Damage Measures and Damage Accumulation

This chapter deals the problem of accumulating damage due to any fatigue load history. First, some desirable properties for a damage model are discussed and different possible alternatives fulfilling these properties are analyzed. Generally, current damage measures, such as the Palmgrem-Miner's rule, do not satisfy these properties. Next, a statistical fatigue regression model, able to predict the Wöhler field for any combination of $\sigma_{min}$, $\sigma_{max}$ or $R = \sigma_{min}/\sigma_{max}$ is presented.
This model is based on physical, statistical and compatibility conditions rather than on arbitrary functions. The probability of failure is assumed to be the most suitable option to assess damage measure. According to this, the procedure for obtaining the basic information for constant load, i. e. the probabilistic Wöhler field, is discussed, and formulas for calculating the associated damage are given.

## 8.1 Introduction

The evaluation of fatigue damage is basic and very important in design of structures, because fatigue is becoming determinant and the cause of a high number of failures of mechanical components and structural elements in real practice.

Fatigue design of structures subject to varying loading is not possible without some basic material fatigue characterization related to the stress range and stress levels, as the primary and secondary parameters, respectively. This information allows one the evaluation of the damage caused by the loading cycles associated with any given load spectrum. Generally, this important information is obtained from tests conducted at constant stress level, either $\sigma_{max}$, $\sigma_{min}$, $\sigma_{mean}$ or $R = \sigma_{min}/\sigma_{max}$, though Wöhler curves obtained from tests run at $\sigma_{mean} = 0$, i.e. for completely reverse stress, are often preferred. The speed of the damage process depends on the microstructure characteristics of the material and increases with the number of cycles, the stress range and the stress level in every cycle, three factors to be taken into account when analyzing damage.

The main objective of this chapter is to check the validity of the model developed in the chapters below (chapter 6: Model derivation and chapter 7: Experimental validation) for fatigue damage due to any stress history.

In most structural dynamic situations the loading process and hence the structural response is assumed to be Gaussian [116], and so, very frequently, the damage accumulation is calculated by simulating a Gaussian time history from a random process defined by a power spectra density ($PSD$) curve. Later, the rain-flow counting algorithm, which is assumed to be the best counting method, and the Palmgrem-Miner rule ([95], [105]), frequently used due to its simplicity, are applied to obtain an estimate of the structural fatigue life. The problem arises because in many realistic applications the Gaussian hypothesis is not correct, since observed structural responses are non-Gaussian ([81], [90]), due to either non-Gaussian external excitations (e.g. wave or wind loads), or to the structural non-linearities. Different authors have pointed out that the non-normal load can be responsible of an increase of the rate of fatigue damage accumulation ([83], [116] and [132]), so all the spectral methods valid for Gaussian loadings may provide non-conservative estimates when applied to non-Gaussian loads [24]. In summary, constant loads and lineal variable loads were used in order to illustrate damage evolution.

An important question was risen in Castillo et al. [41] *what is damage?* Or, equivalently *how is damage related to failure?* A physical concept of failure, such as crack size, seems to be adequate to define a service limit state, but fatigue failure, as an ultimate limit state, requires a probabilistic framework allowing relating damage levels to probabilities of occurrence. In this chapter we try to answer this question, furthermore, several methods to measure damage will be analyzed and discuss to identify which is the best one and which of them are inadequate for measuring damage ([41], [115]).

## 8.2 Damage measures

The problem of defining and selecting damage measures must be done with care if one desires they to be useful in practice. This problem is discussed in this section, with the main ideas taken from Castillo et al. [41].

### 8.2.1 Some requirements for a damage measures

Consider a piece subject to a fatigue load. This piece has an initial damage, which is random. The piece fails when the accumulated damage reaches a given threshold (critical) value. In order to make sense and be a useful tool, a damage measure must be carefully selected to be an indicator of the damage a certain piece of material has suffered during its past life, including fabrication.

Some properties to get a valid damage measure are:

**Property 1.- Increasing with damage:** The damage increases when increases the damage measure.

**Property 2.- Interpretability:** The damage measures must provide a clear information of the associated damage level.

**Property 3.- Dimensionless measures:** To avoid the problem of estimate the lifetime with non-dimensionless variables, dimensionless variables should be chosen.

**Property 4.- Known and fixed range:** The range of variation of the damage measure must be fixed and known, independently of the type of load and, if possible, of the material.

**Property 5.- Of known distribution:** To know the probability of failure of a piece chosen at random, its damage must have a known distribution.

### 8.2.2 Some damage measures

Several proposals of damage measures will be analyzed below. The aim of this study is to illustrate the appropriateness and importance of the above properties [115].

#### Measures based on the number of cycles

As fatigue damage increases with the number of cycles $N$, the number of cycles to failure or any increasing function of it are possible candidates for damage measures. Some possibilities are:

1. *The number of cycles:* The damage measure is the number of cycles $N$. This measure does not satisfy Property 3 above (is not dimensionless), because if we use thousands or dozens of cycles, instead of cycles, we have N/1000 or N/12, respectively.

   According with the model (6.13), we have:

   $$\log N_i \sim G\left(B - \frac{E}{\log \Delta\sigma^* - C}, \frac{D}{\log \Delta\sigma^* - C}\right), \tag{8.1}$$

   and the range $\left(e^{B - \frac{E}{\log \Delta\sigma^* - C}}, \infty\right)$ depends on the stress range $\Delta\sigma_i^*$, so it satisfies Property 5 but not Property 4.

2. *The logarithm of the number of cycles:* Other alternative is the logarithm of the number of cycles N. Unfortunately, this index satisfies neither Property 3 nor Property 4.

   If $\log N$ is a Gumbel distribution (Equation (8.1)), and the range depends on the stress level, this alternative has the same problems and limitations as the previous one.

3. *The normalized logarithm of the number of cycles:* A third alternative is the normalized logarithm of the number of cycles to failure.

   $$D_i = \frac{\log N_i^*}{\mu_i}, \tag{8.2}$$

   where $\mu_i$ is the mean of $\log N_i^*$ when the stress range is $\Delta\sigma_i^*$. Because this equation (8.2) is a linear transformation, we have:

   $$D_i \sim G\left(\frac{\lambda_i}{\mu_i}, \frac{\delta_i}{\mu_i}\right), \tag{8.3}$$

   but this measure it is not easily interpretable, so it does not satisfy Property 2. Furthermore $D_i$ does not satisfy Property 4.

4. *The standardized logarithm of the number of cycles:* The last option analyzed, is the standardized logarithm of the number of cycles:

   $$N_i^* = \frac{\log N_i^* - \mu_i}{\sigma_i}, \tag{8.4}$$

so that

$$N_i^* \sim G\left(\frac{B\log\Delta\sigma^* + E}{\log\Delta\sigma^* - C}, \frac{D}{\log\Delta\sigma^* - C}\right). \tag{8.5}$$

This alternative does not depend on the stress range and material, so we can conclude that $N_i^* \Leftrightarrow N^*$ and does not satisfy all the properties.

**Based on the Palmgren-Miner number**

1. *The Palmgren-Miner number:*

$$M_i = N_i/\mu_i', \tag{8.6}$$

where $\mu_i'$ is the mean value of the number of cycles to failure $N_i$ for a stress level $\Delta\sigma_i$.

The Palmgren-Miner number is dimensionless (because the random variable is divided by its mean) so it satisfies Property 3. Taking logarithms one gets:

$$\log M_i = \log N_i - \log\mu_i' \tag{8.7}$$

and then

$$M_i \sim \log G(\lambda_i - \log\mu_i', \delta_i). \tag{8.8}$$

The range of $M_i$ is $(e^{\lambda_i/\mu_i'}, \infty)$ so it does not satisfy Property 4.

2. *The logarithm the Palmgren-Miner number:* The damage measure $\log M_i$ has a Gumbel distribution too (Equation (8.8)), but its range is $(\lambda_i - \log\mu_i', \infty)$, and then, it does not satisfy Property 4.

**Based on the Gumbel variable**

A very convenient candidate for a damage measure is the normalized variable $Z$ of the Gumbel model.

**Normalization of the Gumbel model** Normalization will be applied with the aim of establishing a relation among the fatigue data pertaining to different load levels, thus enabling us not only a pooled parameter estimation, but the statistical interpretation of the damage measure to be done.

We remind the reader that the cumulative distribution function of the two parameter Gumbel family is given by:

$$F(x;\lambda,\delta) = 1 - \exp\left\{-\exp\left[\frac{x-\lambda}{\delta}\right]\right\}; x \geq \lambda; -\infty < \lambda < \infty; \delta > 0, \tag{8.9}$$

where $\lambda$ and $\delta$ are the location and the scale parameters, respectively. When X follows a Gumbel distribution $G(x;\lambda,\delta)$, we write $X \sim G(x;\lambda,\delta)$. Its mean $\mu$ and variance $\sigma^2$ are:

$$\mu = \lambda - 0.57772\delta, \tag{8.10}$$

$$\sigma^2 = \frac{\pi^2\delta^2}{6}. \tag{8.11}$$

One important property of the Gumbel family is that it is stable with respect to location and scale transformations, and also with respoect to minimum operations (see [33] and [46]). More precisely:

$$X \sim G(\lambda,\delta) \Leftrightarrow \frac{X-a}{b} \sim G\left(\frac{\lambda-a}{b}, \frac{\delta}{b}\right) \tag{8.12}$$

and

$$X_i \sim G(\lambda, \delta) \Leftrightarrow Min(X_1, X_2, \ldots, X_n) \sim G(\lambda - \delta n, \delta). \tag{8.13}$$

Let $X$ be a random sample value coming from a given population. It is well known that, no matter what statistical distribution $X$ belongs to, it can be normalized by means of the one-to-one transformation:

$$U = \frac{X - \mu_X}{\sigma_X}, \tag{8.14}$$

where $\mu_X$ and $\sigma_X$ are the mean value and the standard deviation of $X$, respectively, of the original distribution, and $U$ is the corresponding normalized value. The normalized distribution has mean $\mu_U = 0$ and standard deviation $\sigma_U = 1$. In addition, the new variable $U$ is dimensionless.

According to Equation (8.12), if $X$ follows a Gumbel distribution, as it is generally accepted in the case of fatigue lives, $U$ also follows a Gumbel distribution with parameters $\lambda^*$ and $\delta^*$, given by (see Equation 8.12):

$$\lambda^* = \frac{\lambda - \mu}{\sigma} = \frac{\mu + 0.57772\delta - \mu}{\pi\delta/\sqrt{6}} = \frac{0.57772\sqrt{6}}{\pi}, \tag{8.15}$$

$$\delta^* = \frac{\delta}{\sigma} = \frac{\delta\sqrt{6}}{\pi\delta} = \frac{\sqrt{6}}{\pi}. \tag{8.16}$$

This demonstrates that the Gumbel parameters of the normalized distribution do not depend on the parameters of the original distribution. Thus, it follows, that all distributions sharing common parameters $\lambda$ and $\delta$ transform, after normalization, to the same distribution.

An alternative normalization consists of using the random variable

$$Z = \frac{(\log N^* - B)(\log \Delta\sigma^* - C) - E}{D}, \tag{8.17}$$

that is,

$$Z = C_0 + C_1\sigma_{m_i} + C_2\sigma_{M_i} + C_3\sigma_{m_i}\sigma_{M_i} + (C_4 + C_5\sigma_{m_i} + C_6\sigma_{M_i} + C_7\sigma_{m_i}\sigma_{M_i}) \log N_i. \tag{8.18}$$

The normalized variable $Z$ presented, satisfies all the Properties: increasing with damage, interpretable, non-dimensional, with fixed range, and $Z \sim G(0, 1)$. Thus, we propose Z as a convenient measure for the cumulative fatigue damage associated with a given stress level or load history.

**Based on the failure probability**

In this subsection the failure probability as a damage measure is studied. According to our Gumbel model (6.13), any number of cycles $N$ below the zero-percentile curve leads to no failure and, above this curve, there is a probability of failure dependent on $N$.

All specimens have maximum crack sizes below the failure size, in other words, below the zero percentile curve, the crack grows but cannot reach failure for any possible initial crack siz. On the contrary, above the zero percentiles, some specimens have cracks that have already reached the failure size. Thus, above the zero-percentile curve, we can define our damage measure as the failure probability (see [41], [115]):

$$P_F = F_{G(B-\lambda_i, \delta_i)}(\log N_i) = F_D(D), \tag{8.19}$$

where $P_F$ is non-dimensional and has a uniform distribution ($P_F \sim U(0,1)$). This measure satisfies all desired Properties 1-5.

To define a damage measure below the zero-percentile, in the non-failure zone, a proportionality criterion is used. This criteria was defined by Castillo et al. [41], damage in this zone is proportional to the number of cycles if the stress level is held constant. So, the probability damage measure is:

$$P_F = \begin{cases} \dfrac{N_i}{N_{0,i}} - 1 & \text{if } N_i \leq N_{0,i} \\ F_{G(\lambda_i,\delta_i)}(\log N_i) & \text{if } N_i > N_{0,i}, \end{cases} \tag{8.20}$$

where $N_{0,i}$ is the zero-percentile number of cycles for a stress level $\Delta\sigma_i$.

Finally we can conclude that a piece in the non-failure region has damage measure in the range $[-1, 0]$, where $-1$ corresponds to zero cycles and 0 to the critical number of cycles $N_{i,0}$ in the zero-percentile line. A piece in the failure region has a damage measure in the range $(0, 1)$, where 1 is the maximum damage measure, that corresponds to an infinite life, only attainable for the strongest possible piece.

**Critical comparison**

In this section, a comparison between all the cases studied is made. table 8.1 summarizes the main characteristics and properties of several proposals of damage measures.

Some conclusions derived from this table are:

1. All measures increase with damage, as required.
2. Some measures are easier to evaluate than other.
3. All the measures are dimensionless except the measures based on $N_i$ and $\log N_i$.
4. Some ranges are not independent of the material, load history or both. Only $Z$ and $P_f$ satisfy this material independent property.
5. The measures $Z$ and $P_F$ are the only ones that have a fixed statistical distribution, that is, independent of the stress level.
6. Only measures $Z$ and $P_F$ satisfy all the properties, so these measures are the best, followed by $N^*$.

## 8.3 Cumulate damage associated with a general load history

This section aims at studying the cumulative damage associated with a general load history taking into account the influence of the mean stress in damage accumulation (see Conway [53] and Dowling [60]).

In figure 8.1 we can see directly the number of cycles under a constant stress load with the corresponding probability of failure, but it gives no direct information of the probability of failure associated with a varying stress level history. An accumulation rule becomes necessary to evaluate the damage produced by an arbitrary load history.

figure 8.1 represents isodamage curves in the Wöhler field, which are the curves corresponding to the same damage level for different stress ranges. In this figure two different load histories leading to the same damage are shown. The first one is if the experiment is started (point

Table 8.1: Properties and characteristics of different damage measures for the case of constant stress levels (Legend: $****$ very good, $***$ good, $**$ medium and $*$ bad) [115].

| Damage measure | Property | | | | |
|---|---|---|---|---|---|
| | Increasing | Interpretability | Dimesionless | Range | Distribution |
| $N_i$ | Yes | ** | No | $(e^{\lambda_i}, \infty)$ | $\log G(B - \lambda_i, \delta_i)$ |
| $\log N_i$ | Yes | * | No | $(\lambda_i, \infty)$ | $G(B - \lambda_i, \delta_i)$ |
| $D_i = \dfrac{\log N_i}{\mu_i}$ | Yes | * | Yes | $(\lambda_i/\mu_i, \infty)$ | $G(\lambda_i/\mu_i, \delta_i/\mu_i)$ |
| $N^* = \dfrac{\log N_i - \mu_i}{\sigma_i}$ | Yes | *** | Yes | $(\lambda_i^*, \infty)$ | $G(\lambda_i^*, \delta_i^*)$ |
| $M_i = \dfrac{N_i}{\mu_i}$ | Yes | ** | Yes | $(e^{\lambda_i/\mu_i}, \infty)$ | $\log G(\lambda_i - \log \mu_i', \delta_i)$ |
| $\log M_i = \log N_i - \log \mu_i$ | Yes | * | Yes | $(\lambda_i - \log \mu_i', \infty)$ | $G(\lambda_i - \log \mu_i', \delta_i)$ |
| $Z = \dfrac{\log N_i - B - \lambda_i}{\delta_i}$ | Yes | *** | Yes | $(-\infty, \infty)$ | $G(0, 1)$ |
| $P_F = F_{G(B+\lambda_i, \delta_i)} \log N_i$ | Yes | **** | Yes | $(0, 1)$ | $U(0, 1)$ |

$$\lambda^* = \frac{0.57772\sqrt{6}}{\pi}; \delta^* = \frac{\sqrt{6}}{\pi}$$

$A_0$) at stress level $\Delta\sigma_1$ for a number of cycles (until reaching point $A_1$) and then changed to another stress level $\Delta\sigma_2$ (point $A_2$) for a number of cycles (until reaching point $A_3$) and so on, until the final curve is reached (point $A_7$). In the second load history, everything occurs at the reference level $\Delta\sigma_{ref}$, where the points $B_1, ..., B_7$ are equivalent (in damage) to the points $A_1, ..., A_7$, respectively. In other words, the four steps load history, moving from $\Delta\sigma_1$ and $\Delta\sigma_4$, and the load history at the reference level $\Delta\sigma_{ref}$ lead to the same damage level. The important consequence is that iso-damage curves permit the reduction of a load history to a probability of failure, independently of the previous history of stress level or mean stress [41].

The following two rules permit damage evaluation of any stress history:

1. ***Iso-probability rule:*** *Two load histories produce the same damage if the corresponding probabilities of failure coincide.*

2. ***Proportionality rule:*** *The damage produced under the zero percentile curve is proportional to the number of cycles, with a total maximum damage in that area being one unit.*

### 8.3.1 Procedure to perform a damage analysis

Model (6.13) provides probabilistic bases for calculating the damage accumulation for any type of loading being considered. In fact, due to the possible identification of the probability of failure $P$, represented by the percentile curves in the Wöhler field for any $\sigma_{min}$ and $\sigma_{max}$ with the damage state, the model can be used in cumulative damage calculations for fatigue life prediction of components subject to complex loading histories.

To evaluate the accumulated damage, we proceed as follows:

1. The initial damage is set to 0 (no damage)

2. The damage $p$ after the first cycle is calculated with the stress levels considered in this cycle.

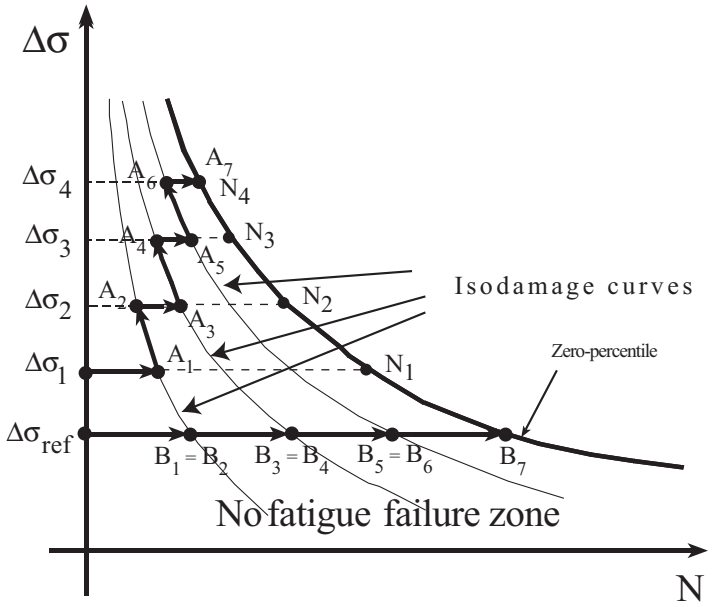


Figure 8.1: Illustration of the isodamage curves. figure from [36].

3. The equivalent number of cycles associated with this damage level $p$ for the stress levels ($\sigma_m^* = \sigma_m^*(N)$ and $\sigma_M^* = \sigma_M^*(N)$), for $N^* = 2$, using the inverse function (quantile) of (6.13), is calculated:

$$\log N_{eq}^* = \frac{\log(-\log(1-p)) - (C_0 + C_1\sigma_m^* + C_2\sigma_M^* + C_3\sigma_m^*\sigma_M^*)}{C_4 + C_5\sigma_m^* + C_6\sigma_M^* + C_7\sigma_m^*\sigma_M^*} \tag{8.21}$$

4. The accumulated damage, represented by the probability of failure, is calculated by the recursive formula:

$$P_{N+\Delta N} = F(N_{eq}^* + \Delta N, \sigma_m^*(N), \sigma_M^*(N)), \tag{8.22}$$

which gives the accumulated damage after $N + \Delta N$ cycles when the unit is subject to the stress history given by $\sigma_m^*(N)$ and $\sigma_M^*(N)$.

5. After this point, the damage can be calculated based on the percentiles, only by repeating steps 3 and 4 successively, until the damage level required is reached.

Figure 8.2 represent an theoretical example of application of this procedure:

1. The initial damage is equal to zero.

2. Knowing the first range of load, defined by $\sigma_{m1}$, $\sigma_{M1}$ and $N_1$, we obtain the probability $p_1$.

3. With the second range of load ($\sigma_{m2}$, $\sigma_{M2}$, $N_2$), we cannot obtain the probability $p_2$ directly. First we calculate the number equivalent of cycles ($N_{eq1}$) in function of $p_1$, to locate us in the correct position inside the S–N field (figure 8.2, (3) signal A). Then, with this number of cycles and the increment between $\Delta N = N_2 - N_1$ we obtain the probability $p_2 = F(N_{eq1} + \Delta N, \sigma_{m2}, \sigma_{M2})$ (figure 8.2, (3) signal B).

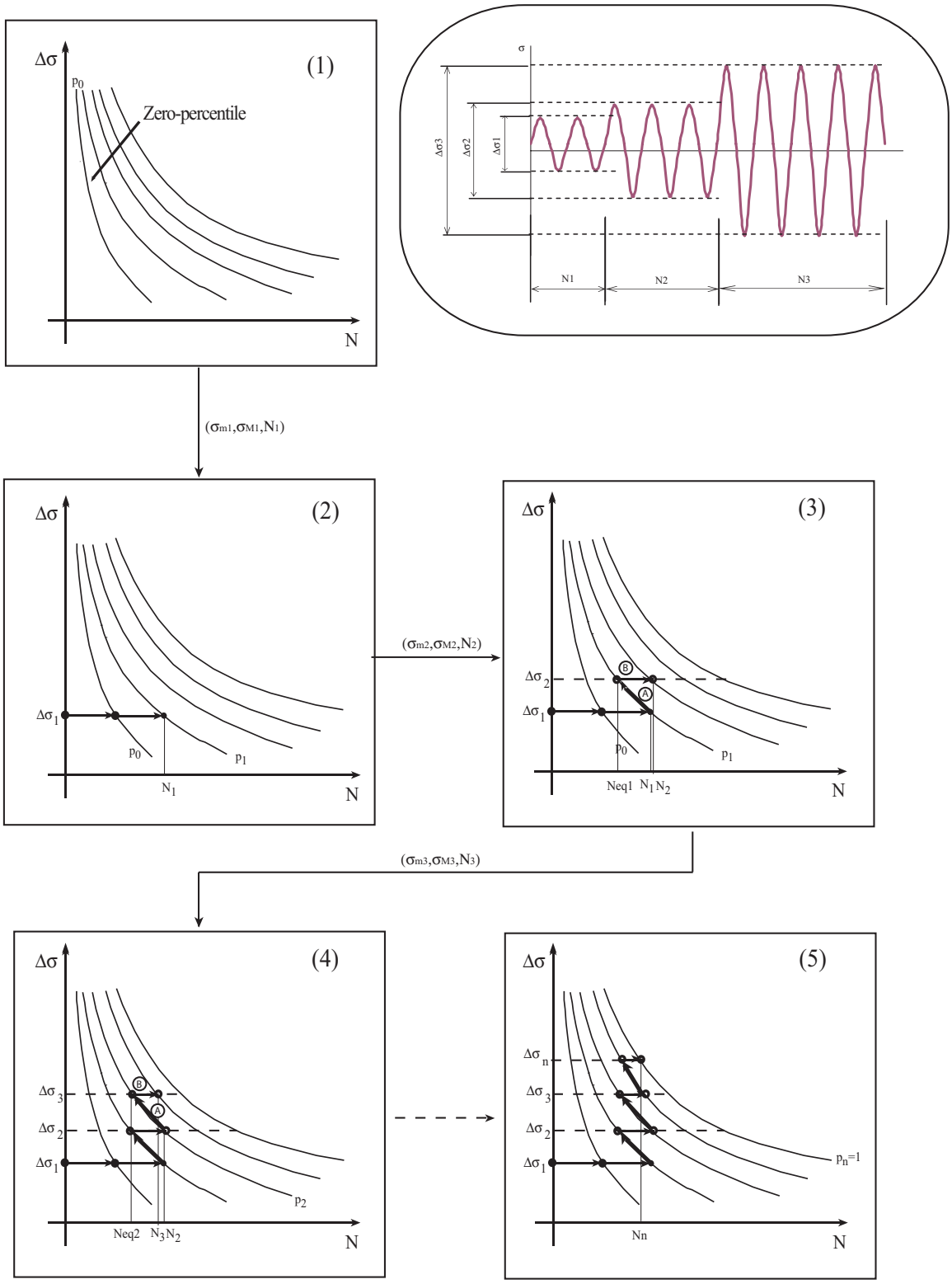


Figure 8.2: Theoretical example of application of the procedure for damage analysis.

4. Like in the step nr. 3, we repeat all the procedure, this time with the load ($\sigma_{m3}$, $\sigma_{M3}$, $N_3$), calculating first $N_{eq2}$ and then $p_3$.

5. Finally our specimen will be broken when the probability of failure will be equal to one $p_n = 1$.

## 8.4 Example of applications. Validation of damage accumulation

As indicated, this model provides probabilistic bases for calculating the damage accumulation for any type of loading being considered. In fact, due to the possible identification of the probability of failure ($p$), represented by the percentile curves in the Wöhler field, with any damage state, the model can be used in cumulative damage calculations for fatigue life prediction of components subject to complex loading histories.

In this section different types of load are analyzed to validate the capacity of the model described in chapter 6. These groups of loads are divided into two types:

1. Constant load, in which the specimen is subjected to a constant $\Delta\sigma$.

2. Variable load, in which the specimen is subjected to a non constant $\Delta\sigma$, but in which there is a lineal relation between load and lifetime.

In all cases, the material used for this validation was 42CrMo4, and the parameter used are those in chapter 7, section 7.6.2.

### 8.4.1 Constant loading

In this subsection a damage analysis of three different load histories is performed. All cases have a constant $\Delta\sigma(N) = 1130MPa$, that correspond with $\Delta\sigma^* = 1.099$ ($\sigma_0 = 955.5$ MPa), but each one has different values of $\sigma_M$, $\sigma_m$ and $\sigma_{mean}$. The characteristics of each load are shown in table 8.2. figure 8.3 shows the different load histories.

Table 8.2: Characteristics of the three different load histories analyzed. Case of constant $\Delta\sigma$.

| Case | $\Delta\sigma^*$ | $\sigma_m^*$ | $\sigma_M^*$ | $\sigma_{mean}^*$ |
|---|---|---|---|---|
| (a) | 1.099 | -0.500 | 0.599 | 0.045 |
| (b) | 1.099 | -0.399 | 0.700 | 0.151 |
| (c) | 1.099 | (odd cycles) -0.399 | 0.700 | (mean value) |
| | | (even cycles) -0.500 | 0.599 | 0.095 |

The results are presented in table 8.3 and figure 8.4. In table 8.3 the different values of the number of cycles for certain probabilities of failure ($p = 0.01, 0.1, 0.5, 0.9$ and $p = 0.99$) are presented. The effect of $\sigma_{mean}$ in the damage accumulation can be appreciated , i.e. higher values of $\sigma_{mean}$ correspond with higher probabilities of failure.

$$\sigma_{mean^*_{(a)}} < \sigma_{mean^*_{(c)}} < \sigma_{mean^*_{(b)}} \rightarrow N^*_{(a)} > N^*_{(c)} > N^*_{(b)}$$

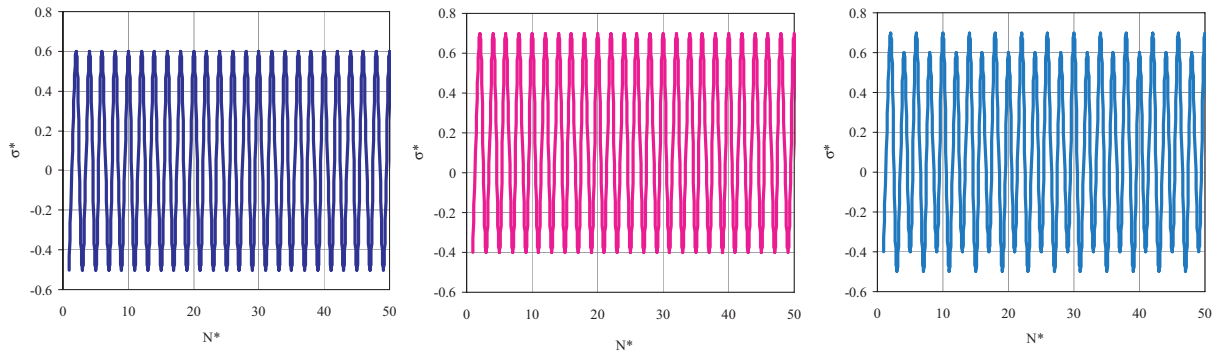


(a) (b) (c)

Figure 8.3: Load histories for the damage analysis, case of constant $\Delta\sigma = 1050$ MPa $\rightarrow \Delta\sigma^* = 1.099$ ($\sigma_0 = 955.5$ MPa). (a) $\sigma_m^* = -0.500$, $\sigma_M^* = 0.599$; (b) $\sigma_m^* = -0.399$, $\sigma_M^* = 0.700$; (c) $\sigma_m^* = -0.500$, $\sigma_M^* = 0.599$ for odd cycles and $\sigma_m^* = -0.399$, $\sigma_M^* = 0.700$ for even cycles.

Table 8.3: Values of the number of cycles $N^*$ for the probabilities of $p = 0.01, 0.1, 0.5, 0.9, 0.99$ for constant $\Delta\sigma$ and cases (a), (b) and (c).

| Case | Number of cycles $N^*$ | | | | |
|---|---|---|---|---|---|
| | $p = 0.01$ | $p = 0.1$ | $p = 0.5$ | $p = 0.9$ | $p = 0.99$ |
| (a) | 10 | 51 | 188 | 434 | 704 |
| (b) | 1 | 5 | 15 | 30 | 45 |
| (c) | 3 | 8 | 27 | 55 | 85 |

**Effect the existence of a discontinuity on the damage accumulation**

Here, the effect of the existence of a discontinuity on the damage accumulation is analyzed. For this, three different cases are studied (see figure 8.5):

- **Case a:** When the discontinuity is situated at the beginning of the sequence ($N^* = 10$).
- **Case b:** When the discontinuity is situated at the end of the sequence ($N^* = 100$).
- **Case c:** When the discontinuities are situated at $N^* = 10$ and $N^* = 30$.

Table 8.4: Values of number of cycles $N^*$ for the probabilities of $p = 0.01, 0.1, 0.5, 0.9, 0.99$ when there exits punctual high cycles in the load sequence.

| Case | Number of cycles $N^*$ | | | | |
|---|---|---|---|---|---|
| | $p = 0.01$ | $p = 0.1$ | $p = 0.5$ | $p = 0.9$ | $p = 0.99$ |
| Original | 7 | 32 | 103 | 217 | 335 |
| (a) | 7 | 9 | 42 | 156 | 274 |
| (b) | 7 | 32 | 99 | 147 | 264 |
| (c) | 7 | 9 | 29 | 87 | 204 |

For all the cases the $\Delta\sigma = 1000$ MPa, corresponding with $\Delta\sigma^* = 1.047$ ($\sigma_0 = 955.5$)MPa. The punctual cycle increase the amplitude a 10%. The results shown in table 8.4 that the

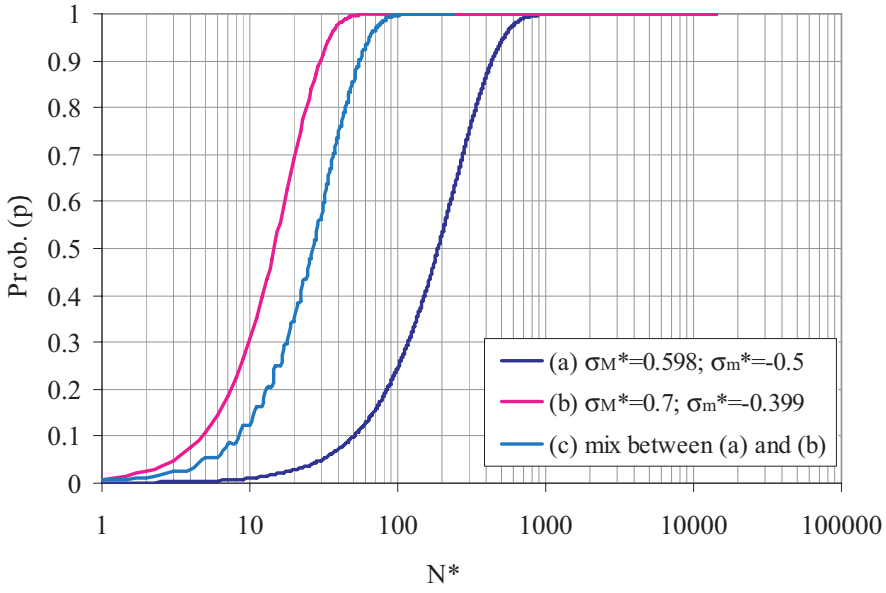


Figure 8.4: Load histories for the damage analysis, case of constant $\Delta\sigma = 1050$ MPa $\rightarrow \Delta\sigma^* = 1.099$ ($\sigma_0 = 955.5$ MPa). (a) $\sigma^*_m = -0.500$, $\sigma^*_M = 0.599$; (b) $\sigma^*_m = -0.399$, $\sigma^*_M = 0.700$; (c) $\sigma^*_m = -0.500$, $\sigma^*_M = 0.599$ for odd cycles and $\sigma^*_m = -0.399$, $\sigma^*_M = 0.700$ for even cycles.

probability of failure changes in function of where the discontinuity is situated. In all cases, the specimen will break before than the original one (without discontinuity inside of the load sequence). Otherwise, the worst case is the one corresponding to discontinuities at $N^* = 10$ and $N^* = 30$ (case (c), figure 8.5), because the $\sigma_{mean}$ is bigger and consequently the damage too. Finally, when the situation of the discontinuities are different, the distribution of probabilities of failure (cdf, figure 8.6) is different. The increment of the probability of failure is function of the equivalent number of cycles ($N^*_{eq}$) that depends also of the probability in the previous cycle (see section 8.3.1 and Equations (8.21) and (8.22)), that is, the evolution of probabilities is different although the increment of amplitude is the same in all the cases.

### 8.4.2 Variable loading

In this section different load histories are analyzed. All the sequences have a lineal amplitude slope, but different $\sigma_m$ and $\sigma_M$ expressions (see figure 8.7). Three different groups are studied:

1. Load history with constant $\sigma^*_m$ and variable $\sigma^*_M$.

2. Load history with constant $\sigma^*_M$ and variable $\sigma^*_m$.

3. Load history with variable $\sigma^*_M$ and $\sigma^*_m$.

The general form of each expression is $\Delta\sigma^* = m \cdot N^* + n = \sigma^*_M - \sigma^*_m$, where $\sigma^*_M = m_1 \cdot N^* + n_1$ and $\sigma^*_m = m_2 \cdot N^* + n_2$. The values of the parameters $m_1, m_2, m, n_1, n_2$ and $n$ are defined in table 8.5.

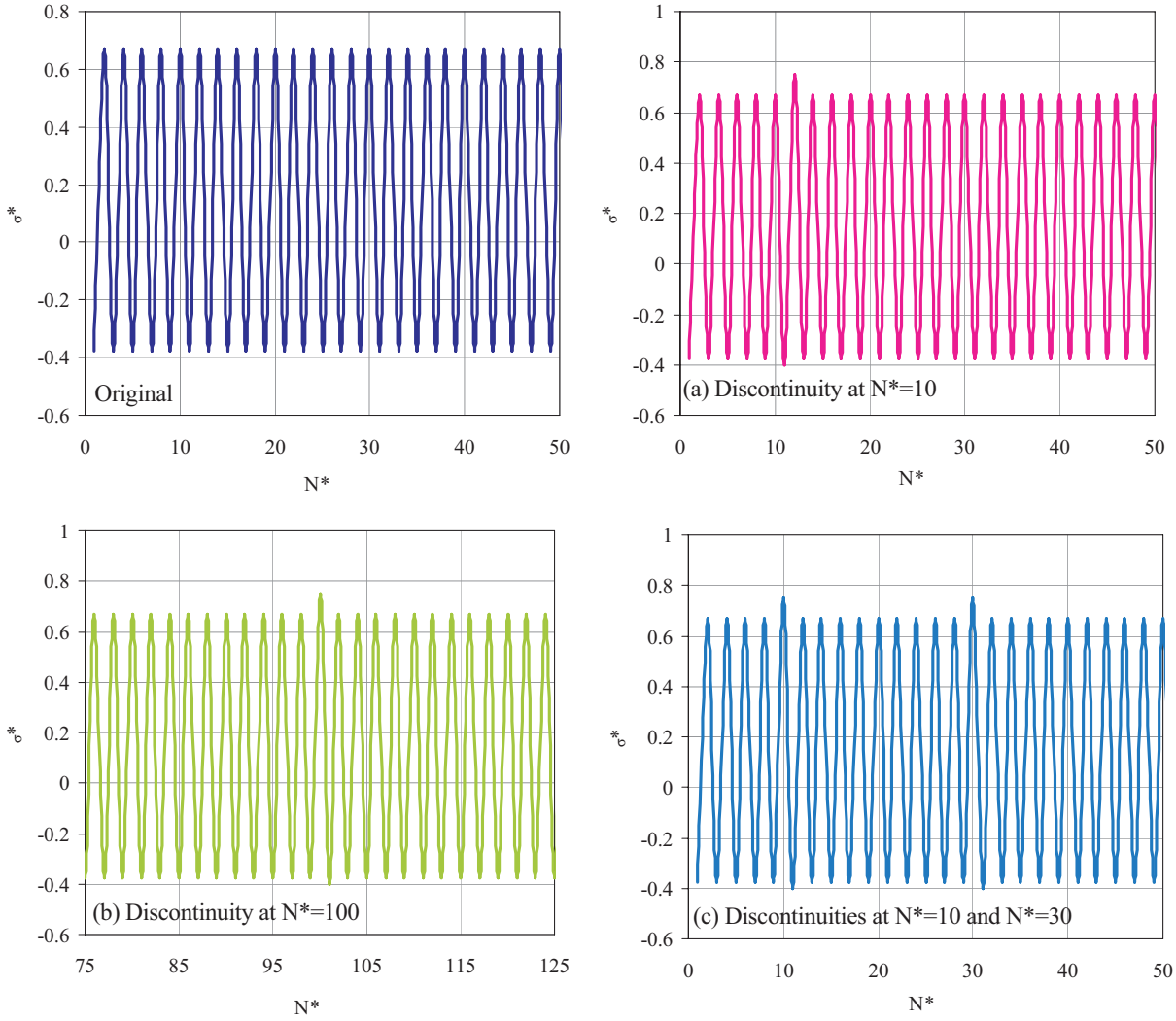


Figure 8.5: Load sequences used for the analysis of damage accumulation when a discontinuity appear in the sequence. From top to the bottom, and left to right: original sequence (without discontinuity), discontinuity situated at $N^* = 10$, discontinuity situated at $N^* = 100$ and punctual cycles situated at $N^* = 10$ and $N^* = 30$ (for $N_0 = 532000$ cycles).

The aim of analyzing a two spectra in each group of load histories is to discover the effect of symmetrical spectra in the damage accumulation. Figure 8.8 represent a scheme of this analysis, the aim is discover if the probability $p_A$ and the probability $p_B$ will be equal.

The cdfs obtained for each group of load histories are shown in figure 8.9. It can be appreciated how the second spectra of each group (designed by $a_2, b_2$ and $c_2$ grow faster than the first ones. This occurs because the second spectra damage begins to grow with a bigger value than in the first one. Furthermore, the damage always grows, that is, if in the beginning the probability is bigger, the failure will produce before than with the first spectra (designed by $a_1, b_1$ and $c_1$).

Finally, if a comparison between all the different cdf's is made, we can conclude that the damage increase with the value of $\sigma_{mean}$. In this example, we have analyzed six different load

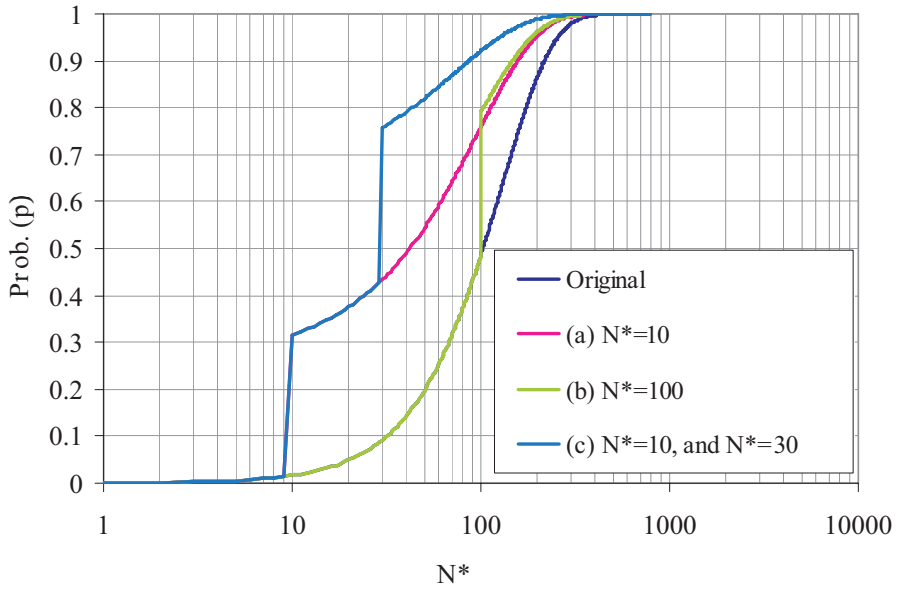


Figure 8.6: Load sequences used for the analysis of damage accumulation when a discontinuity appear in the sequence. From top to the bottom, and left to right: original sequence (without discontinuities), discontinuity situated at $N^* = 10$, discontinuity situated at $N^* = 100$ and discontinuities situated at $N^* = 10$ and $N^* = 30$ (for $N_0 = 532000$ cycles).

Table 8.5: Parameter for the definition of the load histories expressions.

| | $\sigma^*_M$ | | $\sigma^*_m$ | | $\Delta\sigma^*$ | |
|---|---|---|---|---|---|---|
| Case | $m_1$ | $n_1$ | $m_2$ | $n_2$ | m | n |
| $a_1$ | $4.5 \cdot 10^{-4}$ | 0.50 | 0.00 | -0.50 | $2.75 \cdot 10^{-4}$ | 0.50 |
| $a_2$ | $-4.5 \cdot 10^{-4}$ | 0.66 | 0.00 | -0.50 | $-2.75 \cdot 10^{-4}$ | 0.58 |
| $b_1$ | 0.00 | 0.75 | $4.5 \cdot 10^{-4}$ | 0.10 | $2.75 \cdot 10^{-4}$ | 0.33 |
| $b_2$ | 0.00 | 0.75 | $-4.5 \cdot 10^{-4}$ | -0.25 | $-2.75 \cdot 10^{-4}$ | 0.50 |
| $c_1$ | $1.8 \cdot 10^{-4}$ | 0.25 | $9 \cdot 10^{-5}$ | -0.45 | $1.35 \cdot 10^{-4}$ | 0.33 |
| $c_2$ | $-1.8 \cdot 10^{-4}$ | 0.59 | $-9 \cdot 10^{-5}$ | -0.62 | $-1.35 \cdot 10^{-4}$ | 0.61 |

histories with the following $\sigma^*_{mean}$ expressions:

- $a_1$: $\sigma^*_{mean} = 2.75 \cdot 10^{-4} \cdot N^* + 0.50$.
- $a_2$: $\sigma^*_{mean} = -2.75 \cdot 10^{-4} \cdot N^* + 0.58$.
- $b_1$: $\sigma^*_{mean} = 2.75 \cdot 10^{-4} \cdot N^* + 0.33$.
- $b_2$: $\sigma^*_{mean} = -2.75 \cdot 10^{-4} \cdot N^* + 0.50$.
- $c_1$: $\sigma^*_{mean} = 1.35 \cdot 10^{-4} \cdot N^* + 0.33$.
- $c_2$: $\sigma^*_{mean} = -1.35 \cdot 10^{-4} \cdot N^* + 0.61$.

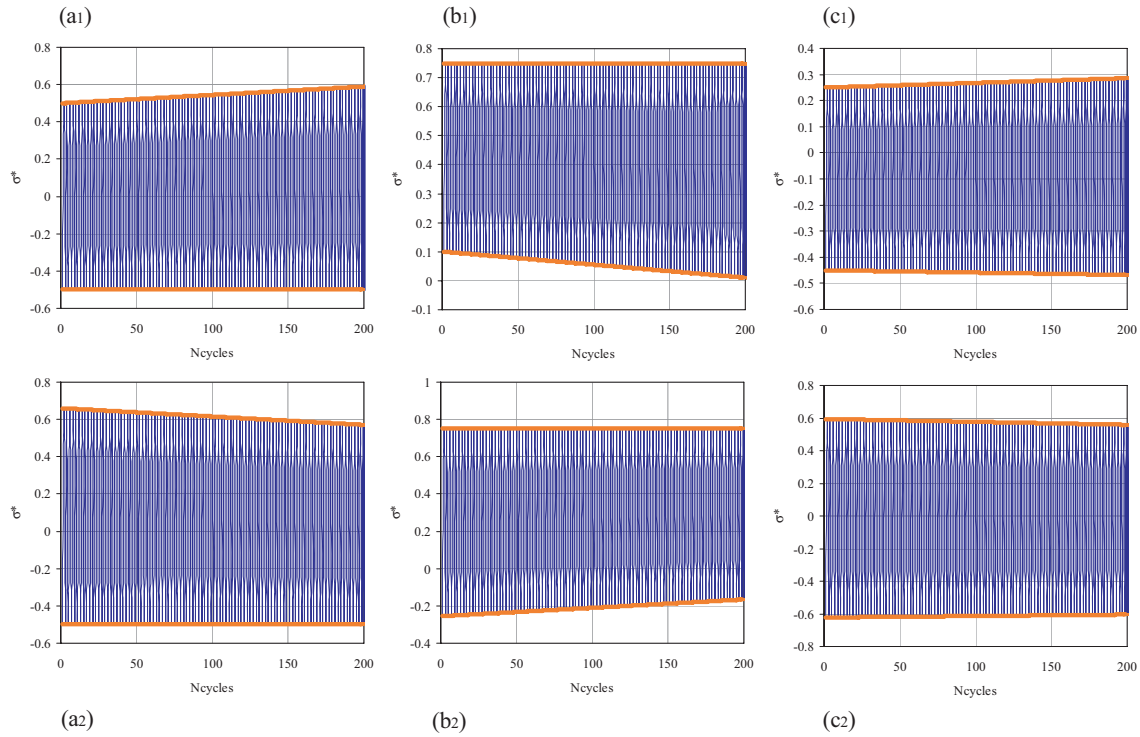


Figure 8.7: Variable load histories analyzed in the damage accumulation: $(a_1), (a_2)$ constant $\sigma^*_m$ and variable $\sigma^*_M$, $(b_1, b_2)$ constant $\sigma^*_M$ and variable $\sigma^*_m$, $(c_1, c_2)$ variable $\sigma^*_M$ and $\sigma^*_m$.

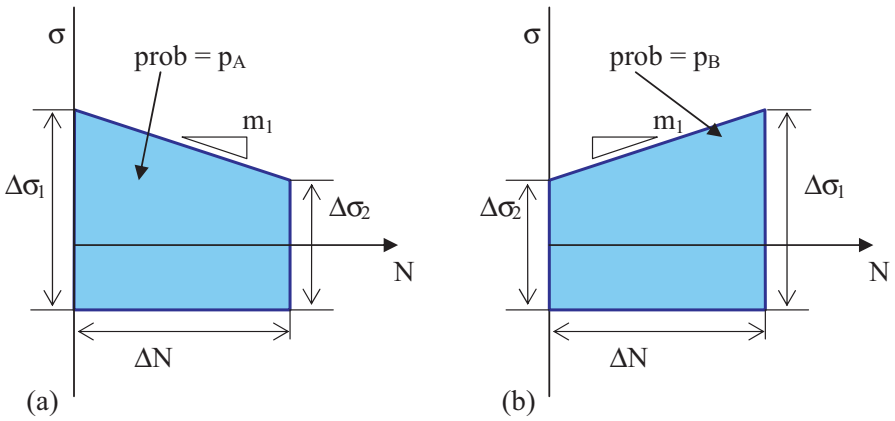


Figure 8.8: Schematic representation of the symmetrical problem.

If we choose a number of cycles, i.e. $N^* = 1$ the $\sigma^*_{mean}$ becomes in:

$$a_1 \rightarrow \sigma^*_{mean} = 0.5001; a_2 \rightarrow \sigma^*_{mean} = 0.5798; b_1 \rightarrow \sigma^*_{mean} = 0.3252;$$

$$b_2 \rightarrow \sigma^*_{mean} = 0.4999; c_1 \rightarrow \sigma^*_{mean} = 0.3251; c_2 \rightarrow \sigma^*_{mean} = 0.6080$$

where it can be appreciated the failure sort of the different load histories:

$$\sigma_{mean_{c_2}} > \sigma_{mean_{a_2}} > \sigma_{mean_{a_1}} > \sigma_{mean_{b_2}} > \sigma_{mean_{b_1}} > \sigma_{mean_{c_1}}$$

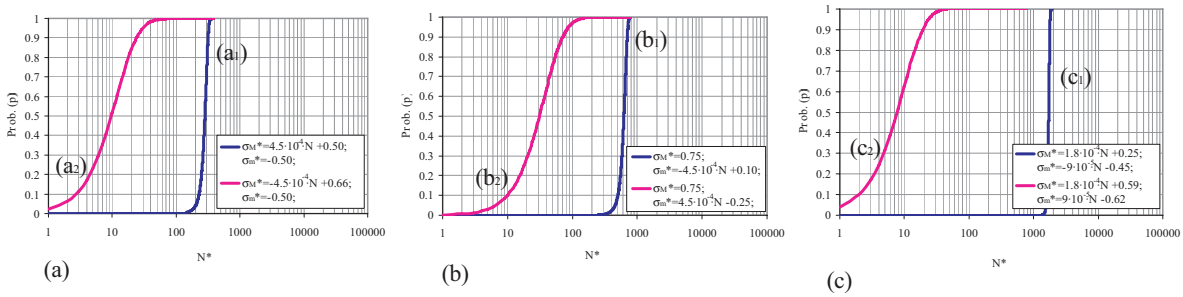


Figure 8.9: Variable load histories analyzed in the damage accumulation: $(a_1), (a_2)$ constant $\sigma_m^*$ and variable $\sigma_M^*$, $(b_1, b_2)$ constant $\sigma_M^*$ and variable $\sigma_m^*$, $(c_1, c_2)$ variable $\sigma_M^*$ and $\sigma_m^*$.

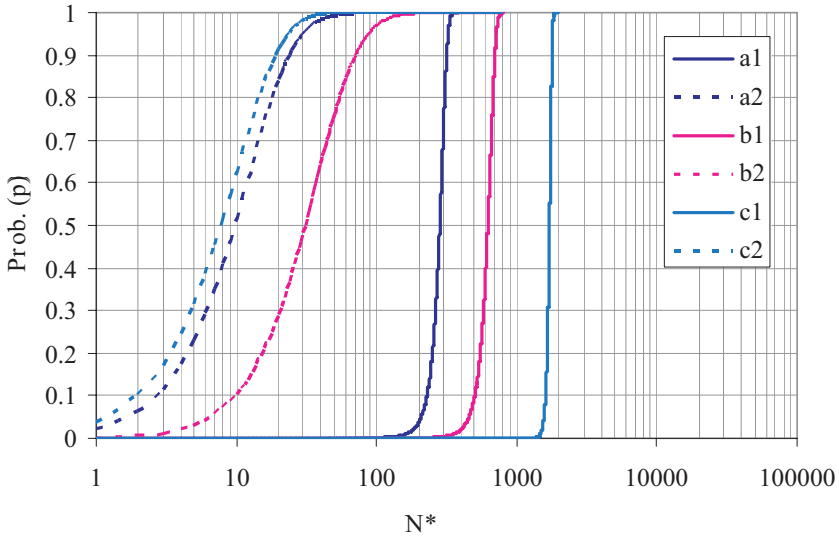


Figure 8.10: Variable load histories analyzed in the damage accumulation: $(a_1), (a_2)$ constant $\sigma_m^*$ and variable $\sigma_M^*$, $(b_1, b_2)$ constant $\sigma_M^*$ and variable $\sigma_m^*$, $(c_1, c_2)$ variable $\sigma_M^*$ and $\sigma_m^*$.

corresponding with

$$p_{failure_{c_2}} > p_{failure_{a_2}} > p_{failure_{a_1}} > p_{failure_{b_2}} > p_{failure_{b_1}} > p_{failure_{c_1}}$$

and with

$$N^*_{failure_{c_2}} < N^*_{failure_{a_2}} < N^*_{failure_{a_1}} < N^*_{failure_{b_2}} < N^*_{failure_{b_1}} > N^*_{failure_{c_1}}$$

Table 8.6 shows the different number of cycles $N^*$ for different probabilities of failure ($p = 0.01, 0.1, 0.5, 0.9$ and $0.99$).

## 8.5 Conclusions

The main conclusions from this chapter are the following:

Table 8.6: Values of number of cycles $N^*$ for the probabilities of $p = 0.01, 0.1, 0.5, 0.9, 0.99$ for different variable load histories.

| Case | Number of cycles $N^*$ | | | | |
|---|---|---|---|---|---|
| | $p = 0.01$ | $p = 0.1$ | $p = 0.5$ | $p = 0.9$ | $p = 0.99$ |
| $(a_1)$ | 161 | 229 | 283 | 317 | 337 |
| $(a_2)$ | 1 | 3 | 9 | 24 | 47 |
| $(b_1)$ | 355 | 501 | 623 | 700 | 744 |
| $(b_2)$ | 3 | 10 | 31 | 71 | 130 |
| $(c_1)$ | 1472 | 1607 | 1716 | 1785 | 1825 |
| $(c_2)$ | 1 | 2 | 7 | 20 | 34 |

- The normalized random variable in (8.17) described in Section 8.2.2 appears to be a useful tool to facilitate the comparison of the cumulative fatigue damage produced by different load histories involving constant or changing stress levels.

- A wide range of possible alternatives for selecting damage indices, including the logarithm of the number of cycles, the number of cycles to failure, the Palmgren–Miner number, its logarithm, its normalized or standardized form, the reference Weibull variable and the failure probability, are possible, and have been described in this paper. However, some of them are more convenient than others in the sense that they satisfy some desirable properties, such as non–dimensionality, fixed range, interpretability, known distribution, invariance with respect to load histories, etc.

- The probability of failure has been demonstrated to be the most convenient damage measure for engineering design, due to the fact that it satisfies all desirable properties and permits evaluating the probability of failure directly.

- The probability of failure is a very reasonable criterion for defining cumulative damage associated with different load histories. In fact, the Wöhler percentile curves allow us an easy interpretation of damage.

- The new model (6.13) is a good method for evaluating the damage in all ranges and load histories: constant or variables.

- The mean stress is the most important factor in the damage accumulation process and it gives to us a precious information. Understanding the variation of the mean stress in our load history the damage accumulation will be obtained easily.

- The existence of discontinuities in a load sequence transform the mean value of the mean stress, and this affect in the damaage accumulation process as indicated in the previous conclusion.

# Part V

# Conclusions

# Chapter 9

# Conclusions

This Chapter is the final chapter of the doctoral thesis presented in this document and its objective is to summarize the conclusions drwan during the elaboration of the doctoral thesis, and to present the future lines of research.
The Chapter is organized as follow: First, the general conclusions for each Chapter are presented. Second, a summary of the original contribution is given. Finally, the future lines of research are described.

## 9.1 Conclusions

The aim of this section is to present the most important conclusions obtained during the elaboration of this doctoral thesis:

**The new Gumbel fatigue model**

- The model is based on statistical and physical considerations, in particular, on compatibility conditions in the Wöhler field that leads to a system of functional equations.

- The model depends on 8 parameters that can be estimated by maximum likelihood and also by non–linear regression methods. It supplies all the material basic probabilistic fatigue information to be used in a damage accumulation assessment for fatigue life prediction of structural and mechanical components under real loading spectra.

- The large number of constraints of the model provide us only physically and statistically valid models, resulting good estimators of fatigue lifetime in the low-cycle range of fatigue (see the example presented in Section 6.8.1).

- Once the parameters of the model have been estimated, the model allows us obtaining any kind of Wöhler field according to the testing condition chosen.

**Experimental validation of the model**

- Two different materials (a low–alloy steel and an aluminum alloy) have been analyzed and their model parameters obtained. The behaviors of these materials are different. The results show less dispersion for the AlMgSi1 alloy than for the 42CrMo4 steel.

- Different models have been obtained without fixed parameters. The model has the capacity of choosing the best parameters for each material.

- The distribution of the points doesn't greatly affect the parameter estimation, but a wide range of data is necessary for a good estimation.

- Model validation have been made for both materials and, furthermore, for the theoretical example presented. The results show the goodness fit of the models for constant ratio: $R$ ratio or stress $\sigma_M$.

- The capacity of the model to be extrapolated has been presented. Two different extrapolation have been made: first, the P-S-N field for both materials, second re-estimation of the model without some of the original data to validate the extrapolation.

- The extrapolation of the model can be done for any range of load, but better results are obtained if the extrapolation is made when one of the middle series is deleted (see Figures 7.14 to 7.17).

**Analysis of the damage accumulation**

- The normalized random variable in Equation (8.17) described in Section 8.2.2 appears to be a useful tool to facilitate the comparison of the cumulative fatigue damage produced by different load histories involving constant or changing stress levels.

- A wide range of possible alternatives for selecting damage indices, including the logarithm of the number of cycles, the number of cycles to failure, the Palmgren- Miner number, its logarithm, its normalized or standardized form, the reference Weibull variable and the failure probability, are possible, and have been described in this paper. However, some of them are more convenient than others in the sense that they satisfy some desirable properties, such as non-dimensionality, fixed range, interpretability, known distribution, invariance with respect to load histories, etc.

- The probability of failure has been demonstrated to be the most convenient damage measure for engineering design, due to the fact that it satisfies all desirable properties and permits evaluating the probability of failure directly.

- The probability of failure is a very reasonable criterion for defining cumulative damage associated with different load histories. In fact, the Wöhler percentile curves allow us an easy interpretation of damage.

- The model can be used for all range of load and for any type of load: constant or variable.

- The mean stress is the most important factor in the damage accumulation process and it gives us a precious information. Understanding the variation of the mean stress in our load history the damage accumulation will be obtained easily.

- The existence of discontinuities in a load sequence transform the mean value of the mean stress, and this affect in the damaage accumulation process as indicated in the previous conclusion.

## 9.2 Summary of Contributions

The principal contributions provided in this doctoral thesis are:

- A new fatigue model useful for all range of load is defined. The model can be used for the analysis of material subjected to fatigue load in the range of tension-tension or tension-compression test.
- The new fatigue model is a good tool to know the damage accumulation. The model provides with a easy methodology good results in the analysis of the damage accumulation with constant and variable load histories. In the case of random load histories, using a second normalization, the model gives us a useful information of the damage process.
- A probabilistic useful model is developed. The advantages of this statistical approach to the fatigue of materials are diverse, as the possibility of knowing the probability of failure on a certain moment, or other statistical characteristics as the mean value of failure, lifetime, cutoff of a material subjected to fatigue loads.

## 9.3 Future work

Finally, after the elaboration of this doctoral thesis, in which a new fatigue model is presented, defined and developed, a continuation of this research is planned. The principal ideas/subjects that need more analysis in this research are:

1. Realize constant fatigue test with diverse metallic material with the objective of validate the new Gumbel fatigue model and to know the characteristic parameter of more materials. The methodology for this is explained in chapter 6 of this doctoral thesis.

2. Validate the new model for the low–cycle and for the high–cycle range of fatigue. This doctoral thesis has validated the model for the central region of number of cycles, but for

diverse application of the industrial engineering the materials are subjected to fatigue load belonging in the other two ranges of fatigue lifetime.

3. Elaborate a research in which the objective is to find and define an optimum testing strategy.

4. Study the effect of other parameters in the damage accumulation process using the Gumbel fatigue model (6.13). With respect to the influence of the frequency, normally is assumed that it has not influence in the lifetime on the fatigue tests [102], but this is not true when factors such as corrosion, high temperatures or random loads are analyzed. This influence depend of the material tested, and the type of test realized. Normally this factor is analyzed when the fatigue cracks growth are studied (see [14], [16], [102] or [119]). The effect of high temperatures is also a good subject for a new line of research. Its well known the use of metallic material in the aerospace industry, in which the material is subjected to random fatigue load histories in combination with high temperatures.

5. Validate the model for other type of materials, such as composite materials, heterogenous material (concrete), or new materials in which with diverse techniques the material is modified to obtain higher lifetimes.

# Appendix A

# Derivation of the Model

The functional equation (6.10) can be written as:

$$(\sigma_M^* - C_M(\sigma_M^*))D_m(\sigma_m^*) - D_m(\sigma_m^*)\sigma_m^* - D_M(\sigma_M^*)\sigma_M^* + D_M(\sigma_M^*)(C_m(\sigma_m^*) + \sigma_m^*) = 0, \quad \text{(A.1)}$$

and solved as follows (see Aczél [11] and Castillo et al. [49] and [46]):

$$\begin{pmatrix} \sigma_M^* - C_M(\sigma_M^*) \\ 1 \\ D_M(\sigma_M^*)\sigma_M^* \\ D_M(\sigma_M^*) \end{pmatrix} = \begin{pmatrix} 1 & 0 \\ 0 & 1 \\ a_0 & b_0 \\ c_0 & d_0 \end{pmatrix} \begin{pmatrix} \sigma_M^* - C_M(\sigma_M^*) \\ 1 \end{pmatrix} \quad \text{(A.2)}$$

$$\begin{pmatrix} D_m(\sigma_M^*) \\ -D_m(\sigma_m^*)\sigma_m^* \\ -1 \\ C_m(\sigma_m^*) + \sigma_m^* \end{pmatrix} = \begin{pmatrix} m_0 & n_0 \\ p_0 & q_0 \\ -1 & 0 \\ 0 & 1 \end{pmatrix} \begin{pmatrix} 1 \\ C_m(\sigma_m^*) + \sigma_m^* \end{pmatrix} \quad \text{(A.3)}$$

with

$$\begin{pmatrix} 1 & 0 & a_0 & c_0 \\ 0 & 1 & b_0 & d_0 \end{pmatrix} \begin{pmatrix} m_0 & n_0 \\ p_0 & q_0 \\ -1 & 0 \\ 0 & 1 \end{pmatrix} = \begin{pmatrix} 0 & 0 \\ 0 & 0 \end{pmatrix} \quad \text{(A.4)}$$

from which one gets:

$$m_0 = a_0; \quad n_0 = -c_0; \quad p_0 = b_0; \quad q_0 = -d_0. \quad \text{(A.5)}$$

and replacing (A.5) into (A.2) and (A.3) and operating, one gets the solution of (6.10):

$$D_M(\sigma_M^*) = \frac{a_0 d_0 - b_0 c_0}{a_0 - c_0 \sigma_M^*} \quad \text{(A.6)}$$

$$C_M(\sigma_M^*) = \frac{b_0 - \sigma_M^*(d_0 - a_0 + c_0 \sigma_M^*)}{a_0 - c_0 \sigma_M^*} \quad \text{(A.7)}$$

$$D_m(\sigma_m^*) = \frac{a_0 d_0 - b_0 c_0}{d_0 + c_0 \sigma_m^*} \quad \text{(A.8)}$$

$$C_m(\sigma_m^*) = \frac{b_0 - \sigma_m^*(d_0 - a_0 + c_0 \sigma_m^*)}{d_0 + c_0 \sigma_m^*}. \quad \text{(A.9)}$$

where $a_0, b_0, c_0$ and $d_0$ are arbitrary constants.

Similarly, the functional equation (6.11) can be written as

$$\mathbf{A}^T\mathbf{B} = 0, \tag{A.10}$$

where

$$\mathbf{A} = \begin{pmatrix} B_M(\sigma_M^*)C_M(\sigma_M^*)\sigma_M^* - E_M(\sigma_M*)\sigma_M^* - B_M(\sigma_M^*)(\sigma_M^*)^2 \\ B_M(\sigma_M^*)C_M(\sigma_M^*) - E_M(\sigma_M^*) \\ B_M(\sigma_M^*)\sigma_M^* \\ C_M(\sigma_M^*)\sigma_M * -(\sigma_M^*)^2 \\ C_M(\sigma_M^*) \\ B_M(\sigma_M^*) \\ \sigma_M^* \\ 1 \end{pmatrix} \tag{A.11}$$

and

$$\mathbf{B} = \begin{pmatrix} 1 \\ -C_m(\sigma_m^*) - \sigma_m^* \\ C_m(\sigma_m^*) + 2\sigma_m^* \\ -B_m(\sigma_m^*) \\ B_m(\sigma_m^*)C_m(\sigma_m^*) - E_m(\sigma_m^*) + B_m(\sigma_m^*)\sigma_m^* \\ -C_m(\sigma_m^*)\sigma_m^* - (\sigma_m^*)^2 \\ -B_m(\sigma_m^*)C_m(\sigma_m^*) + E_m(\sigma_m^*) - 2B_m(\sigma_m^*)\sigma_m^* \\ B_m(\sigma_m^*)C_m(\sigma_m^*)\sigma_m^* - E_m(\sigma_m^*)\sigma_m^* + B_m(\sigma_m^*)(\sigma_m^*)^2 \end{pmatrix}. \tag{A.12}$$

To solve this functional equation, we write

$$\begin{pmatrix} B_M(\sigma_M^*)C_M(\sigma_M^*)\sigma_M^* - E_M(\sigma_M*)\sigma_M^* - B_M(\sigma_M^*)(\sigma_M^*)^2 \\ B_M(\sigma_M^*)C_M(\sigma_M^*) - E_M(\sigma_M^*) \\ B_M(\sigma_M^*)\sigma_M^* \\ C_M(\sigma_M^*)\sigma_M * -(\sigma_M^*)^2 \\ C_M(\sigma_M^*) \\ B_M(\sigma_M^*) \\ \sigma_M^* \\ 1 \end{pmatrix} = \begin{pmatrix} \alpha & \beta & \gamma & \delta \\ \epsilon & \phi & \xi & \eta \\ m_1 & n_1 & p_1 & q_1 \\ r_1 & s_1 & t_1 & u_1 \\ 1 & 0 & 0 & 0 \\ 0 & 1 & 0 & 0 \\ 0 & 0 & 1 & 0 \\ 0 & 0 & 0 & 1 \end{pmatrix} \begin{pmatrix} C_M(\sigma_M^*) \\ B_M(\sigma_M^*) \\ \sigma_M^* \\ 1 \end{pmatrix} \tag{A.13}$$

$$\begin{pmatrix} 1 \\ -C_m(\sigma_m^*) - \sigma_m^* \\ C_m(\sigma_m^*) + 2\sigma_m^* \\ -B_m(\sigma_m^*) \\ B_m(\sigma_m^*)C_m(\sigma_m^*) - E_m(\sigma_m^*) + B_m(\sigma_m^*)\sigma_m^* \\ -C_m(\sigma_m^*)\sigma_m^* - (\sigma_m^*)^2 \\ -B_m(\sigma_m^*)C_m(\sigma_m^*) + E_m(\sigma_m^*) - 2B_m(\sigma_m^*)\sigma_m^* \\ B_m(\sigma_m^*)C_m(\sigma_m^*)\sigma_m^* - E_m(\sigma_m^*)\sigma_m^* + B_m(\sigma_m^*)(\sigma_m^*)^2 \end{pmatrix} = \begin{pmatrix} 1 & 0 & 0 & 0 \\ 0 & 1 & 0 & 0 \\ 0 & 0 & 1 & 0 \\ 0 & 0 & 0 & -1 \\ a & b & c & d \\ e & f & g & h \\ m & n & p & q \\ r & s & t & u \end{pmatrix} \begin{pmatrix} 1 \\ -C_m(\sigma_m^*) - \sigma_m^* \\ C_m(\sigma_m^*) + 2\sigma_m^* \\ B_m(\sigma_m^*) \end{pmatrix} \tag{A.14}$$

with

$$\begin{pmatrix} \alpha & \epsilon & m_1 & r_1 & 1 & 0 & 0 & 0 \\ \beta & \phi & n_1 & s_1 & 0 & 1 & 0 & 0 \\ \gamma & \xi & p_1 & t_1 & 0 & 0 & 1 & 0 \\ \delta & \eta & q_1 & u_1 & 0 & 0 & 0 & 1 \end{pmatrix} \begin{pmatrix} 1 & 0 & 0 & 0 \\ 0 & 1 & 0 & 0 \\ 0 & 0 & 1 & 0 \\ 0 & 0 & 0 & -1 \\ a & b & c & d \\ e & f & g & h \\ m & n & p & q \\ r & s & t & u \end{pmatrix} = \begin{pmatrix} 0 & 0 & 0 & 0 \\ 0 & 0 & 0 & 0 \\ 0 & 0 & 0 & 0 \\ 0 & 0 & 0 & 0 \end{pmatrix} \tag{A.15}$$

from which we get:

$$a = -\alpha; \quad b = -\epsilon; \quad c = -m_1; \quad d = r_1; \quad m = -\gamma; \quad n = -\xi; \quad p = -p_1; \quad q = t_1; \tag{A.16}$$

$$e = -\beta; \quad f = -\phi; \quad g = -n_1; \quad h = s_1; \quad r = -\delta; \quad s = -\eta; \quad t = -q_1; \quad u = u_1; \tag{A.17}$$

From the fourth row of (A.13) and using $C_M(\sigma_m^*)$ from (A.7) one deduces that $B_M(\sigma_M^*)$ must be of the following form:

$$B_M(\sigma_M^*) = \frac{m_2 + n_2\sigma_M^* + p_2(\sigma_M^*)^2}{a_0 - c_0\sigma_M^*}. \tag{A.18}$$

From the first and second rows of (A.13) and using again $C_M(\sigma_m^*)$ from (A.7) one deduces that $E_M(\sigma_M^*)$ must be of the following for:

$$E_M(\sigma_M^*) = \frac{m_3 + n_3\sigma_M^* + p_3(\sigma_M^*)^2 + q_3(\sigma_M^*)^3}{(\sigma_M^* - n_1)(a_0 - c_0\sigma_M^*)^2}. \tag{A.19}$$

Similarly, from the fifth and sixth rows of (A.14) and using $C_m(\sigma_m^*)$ from (A.9) one can derive the following two expressions for $B_m(\sigma_m^*)$ and $E_m(\sigma_m^*)$, respectively:

$$B_m(\sigma_m^*) = \frac{m_4 + n_4\sigma_m^* + p_4(\sigma_m^*)^2}{d_0 + c_0\sigma_m^*} \tag{A.20}$$

$$E_m(\sigma_m^*) = \frac{m_5 + n_5\sigma_m^* + p_5(\sigma_m^*)^2}{(d_0 + c_0\sigma_m^*)^2}. \tag{A.21}$$

We note that in order to deduce that the numerator of $E_m(\sigma_m^*)$ is a second degree polynomial equation, one has also to use the seventh and eighth rows of (A.14) and compare the resulting expressions for $B_m(\sigma_m^*)$ and $E_m(\sigma_m^*)$ with those in (A.20) and (A.21).

Replacing (A.18), (A.19), (A.20) and (A.21) into (6.11) one obtains a polynomial in $\sigma_m^*$ and $\sigma_M^*$, which must be identically equal to zero, that is, all its coefficients must be null. This leads to $p_2 = 0$ and $p_4 = 0$, which replaced into (6.7) provides the model:

$$\left[\frac{\log N^* - \left[B_m(\sigma_m^*) + \frac{E_m(\sigma_m^*)}{\Delta\sigma^* - C_m(\sigma_m^*)}\right]}{\frac{D_m(\sigma_m^*)}{\Delta\sigma^* - C_m(\sigma_m^*)}}\right]^{A_m} = \left[\frac{\log N^* - \left[B_M(\sigma_M^*) + \frac{E_M(\sigma_M^*)}{\Delta\sigma^* - C_M(\sigma_M^*)}\right]}{\frac{D_M(\sigma_M^*)}{\Delta\sigma^* - C_M(\sigma_M^*)}}\right]^{A_M} = \tag{A.22}$$

$$= 1 - \exp\left\{-\left[C_0 + C_1\sigma_m^* + C_2\sigma_M^* + C_3\sigma_m^*\sigma_M^* + (C_4 + C_5\sigma_m^* + C_6\sigma_M^* + C_7\sigma_m^*\sigma_M^*)\log N^*\right]^A\right\} \tag{A.23}$$

in which the parameters have been redefined.

# Appendix B

# Specimen Characterization

## B.1 Material characterization

### B.1.1 Metallographic test

#### Standard

The metallographic test is based on the ASTM E7-03 [4]. This standard describes the aim of the test, terminology, and test procedure.

#### Procedure

Two solid rectangular specimens are necessary (dimensions $1 \times 1 \times 0.5$ cm). Furthermore, to analyze the C/S contents some grams of steel filings are necessary. The material surface is filed.

The WD-XRF test measures the wave lengths of different chemical components (in percentage). Then, to know the C/S content in the material, a IR-Detection test is made. This test defines the percentage of $CO_2$ and $SO_2$ that exists in the specimen.

#### Results: 42CrMo4

Table B.1: Result of metallographic test for the 42CrMo4 material

| Element | C | Si | Mn | S | P | Cu | Ni | Cr | Mo | Fe |
|---|---|---|---|---|---|---|---|---|---|---|
| Content | 0.40 | 0.24 | 0.76 | 0.033 | 0.012 | 0.18 | 0.11 | 1.2 | 0.23 | Rest |
| DIN 1.7225 | 0.38-0.45 | $\leq$0.40 | 0.60-0.90 | $\leq$0.035 | $\leq$0.035 | - | - | 0.90-1.20 | 0.15-0.30 | Rest |

### B.1.2 Static tests

#### Standard

The tension test is based on the ASTM EM8-08 [7]. This standard describes the aim of the test, terminology, and test procedure.

#### Procedure

Machines used for tension testing shall conform to the Practices E4 [6]. To transmit the measured force applied by the testing machine to the test specimens various types of gripping devices may

be used. To ensure axial tensile stress within the gage length, the axis of the test specimens should coincide with the center line of the heads of the testing machine. In figure B.1 some pictures of the testing machine are shown.

(a) (b) (c)

Figure B.1: Tension testing machine. (a) machine, (b) detail of specimens in the machine, (c) detail of the broken specimen.

Figure B.2 and figure B.3 present the dimensions of the specimens used in these tests for the 42CrMo4 steel and the AlMgSi1 alloy respectively.

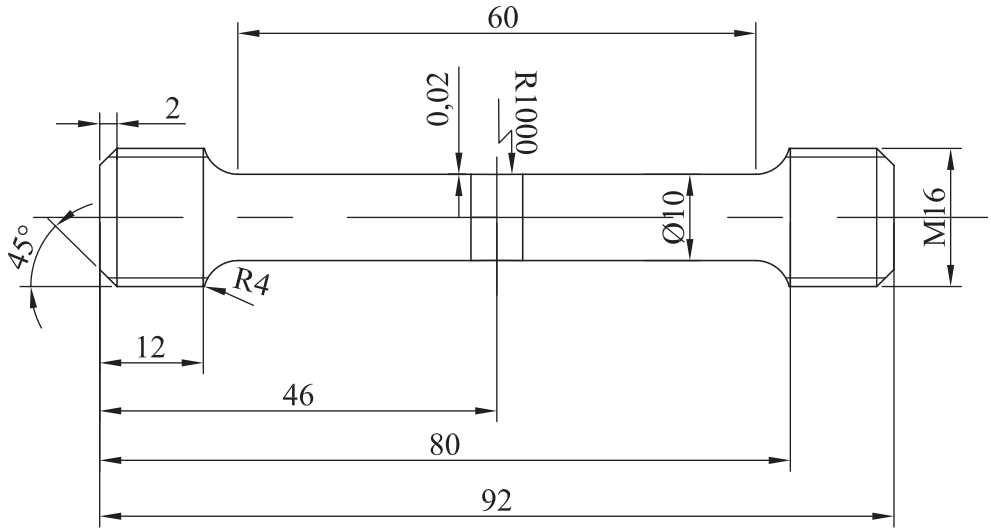


Figure B.2: Geometric definition of the tension test specimen for the 42CrMo4 steel.

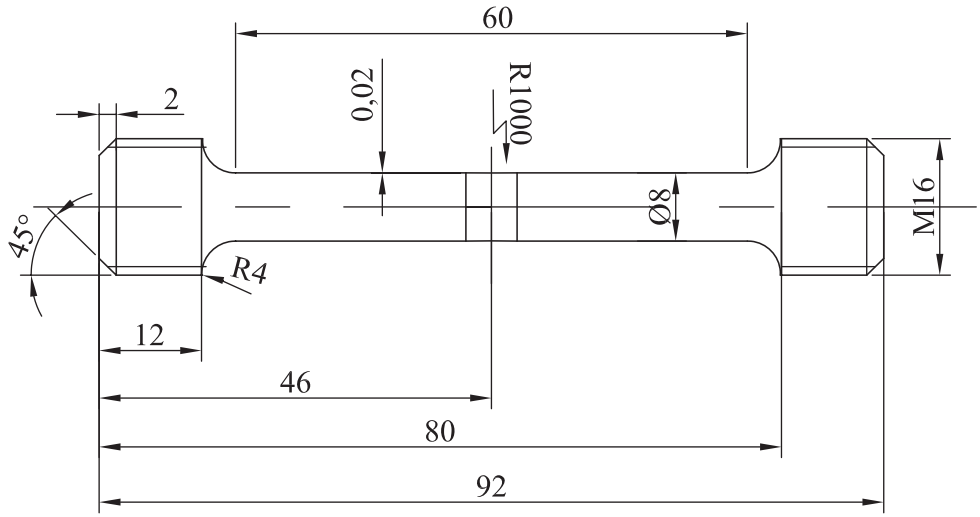


Figure B.3: Geometric definition of the tension test specimen for the AlMgSi1 alloy.

**Results**

Tables B.2 B.3 present the static parameters of the 42CrMo4 and the AlMgSi1 materials.

Figures B.4 to B.6 show the $\epsilon$–$\sigma$ curves obtained in the tension tests. Figures B.7 to B.9 show the corresponding curves for the AlMgSi1 material.

Table B.2: Static tests results for the 42CrMo4 steel.

| Nr. Test | Date | T [C] | d [mm] | Ry [MPa] | Rp0.2 [MPa] | Fm [kN] | Rm [MPa] | Ag [%] | A [%] | E modul [MPa] |
|---|---|---|---|---|---|---|---|---|---|---|
| 1 | 13/06/07 | 21.70 | 9.97 | 978.00 | 966.00 | 83.13 | 1065 | 6.00 | 14.10 | 201820 |
| 2 | 14/06/07 | 21.70 | 9.97 | 976.00 | 969.00 | 83.40 | 1068 | 6.00 | 14.00 | 206610 |
| 3 | 15/06/07 | 21.70 | 9.97 | 972.00 | 967.00 | 83.40 | 1068 | 5.90 | 14.10 | 206180 |
| | $\mu$ | 21.70 | 9.97 | 975.33 | 967.33 | 83.31 | 1067 | 5.97 | 14.13 | 204870 |
| | $\sigma^2$ | 0.00 | 0.00 | 2.16 | 1.08 | 0.11 | 1.23 | 0.04 | 0.04 | 1873.91 |

Table B.3: Static tests results for the AlMgSi1 alloy.

| Nr. Test | Date | T [C] | d [mm] | Rp0.2 [MPa] | Fm [kN] | Rm [MPa] | Ag [%] | A [%] | E modul [MPa] |
|---|---|---|---|---|---|---|---|---|---|
| 1 | 31/07/07 | 21.50 | 7.77 | 359.00 | 18416 | 388.00 | 6.00 | 10.50 | 72308 |
| 2 | 31/07/07 | 21.60 | 7.77 | 369.00 | 18789 | 396.00 | 6.00 | 10.60 | 72258 |
| 3 | 31/07/07 | 21.70 | 7.77 | 365.00 | 18557 | 391.00 | 5.80 | 10.40 | 71681 |
| | $\mu$ | 21.60 | 7.77 | 364.33 | 18587 | 391.7 | 5.93 | 10.5 | 72082.33 |
| | $\sigma^2$ | 0.07 | 0.00 | 3.56 | 1.33 | 2.86 | 0.08 | 0.07 | 246.40 |

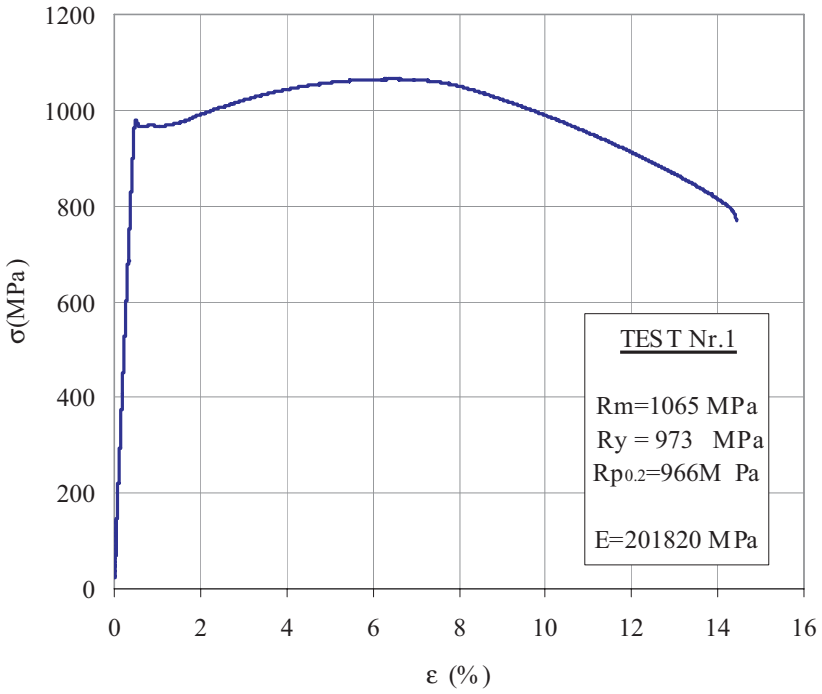


Figure B.4: Static test result for the 42CrMo4 steel. Specimen Nr. 1.

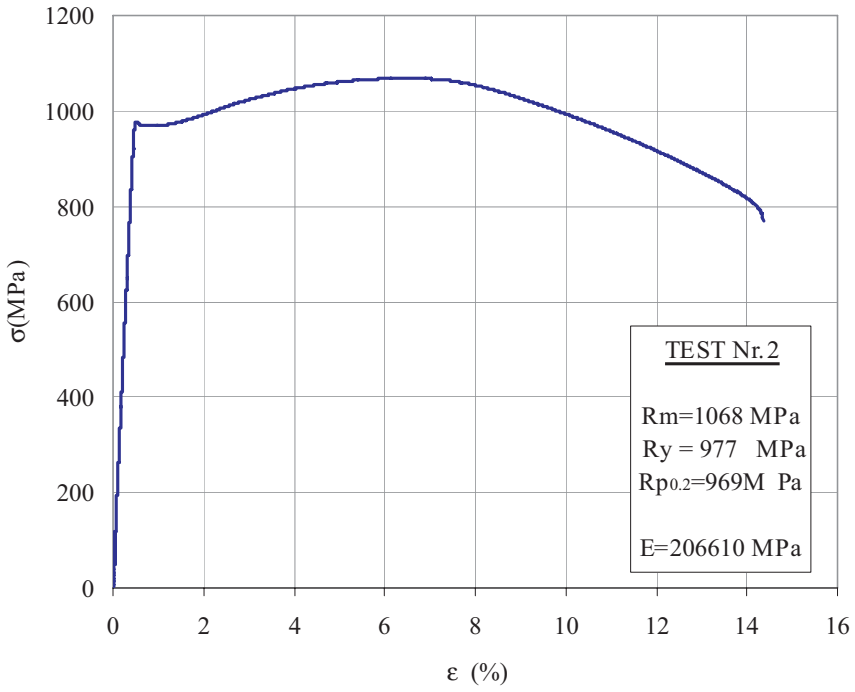


Figure B.5: Static test result for the 42CrMo4 steel. Specimen Nr. 2.

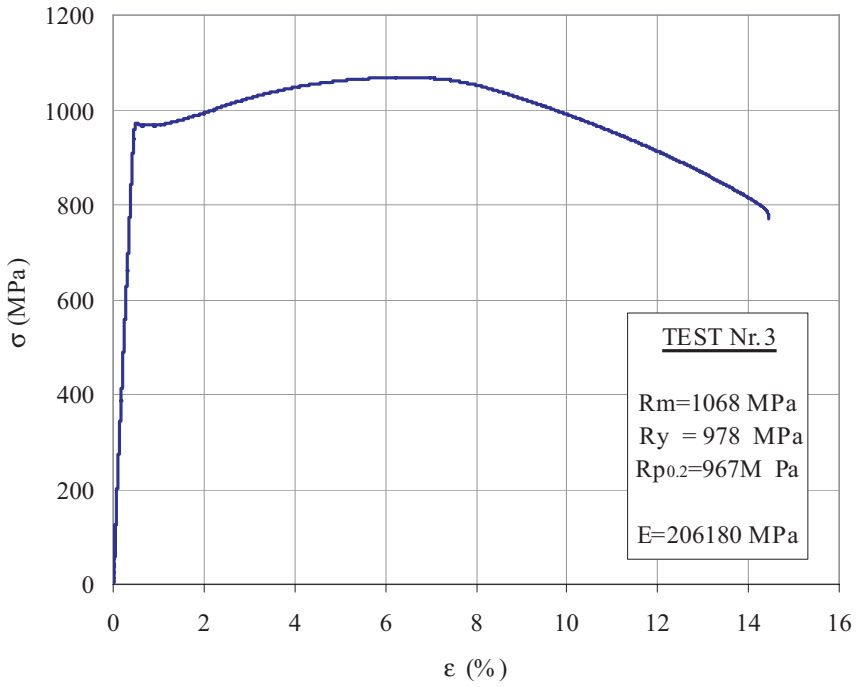


Figure B.6: Static test result for the 42CrMo4 steel. Specimen Nr. 3.

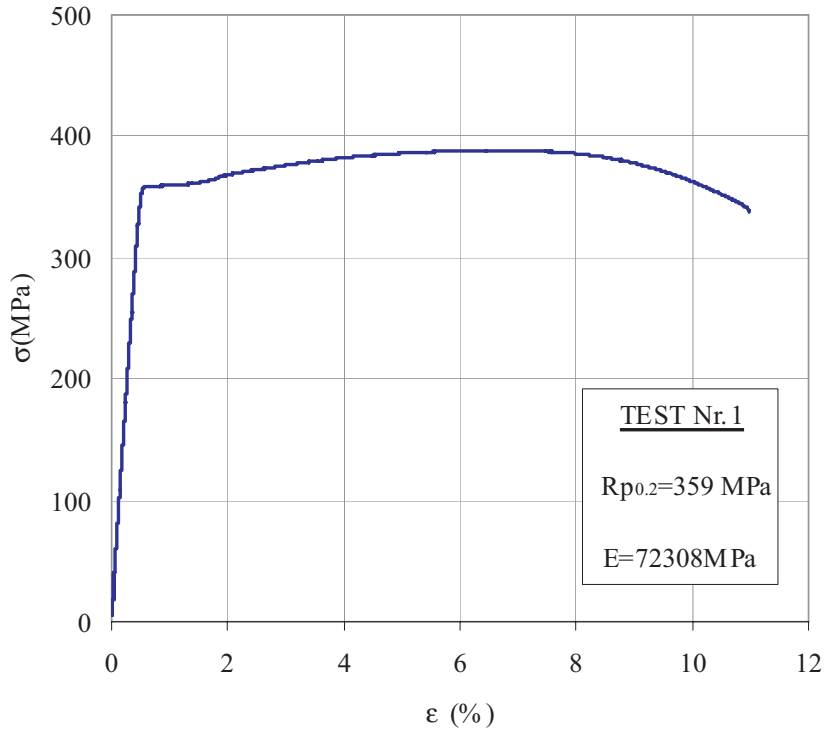


Figure B.7: Static test result for the AlMgSi1 alloy. Specimen Nr. 1.

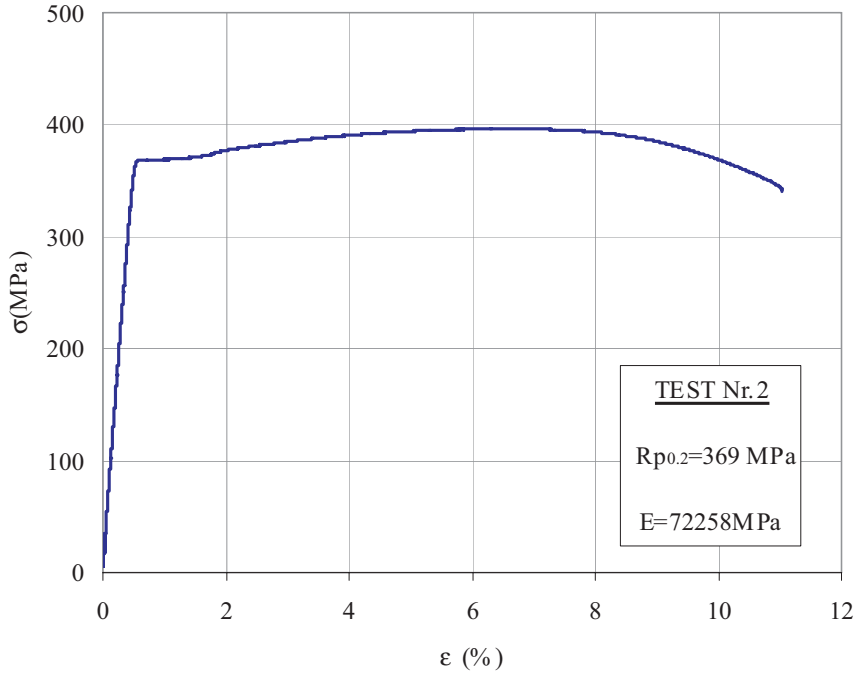


Figure B.8: Static test result for the AlMgSi1 alloy. Specimen Nr. 2.

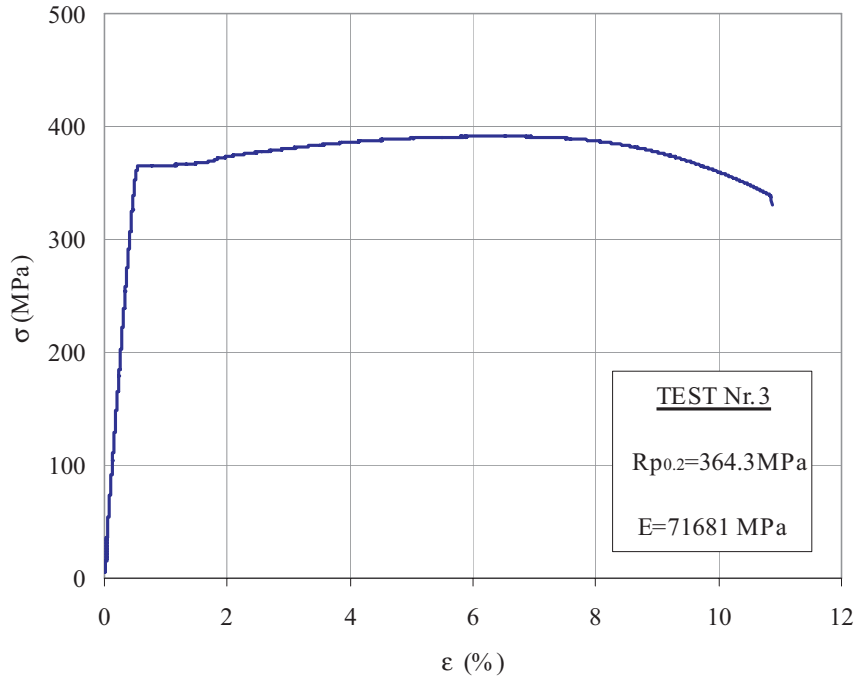


Figure B.9: Static test result for the AlMgSi1 alloy. Specimen Nr. 3.

## B.2 Geometric specimens definition

### B.2.1 42CrMo4

The geometrical specimen definition for the 42CrMo4 steel is shown in figure B.10.

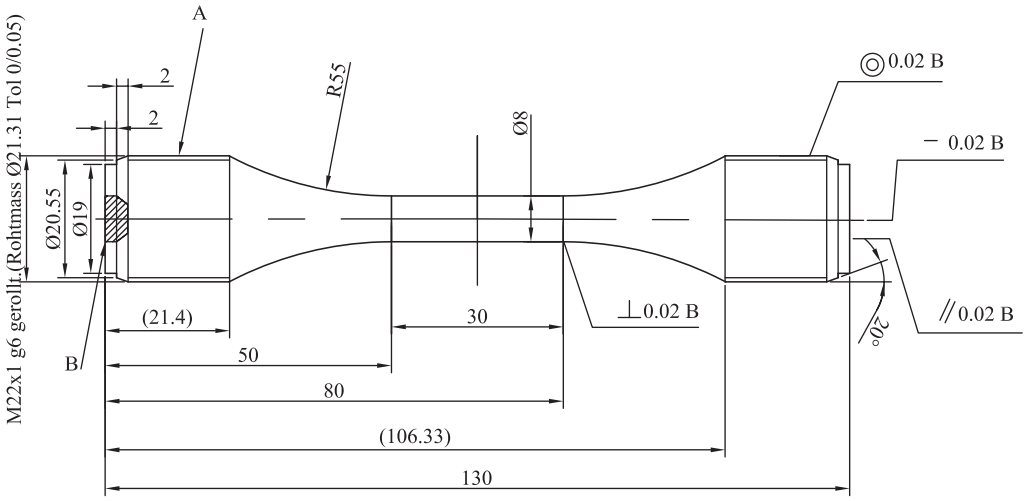


Figure B.10: Geometric fatigue test definition for the 42CrMo4 steel.

### B.2.2 AlMgSi1

The geometrical specimen definition for the AlMgSi1 alloy is shown in figure B.11.

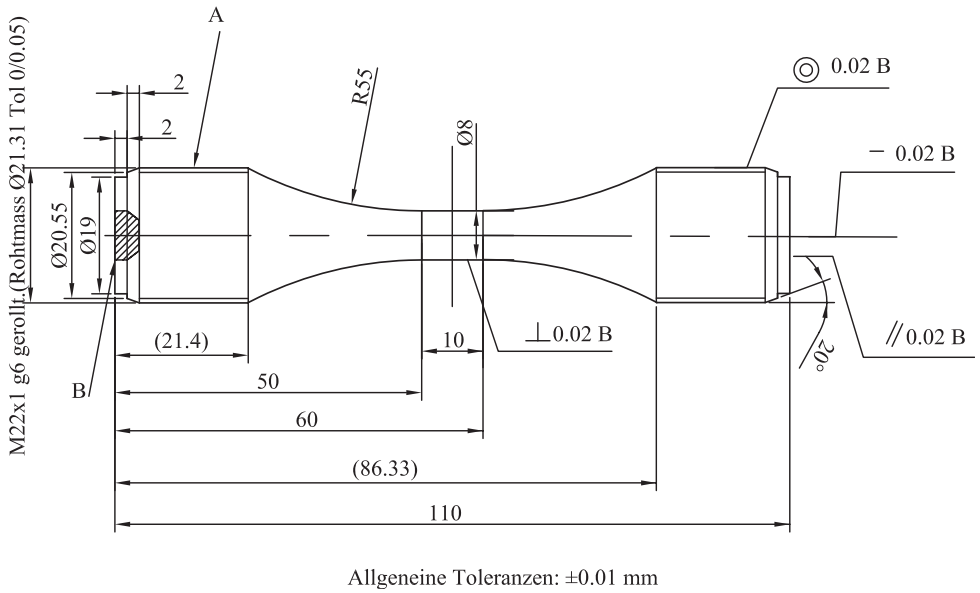


Figure B.11: Geometric fatigue test definition for the AlMgSi1 alloy.

# Appendix C

# Experimental Protocols

## C.1 Constant load tests

Next tables present the experimental protocol made in the constant load test for the materials analyzed.The table shown by different columns the number of test (Nr.), the diameter of the specimen ($\phi$), the maximum stress ($\sigma_M$), the static and dynamic force ($F_{Stat}$ and $F_{Dyn}$), the machine use, the frequency ($f$), the start and finish date and the number of cycles to failure obtained in each test point.

### C.1.1 42CrMo4 steel

Table C.1: Experimental protocol for the 42CrMo4 steel. Constant load tests

| Nr. | $\phi$ | $\sigma_M$ | $F_{Stat}$ | $F_{Dyn}$ | Machine | $f$ | *Date* | | *Cycles* |
|---|---|---|---|---|---|---|---|---|---|
| | $[mm]$ | $[MPa]$ | $[kN]$ | $[kN]$ | | $[Hz]$ | *Start* | *End* | |
| 1 | 8.00 | 955.50 | 24.46 | 23.58 | Rumul | 101.36 | 25/06/2007 | 25/06/2007 | 65277 |
| 2 | 8.00 | 955.50 | 24.90 | 23.13 | Rumul | 88.90 | 25/06/2007 | 25/06/2007 | 23700 |
| 3 | 8.00 | 955.50 | 25.41 | 22.63 | Rumul | 90.00 | 26/06/2007 | 26/06/2007 | 52700 |
| 4 | 8.00 | 955.50 | 25.97 | 22.03 | Rumul | 90.10 | 26/06/2007 | 26/06/2007 | 40900 |
| 5 | 8.00 | 955.50 | 27.03 | 21.04 | Rumul | 90.29 | 24/08/2007 | 25/08/2007 | 85900 |
| 6 | 8.00 | 955.50 | 26.75 | 21.28 | Rumul | 90.50 | 25/08/2007 | 25/08/2007 | 124300 |
| 7 | 8.00 | 955.50 | 27.14 | 20.90 | Rumul | 90.70 | 26/08/2007 | 26/08/2007 | 222900 |
| 8 | 8.00 | 955.50 | 26.51 | 21.54 | Rumul | 89.34 | 29/06/2007 | 29/06/2007 | 93500 |
| 9 | 8.01 | 877.80 | 15.80 | 28.38 | Torsion-Tension | 3.00 | 23/07/2007 | 24/07/2007 | 17281 |
| 10 | 8.01 | 877.80 | 17.33 | 26.90 | Torsion-Tension | 5.00 | 24/07/2007 | 24/07/2007 | 48787 |
| 11 | 8.00 | 877.80 | 17.66 | 26.46 | Torsion-Tension | 5.00 | 08/08/2007 | 13/08/2007 | 81244 |
| 12 | 8.00 | 877.80 | 13.01 | 31.11 | Torsion-Tension | 2.00 | 08/08/2007 | 08/08/2007 | 3373 |
| 13 | 8.01 | 877.80 | 14.41 | 29.76 | Torsion-Tension | 3.00 | 16/08/2007 | 16/08/2007 | 21812 |
| 14 | 8.01 | 877.80 | 13.72 | 30.46 | Torsion-Tension | 3.00 | 16/08/2007 | 16/08/2007 | 7265 |
| 15 | 8.00 | 877.80 | 17.85 | 26.27 | Rumul | 90.77 | 15/08/2007 | 15/08/2007 | 125800 |
| 16 | 8.00 | 780.27 | 7.05 | 32.18 | Torsion-Tension | 3.00 | 14/08/2007 | 14/08/2007 | 11439 |
| 17 | 8.00 | 780.27 | 8.61 | 30.60 | Torsion-Tension | 4.00 | 14/08/2007 | 14/08/2007 | 14973 |
| 18 | 8.00 | 780.27 | 10.19 | 29.04 | Torsion-Tension | 7.00 | 14/08/2007 | 14/08/2007 | 32055 |
| 19 | 8.00 | 780.27 | 11.76 | 27.46 | Rumul | 90.78 | 08/08/2007 | 08/08/2007 | 483000 |
| 20 | 8.00 | 780.27 | 10.97 | 28.24 | Torsion-Tension | 3.00 | 15/08/2007 | 15/08/2007 | 36708 |

| Nr. | $\phi$ | $\sigma_M$ | $F_{Stat}$ | $F_{Dyn}$ | Machine | $f$ | *Date* | | *Cycles* |
|---|---|---|---|---|---|---|---|---|---|
| | $[mm]$ | $[MPa]$ | $[kN]$ | $[kN]$ | | $[Hz]$ | *Start* | *End* | |
| 21 | 8.00 | 780.27 | 12.94 | 26.30 | Rumul | 90.82 | 15/08/2007 | 15/08/2007 | 532200 |
| 22 | 8.00 | 780.27 | 12.54 | 26.69 | Rumul | 90.74 | 14/08/2007 | 14/08/2007 | 123100 |
| 23 | 8.00 | 682.73 | 3.34 | 30.99 | Torsion-Tension | 3.00 | 30/07/2007 | 31/07/2007 | 183024 |
| 24 | 8.00 | 682.73 | 1.58 | 32.77 | Torsion-Tension | 3.00 | 31/07/2007 | 31/07/2007 | 19331 |
| 25 | 8.00 | 682.73 | 3.97 | 30.36 | Torsion-Tension | 6.00 | 13/08/2007 | 14/08/2007 | 347102 |
| 26 | 8.00 | 682.73 | 2.46 | 31.86 | Torsion-Tension | 1.00 | 15/08/2007 | 16/08/2007 | 33925 |
| 27 | 8.00 | 682.73 | 4.59 | 29.74 | Torsion-Tension | 7.00 | 14/08/2007 | 15/08/2007 | 381543 |

### C.1.2 AlMgSi1 alloy

Table C.2: Experimental protocol for the AlMgSi1 alloy. Constant load tests

| Nr. | $\phi$ | $\sigma_M$ | $F_{Stat}$ | $F_{Dyn}$ | Machine | $f$ | *Date* | | *Cycles* |
|---|---|---|---|---|---|---|---|---|---|
| | $[mm]$ | $[MPa]$ | $kN$ | $kN$ | | $[Hz]$ | *Start* | *End* | |
| 1 | 8.00 | 327.87 | 3.66 | 12.82 | Rumul | 78.02 | 17/08/2007 | 17/08/2007 | 19100 |
| 2 | 8.00 | 327.87 | 5.49 | 10.99 | Rumul | 78.90 | 17/08/2007 | 17/08/2007 | 34000 |
| 3 | 8.00 | 327.87 | 6.41 | 10.07 | Rumul | 78.27 | 26/08/2007 | 26/08/2007 | 42800 |
| 4 | 8.00 | 327.87 | 9.16 | 7.32 | Rumul | 78.23 | 25/08/2007 | 25/08/2007 | 153100 |
| 5 | 8.00 | 327.87 | 7.78 | 8.70 | Rumul | 78.21 | 27/08/2007 | 27/08/2007 | 63800 |
| 6 | 8.00 | 327.87 | 10.53 | 5.95 | Rumul | 78.29 | 27/08/2007 | 27/08/2007 | 360400 |
| 7 | 8.00 | 291.44 | 2.75 | 11.90 | Rumul | 78.20 | 17/08/2007 | 17/08/2007 | 28700 |
| 8 | 8.00 | 291.44 | 5.49 | 9.15 | Rumul | 78.27 | 27/08/2007 | 27/08/2007 | 71700 |
| 9 | 8.00 | 291.44 | 4.58 | 10.07 | Rumul | 78.26 | 20/08/2007 | 20/08/2007 | 59900 |
| 10 | 8.00 | 291.44 | 6.87 | 7.78 | Rumul | 78.25 | 27/08/2007 | 27/08/2007 | 143500 |
| 11 | 8.00 | 291.44 | 8.24 | 6.41 | Rumul | 78.12 | 27/08/2007 | 27/08/2007 | 326400 |
| 12 | 8.00 | 255.01 | 1.83 | 10.98 | Rumul | 78.35 | 20/08/2007 | 20/08/2007 | 48000 |
| 13 | 8.00 | 255.01 | 2.75 | 10.07 | Rumul | 78.19 | 06/09/2007 | 06/09/2007 | 57900 |
| 14 | 8.00 | 255.01 | 3.66 | 9.15 | Rumul | 78.40 | 20/08/2007 | 20/08/2007 | 113100 |
| 15 | 8.00 | 255.01 | 5.95 | 6.86 | Rumul | 78.33 | 11/09/2007 | 11/09/2007 | 348300 |
| 16 | 8.00 | 255.01 | 4.81 | 8.01 | Rumul | 78.35 | 11/09/2007 | 11/09/2007 | 172500 |
| 17 | 8.00 | 218.58 | -1.58 | 12.57 | Rumul | 78.28 | 12/09/2007 | 12/09/2007 | 37100 |
| 18 | 8.00 | 218.58 | -0.70 | 11.68 | Rumul | 78.30 | 12/09/2007 | 12/09/2007 | 54400 |
| 19 | 8.00 | 218.58 | 0.18 | 10.81 | Rumul | 78.23 | 12/09/2007 | 12/09/2007 | 80300 |
| 20 | 8.00 | 218.58 | 1.06 | 9.92 | Rumul | 78.33 | 13/09/2007 | 13/09/2007 | 96300 |
| 21 | 8.00 | 218.58 | 1.94 | 9.06 | Rumul | 78.42 | 13/09/2007 | 13/09/2007 | 175500 |
| 22 | 8.00 | 218.58 | 2.82 | 8.17 | Rumul | 78.44 | 13/09/2007 | 13/09/2007 | 172800 |
| 23 | 8.00 | 218.58 | 3.70 | 7.29 | Rumul | 78.42 | 13/09/2007 | 13/09/2007 | 526500 |

# Appendix D

# SISIFO program

## D.1 Introduction

This appendix summarizes the work done by the author during her stay at the Empa Reseach Institute.

The principal objectives are:

1. Solve the problem by using different programs to first estimate the model parameters and, then, extend the analysis of different situations that appear in the daily practice of fatigue of materials.

2. Develop a compiler tool (Matlab) for the new fatigue model together with an a user interface (SISIFO) to facilitate the use of the program.

3. Present the different parts of the program and explaining the objectives of each one.

4. Describe all the components of the program.

5. Show by means of simple examples how the program works.

The report is organized as follows:

1. The fatigue model considerations are presented in section D.2 together with the required background and how the problem can be solved.

2. In section D.3 the program (SISIFO) is presented. Different sections and subsections describe its components and the steps needed to use it.

3. Section D.4 describes a general example of application in order to facilitate the understanding of the complete process of the parameter estimation and the damage analysis.

## D.2 Background of SISIFO program: the new fatigue Castillo's model

In this section the most important considerations related to program codes, and the main simplifications made are described.

### D.2.1 Simplification of Castillo's model

In this work one of the submodels presented in section 6.5.6 is implemented as a computer program. This model depends on 4 parameters ($C_0$, $C_1$, $C_2$ and $C_5$), the rest of parameters are assumed null, that is, $C_3 = C_4 = C_7 = 0$ and $C_6 = -C_5$. The final expression of the model is:

$$p = 1 - \exp\left\{-\exp\left[C_0 + C_1\sigma_m^* + C_2\sigma_M^* - (C_5(\sigma_M^* - \sigma_m^*))\log N^*\right]\right\}, \tag{D.1}$$

where $p = F(N^*; \sigma_m^*, \sigma_M^*)$, which supplies a complete probabilistic information for any Wöhler curves of the material related to whichever given stress level.

Finally, the restrictions of this submodel stated in Equation (6.13) are:

$$\begin{aligned} C_0 &\leq 0; \\ C_5 &\leq 0; \\ \min(\log N^*) &\geq -C_1/C_5; \\ \min(\log N^*) &\geq C_2/C_5; \end{aligned} \tag{D.2}$$

### D.2.2 Parameter estimation

The parameter estimation of the model was given in section 6.6, and the program is prepared to estimate the parameter by two methods (maximum likelihood and least–squares).

### D.2.3 Validation of the model

The methods used to validate the model were shown in section 7.7.

### D.2.4 Damage accumulation

The damage accumulation is based on the methodology presented in section 8.3.1.

## D.3 Progam SISIFO

### D.3.1 Introduction and general organization

The interface *SISIFO* has been created to solve the problems of estimation and analysis of the new fatigue model defined and described by Castillo et al. [40]. The principal objective of the program is to reproduce all the necessary steps (described in section 6.7) for the complete analysis of a material subjected to a certain load history. Other secondary objectives of the program are:

1. Provide the necessary information for the correct use of the different components in the program, such as type of data, files, etc.
2. Work with data series from experimental tests. Make the normalization of data following strategy described in chapter 6.
3. Estimate the model parameters, characteristic of each material.
4. Validate the model resulting after the estimation process.
5. Obtain the S–N curves and the P–S–N curves.

6. Define the method of extrapolation to other load conditions.

7. Analyze the damage accumulation of a specimen subject to a non constant load history.

8. Perform the rainflow analysis and filtering of the rainflow matrix depending on the endurance limit of the material.

*SISIFO* has been created using the *GUIDE* tool of the *MATLAB* program. *GUIDE* (Graphical User Interface Development Environment) is a set of tools that can extend all the options of *MATLAB*, designing easily interfaces (*GUIs*). A *GUI* is a graphical user interface that contains components, that enable a user to perform interactive tasks. *SISIFO* is a set of menus, toolbars, push buttons, radio buttons, pop-up menus etc, in which additional plots are displayed easily.

The first screen of SISIFO represents the start of the process. The program is divided in two basic parts: parameter estimation and damage analysis (see figure D.1 and figure D.2). The parameter estimation menu permits the user to analyze series of experimental data and estimate the set of parameters of the Castillo model. Furthermore the user can plot the S–N curves, the P–S–N curves, validate the model and extrapolate the problem to other load conditions. The second part of the program permits defining a load history (given by the user) and analyzes the damage accumulation of this load history. In addition a rainflow analysis can be performed.

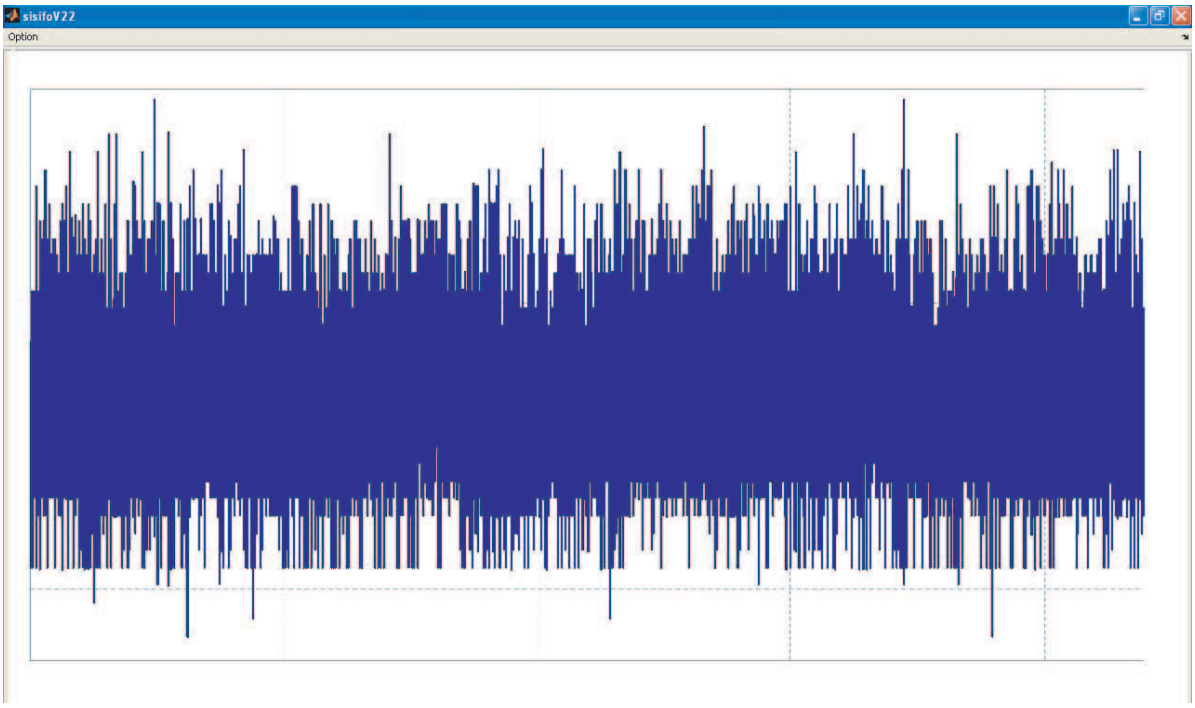


Figure D.1: Start screen of the SISIFO program.

The methodology of work is presented in figure D.3 where the steps mentioned in section 6.7 are represented.

The chapter is organized in two sections and diverse subsections in which all the components of the program are described. In section D.4 some examples of application will be explained.

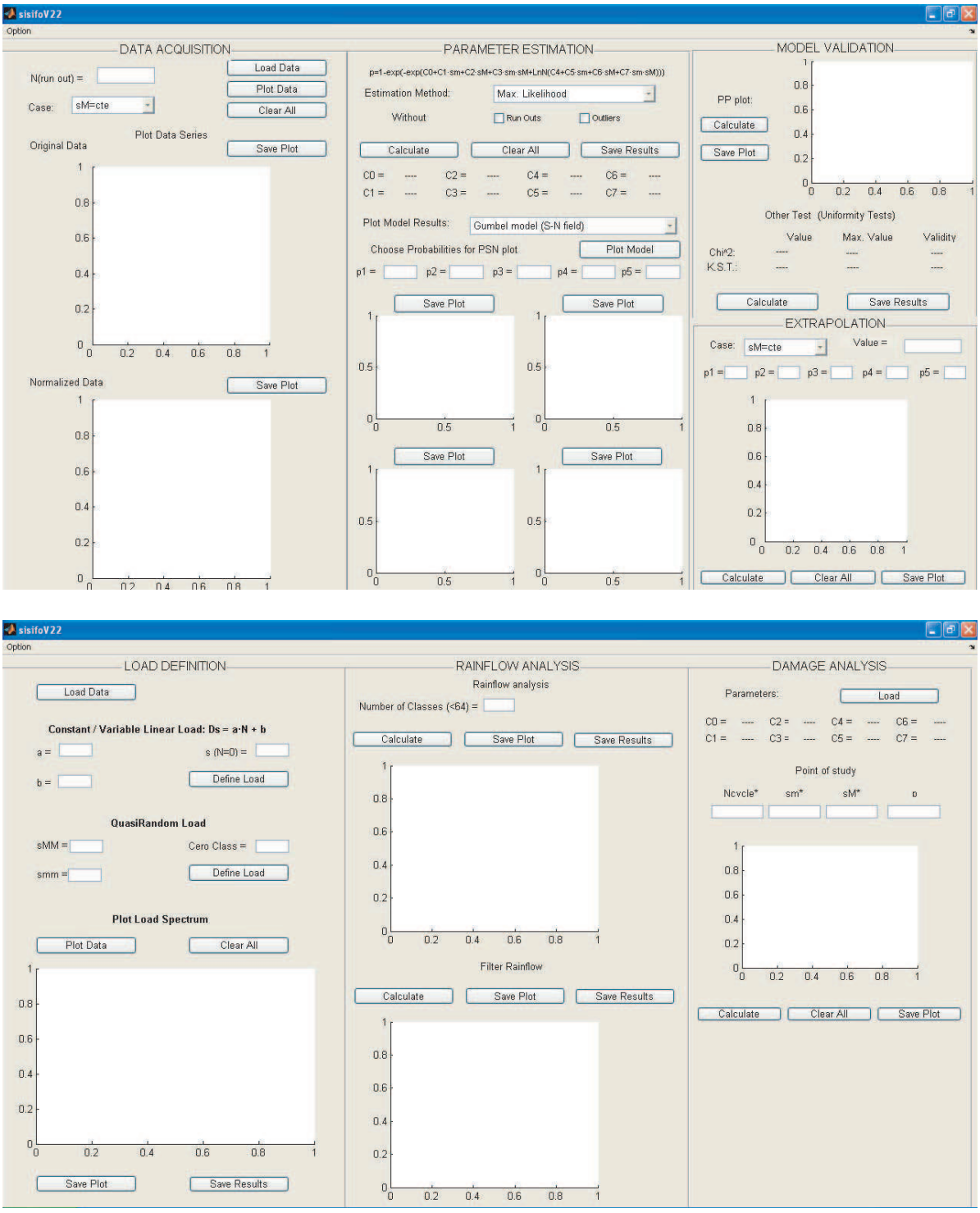


Figure D.2: Main windows of the program: the parameter estimation window (top figure) and the damage analysis window (bottom figure).

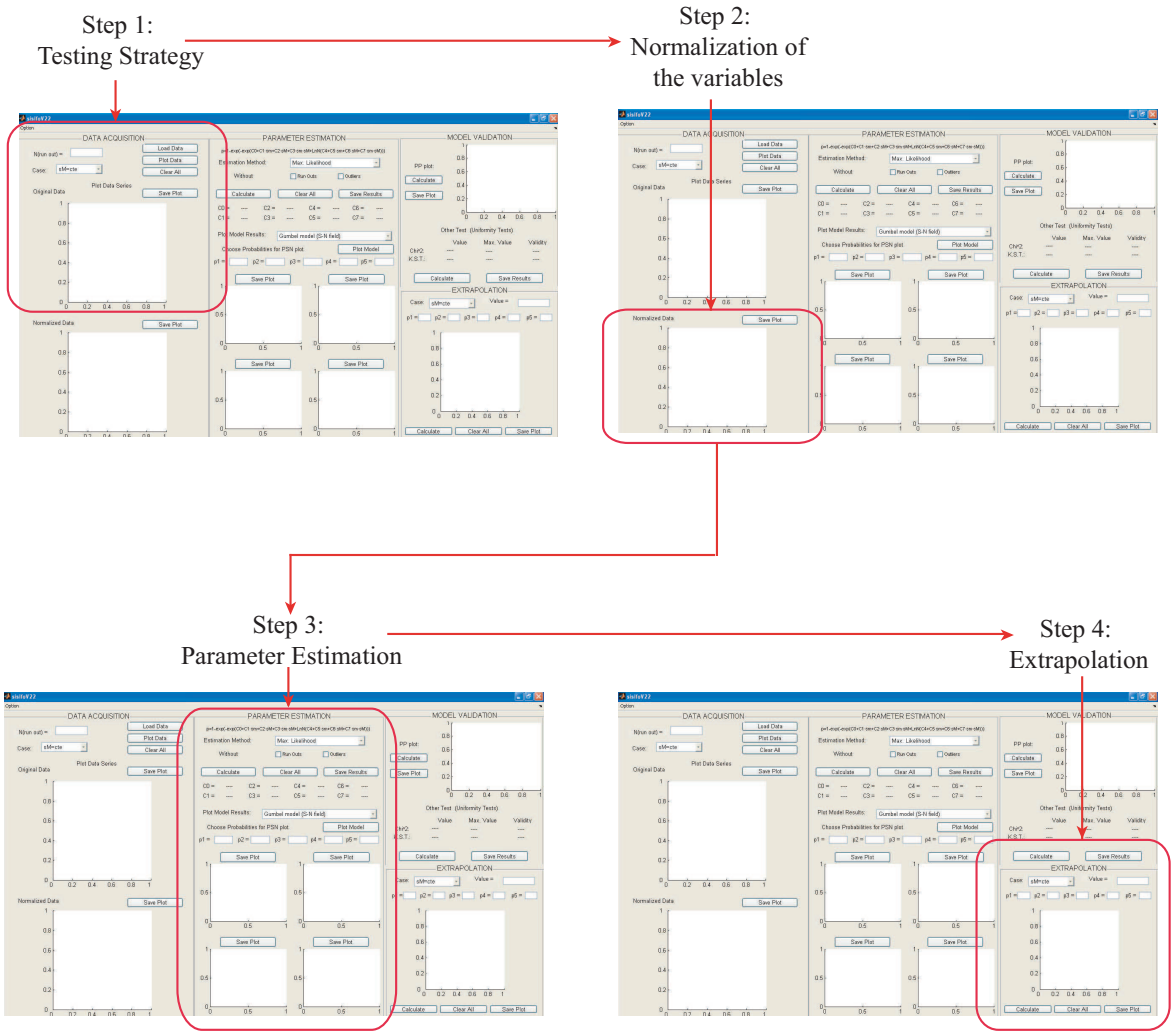


Figure D.3: Representation of the different steps to use the Castillo model in the SISIFO program.

### D.3.2 Program installation

For the use of the SISIFO program no installation process is necessary, because the executable file called *sisifoV22.exe* can be directly used.

If MATLAB is not installed, we need to install a MATLAB component called *mcrInstaller.exe*. The steps to be followed are:

1. Install the file called *mcrInstaller.exe* from the program CD. With this installation the computer is prepared to execute MATLAB codes. For the complete installation the user must follow the steps described in figures D.4 and D.5.

2. Execute the file *sisifoV22.exe*.

3. Use the program.

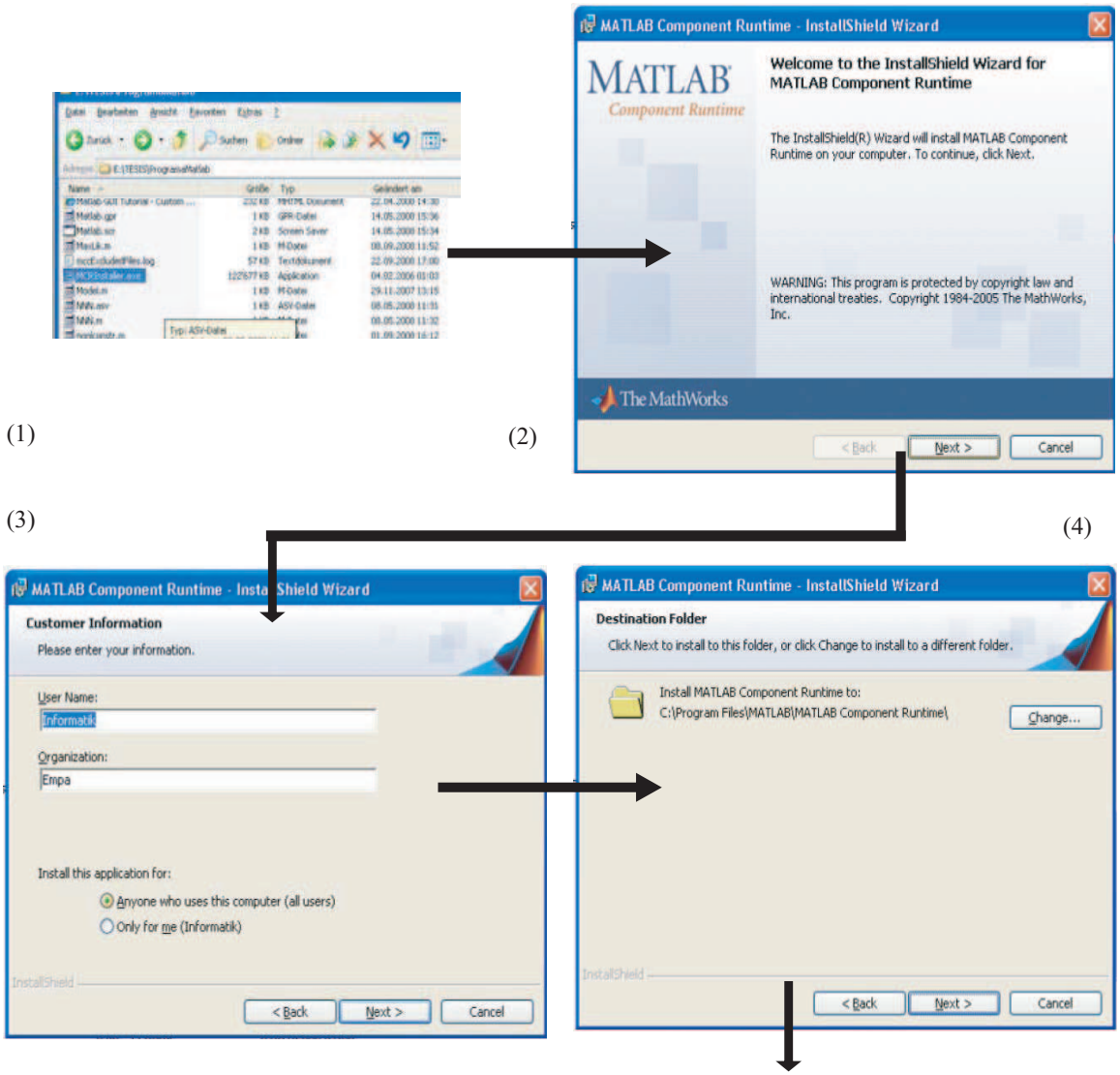


Figure D.4: Representation of the different steps to be followed for the installation of the SISIFO program. Steps 1 to 4.

### D.3.3 Menu 1: parameter estimation

In this section the parameter estimation menu is described. To access this part of the program, the option *Parameter estimation* has to be chosen from the *Option* menu (see figure D.6).

The parameter estimation window is formed by four panels: Data acquisition, Parameter estimation, Model validation and Extrapolation (see figure D.7).

#### Data acquisition

The objective of this panel is to load data from experimental tests and prepare them for the Parameter estimation in the next panel. The homogenization of the data is also realized inside this panel.

The methodology is the following:

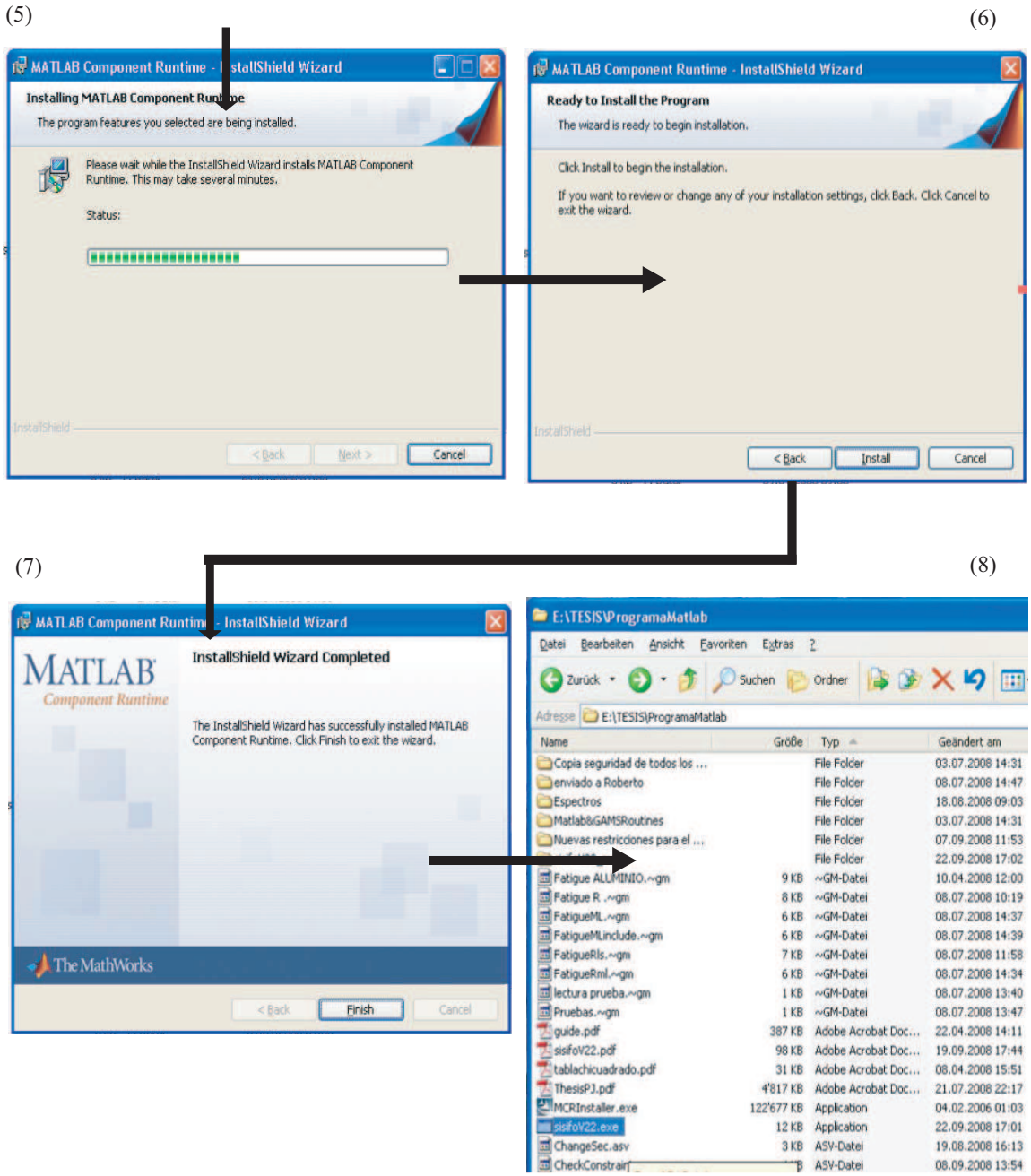


Figure D.5: Representation of the different steps to be followed for the installation of the SISIFO program. Steps 5 to 8.

1. Define the maximum number of cycles $N_{RunOut}$.
2. Choose the testing conditions case ($\sigma_M = cte$, $R = cte$).
3. Load data from an external file.
4. Plot data and homogenize data.

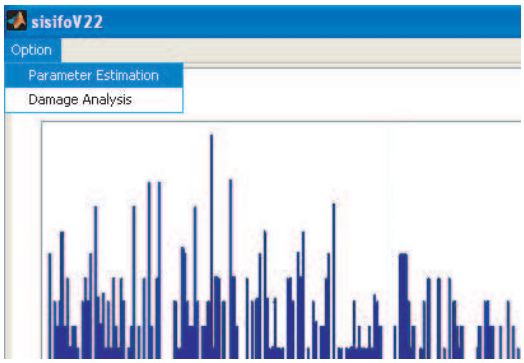


Figure D.6: Entering the Parameter estimation menu of SISIFO.

If the user specifies an incorrect number of cycles, i.e. with ortographic mistakes, a screen with an error dialog box will appear, informing about this error and how to solve it. One example is shown in figure D.8.

There are two different cases of test conditions that SISIFO is able to analyze: test with $\sigma_M = cte$ or test with $R = cte$, where $\sigma_M$ is the maximum stress and $R$ is the stress ratio, defined as $R = \sigma_m/\sigma_M$. The user can choose the corresponding option from the pop-up menu (see figure D.9).

The data to be analyzed is read by the program by using the button *Load Data* (see figure D.10). The data file is an excel file .xls. The structure of this file is shown in figure D.11:

- *First column:* Number of cycles $N$. It represents the abscissas of the S–N curve.
- *Second column:* $\Delta\sigma$ in the case of $\sigma_M = cte$ or $\sigma_M$ in the case of $R = cte$. It represents the ordenate of the S–N curves.
- *Third column:* The constant value chosen in the pop-up menu ($\sigma_M$ or $R$).
- *Fourth column:* Outliers are defined by a value of 1.

Before plotting data, the user has to specify the different data labels such as the name of the data set and axes (a panel will appear on the screen after loading of the data file). In this panel the following information appears (see figure D.12):

- Number of data sets: a real number. A maximum of four data set is permitted. Normally three or four sets are recommended.
- Label of each data sets.
- Axes information, the label of each axis.

  If the user wants to enter a Greek symbol, i.e. $\sigma, \Delta\sigma$, MATLAB is prepared to accept LaTeX code. In table D.1 some of the most useful codes are presented:

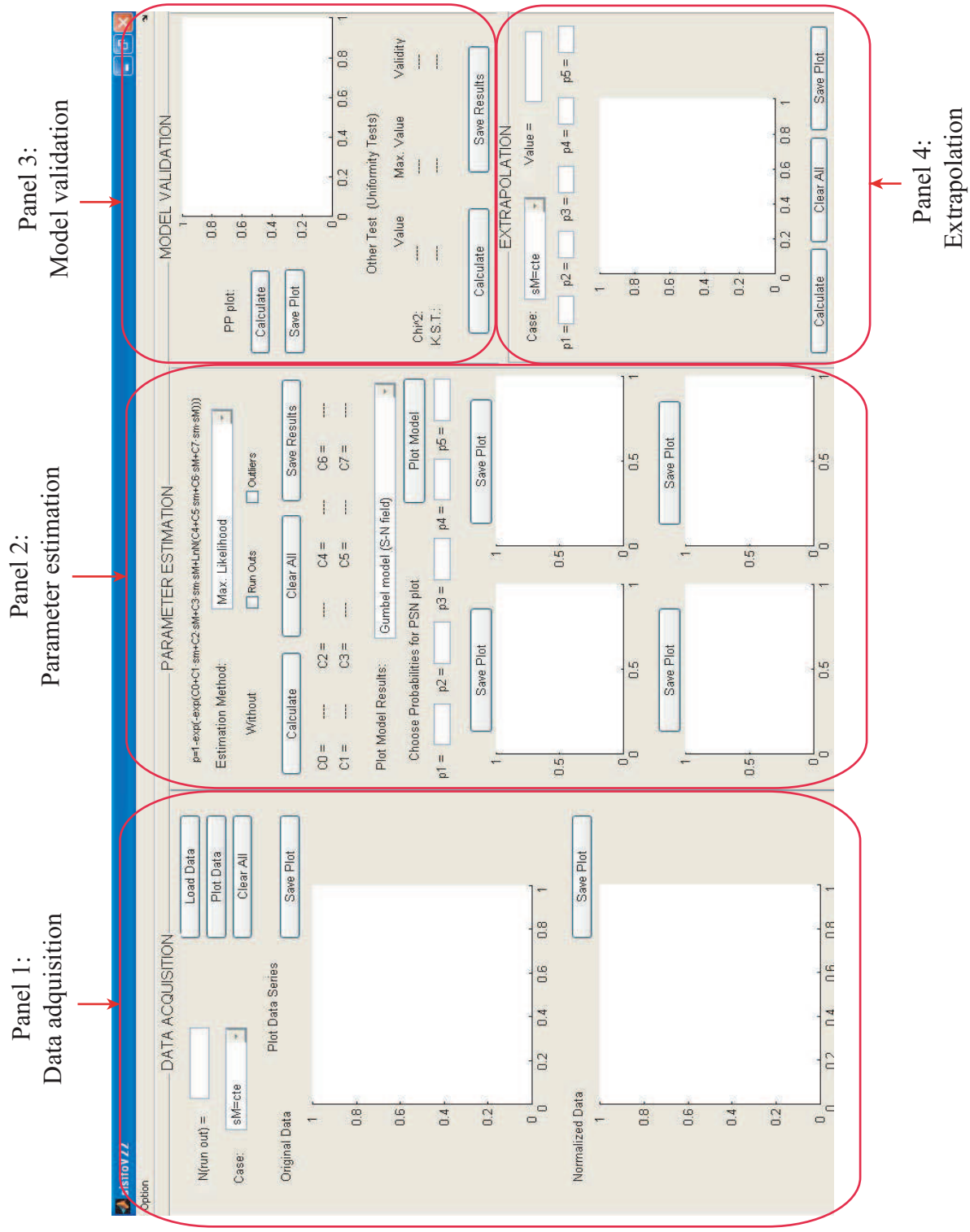


Figure D.7: Panels that form the Parameter estimation window of SISIFO.

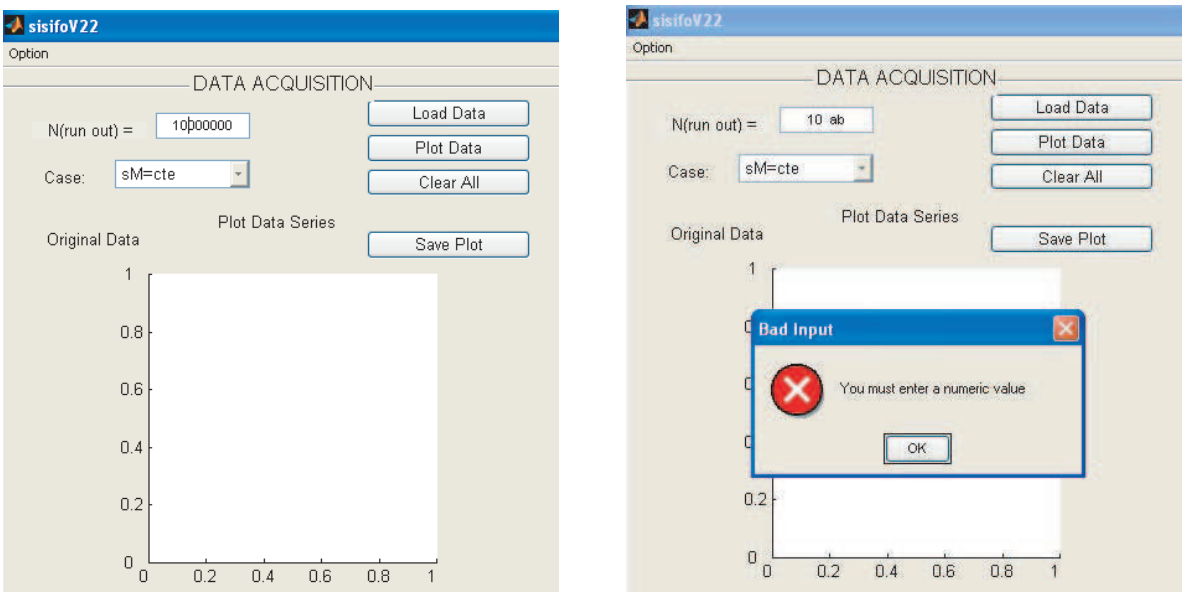


Figure D.8: Definition of the maximum number of cycles (run outs). Left side, a correct definition; right side, bad input.

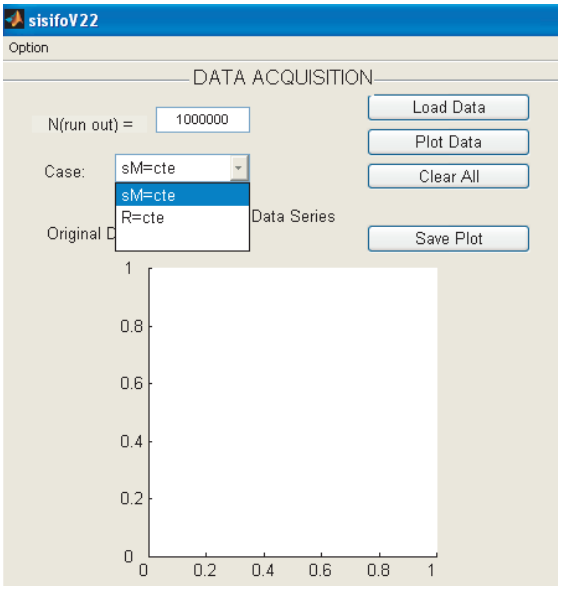


Figure D.9: Example of the testing option chosen by the user for the data analysis.

Table D.1: Useful symbols in MATLAB code.

| Symbol | Code | Symbol | Code |
|---|---|---|---|
| $\sigma$ | $\backslash sigma$ | $\Delta\sigma$ | $\backslash Delta \backslash sigma$ |
| $a_b$ (subindex) | a_b | $a^b$ (superindex) | a$\hat{}$b |
| $\log N$ | $\backslash log$ N | $\exp a$ | $\backslash$ exp a |

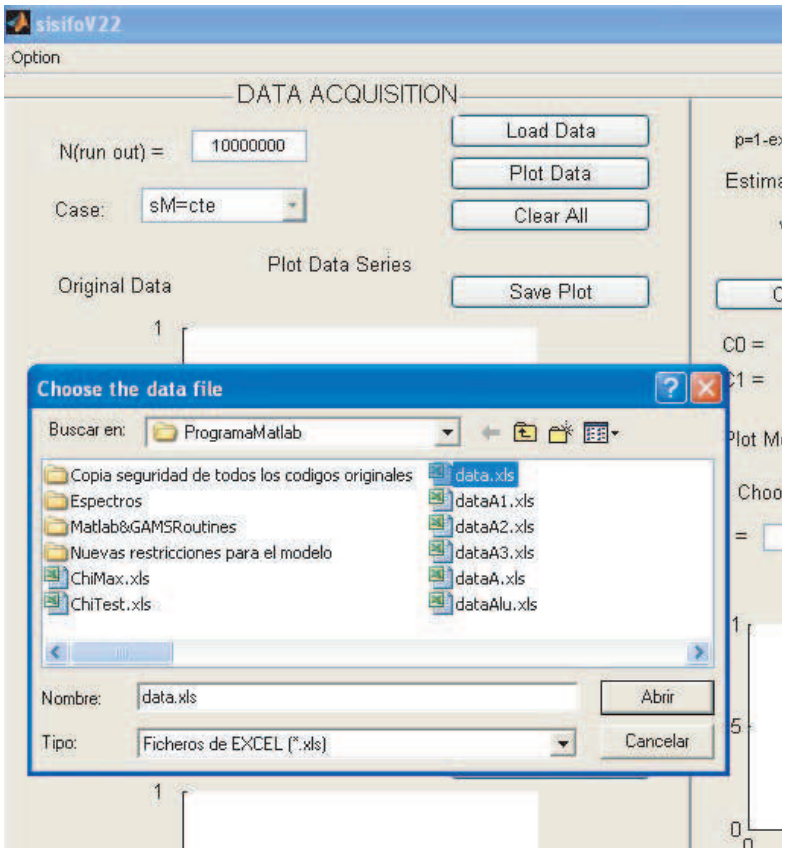


Figure D.10: Example for loading data.

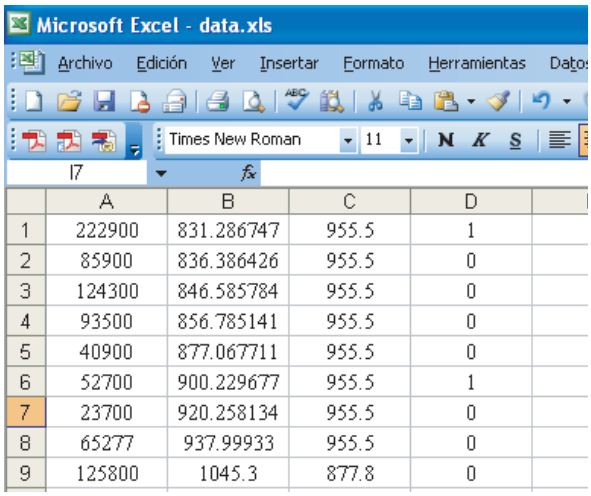


| | A | B | C | D |
|---|---|---|---|---|
| 1 | 222900 | 831.286747 | 955.5 | 1 |
| 2 | 85900 | 836.386426 | 955.5 | 0 |
| 3 | 124300 | 846.585784 | 955.5 | 0 |
| 4 | 93500 | 856.785141 | 955.5 | 0 |
| 5 | 40900 | 877.067711 | 955.5 | 0 |
| 6 | 52700 | 900.229677 | 955.5 | 1 |
| 7 | 23700 | 920.258134 | 955.5 | 0 |
| 8 | 65277 | 937.99933 | 955.5 | 0 |
| 9 | 125800 | 1045.3 | 877.8 | 0 |

Figure D.11: Example of data file.

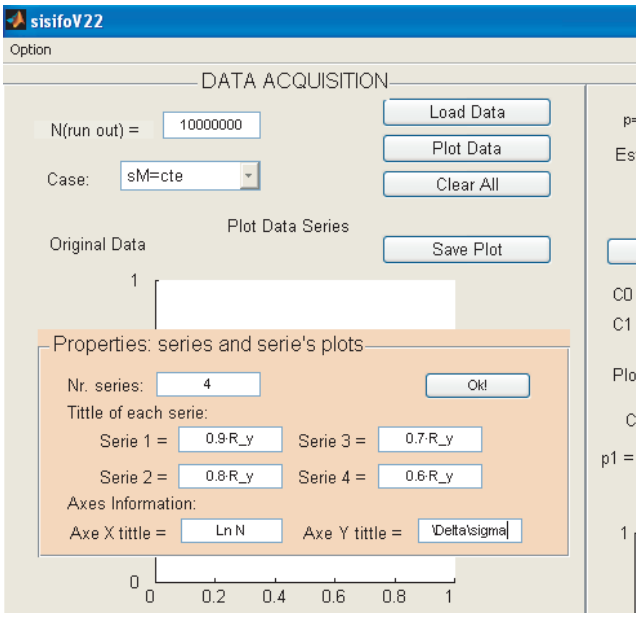


Figure D.12: Definition of the data sets labels.

The data sets are plotted on two different charts: first without normalization (see figure D.13). For the normalization process SISIFO uses by default $N_0 = 1$ and $\sigma_0 = 1000$ MPa.

There are other two different buttons in this panel: *Clear all* and *Save Plot*. The first is used to clear all the data and the plots, useful when the user wants to change the data at the beginning of the parameter estimation process. The second is used to save the plot, in this case a new window will appear on the screen, in which the user can choose different options, such as change the symbol of the series, the colour, name, etc (see figure D.14).

### Parameter estimation

The objective of this panel is to estimate the parameters of the model. To this end the Castillo fatigue model is used [40]. For the estimation process SISIFO uses the normalizated data in the previous panel.

The steps to use this panel are:

1. Choose the estimation method. The user can choose between "maximum likelihood" or "least-squares regression".

2. Choose the data to be used with or without run-outs and with or without outliers.

3. Estimate the parameters. The user can choose some estimation methods.

4. Plot the results. The user can choose from two different plot options: S–N curves or P–S–N curves.

The estimation methods were presented in section 6.6: maximum likelihood (section 6.6.1) and least-squares (section 6.6.2). The user may choose the method in the pop-up menu (see figure D.15).

The user can estimate the parameters of the model for different cases (see figure D.16). The differences between these cases refer to the existence of run-outs or outliers. If the user checks the

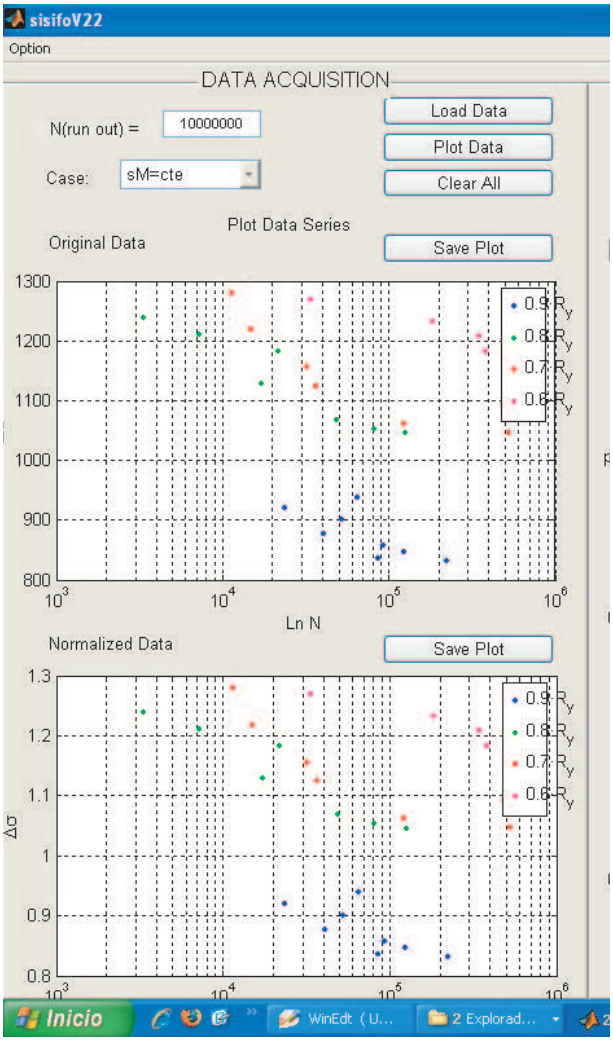


Figure D.13: The two plots obtained with SISIFO: upper figure, plot of the initial data, and lower figure, plot of the normalized data.

*Without run-out* or *Without outliers* check boxes, the program modifies the data sets deleting the corresponding, run-out and outlier data respectively. Furthermore, when one of these check boxes is selected, the data plot of the first panel changes and shows the data selected for the estimation.

The data filter works in two different ways: in the case that the user chooses estimation without run-outs, the program reviews all the test data and deletes data in which the number of cycles to failure is larger than $N_0$ defined in the first panel; if the user chooses estimation without outliers, the program analyzes the fourth column of the data file, if the value in the cell is equal to one, an outlier is defined and the program deletes this row for the parameter estimation.

When the user presses the button *Calculate* a new window appears on the screen of SISIFO (see figure D.17). In this window some estimation options may be selected:

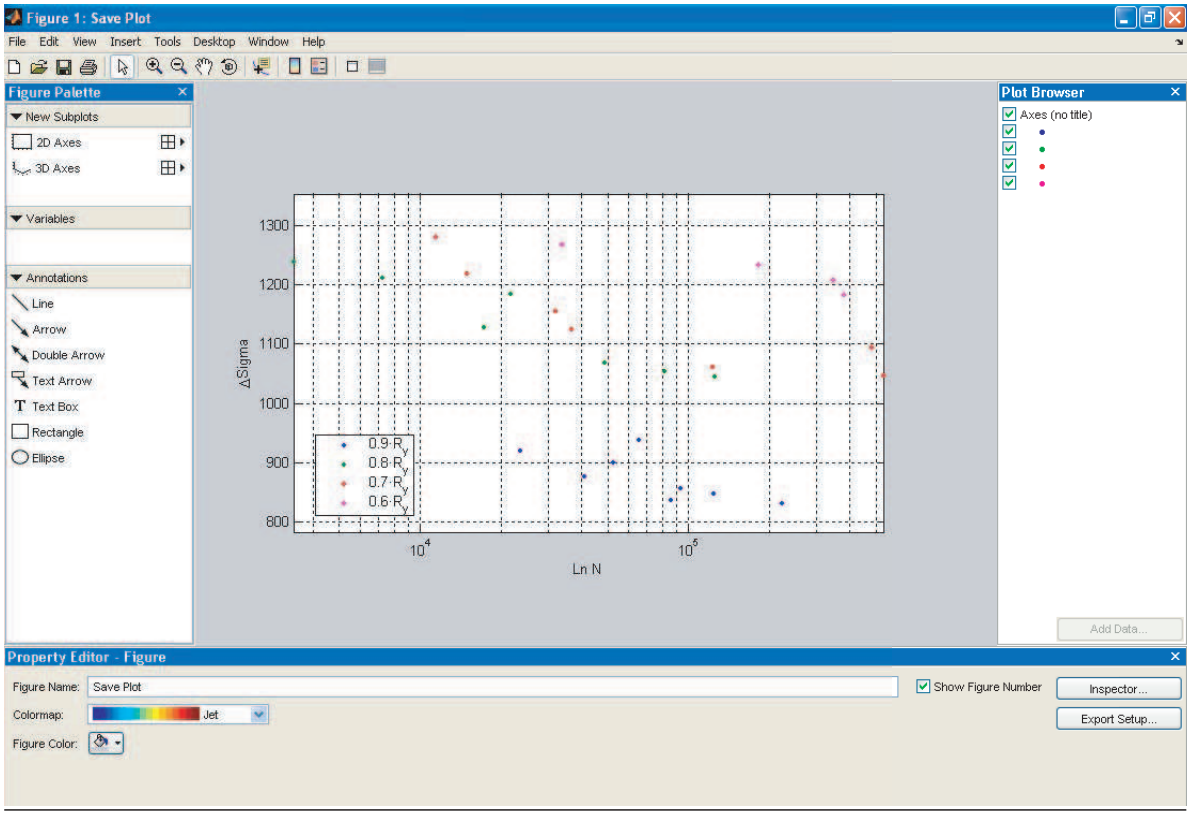


Figure D.14: Plot options in the Save plot window.

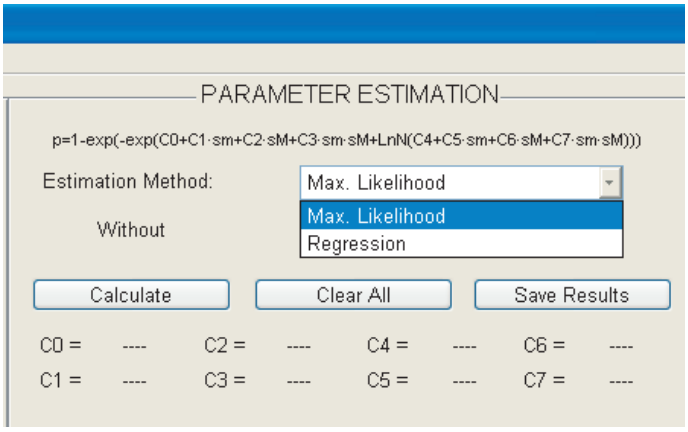


Figure D.15: Parameter estimation methods represented in the corresponding pop-up menu in SISIFO.

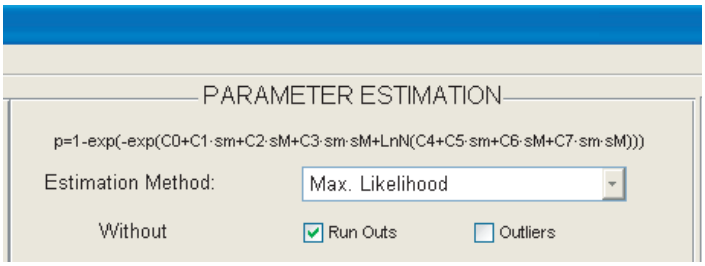


Figure D.16: SISIFO Check boxes to choose the final data for the parameter estimation, with or without run-outs and/or outliers.

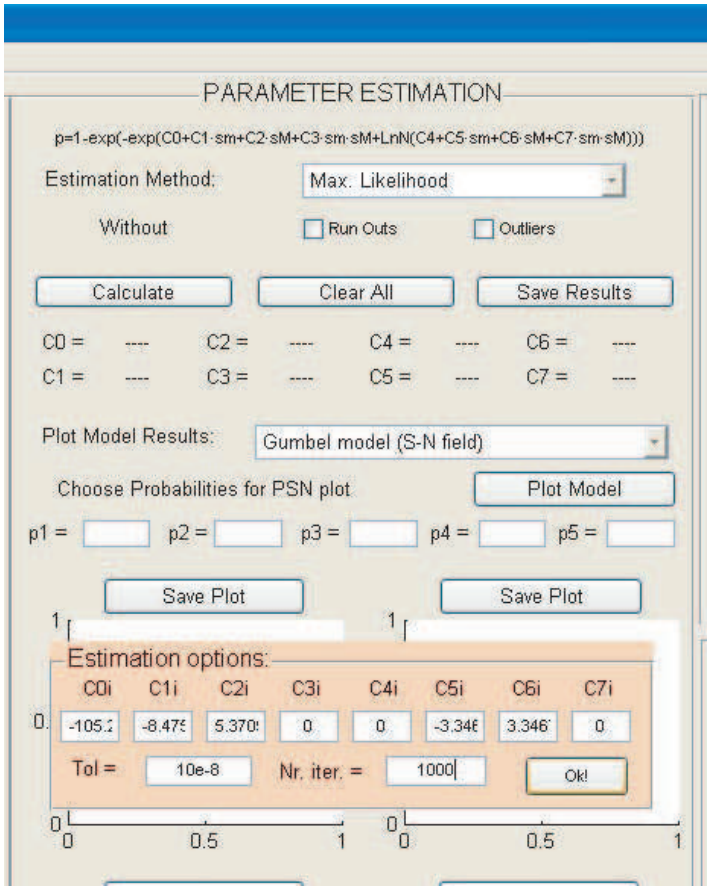


Figure D.17: Definition of the parameter estimation options.

- *Initial parameters, $x_0$:* It is necessary to define a set of initial parameters for the MATLAB estimations (always a local optimum). With these parameters the program tries to obtain the best estimates. These initial parameters must satisfy the constraints of the model (defined in section 6.4). If these initial parameters don't satisfy the constraints, a dialog box will appear on the screen indicating us the problem (see figure D.18).

- *Tolerance, $Tol$:* The user has the option of increasing the tolerance value of the parameter estimation algorithm. In the case that the user doesn't specify a value, SISIFO chooses a default value of $Tol = 10^{-4}$.

- *Number of iterations, $Nr.iter$:* The user has the option of increasing the maximum number of iterations to be used in the optimization process. In the case that the user doesn't specify as value, the program chooses a default value $Nr.Iter = 400$.

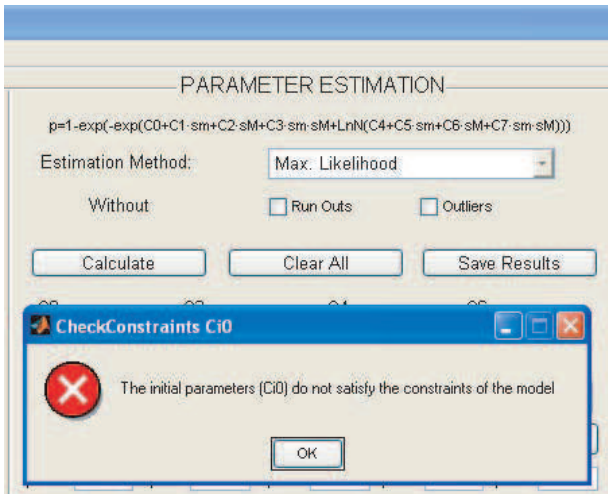


Figure D.18: Dialog box: Error on initial parameters.

If the calculated parameters don't satisfy the constraints of the model, a screen similar to figure D.18 will appear indicating us the problem, otherwise the resulting parameters will appear on this panel (see figure D.19).

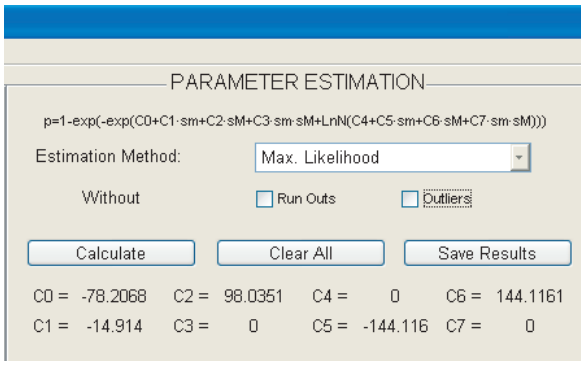


Figure D.19: Parameters calculated by the SISIFO program.

The results can be plotted in two different ways: the S–N curves or the P–S–N curves. The user has to choose the type of graphic in the pop-up menu shown in figure D.20.

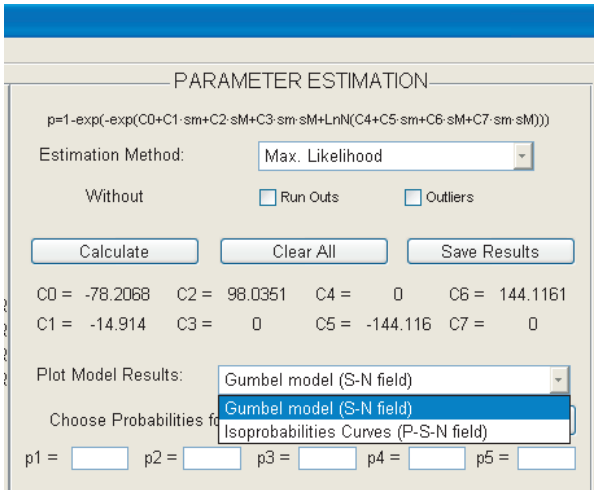


Figure D.20: Different plot options of the estimation results.

In both cases, having chosen one option, a new window will appear (see figure D.21). In this window the user defines the ranges of the plots. If the probability stress field plot (P–S–N field) is chosen, the user may specify the different probabilities (between zero and one $\in [0, 1]$). These will appear in the graphic (see figure D.22). Note that the program is prepared for the analysis and estimation of a maximum of four different sets of data. In order to display the results the user needs to press the *Plot Model* button.

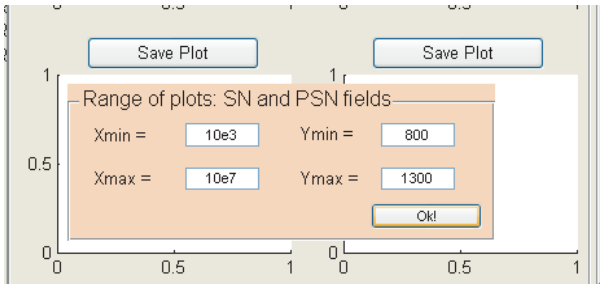


Figure D.21: Plot ranges of the chart.

One example of the type of graphics obtained with the program is shown in figure D.23. The experimental data is plotted by dots and the model results as continuous lines.

Finally, this panel has also the buttons *Save Plot* and *Clear all*. They work as explained in the first panel.

The button *Save result* of this panel saves the obtained parameters estimates in an excel file (.xls). The program saves the file with the default path, and the name *Param.xls*. When the file has been saved a dialog box will appear on the SISIFO screen confirming the creation of the file *Param.xls* (see figure D.24).

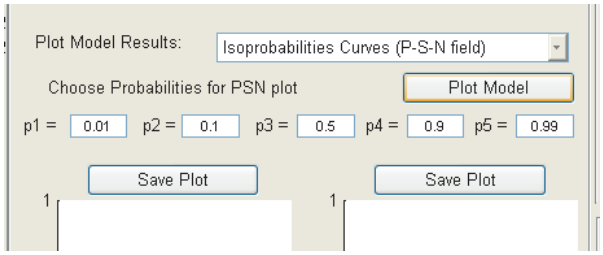


Figure D.22: Probability definition of the P–S–N curves.

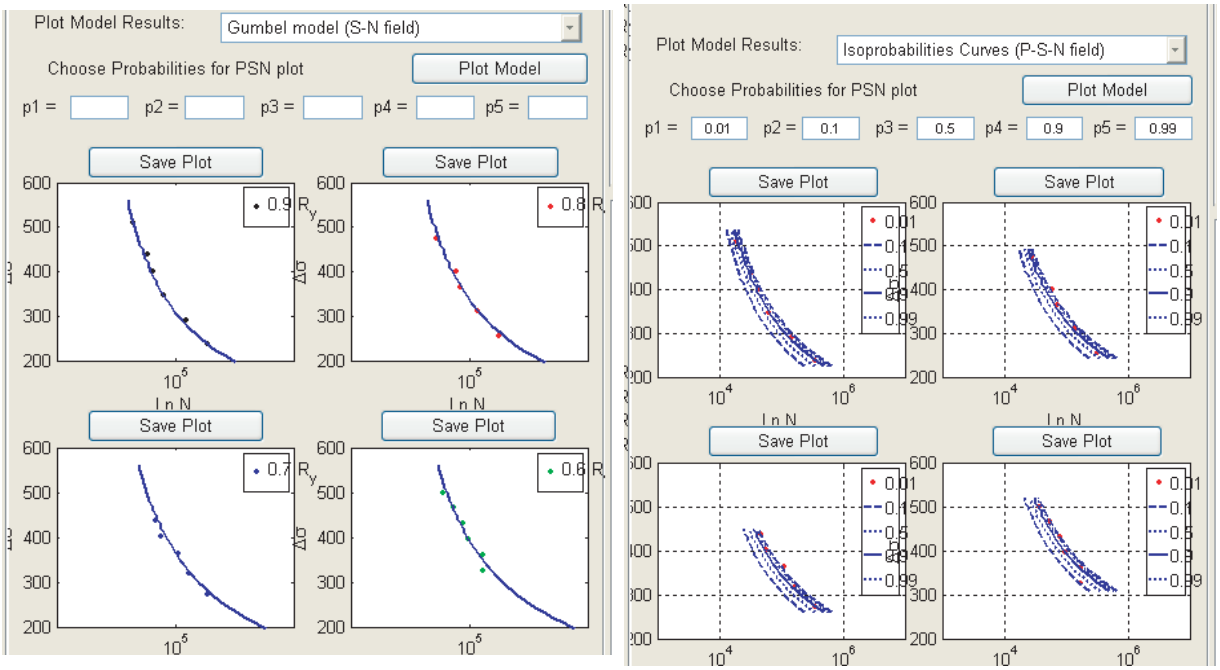


(a) (b)

Figure D.23: Example of graphics obtained after the parameter estimation: (a) S–N curves; (b) P–S–N curves.

### Model validation

The objective of this panel is to validate the model with the obtained parameters of the previous panel: Parameter estimation, based on the concepts and methods explained in section 7.7. From a user point of view it is easy to work with panels in the SISIFO program because the user only needs to press buttons to obtain the results, without the necessity of loading files or defining certain values.

For the evaluation of the PP–plot, the user has to press the button near to the PP–plot graphic called *Calculate* and SISIFO will generate the corresponding PP–plot (see figure D.25). For the evaluation of the Kolmogoronov-Smirnov Test (K.S.T.) and the $\chi^2$ Test, the user has to press the button called *Calculate* at the bottom of the panel (see figure D.26).

The button *Save plot* works similar to the first panel 4.2. The button called *Save Result*

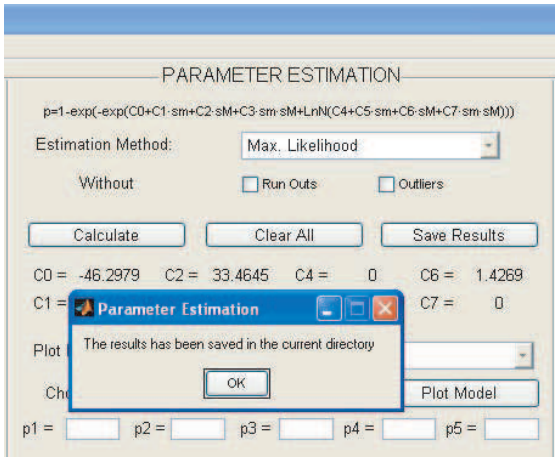


Figure D.24: Dialog box confirming the creation of the file *Param.xls*.

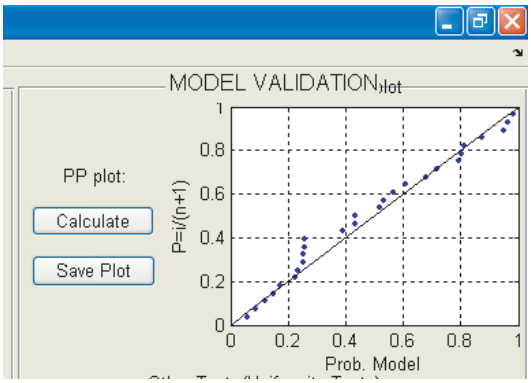


Figure D.25: PP–plot obtained by the SISIFO program.

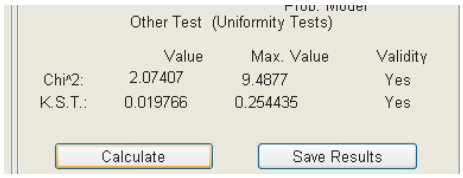


Figure D.26: Resulting of the model validation performed by the SISIFO program.

saves the result in an excel file (.xls) called *ValidationTest.xls*. In figure D.27 the confirmation of the file creation is shown.

In figure D.28 an example of the created file is shown. The first row corresponds to the results obtained in the $\chi^2$ test, and the second row to the Kolmogoronov-Smirnov test ($KST$ test). The first column represents the value obtained with the estimated parameters, the second with the critical value for each validation test and the last column corresponds to the difference between the first two columns. If this difference is negative the set is not uniform.

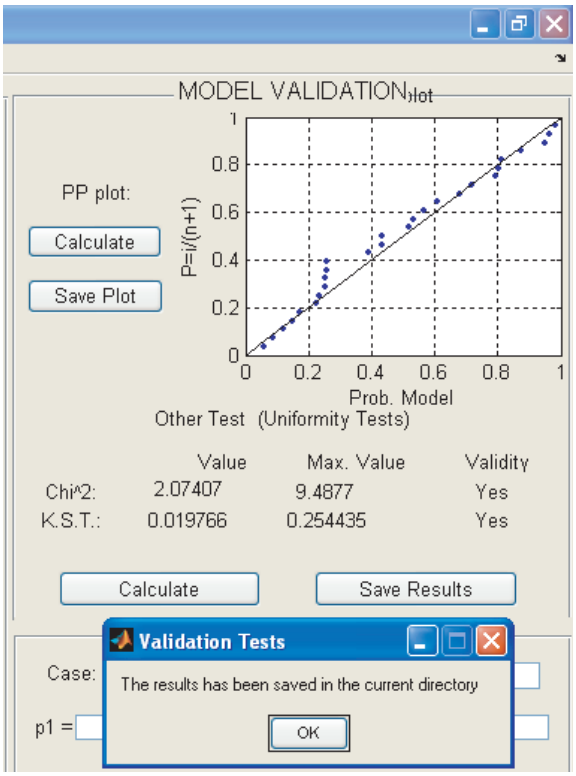


Figure D.27: Confirmation after creating the validation file.

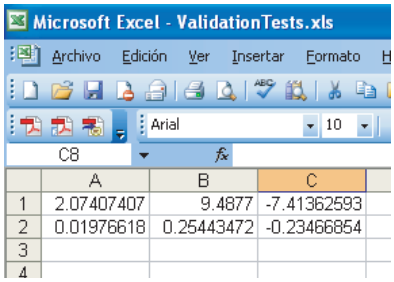


Figure D.28: Example of the *ValidationTest.xls* file.

### Extrapolation

Finally the last panel in this menu is the panel called *Extrapolation*. Its objective is to show a certain S–N or P–S–N curve for a certain constant value ($\sigma_M$ or $R$ ratio).

The steps required to obtain these curves are:

1. Choose the case of study, $\sigma_M$ or $R$ constant values.
2. Choose certain probabilities for the P–S–N curves or any probability to plot the S–N curves.

The case study is chosen from a Pop-up menu (see figure D.29). After having chosen the case, the user defines a constant value corresponding to each case ($\sigma_M$ or $R$ respectively).

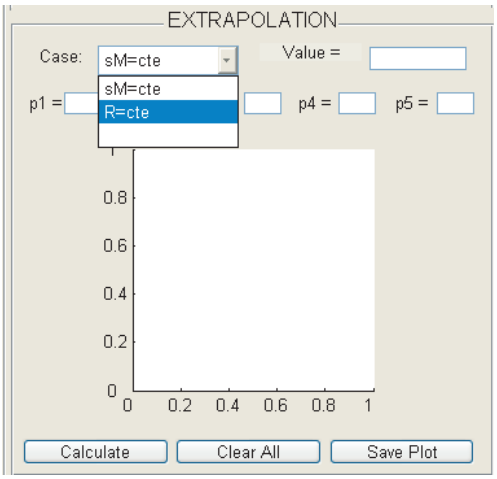


Figure D.29: Definition of the case study in the extrapolation panel.

The S–N curves are plotted when the text boxes with labels $p_1, p_2, p_3, p_4$ and $p_5$, that define the different probabilities are not filled, otherwise the P–S–N field will appear in the Figure. In the figure D.30 an example of the extrapolation is shown, the left side represents the S–N curves for the case and value chosen and the right side represents the P–S–N curves for the same value and case study.

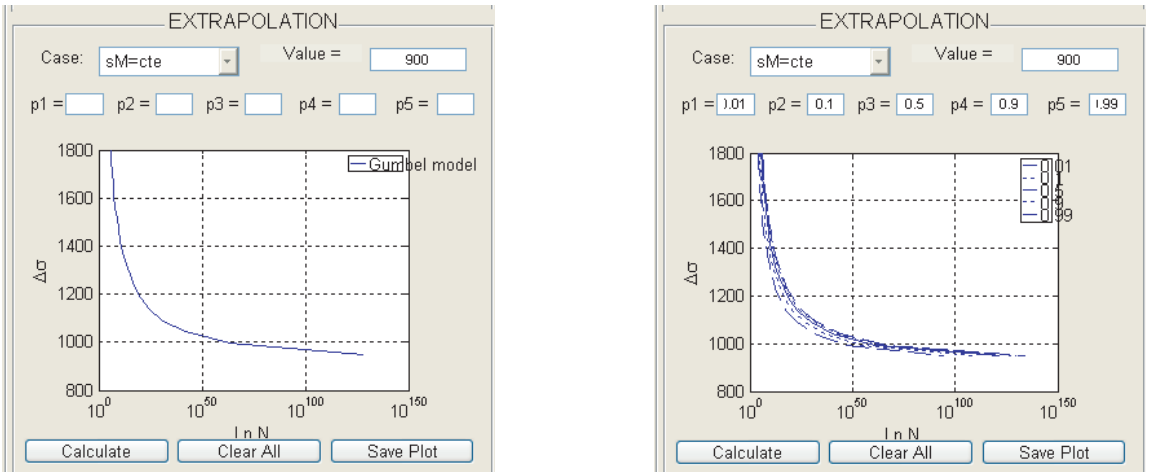


Figure D.30: Example of extrapolation: left side, S–N curves for a $\sigma_M = 900$MPa; right side, P–S–N curves for the same value and case of study.

The buttons *Clear All* and *Save Plot* work similar to those in the first panels (section D.3.3).

### D.3.4 Menu 2: damage analysis

In this section, the Damage analysis menu is described. To access this menu the option *Damage Analysis* has to be chosen in the *Option* menu (see figure D.31).

This menu consists of three panels: Load definition, Rainflow analysis and Damage analysis (see figure D.33).

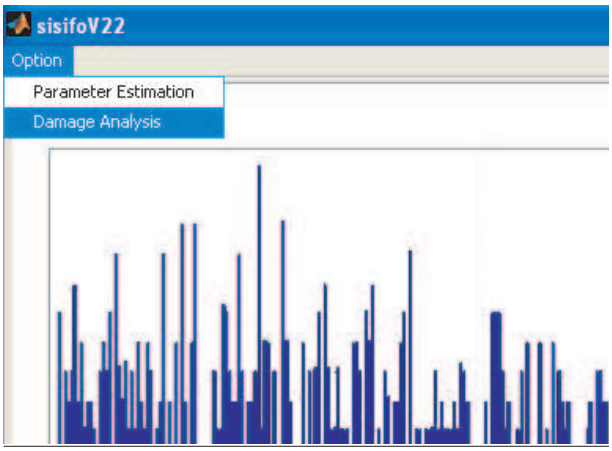


Figure D.31: Entering the Damage analysis menu of SISIFO.

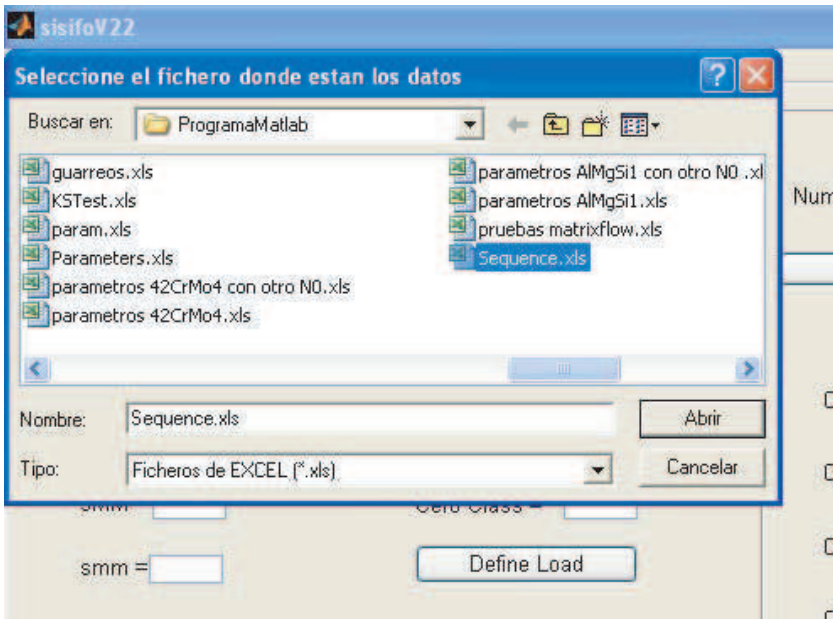


Figure D.32: Loading a load sequence in the SISIFO program.

### Load definition

The objective of this panel is to load or to define a load history that will be used for the Damage analysis.

The methodology of using is as follows:

1. Define a load history.
2. Plot the spectrum and save the load sequence.

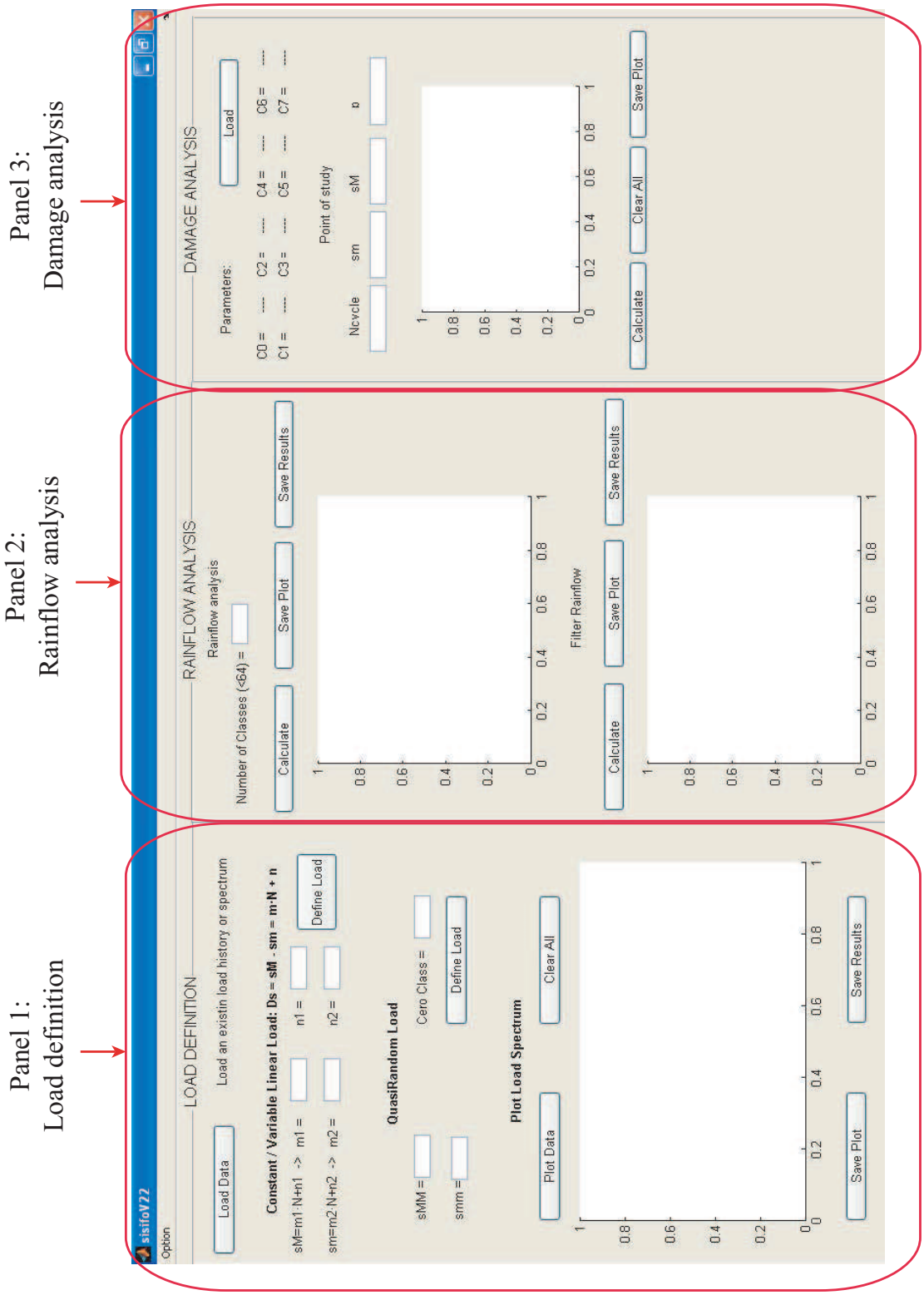


Figure D.33: Different panels in the Damage analysis menu of the SISIFO program.


Figure D.34: Different types of load histories: (a) $\Delta\sigma = 900$ MPa,(b) $\Delta\sigma = 0.1 \cdot N + 900$ MPa,(c) $\Delta\sigma = 0.4 \cdot N + 600$ MPa.

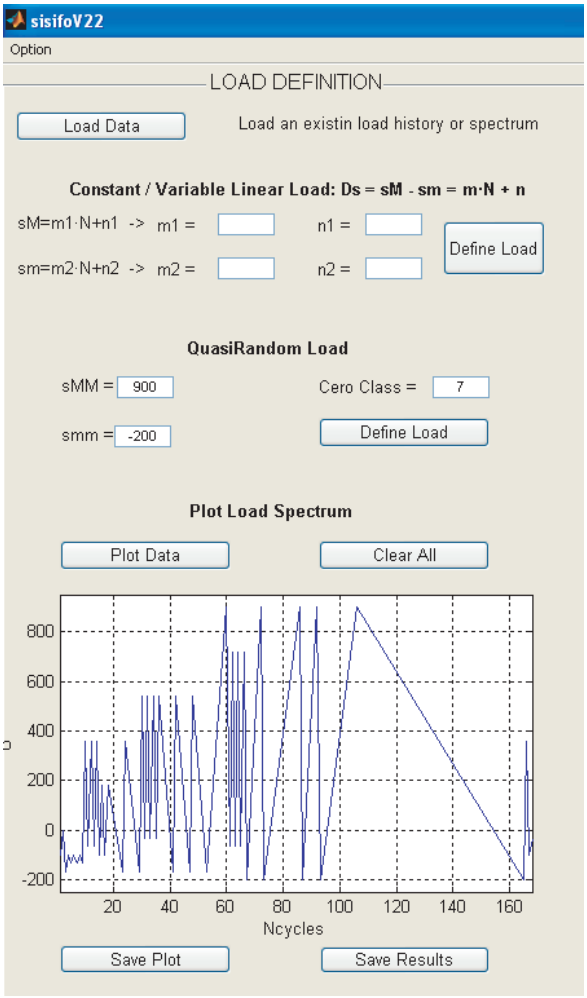


Figure D.35: Representation of a quasi-random load history in SISIFO.

To define the load history the user has three different options:

1. *Load a load history file with all the information about the sequence of loads:* The user will press the button called *Load*, and choose the correct file (see figure D.32). This file (.xls file) will be formed by three columns, the first column represents the number of cycles, the second the minimum stress $\sigma_m$ and the third column represents the maximum stress $\sigma_M$.

2. *Define a constant load history or a variable linear load history:* The user creates the load history ($\Delta\sigma = \sigma_M - \sigma_m = m \cdot N + n$) defining the expressions of $\sigma_M = m_1 \cdot N + n_1$ and $\sigma_m = m_2 \cdot N + n_2$. The constants $m_1$, $m_2$, $n_1$ and $n_2$ are chosen by the user. Finally, the parameter $m$ corresponds to the slope of the load history, how the load increase/decrease with the number of cycles and $n$ corresponds to the value of $\Delta\sigma$ when $N = 0$. The meaning of $m_1, m_2$ and $n_1$ and $n_2$ is the same than $m$ and $n$. Three examples of load histories are shown in figure D.34.

   In the sequence plot the program shows three different lines, two of them correspond to the definition of $\sigma_m$ and $\sigma_M$ (red lines) and the third one represents the load sequence (in blue).

3. *Load a quasi-random load spectrum:* First the user needs to load the spectrum using the button called *Load* (as in the first point). After this, the user defines the stresses that define the load sequence (because normally the spectra are dimensionless and based on classes) and defines the position of the zero load *Zero Class* (see figure D.35).

   The sequence shown in this case is the result of the algorithm of four points. The sequence represents the real cycles of the load history.

In order to plot the different load histories the user presses the button called *Plot Load*. The button *Save Plot* and *Clear All* work similar as in section D.3.2. The button called *Save sequence* creates an excel file in the current directory with all the information of the load history in three columns (first, number of cycles; second, minimum stress and third column maximum stress in the cycle), but it is implemented only for quasi-random spectra.

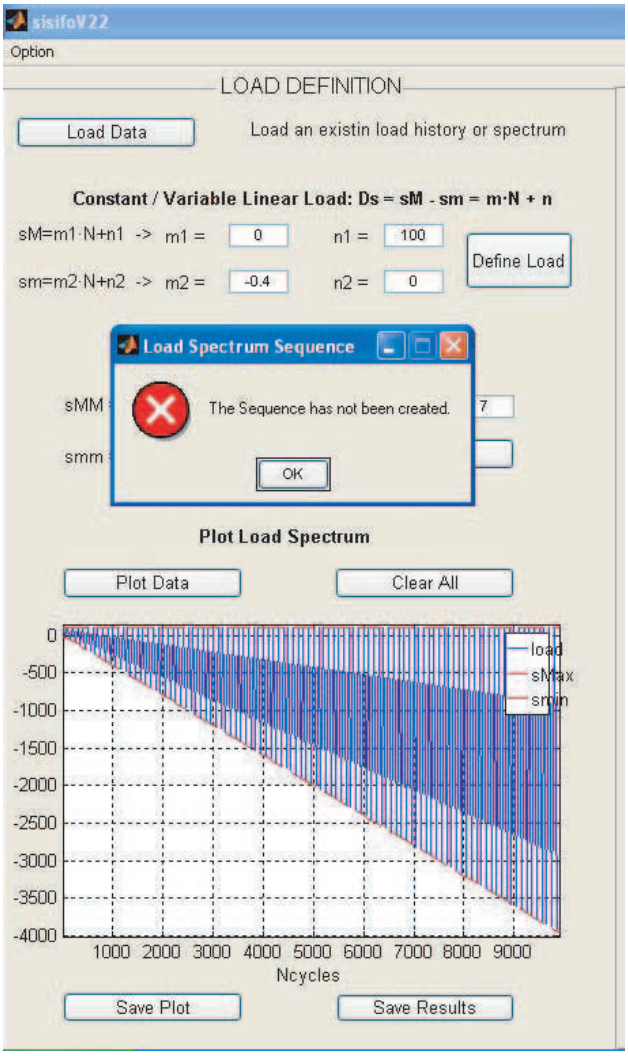


Figure D.36: Error dialog box used to tell the user that the sequence file has not been created.

If the user presses the button called *Save results* when the load history is different, a new Dialog box will appear in SISIFO indicating us that the file has not been created (see figure D.36, in which a variable load history is presented but not a quasi-random one, so SISIFO tells

us that the file has not been created). The aim of this is to obtain a sequence file that can be applicated to a fatigue test machine.

### Rainflow analysis

The objective of this panel is to calculate the Rainflow matrix for that load history.

For the rainflow analysis the program needs only the number of classes (normally less than 64). After pressing the button *Calculate* a plot with the rainflow analysis in a color scale is obtained. The user can save the results in an excel file (.xls) by pressing the button *Save Results*. In figure D.37 a rainflow plot is shown.

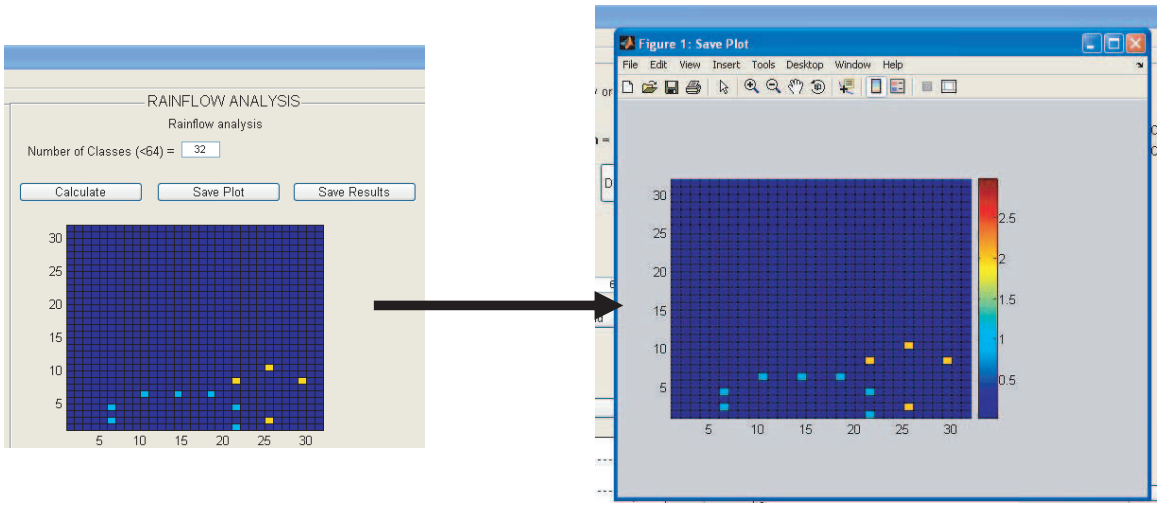


Figure D.37: Rainflow matrix in color scale. The color scale of the right side represents the frequence of cycles in the rainflow matrix.

The second part of this panel corresponds to a filter that the user may apply to the load sequence. The objective is to delete cycles lower than the endurance limit of the material. This is useful to reproduce the damage calculations and time on fatigue test machines. In this case, a new window will appear in the program and the user specifies in it the necessary data to filter the rainflow matrix: Endurance limit, $R$-ratio and a security factor (between zero and one) to use in the filter process.

There are two options for the $R$-ratio, equal to minus one or equal to zero. In the first case, the endurance limit doubled in order to get the endurance range instead of the amplitude parameter definition window (see figure D.38). In the case of $R = 0$ the endurance limit is equal to the limit defined by the user. The security factor modifies the final value of the endurance limit.

Finally, the buttons *Save Plot* and *Save Results* work similar to the buttons explained in the previous sections.

### Damage analysis

The objective of the last panel of the SISIFO program is to analyze the damage accumulation (defined by the probability of failure $p$) of a material subjected to a certain load history.

The methodology is the following:

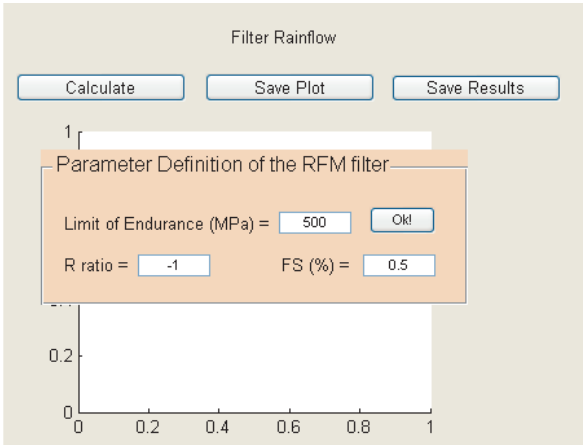


Figure D.38: Parameter definition for the Rainflow filter analysis.

1. Load the model parameters. If they don't exist the program sends the user to the first menu of SISIFO in order to calculate the parameters (see figure D.39).

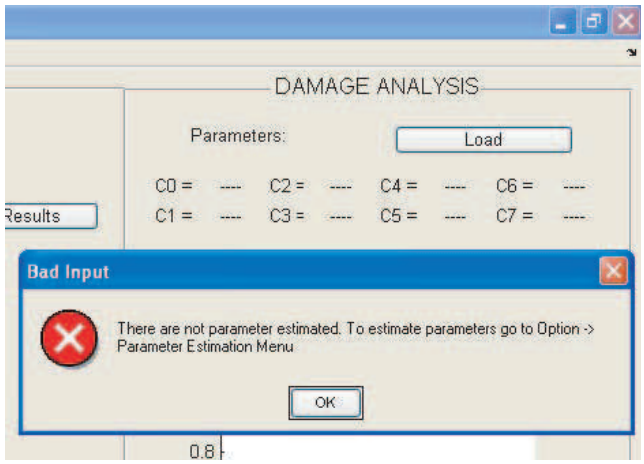


Figure D.39: Dialog box indicating the absence of the parameter file.

2. Define the point of study, that is, number of cycles ($N$), minimum stress ($\sigma_m$) and maximum stress ($\sigma_M$).

3. Press Calculate. The program calculates the probability of failure ($p$) for the point defined in the previous step and plot the cumulative distribution function (cdf) for this load and parameters (see figure D.40).

   It is very important that the user specifies a good value for $\sigma_m$, $\sigma_M$ and $N$.

Finally, the buttons *Save Plot* and *Save Results* work similar to the buttons explained in the previous sections.

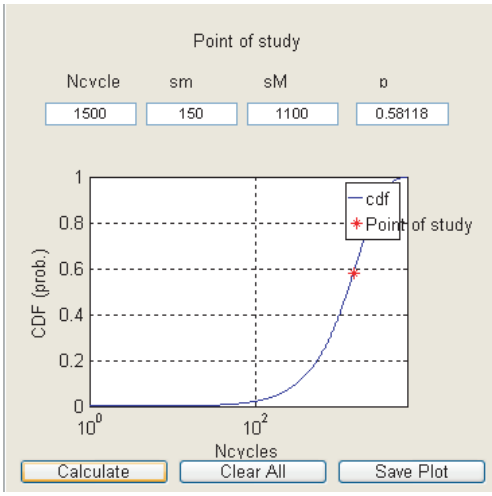


Figure D.40: Representation of the probability of failure calculated with the model parameters for a certain point of study. The red point corresponds to the point of study, the blue line corresponds to the cdf of the model for all number of cycles with this load.

## D.4 Example of application

In this section, some illustrative examples of applications are given with the aim of showing how the SISIFO program works. The section is organized in three subsections: first, an example of how the parameters of a material can be estimated is given, second, it is shown how the damage accumulation can be analyzed and finally, an example of how a rainflow matrix can be estimated and filtered.

### D.4.1 Estimation of the Castillo model parameters

#### Presentation of the problem

Consider a metallic material. We want to know the lifetime of these material subjected to a certain variable load history, using the new fatigue model defined by Castillo et al. [40].

The data of the problem are:

- A set of experimental data tests have been obtained from fatigue tests. The results are shown in table D.2. The data consists of four different series for constant $\sigma_M$.
- The number of cycles defined for runouts are $N = 10000000$ cycles.

Following the methodology defined by Castillo et al. [40] (see section 6.7) the steps in the damage accumulation analysis will be:

1. *Design of the testing strategy:* Presented in table D.2.
2. *Choose the normalizing variables $N_0$ and $\sigma_0$:* Defined by SISIFO (see section D.3.2).
3. *Estimate the model parameters:* Using the SISIFO program (see section D.4.2).
4. *Extrapolate to other testing conditions:* Calculate the damage accumulation for the load history described before and estimate the trend of the S–N curves in the case of i.e. $R = -1$.

Table D.2: Resulting lifetimes from the laboratory tests.

| Nr. Test | $\sigma_{min}$ | $\sigma_{max}$ | Ncycles | Nr. Test | $\sigma_{min}$ | $\sigma_{max}$ | Ncycles |
|---|---|---|---|---|---|---|---|
| 1 | -182.15 | 327.87 | 19100 | 18 | -281.42 | 218.58 | 37100 |
| 2 | -109.29 | 327.87 | 34000 | 19 | -246.42 | 218.58 | 54400 |
| 3 | -72.86 | 327.87 | 42800 | 20 | -211.42 | 218.58 | 80300 |
| 4 | 36.43 | 327.87 | 153100 | 21 | -176.42 | 218.58 | 96300 |
| 5 | 109.29 | 327.87 | 10000000 | 22 | -141.42 | 218.58 | 175500 |
| 6 | -18.22 | 327.87 | 63800 | 23 | -106.42 | 218.58 | 172800 |
| 7 | 91.08 | 327.87 | 360400 | 24 | -71.42 | 218.58 | 526500 |
| 8 | 182.15 | 327.87 | 10000000 | 25 | -36.42 | 218.58 | 8639500 |
| 9 | 72.86 | 327.87 | 81600 | 26 | -182.15 | 255.01 | 48000 |
| 10 | -182.15 | 291.44 | 28700 | 27 | -145.72 | 255.01 | 57900 |
| 11 | -72.86 | 291.44 | 71700 | 28 | -109.29 | 255.01 | 113100 |
| 12 | -109.29 | 291.44 | 59900 | 29 | 27.32 | 255.01 | 7500000 |
| 13 | -18.22 | 291.44 | 143500 | 30 | -18.22 | 255.01 | 348300 |
| 14 | 36.43 | 291.44 | 326400 | 31 | -63.75 | 255.01 | 172500 |
| 15 | 109.29 | 291.44 | 10000000 | 32 | 55.01 | 255.01 | 10000000 |
| 16 | 91.08 | 291.44 | 10000000 | 33 | 72.86 | 255.01 | 238200 |
| 17 | 72.86 | 291.44 | 207700 | | | | |

**Preparation of the data**

Before estimating the model parameters, the normalization of the data is performed. For this we need to load our data in SISIFO and show the normalization of the data.

The file *example1.xls* contains all the test data and also defines which of these points are outliers (indicated by a value equal to one in the fourth column). figure D.41 shows how the data looks like.

Figure D.42 presents the plots obtained by SISIFO, the upper figure corresponds to the original data and the lower one to the normalized data.

**Parameter estimation**

After the data normalization the parameter estimation is carried out. The maximum likelihood method is chosen for the estimation and for this example the estimation is done without runouts and outliers (note that in figure D.43 the check boxes *RunOut* and *Outliers* are checked).

The initial parameters correspond to

$$C_{initial} = (-10.19593, 44.77213, -39.18622, 0.0, 0.0, -5.66951, 5.66951, 0.0)$$

which satisfy all the model constraints. The final parameters are shown in figure D.43. The parameters obtained have been saved in the current directory (see figure D.44).

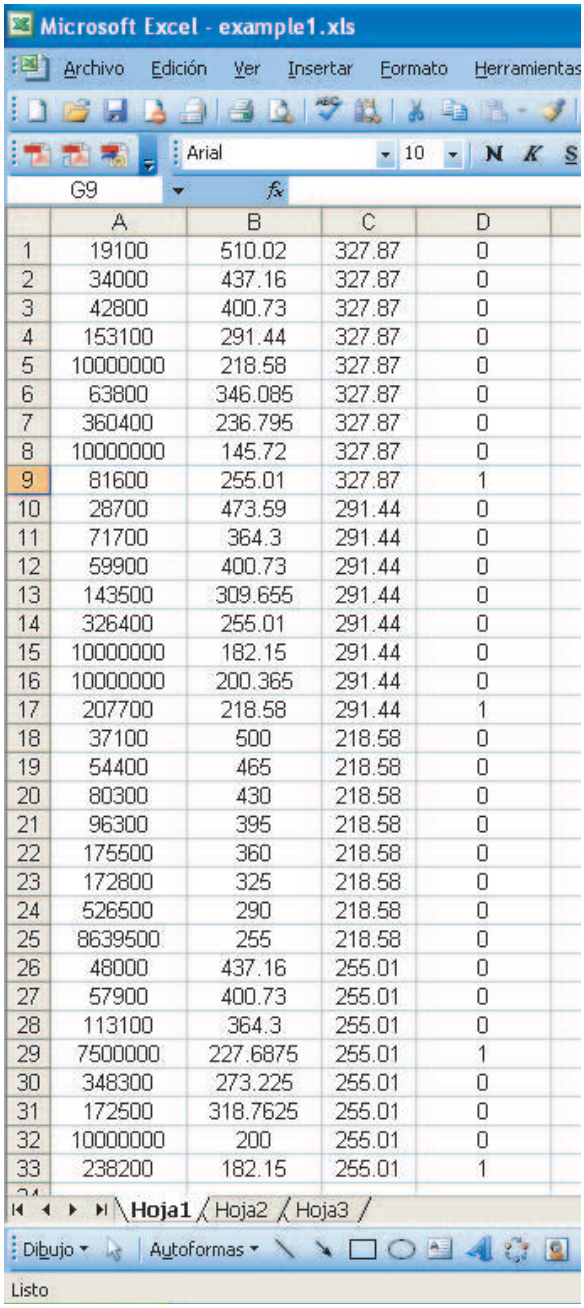


| | A | B | C | D |
|---|---|---|---|---|
| 1 | 19100 | 510.02 | 327.87 | 0 |
| 2 | 34000 | 437.16 | 327.87 | 0 |
| 3 | 42800 | 400.73 | 327.87 | 0 |
| 4 | 153100 | 291.44 | 327.87 | 0 |
| 5 | 10000000 | 218.58 | 327.87 | 0 |
| 6 | 63800 | 346.085 | 327.87 | 0 |
| 7 | 360400 | 236.795 | 327.87 | 0 |
| 8 | 10000000 | 145.72 | 327.87 | 0 |
| 9 | 81600 | 255.01 | 327.87 | 1 |
| 10 | 28700 | 473.59 | 291.44 | 0 |
| 11 | 71700 | 364.3 | 291.44 | 0 |
| 12 | 59900 | 400.73 | 291.44 | 0 |
| 13 | 143500 | 309.655 | 291.44 | 0 |
| 14 | 326400 | 255.01 | 291.44 | 0 |
| 15 | 10000000 | 182.15 | 291.44 | 0 |
| 16 | 10000000 | 200.365 | 291.44 | 0 |
| 17 | 207700 | 218.58 | 291.44 | 1 |
| 18 | 37100 | 500 | 218.58 | 0 |
| 19 | 54400 | 465 | 218.58 | 0 |
| 20 | 80300 | 430 | 218.58 | 0 |
| 21 | 96300 | 395 | 218.58 | 0 |
| 22 | 175500 | 360 | 218.58 | 0 |
| 23 | 172800 | 325 | 218.58 | 0 |
| 24 | 526500 | 290 | 218.58 | 0 |
| 25 | 8639500 | 255 | 218.58 | 0 |
| 26 | 48000 | 437.16 | 255.01 | 0 |
| 27 | 57900 | 400.73 | 255.01 | 0 |
| 28 | 113100 | 364.3 | 255.01 | 0 |
| 29 | 7500000 | 227.6875 | 255.01 | 1 |
| 30 | 348300 | 273.225 | 255.01 | 0 |
| 31 | 172500 | 318.7625 | 255.01 | 0 |
| 32 | 10000000 | 200 | 255.01 | 0 |
| 33 | 238200 | 182.15 | 255.01 | 1 |

Figure D.41: Definition of the data file *example1.xls*.

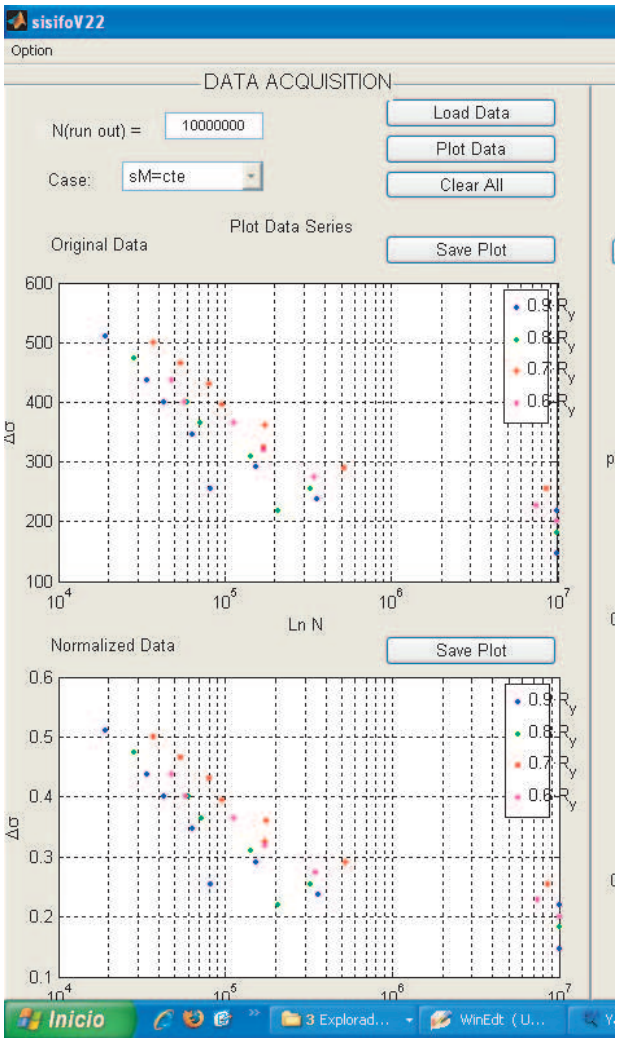


Figure D.42: Graphics representing the original and normalized data.

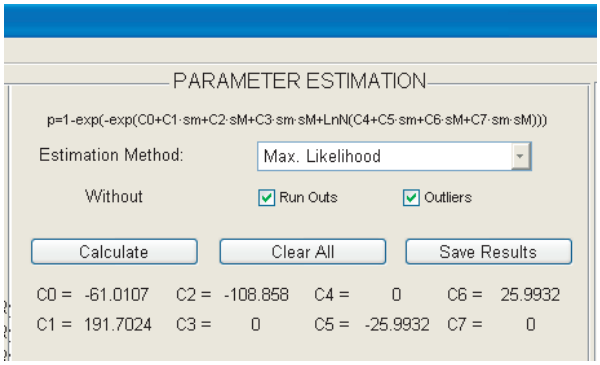


Figure D.43: Parameter estimation with all the data, using the maximum likelihood method.

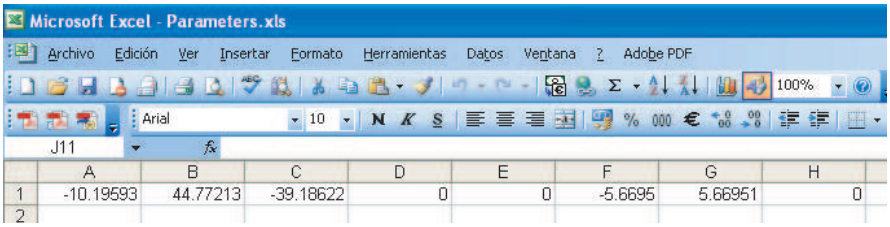


Figure D.44: File saved by SISIFO with the estimated parameters.

The S–N and P–S–N curves are shown in figure D.45. We can observe that with these parameters the curves fit well with the experimental data.

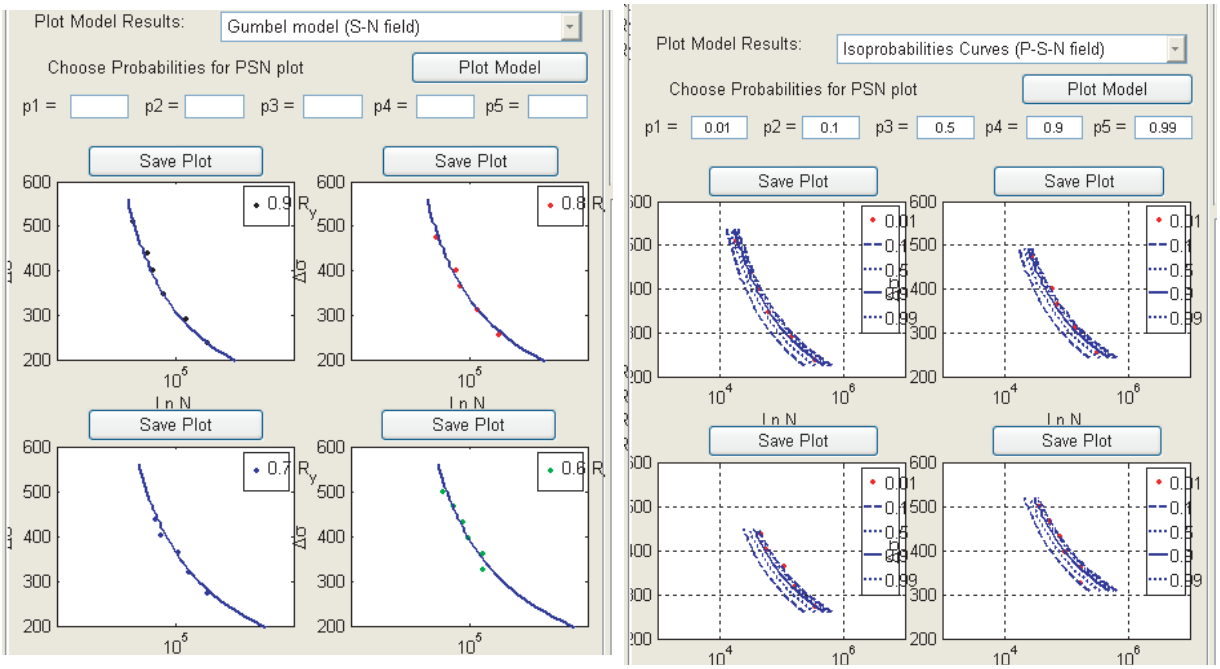


(a) (b)

Figure D.45: S–N curves and P–S–N curves obtained with the parameter estimation.

### Model validation

For the model validation the last parameters obtained are chosen. Pressing the two buttons called *Calculate* (first one close to PP–plot and second one on the validation uniformity test) in the model validation panel we obtain the results shown in figure D.46.

### Extrapolation to other load conditions

We want the model to extrapolate and plot a new P–S–N curve corresponding to the value $R = -1$. For this we choose the case $R = cte$ in the pop-up menu and then we define the value to minus one. Pressing the button *Calculate* the new curve is shown (see figure D.47).

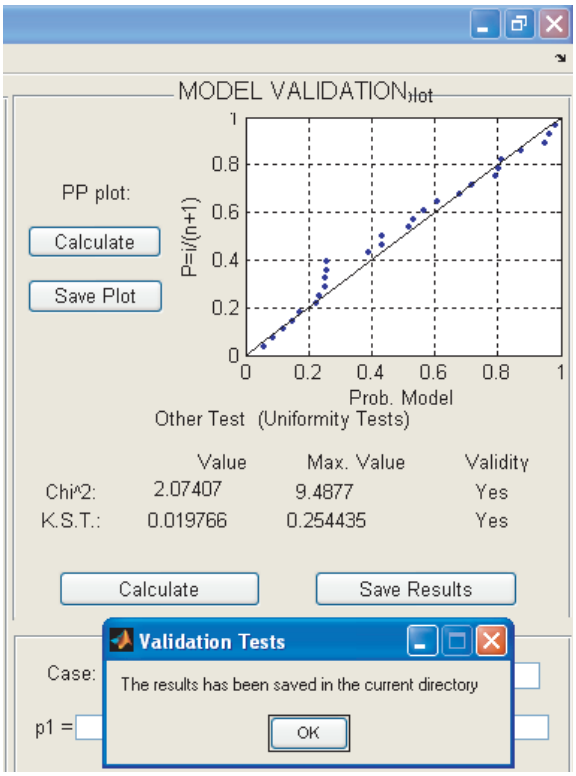


Figure D.46: Obtained results for the model validation.

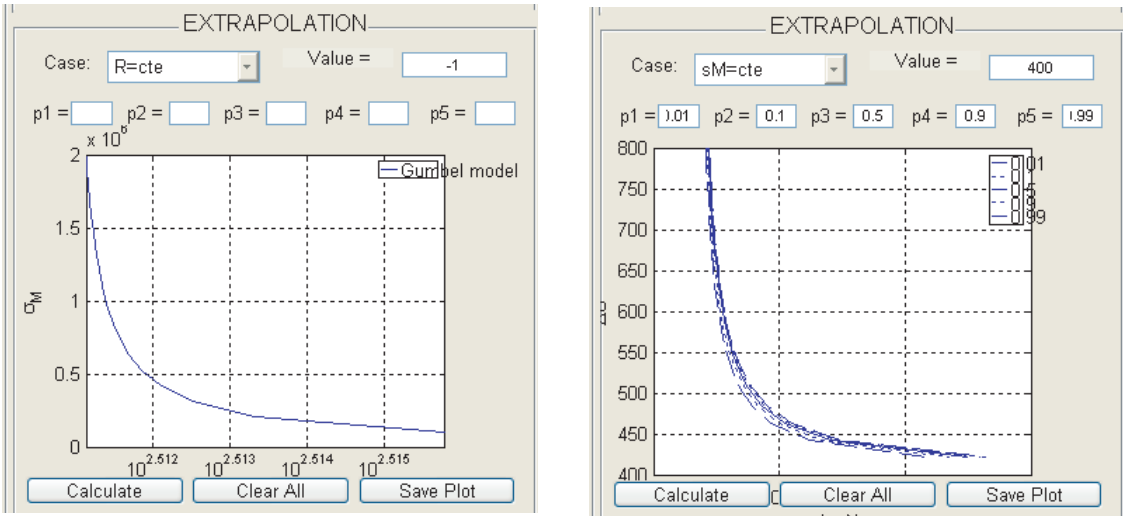


(a) (b)

Figure D.47: P–S–N curve obtained for $R = -1$, extrapolated from the original data.

Before going to the second menu for the damage analysis we want to show how the first menu looks like when all the panels are in use. This is presented in figure D.48.

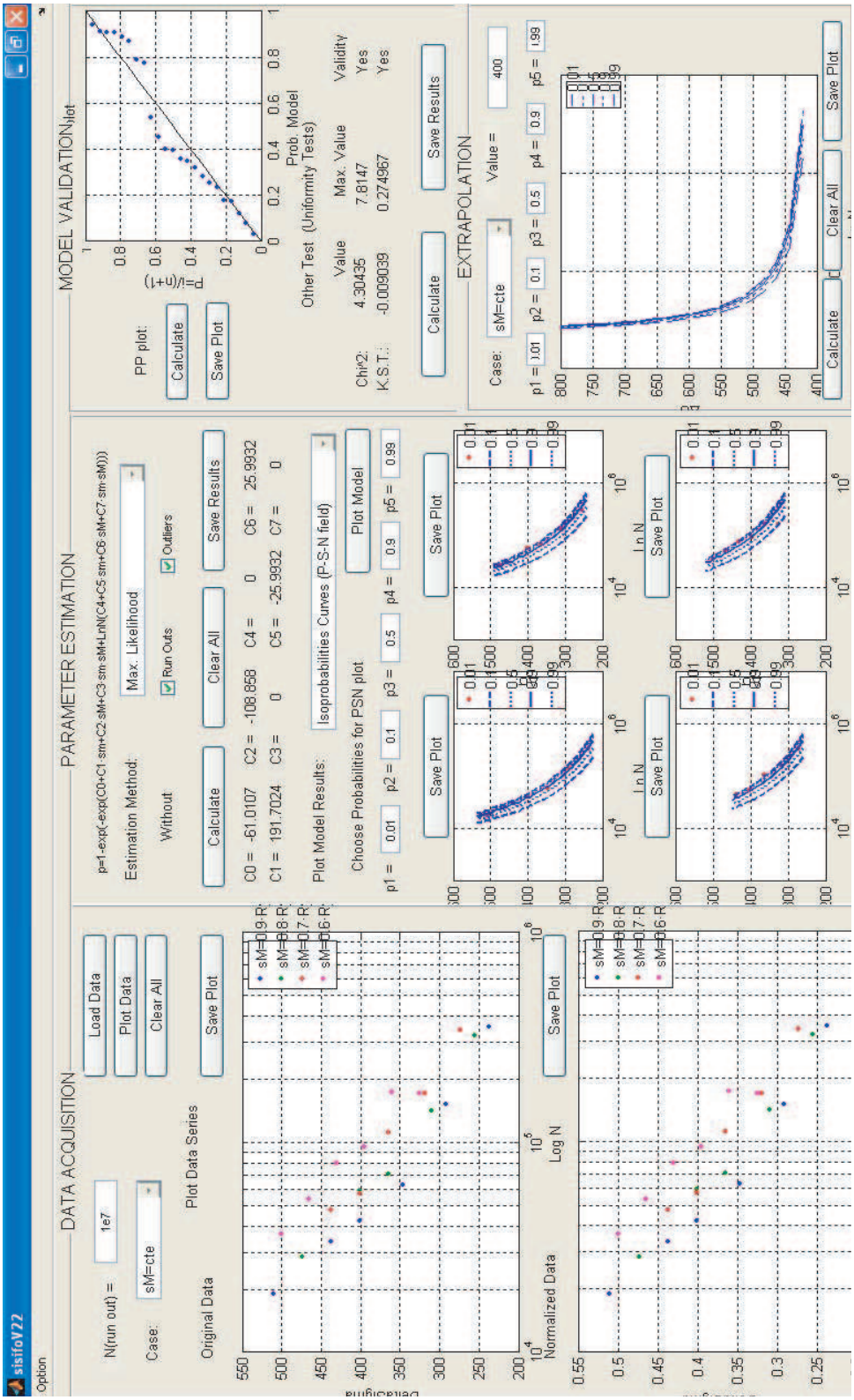


Figure D.48: Representation of the Menu 1: Parameter estimation after using all the panels.

### D.4.2 Analysis of the damage accumulation

#### Presentation of the problem

Consider a metallic material. We want to analyze the damage accumulation of a material subjected to a certain variable load history, using the new fatigue model defined by Castillo et al. [40].

The data of the problem is:

- A set of experimental data tests have been obtained from fatigue tests. The results are shown in table D.3. The data consists of four different series for constant $\sigma_M$.
- The number of cycles defined for runout are $N = 10000000$ cycles.
- Endurance limit is 420 MPa for $R = 0$.
- The damage accumulation will be analyzed for the following load history: $\Delta\sigma = 1250$ MPa .

Table D.3: Resulting lifetimes from the laboratory tests for the Example Nr.2.

| Nr. Test | $\sigma_{min}$ | $\sigma_{max}$ | Ncycles | Nr. Test | $\sigma_{min}$ | $\sigma_{max}$ | Ncycles |
|---|---|---|---|---|---|---|---|
| 1 | 17.502 | 955.50 | 65277 | 15 | -167.50 | 877.80 | 125800 |
| 2 | 35.24 | 955.50 | 23700 | 16 | -500.00 | 780.30 | 11439 |
| 3 | 55.27 | 955.50 | 52700 | 17 | -437.50 | 780.30 | 14973 |
| 4 | 78.43 | 955.50 | 40900 | 18 | -375.00 | 780.30 | 32055 |
| 5 | 119.11 | 955.50 | 85900 | 19 | -312.50 | 780.30 | 483000 |
| 6 | 108.91 | 955.50 | 124300 | 20 | -343.75 | 780.30 | 36708 |
| 7 | 124.21 | 955.50 | 222900 | 21 | -265.63 | 780.30 | 532200 |
| 8 | 98.71 | 955.50 | 93500 | 22 | -281.25 | 780.30 | 123100 |
| 9 | -250.00 | 877.80 | 17281 | 23 | -550.00 | 682.74 | 183024 |
| 10 | -190.00 | 877.80 | 48787 | 24 | -620.00 | 682.74 | 19331 |
| 11 | -175.00 | 877.80 | 81244 | 25 | -525.00 | 682.74 | 347102 |
| 12 | -360.00 | 877.80 | 3373 | 26 | -585.00 | 682.74 | 33925 |
| 13 | -305.00 | 877.80 | 21812 | 27 | -500.00 | 682.74 | 381543 |
| 14 | -332.50 | 877.80 | 7265 | | | | |

In this section the parameter estimation is made as in the first example. Since the results of the parameter estimates are presented in table D.4, we go directly to the analysis of damage accumulation for the load history defined above.

Table D.4: Parameters estimated with SISIFO for Example Nr.2.

| $C_0$ | $C_1$ | $C_2$ | $C_3$ | $C_4$ | $C_5$ | $C_6$ | $C_7$ |
|---|---|---|---|---|---|---|---|
| -46.29 | -3.77 | 33.464 | 0.00 | 0.00 | -1.43 | 1.43 | 0.00 |

#### Defining the variable load history

In this section the load history is created. The load history corresponds to the expression $\Delta\sigma = 1250$ MPa, that is $m = 0$ and $n = 1250$ MPa (constant load history), with $\sigma_m = -250$ MPa and $\sigma_M = 1000$ MPa.

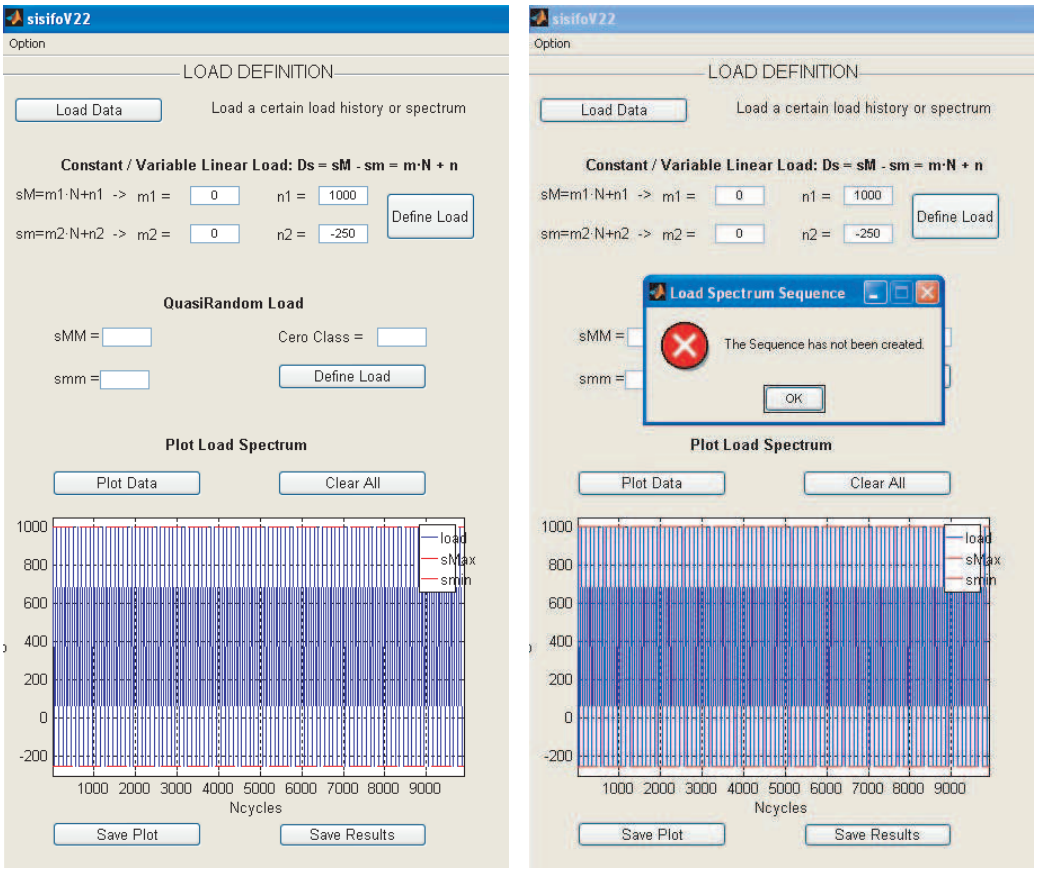


Figure D.49: (a) Load history definition: $\Delta\sigma = 1250$ MPa (constant load history), with $\sigma_m = -250$ MPa and $\sigma_M = 1000$ MPa. (b) Error dialog box created by SISIFO when the file *sequence.xls* can not be created.

The sequence is defined by pressing the button *Define load*. Pressing *Plot Results* we obtain the graphic N cycles vs. $\sigma$. figure D.49 (a) shows the error dialog box created by SISIFO when the load history defined is not a random load history and the program is not prepared to create sequences of this type of loads.

The program is not prepared to make the rainflow analysis to this type of load sequences. figure D.49 (b) shows the Dialog box that SISIFO creates when we press the button *Calculate* on the Rainflow analysis panel.

### Damage analysis

Finally, the damage is analyzed. First we need to load the parameter values of our material by pressing the button called *Load Parameters*.

We want to know the probability of failure when the material is subjected to the load defined in section D.4.3, or, more precisely, when the number of cycles is equal to $N = 4000$, $\sigma_m = -250$ MPa and $\sigma_M = 1000$ MPa. figure D.51 shows the results of this analysis when we press the *Calculate* button.

Concluding with this section, figure D.52 shows how the second menu looks like when all the

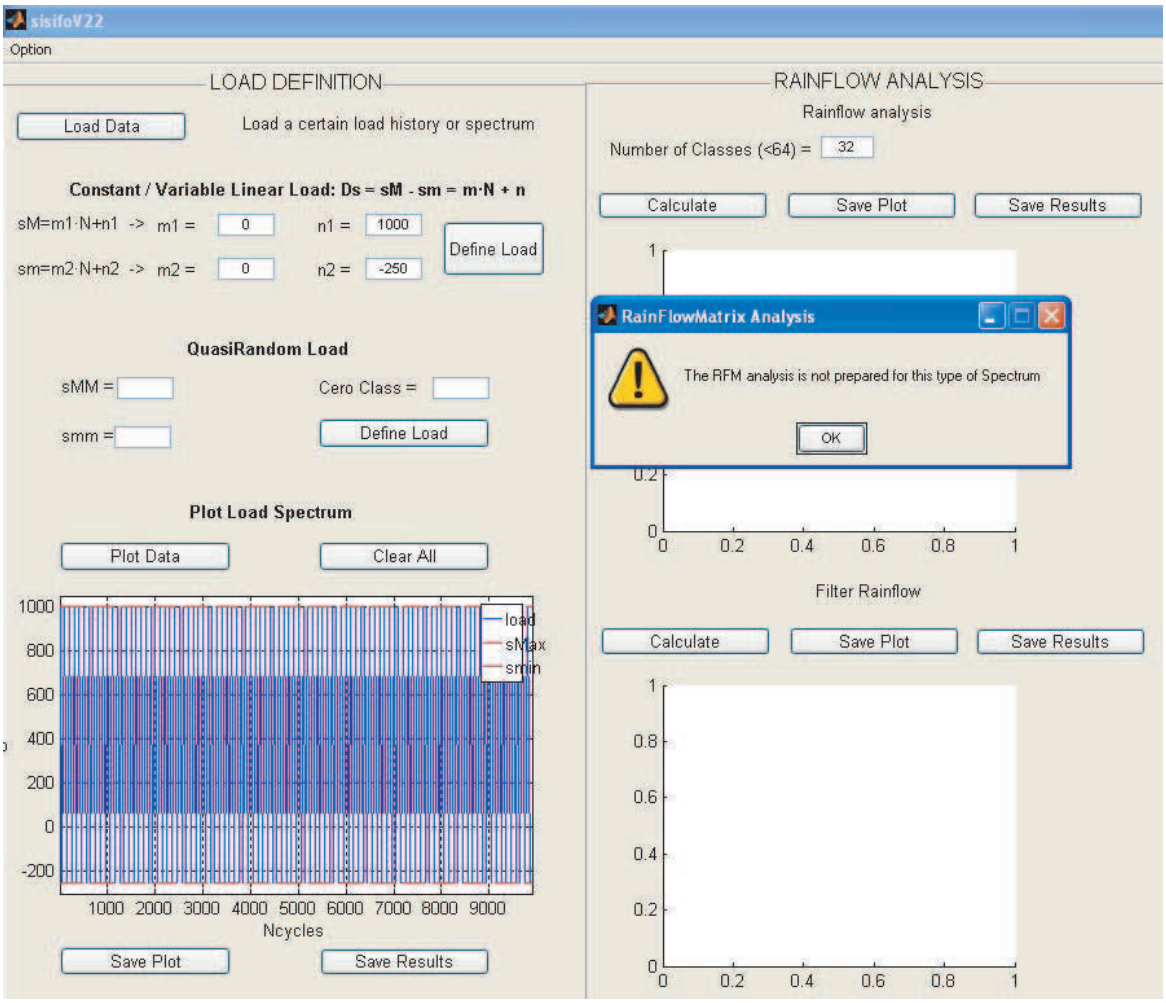


Figure D.50: Error dialog box created by SISIFO when the rainflow analysis cannot be carried out.

procedures have been used.

### D.4.3 Rainflow analysis in a quasi-random load history

Rainflow analysis is normally made to work easily with complex load histories, as quasi-random load histories. In this section an example of rainflow analysis is made: first obtaining the rainflow matrix and then filtering the resulting sequence.

The rainflow matrix represents a certain number of classes (less than 64) containing the frequency of cycles between a certain minimum stress (from) to a maximum stress (to). The diagonal of this matrix is equal to zero because these cycles would have an amplitude equal to zero.

The steps for obtaining the rainflow matrix (RFM) are:

1. Load a sequence. For this we choose the option *Load data* from the panel *Load definition*. We choose the file *example2.xls*.

2. Definition of the maximum and minimum stresses, and the position of the zero load. We

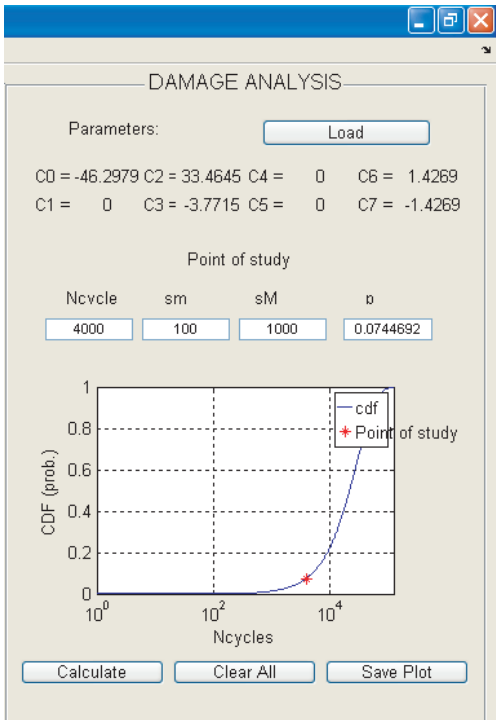


Figure D.51: Damage results obtained with SISIFO, for the load history $\Delta\sigma = 1250$ MPa in the point $N = 4000$, $\sigma_m = -250$ MPa and $\sigma_M = 1000$ MPa

choose the values of $\sigma_M = 900$ MPa, $\sigma_m = -200$MPa, and zero class in 7 (in a sequence with 12 classes). figure D.53 shows the resulting spectrum.

3. Select the number of classes in our RFM equal to 32. Press the button called *Calculate*. The resulting RFM is shown in figure D.54 (a). Note that the diagonal is equal to zero and there is a quasi symmetric distribution of the points. The results are saved by pressing the button *Save Results*.

To optimize the time in our fatigue test with random loads and/or in the calculation of the damage accumulation we decide to do a filtering of the rainflow matrix obtained before with the aim of deleting the cycles with an amplitude $\Delta\sigma \leq \Delta\sigma_{lim}$ (limit of endurance). In the section D.4.2 the values for the $R$ ratio, security factor (FS) and the $\Delta\sigma_{limit}$ are defined. Pressing the button *Calculate*, filling the different text boxes and finally pressing *Ok!* we obtain the filtered rainflow matrix (see figure D.54 (b)).

It can be appreciated that both rainflow matrices are equal. But the width of the empty diagonal of the filtered matrix is bigger, because all the small non damaging cycles have been deleted (see figure D.54). Pressing the button *Save results* the file *RFMfiltered.xls* is created and the new sequence (without the smallest cycles) is also created (file called *sequenceFiltered.xls*).

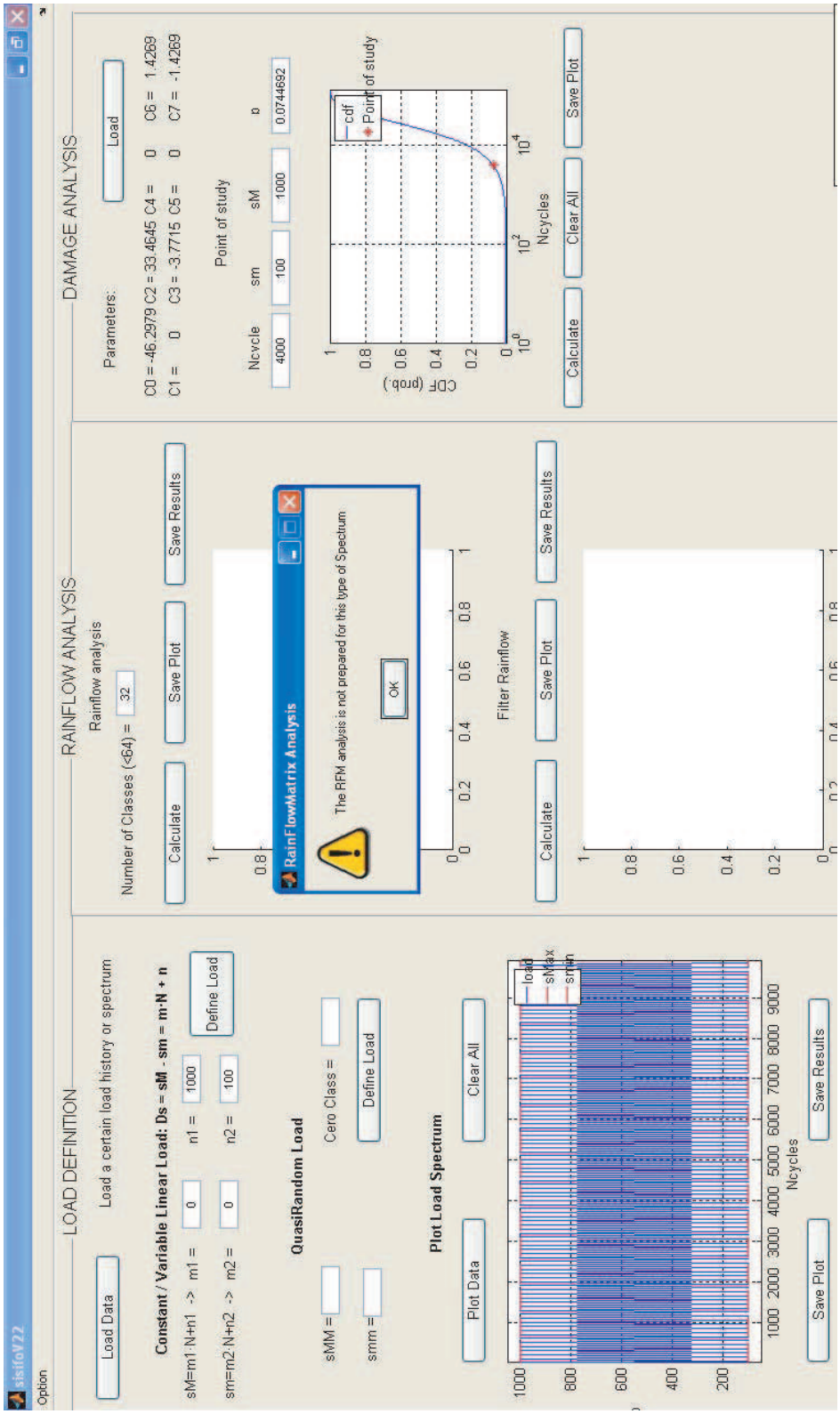


Figure D.52: Representation of Menu 2: Damage Analysis after using it.

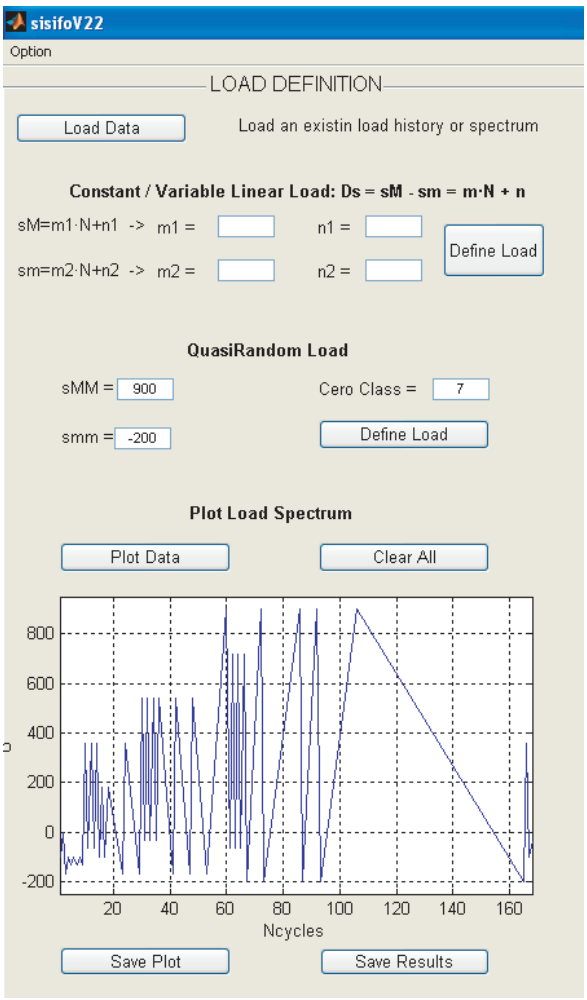


Figure D.53: Random spectrum used for the example of rainflow analysis.

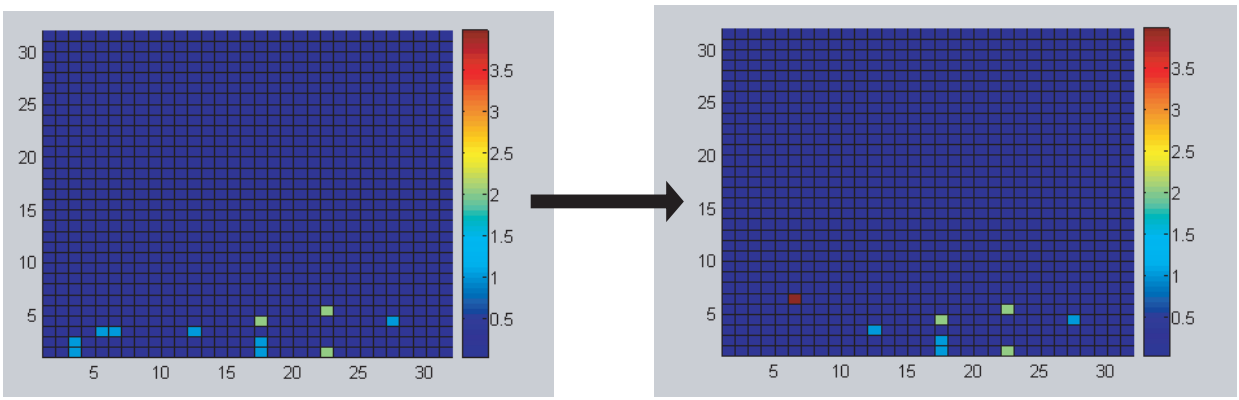


(a) (b)

Figure D.54: Comparison between the rainflow matrix (a) and the filtered rainflow matrix (b).

# Appendix E

# Nomenclature

| Symbol | Nomenclature |
|---|---|
| Chapter 3 | Basic concepts |
| $\sigma$ | Stress of a cycle |
| $\sigma_{min}$, $\sigma_m$ | Minimum stress of a cycle |
| $\sigma_{max}$, $\sigma_M$ | Maximum stress of a cycle |
| $\sigma_{mean}$ | Mean stress in a cycle |
| $\Delta\sigma$ | Stress range of a cycle |
| $\sigma_a$ | Stress amplitude of a cycle |
| $R$ | Stress ratio |
| $A$ | Amplitude ratio |
| Chapter 3 | Fatigue under fracture mechanics point of view |
| $a$ | Crack length |
| $F$ | Dimensionless function used in the fracture mechanics approach |
| $K$ | Stress intensity factor |
| $\Delta K$ | Stress intensity factor range |
| $\alpha$ | Relative crack length |
| $b$ | Width dimension of a member |
| $\frac{da}{dN}$ | Crack growth rate |
| $C$ | Constant used in the fatigue crack growth |
| $m$ | Constant used in the fatigue crack growth |
| $\Delta K_{th}$ | Fatigue crack growth intensity factor threshold |
| $K_c$ | Fatigue crack growth intensity factor critic (failure) |
| $\Delta\bar{K}$ | Equivalent zero-to-tension ($R = 0$) stress intensity factor |
| $\gamma$ | Constant of the material used in the fatigue crack growth theories |
| $\frac{da}{dt}$, $\dot{a}$ | Time based growth rate, crack growth velocity |
| $A$, $n$ | Constant of the material used in the crack velocity formulation |
| $C_1$, $C_2$ | Material parameter used by Broek & Schijve [30] in the crack growth formulation |
| $P$, $Q$ | Material parameter used by Frost & Dugdale [69] in the crack growth formulation |
| $f_\tau$ | Strength applied in the Yokobori [134] crack growth formulation |
| $f_i$ | Image strength in the Yokobori [134] crack growth formulation |
| $\rho$ | Distance from the head of crack to the dislocation. Used by the Yokobori [134] crack growth formulation |
| $\phi$ | Crack angle. Used by the Yokobori [134] crack growth formulation |

| Symbol | Nomenclature |
|---|---|
| Chapter 3 | Stress based approach to fatigue |
| $\sigma_e$ | Equivalent stress |
| $\sigma_u$ | Ultimate strength |
| $\sigma_y$ | Yield stress |
| $\sigma'_f$ | Reversal fatigue strength |
| $M$ | Mean stress sensitivity factor |
| Chapter 3 | Strain based approach to fatigue |
| $\epsilon$ | Strain |
| $l$ | Instantaneous length |
| $l_0$ | Original length |
| $\Delta l$ | Longitudinal deformation |
| $A$ | Cross-sectional area |
| $A_0$ | Original cross-sectional area |
| $S$ | Engineering stress |
| $e$ | Engineering strain |
| $\%EI$ | Percentage of elongation |
| $\%RA$ | Reduction of area |
| $E$ | Modulus of elasticity |
| $K$ | Monotonic strength coefficient. Used by Ramberg and Osgood [112] |
| $n$ | Monotonic strain hardening exponent. Used by Ramberg and Osgood [112] |
| $\sigma_f$ | True fracture strength |
| $\epsilon_f$ | True fracture ductility |
| $\epsilon^e$ | Elastic strain |
| $\epsilon^p$ | Plastic strain |
| $K'$ | Cyclic strength coefficient. Used by Ramberg and Osgood [112] |
| $n'$ | Cyclic strain hardening exponent. Used by Ramberg and Osgood [112] |
| $\Delta\epsilon$ | Strain range |
| $\sigma'$ | Fatigue strength coefficient |
| $\epsilon'$ | Fatigue ductility coefficient |
| $b$ | Fatigue strength exponent |
| $c$ | Fatigue ductility exponet |
| $\epsilon_a$ | Strain amplitude |
| $N_f$ | Number of cycles to failure |
| Chapter 4 | Models used in fatigue |
| $a$, $b$ | Parameters of the Basquin function [20] |
| $\sigma_\infty$ | Fatigue limit used by Stromeyer [128] |
| $a$, $b$, $B$ | Parameters of the Palmgren function [105] |
| $\frac{N_i}{N_{f_i}}$ | Fraction of lifetime used in the Palmgren-Miner rule [95] |
| $\Delta\sigma_i$ | Stress ranges used by Dixon & Mood [57] |
| $p_i$ | Probability of failure |
| $\mu(X)$ | Mean value of the $X$ variable |
| $\sigma(X)$ | Standard deviation of the $X$ variable |
| $\varphi(N)$ | Bastenaire's auxiliary function [21] |
| $A$, $E$, $c$ | Bastenaire's function parameters [21] |
| $S_A$ | Fatigue strength used by Spindel & Haibach [126] |

| Symbol | Nomenclature |
|---|---|
| $k$ | Slope of the S–N curves [126] |
| $\alpha$ | Spindel parameter [126] |
| $N_E$ | Cutoff of the S–N curves by Spindel [126] |
| $S_E$ | Endurance limit [126] |
| $Y$ | Lifetime in the Pascual & Meeker model [107] |
| $\beta_0$, $\beta_1$ | Pascual-Meeker model parameters [107] |
| $\gamma$ | Fatigue limit of the specimen [107] |
| $\epsilon$ | Error term in the Pascual-Meeker equation [107] |
| $F(x;\lambda,\delta,\beta)$ | Weibull cumulative distribution function |
| $\lambda$ | Location parameter in the Weibull distribution |
| $\delta$ | Scale parameter in the Weibull distribution |
| $\beta$ | Shape parameter in the Weibull distribution |
| $B$ | Threshold value of lifetime used by Castillo et al. [36] |
| $C$ | Endurance limit used by Castillo et al. [36] |
| $E$ | Position of the corresponding zero-percentile hyperbola [36] |
| $D$ | Scale factor [36] |
| $A$ | Weibull shape parameter of the whole cdf in the S–N field [36] |
| $N^*$ | Normalized number of cycles [36] |
| $\Delta\sigma^*$ | Normalized stress level [36] |
| $N_{ref}$ | Number of cycles of reference used for the normalization [36] |
| $\Delta\sigma_{ref}$ | Stress level of reference used in the normalization [36] |
| Chapter 6 | Derivation of the Gumbel fatigue model |
| $N_0$ | Equivalent number of cycles used in the normalization [40] |
| $\sigma_0$ | Equivalent stress used in the normalization [40] |
| $N^*$ | Normalized number of cycles [40] |
| $\sigma^*$ | Normalized stress [40] |
| $\sigma_m^*$ | Normalized minimum stress [40] |
| $\sigma_M^*$ | Normalized maximum stress [40] |
| $C_1, C_2, C_3, C_4, C_5, C_6$ and $C_7$ | Parameters of the Gumbel fatigue mode [40] |
| $\Delta\sigma_{m_0}$ | Asymptotic value of $\Delta\sigma$ for constant $\sigma_m$[40] |
| $\Delta\sigma_{M_0}$ | Asymptotic value of $\Delta\sigma$ for constant $\sigma_M$[40] |
| $\log N_{m_0}$ | Asymptotic value of $\log N$ for constant $\sigma_m$ [40] |
| $\log N_{M_0}$ | Asymptotic value of $\log N$ for constant $\sigma_M$ [40] |
| $\gamma$ | Euler-Mascheroni number |
| $L$ | Log-Likelihood function |
| $I_1$ | Set of non-runouts |
| $I_0$ | Set of runouts |
| $H(N_i)$ | Auxiliary function of the log-likelihood formulation |
| $Covar$ | Covariance matrix of the estimation parameter process |
| $\mathbf{C}$ | Parameters estimated maximum likelihood |
| $Q$ | Regression Weibull-Gumbel equation |

| Symbol | Nomenclature |
|---|---|
| Chapter 7 | Experimental validation of the model |
| $L_1$ | Total length of the specimen |
| $L_2$ | Useful length of the specimen |
| $d$ | Diameter of the specimen |
| $r$ | Curvature radius of the specimen |
| $D$ | Value of the Kolmogorov-Smirnov test |
| $F(H(N_i^*))$ | Sample order statistics |
| $i$ | Position of the sample |
| $n$ | Total number of specimens (sample size) |
| $\chi^2$ | Value of the $Chi^2$ test |
| Chapter 8 | Damage measures and damage accumulation |
| $M_i$ | Palmgren-Miner number |
| $Z$ | Normalized variable related with the Castillo fatigue model [40] |
| $P_F$ | Probability of failure |
| $N_{eq}^*$ | Equivalent number of cycles used in the damage accumulation formulation of the Castillo fatigue model [40] |
| $P_{N+\Delta N}$ | Accumulated damage [40] |
| Appendix B | Specimen characterization |
| $T$ | Temperature (C) |
| $R_y$ | Yield strength (MPa) |
| $Rp_{0.2}$ | Yield strength at $\epsilon = 0.2\%$ of strain |
| $R_m$ | Ultimate strength |
| $\mu$ | Mean value |
| $\sigma$ | Standard deviation |

# Bibliography


[1] *ASTM Standard E1049. Standard Practices for Cycle Counting in Fatigue Analysis.* Philadelphia, 1985.

[2] *MIL-HDBK-5G: Application of Fracture Mechanics for Selection of Metallic Structural Materials. Mlitary Handbook*, 1994.

[3] *ASTM Standard E739. Standard Practice for Statistical Analysis of Linear or Linearized stress–life (S–N) and strain–life ($\epsilon$–N) fatigue data.* Philadelphia, 1998 (reapproved).

[4] *Standard Terminology Relating to Metallography.* Annual Book of ASTM Standards, vol. 03.01 edition, 2003.

[5] *Annual Book of ASTM Standards. ASTM E606-92.* Vol. 03.01.2005 edition, 2005.

[6] *Practices for Force Verification to Testing Machines.* Annual Book of ASTM Standards, vol. 03.01 edition, 2007.

[7] *Standart Test Methods for Tension Testing of Metallic Materiasls [Metric].* Annual Book of ASTM Standards, vol. 03.01 edition, 2008.

[8] N. H. Abel. Méthode génerale pour trouver des functions d'une seule quantité variable lorsqu'une propieté de ces fonctions est exprimée par une equation entre deux variables. *Mag. Naturvidenskab*, 1:1–10, 1823.

[9] N. H. Abel. Unterschungen uber die Reihe $1 + (m/1)x + (m(m-1))(1.2)x^2 + ....$ *Journal Reine Angewandte Mathematical*, 1:311–319, 1826.

[10] N. H. Abel. Untersuchungen der Functionen zweier unabhangigen veranderlichen Grössen $x$ und $y$, wie $f(x, y)$ welche die Eigenschaft haben, dass $f[z; f(x; y)]$ eine Symmetrische Function von $x, y$ und $z$ ist. *Journal Reine Angewandte Mathematical*, 1:5–11, 1826.

[11] J. Aczél. Lectures in functional equations and their applications. *Mathematics in science and Engineering. Academic Press*, 19, 1966.

[12] J. Aczél. *Functional equations: History, applications and theory.* Dordrecht, 1984.

[13] J. Aczél and J. Dhombres. *Functional Equations in several variables.* Cambridge University Press,, 1989.

[14] H. Alawi and M. Shabans. Fatigue crack growth under random loading. *Engineering Fracture Mechanics*, 32(5):845–854, 1989.

[15] A. Anatolij. *Linear functional equations.* Russian Estate University, 1996.

[16] Y.M. Baik and K.S. Kim. The combined effect of frequency and load level on fatigue crack growth in stainless steel 304. *International Journal of Fatigue*, 23:417–425, 2001.

[17] R. Balasubrahmayan and K.S. Lau. *Functional equations in probability theory.* Boston Academic Press, 1991.

[18] J. A. Bannantine, J. J. Comer, and J. L. Handrock. *Fundamentals of Metal Fatigue Analysis.* Prentice Hall, New York, 1990.

[19] J.M. Barson and S.T. Rolfe. *Fracture and Fatigue Control in Structures.* Prentice Hall, Upper Saddle River, New Jersey, 2nd edition, 1987.

[20] O. H. Basquin. The exponential law of endurance tests. *American Society for Testing and Materials Proceedings*, 10:625–630, 1910.

[21] F. A. Bastenaire. *Etúde Statistique et Physique de la Dispersion des Résistances et des Endurances a la Fatigue.* PhD thesis, Faculty of Sciences, University of Paris, Paris, France, 1960.

[22] F. A. Bastenaire. New method for the statistica1 evaluation of constant stress amplitude fatigue-test results. *Probabilistic Aspects of Fatigue, American Society for Testing and Materials*, ASTM STP 511:3–28, 1972.

[23] C. Bathias and R.M. Pelloux. *Etúde de la zone plastifiée à fond de fissure: application à la propagation des fissures de fatigue dans les aciers maraging et les aciers austénitiques.* Saclay, 1972.

[24] D. Benasciutti and R. Tovo. Fatigue life assessment in non-Gaussian random loadings. *International Journal of Fatigue*, 28:733–746, 2006.

[25] B.A. Bilby, A. H. Cottrell, and K. H. Swiden. Analysis of stresses and strains near the end of a crack transversing a plate. *Proceedings of the Royal Society*, A272:304, 1963.

[26] J. Bogdanoff and F. Kozin. Effect of length on fatigue life of cables. *Journal of Engineering Mechanics*, 113:925–940, 1987.

[27] C. Boller and T. Seeger. *Materials Data for Cycling Loading. Part B: Low-Alloy Steels.* Elsevier, ISBN: 0-444-42871-2 edition, 1987.

[28] C. Boller and T. Seeger. *Materials Data for Cycling Loading. Part D: Aluminium and Titanium Alloys.* Elsevier, ISBN: 0-444-42873-9 edition, 1987.

[29] P. W. Bridgman. Stress distribution at the neck of tension specimen. *American Society for Testing and Materials Proceedings*, 32:553–572, 1944.

[30] D. Broek. *Elementary Engineering Fracture Mechanics.* Kluwer Academic Publications, Dordrecht, The Netherlands, 4th edition, 1986.

[31] E. Buckingham. On physically similar systems; illustrations of the use of dimensional equations. *Physical Review*, 4:345–376, 1914.

[32] R.G. Carlson. *Fatigue Studies of Inconel, BMI-1335, UC-25 Metallurgy and Ceramics.* Ohio, 1959.

[33] E. Castillo. *Extreme value theory in engineering.* Academic Press, 1988.

[34] E. Castillo, A. Fernández, J. R. Ruiz, and J. M. Sarabia. Statistical models for analysis of fatigue life of longs elements. *Journal of Mechanical Engineering, ASCE*, 116:1036–1049, 1990.

[35] E. Castillo and A. Fernández-Canteli. A general regression model for lifetime evaluation and prediction. *International Journal of Fracture*, 107:117–137, 2001.

[36] E. Castillo and A. Fernández-Canteli. A parametric lifetime model for the prediction of high-cycle fatigue based on stress level and amplitude. *Fatigue Fracture Engineering Materrial Structure*, 29:1031–1038, 2006.

[37] E. Castillo, A. Fernández-Canteli, V. Esslinger, and B. Thürlimann. Statistical model for fatigue analysis of wires, strands and cables. *International Association for Bridge and Structural Engineering*, P-82/85:1–40, 1985.

[38] E. Castillo, A. Fernández-Canteli, and A.S. Hadi. On fitting a fatigue model to data. *International Journal of Fatigue*, 21:97–106, 1999.

[39] E. Castillo, A. Fernández-Canteli, A.S. Hadi, and M. López-Aenlle. A fatigue model with local sensitivity analysis. *International Journal of Fatigue*, 30:149–168, 2007.

[40] E. Castillo, A. Fernández-Canteli, R. Koller, M.L. Ruiz-Ripoll, and A. García. A statistical fatigue model covering the tension and compression Wöhler fields. *Probabilistic Engineering Mechanics*, doi:10.1016/j.probengmech.2008.06.003, 2007.

[41] E. Castillo, A. Fernández-Canteli, M. López-Aenlle, and M.L. Ruiz-Ripoll. Some fatigue damage measures for longitudinal elements based on the Wöhler field. *Fatigue & Fracture of Engineering Materials & Structures*, 30:1063–1075, 2007.

[42] E. Castillo, A. Fernández-Canteli, and M.L. Ruiz-Ripoll. A general model for fatigue damage due to any stress history. *International Journal of Fatigue*, 30:150–164, 2008.

[43] E. Castillo and J. Galambos. Lifetime regression models based on a functional equation of physical nature. *Journal of Applied Probability*, 24:160–169, 1987.

[44] E. Castillo and A.S. Hadi. Modeling lifetime data with applicaiton to fatigue models. *Journal of the American Statistical Association*, 90, No. 431:1041–1054, 1995.

[45] E. Castillo, A. Iglesias, and M.R. Ruiz-Cobo. *Functional equations in applied sciences.* Amsterdam, 2005.

[46] E. Castillo, A. Iglesias, and R. Ruiz-Cobo. *Functional equation in applied science.* Elsevier, 1st. edition, 2004.

[47] E. Castillo, M. López-Aenlle, A. Ramos, A. Fernández-Canteli, R. Kieselbach, and V. Esslinger. Specimen length effect on parameter estimation in modelling fatigue strength by Weibull distribution. *International Journal of Fatigue*, 28:1047–1058, 2006.

[48] E. Castillo, A. Ramos, R. Koller, M. López-Aenlle, and A. Fernández-Canteli. A critical comparison of two models for assessment of fatigue data. *International Journal of Fatigue*, 30, No. 1:45–57, 2008.

[49] E. Castillo and M.R. Ruiz-Cobo. *Functional equations in science and engineering.* Marcel Dekker, New York, 1992.

[50] L. F. Jr. Coffin. A study of the effect of cyclic thermal stresses on a ductile metal. *Transactions of ASME*, 76:931–950, 1954.

[51] V.J. Colangelo and F.A. Heiser. *Analysis of Metallurgical Failures.* Wiley, New York, 1974.

[52] J.A. Collins. *Failure of Materials in Mechanical Design.* Wiley, New York, 1993.

[53] J. B. Conway and L. H. Sjodahlo. *Analysis and representation of fatigue data.* ASM International, Cincinatti, 1991.

[54] D. R. Cox. Regression models and life-tables. *Journal of the Royal Statistical Society*, 2:187–202, 1972.

[55] J. G. Dhombres and R. Ger. Conditional cauchy equations. *Glasnik Matematicki Series III*, 13:39–62, 1975.

[56] G.E. Dieter. *Mechanical Metallurgy.* McGraw-Hill, New York, 1976.

[57] W. J. Dixon and A. M. Mood. A method for obtaining and analyzing sensitivity data. *Journal of the American Statistical Association*, 43:109–126, 1948.

[58] N. E. Dowling. Fatigue at notches and the local strain and fracture mechanics approaches. *Fracture Mechanics, American Society of Testing and Materials*, ASTM STP 677, 1979.

[59] N.E. Dowling. *Mechanical Behavior of Materials. Engineering Method for Deformations, Fracture and Fatigue.* Pearson, New Jersey, 3nd edition, 1998.

[60] N.E. Dowling and S. Thangjitham. An overview and discussion of basic methodology for fatigue. *Fatigue and Fracture Mechanics. ASTM STP 1389*, 31:3–36, 2000.

[61] H. Drees, L. Haan, and D. Li. On large deviation for extremes. *Statistical Probabilistic Letters*, 64(1):51–62, 2003.

[62] S. Durham, J. Lynch, and W.J. Padgett. $TP_2$-ordering and the IFR property with applications. *Probability in the Engineering and Informational Science*, 4:73–88, 2000.

[63] B. Efron and R. J. Tibshirani. *An Introduction to the Bootstrap.* Chapman & Hall/CRC, 1993.

[64] A. Fernández-Canteli. *Criterios para la normalización de ensayos de fatiga en armaduras activas y pasivas de hormigón armado y pretensado.* PhD thesis, Universidad Politécnica de Madrid, Madrid, 1981.

[65] A. Fernández-Canteli. Statistical interpretation of the miner-number using an index of probability of total damage. In *ABSE Colloquium Lausanne. pp. 309–319*, 1982.

[66] A. Fernández-Canteli, V. Esslinger, and B. Thürlimann. *Ermüdungsfestigkeit von Bewehrungs–und Spannstählen.* Bericht Nr. 8002-1, IBK. ETH Zrich, Birkhäuser Verlag, ISBN:3-7643-1613-6 edition, 1984.

[67] A.G. Forman. *Journal of Basic Engineering*, 89:459–464, 1967.

[68] A. M. Freudenthal. Statistical aspects ol fatigue. *American Society for Testing and Materials*, ASTM STP 121:3, 1952.

[69] N. E. Frost and D.S. Dugdale. The propagation of fatigue craks in sheet specimens. *Journal of the Mechanics and Physics of Solids*, 6, No. 2:92–110, 1965.

[70] J. Galambos. *The Asymptotic Theory of Extreme Order Statistics.* Krieger Publ., Melbourne, Florida, second edition edition, 1987.

[71] G. Galileo. *Discorsi e dimostrazioni intorno a due nouve scienze.* Leyden, 1638.

[72] G. Genest and J. V. Zidek. Combining probability distributions: a critique and a annoted bibliography. *Statistical Science*, 1:114–148, 1986.

[73] W.Z. Gerber. Calculation of the allowable stresses in iron structures. *Z. Bayer Archit Ing Ver*, 6:101–110, 1874.

[74] J. Goodman. *Journal of Mechanics Applied to Engineering.* Longmans, Green, New York, 1st edition, 1899.

[75] J. Goodmann. *Mechanics applied to Engineering.* Longmans, Green and Co., London, 1919.

[76] E. Haibach. Modified linear damage accumulation hypothesis. In *Proceedings of the Conference on Fatigue of welded Structures, pp. xx-xxii.* Brighton, England, 1970.

[77] E. Haibach. *Betriebsfestigkeit. Verfahren und Daten zur Bauteilberechnung.* Düsseldorf: VDI-Verlag, 1989.

[78] E. Haibach and B. Atzori. Ein statistisches Verfahren fr das erneute Auswerten von er anregende. *Aluminium*, 51, No. 4:267–272, 1975.

[79] B.P. Haigh. Experiments on the fatigue of brasses. *Journal of the Institute of Metals*, 18:55–86, 1917.

[80] Fei H.L. and Xu X.L. Lu X.W. Procedures for testing outlying observations with aweibull or extreme-value distribution. *Acta Math Appl Sinica*, 21(4):549–61, 1998.

[81] S.L.J Hu and L.D. Lutes. Non-normal description of morrison-type wave forces. *Journal of Engineering Mecchanics, ASCE*, 113(3):196–209, 1987.

[82] J. Kepler. *Chilias logarithmorum ad totidem numeros rotundos.* Marburg, 1624.

[83] D.P. Kihl, S. Sarkani, and J.E. Beach. Stochastic fatigue damage accumulation under broadband loadings. *International Journal of Fatigue*, 17(5):321–9, 1995.

[84] J. Kohout and S. Vechet. New functions for description of fatigue curves and their advantages. In *Proceedings of the Seventh International Fatigue Congress, Vol. II, pp.783–8.* Beijing, 1999.

[85] J. Kohout and S. Vechet. Regression of fatigue curves using functions with graphs close to broken line. In *Proceedings of Sixth National Conference Degradation of Properties of Structural Materials by Fatigue, pp. 29–33 (ISBN 80-7100-629-7).* Zilina, Slovakia, 1999.

[86] J. Kohout and S. Vechet. A new function for fatigue curves characterization and its multiple merits. *International Journal of Fatigue. Technical note*, 23:175–183, 2001.

[87] M. Kuczma. Functional equations on restricted domains. *Aequationes Mathematicae*, 18:1–34, 1978.

[88] T. E. Langlais and J. H. Vogel. Overcoming limitations of the conventional strain-life fatigue damage model. *Journal of Engineering Materials and Technology*, 117:103–108, 1995.

[89] A. M. Legendre. *Elements de geometrie*. Note II edition, 1791.

[90] L.D. Lutes, M. Corazao, S.L.J. Hu, and J.J. Zimmermann. Stochastic fatigue damage accumulation. *Journal of Structural Engineering ASCE*, 110(ST11):2585–2601, 1984.

[91] J.Y. Mann. The historical development of reseach on the fatigue of materials and structures. *The Journal of the Australian Institute of Metals*, pages 222–241, 1958.

[92] S. S. Manson. *Behavior of materials under conditions of thermal stress*. University of Michigan Engineering Research Institute, MI, 1953.

[93] M. Matsuishi and T. Endo. *Fatigue of metals subjected to varying stress*. Fukuoka, Japan, 1968.

[94] I. Milne. The importance of the managment of structural integrity. *Engineering Failure Analysis*, 1, No. 3:171 – 181, 1958.

[95] M.A. Miner. Cumulative damage in fatigue. *Journal of Applied Mechanics*, 12:159–164, 1945.

[96] J. Morrow. *Fatigue properties of metals. Section 3.2 of Fatigue Design Handbook*. Society for Automotive Engineers, Warrendale, AE-4 edition, 1964.

[97] J. Morrow. Fatigue design handbook. section 3.2. *Advances in Engineering, SAE, Warrendale, PA*, 4:21–29, 1968.

[98] J. D. Morrow. Cyclic plastic strain energy and fatigue of metals. in internal friction, damping and cyclic plasticity. *ASTM, West Conshohocken, PA*, pages 45–86, 1965.

[99] A. Naess and B. Hungness. Estimating confidence intervals of long period design by bootstrapping. *Journal of Offshore Mechanics and Arctic Engineering-Transactions of the ASME*, 124 (1):2–5, 2002.

[100] J. Napier. *Cannon of Logarithms*. 1614.

[101] W. Nelson. Analysis of residuals from censored data. *Technometrics*, 15:697–715, 1973.

[102] S. Nirbhay, R. Khelawan, and G.N. Mathur. Effect of stress ratio and frequency on fatigue crack growth rate of 2618 aluminium alloy silicon carbide metal matrix composite. *Bulletin of Materials Science*, 24(2):169–171, 2001.

[103] N. Oresme. *Questiones super geometriam Euclidis*. Manuscript, Paris, 1347.

[104] N. Oresme. *Tractatus de configurationibus qualitatum et motuum*. Manuscript, Paris, 1352.

[105] A. Palmgrem. Die Lebendauer von Kugellagern. *Ver. Deut. Ingr.*, 68:339–341, 1924.

[106] P. C. Paris and F. Erdogan. A critical analysis of crack propagation law. *Transactions of the ASME Journal Basic Engineering*, 85, 4:528–538, 1963.

[107] F.G. Pascual and W.Q. Meeker. Estimating fatigue curves with the random fatigue-limit model. *Technometrics*, 41, No. 4:277–290, 1999.

[108] R. Picciotto. *Tensile fatigue characteristics of sized polyester/viscose yarn and their effect on weaving performance. Masters Thesis.* PhD thesis, North Carolina State Univ., North Carolina, 1970.

[109] L.P. Pook and N.E. Frost. A fatigue crack growth theory. *International Journal of Fracture*, 9:53–61, 1973.

[110] Koller R., Ruiz-Ripoll M.L., García A., Fernández-Canteli A., and Castillo E. Experimental validation of a statistical model for the Wöhler field corresponding to any stress level and amplitude. *International Journal of Fatigue*, doi:10.1016/j.ijfatigue.2008.09.003.

[111] D. Radaj and C.M. Sonsino. *Fatigue Assessment of Welded Joints by Local Approaches.* Abington Publishing, Cambridge, 1998.

[112] W. Ramberg and W. R. Osgood. Description of stress-strain curves by three parameters. *NACA Technical Note*, 902, 1943.

[113] T.M. Rassias. *Functional equations and inequalities.* Dordrecht: Lluwer Academic Publisher, 2000.

[114] R. C. Rice et al. *Fatigue Design Handbook.* Society of Automotive Engineers, Warrendale, PA, 3rd edition, 1997.

[115] M.L. Ruiz-Ripoll, A. García, E. Castillo, A. Fernández-Canteli, and R. Koller. Fatigue damage measures with a statistical model for the whler field. In *Proceding for the IALCEE'08. First International Conference in Life Cycling Engineering. pp. 221–227.* Taylor & Francis Group, London, 2008.

[116] S. Sarkani, G. Michaelov, D.P. Kihl, and J.E. Beach. Fatigue of welded steel joints under wideband loadings. *Probabilistic Engineering Mechanics*, 11:221–227, 1996.

[117] J. Schijve. *NLR-TR-101-361.* Amsterdam, 1962.

[118] W. Schütz. *View points of material selection for fatigue loaded structures.* Darmstadt, 1968.

[119] M. Shankar and J.B. Ahna. Frequency effects on fatigue behavior of nextel720$^{TM}$/alumina at room temperature. *Journal of the European Ceramic Society*, 28:2783–2789, 2008.

[120] C.G. Small. *Functional equations, how to solve them.* Springer. Boston Academic Press, New York, 2007.

[121] J. Smital. *On functions and functional equations.* Hilger, New York, 1988.

[122] J.O. Smith. *The effect of range of stress on the fatigue strength of metals.* Urbana, Il, 1942.

[123] K.N. Smith, P. Watson, and T.H. Topper. A stress-strain function for the fatigue of metals. *Journal of Materials*, 5:767–778, 1970.

[124] C. R. Soderberg. Fatigue of safety and working stress. *Transactions of the American Society of Mechanical Engineers*, 52 (Part APM-52-2):13–28, 1930.

[125] C.R. Soderberg. Factor of safety and working stress. *Transactions of the ASTM*, 52:13–28, 1939.

[126] J.E. Spindel and E. Haibach. Some consideration in the statistical determination of the shape of S–N curves. *Statistical Analysus of Fatigue Data, ASTM*, ASTM STP 744:89–113, 1981.

[127] P. Starke, F. Walther, and D. Eifler. PHYBAL-A new method for lifetime prediction based on strain, temperature and electrical measurements. *International Journal of Fatigue*, 28(9):1028–1036, 2006.

[128] C. E. Stromeyer. The determination of fatigue limits under alternating stress conditions. *Proceedings of the Royal Society of London. Series A*, 90, No. 620:411–425, 1914.

[129] E.K. Walker. The effect of the stress ratio during crack propagation and fatigue for 2024-T3 and 7075-T6 aluminium. *ASTM-SPT*, 462:1–14, 1970.

[130] W. Weibull. *Fatigue testing and analysis of results*. Pergamon, Oxford, 1st edition, 1961.

[131] J. S. Wilson and B. P. Haigh. Stresses in bridges. *Engineering (London)*, 116:411–413, 1923.

[132] S.R. Winterstein. Nonlinear vibration models for extremes and fatigue. *Journal of Engineering Mechanic ASCE*, 114(10):772–90, 1988.

[133] B. Wolf, C. Fleck, and D. Eifler. Characterization of the fatigue behaviour of the magnesium alloy AZ91D by means of mechanical hysteresis and temperature measurements. *Technical Note. International Journal of Fatigue*, 26:1357–1363, 2004.

[134] T. Yokobori, S. Konosu, and A.T.Jr. Yokobori. Micro and Macro Fracture Mechanics Approach to Brittle Fracture and Fatigue Crack Growth. advances in Research on the Strength and Fracture of Materials. Master's thesis, Engineering Science and Mechanics Departament Virginia Polytechnic Institute and State University, Waterloo, Canada, 1977.

[135] L. Yung-Li, J. Pan, R. Hathaway, and M. Barkey. *Fatigue Testing and Analysis. Theory and Practice*. Elsevier. Butterworth Heinemann, Oxford, 1st edition, 2004.

[136] J. Zhang and D.B. Kececioglu. New approaches to determine the endurance strength distribution. In *4th ISSAT International Conference on Reliability & Quality in Design*. Seattle, WA, 1998.